Investigating the role of ASPP2 in post-implantation mouse embryos

Elizabeth Sandham

Supervisors: Professor Shankar Srinivas, Dr Christophe Royer

Thesis submitted for the Degree of MSc by Research in Physiology, Anatomy & Genetics

Submission: June 2021
Word count: 26,000 words

I, Elizabeth Sandham, confirm that the work presented in this thesis is my own work, unless indicated otherwise.

Acknowledgements

I would like to offer my sincere thanks to my supervisors Professor Shankar Srinivas and Dr Christophe Royer. Their support, guidance and advice has enabled me to complete my research and this thesis. Professor Shankar Srinivas welcomed me into his research group and helped to guide my experiment and my thesis. Dr Christophe Royer has been wonderful in helping me to train for, plan and execute my experiments. The Srinivas group as a whole has provided the most supportive, friendliest environment for carrying out my research.

Abstract

My research focuses on the role of ASPP2 (Apoptosis-stimulating of p53 protein 2, encoded by the *TP53BP2* gene) during early post-implantation development. ASPP2 has multiple important biological functions, including roles in the control of cell polarity, tight junction formation, cell proliferation, differentiation and apoptosis.

To study the molecular basis of ASPP2 function in post-implantation development, I generated a mouse line in which exon 4 of *ASPP2* is flanked by LoxP sites. Using genetic crossings, this allowed me to generate various mouse lines that were used to study the function of ASPP2 in the whole embryo and in specific tissues.

My results indicate that gastrulation is able to proceed in $ASPP2^{-/-}$ embryos – all 3 germ layers appear to form correctly. However, the embryo becomes progressively more disordered as development proceeds, resulting in embryonic lethality by E9.5. Somites are present at E8.5 and E9.5, showing that mesoderm-derived structures can form. The somites, however, are smaller than their wildtype counterparts. Additionally, instead of the normal structure of a single layer of somitic cells surrounding a central cavity, the somites have a disorganised structure with multiple cell layers and often lack a cavity.

Heart formation is also affected in these mutant embryos. By E9.5, there is no heart structure, with the absence of a beating heart. I crossed the $ASPP2^{flox/flox}$ mouse line to a line expressing CRE under the *Mesp1* promoter, which controls early cardiac progenitor formation. These mice developed normal hearts at E8.5 and E9.5, implying that the perturbation in cardiac development is a secondary defect, likely caused by disturbances to the surrounding tissues meaning that the cardiac progenitors do not receive the signals they require to continue developing.

Thus, my research has indicated that ASPP2 is essential for post-implantation embryonic development. The mesoderm initially forms correctly but as the embryo continues to develop,

the mesoderm-derived somites become disrupted, indicating a role for ASPP2 in regulating the epithelial architecture of the somites. Similarly, as seen in the heart, the disorganisation of structures leads to secondary defects later in development, ultimately resulting in embryonic lethality. These results demonstrate the importance of ASPP2 and shed light on some of the functions that it may play in development.

Contents

Chapter 1: Introduction

1.1 ASPP2 and cell polarity

Embryogenesis involves the gain of polarity to allow the determination of axes and the patterning of the embryo. In addition, the cells must proliferate and differentiate as development progresses. ASPP2 may act as a linking factor between polarity, proliferation and differentiation, thus potentially playing a crucial role in embryogenesis.

1.1.1 ASPP2 and its binding partners

ASPP2 is also known as p53-binding protein 2 (53BP2) as it was originally identified in a yeast two-hybrid screening as a binding partner of tumour suppressor p53 [1]. ASPP2 is a protein composed of 1134 amino acids and belongs to the evolutionarily conserved ASPP family of proteins, thus named due to the fact that these proteins are apoptosis-stimulating proteins of p53, and are ankyrin repeat-, SH3 domain- and proline-rich region-containing proteins [2]. These proteins, as the name suggests, regulate the activity of p53 and contain signature sequences in their C-termini; ankyrin repeats, a SH3 domain and a proline-rich region. ASPP2 and related protein ASPP1 also have RAS-association domains located at their N-termini [3]. Therefore, ASPP2 is able to bind both active RAS and p53. It cooperates with the former to stimulate the apoptotic function of the latter [2], [3]. In doing so, ASPP2 may act to regulate cell proliferation.

Other proteins that ASPP2 may bind include apoptotic regulator B-Cell lymphoma 2 (Bcl-2) and NF-κβ subunit p65, a protein that is involved in a diverse array of functions including cell transcription and cell death [4], [5]. The activity of p65 can inhibit apoptosis induced by ASPP2, further adding to regulatory cell death mechanisms that ASPP2 may be involved in.

Additionally, ASPP2 may bind APCL, a brain-specific homologue of the Adenomatous polyposis coli (APC) tumour suppressor, and the two may form a complex in the perinuclear region (although this interaction was shown using over-expression and is yet to be confirmed) [6]. APCL interacts with Wnt effector β-catenin and targets it for degradation. It can also bind cytoskeletal proteins, thus playing a role in actin assembly, cell-cell adhesion and microtubule network formation. Furthermore, ASPP2 partially co-localises and forms a complex with β-catenin itself, negatively regulating its transcriptional activity [7], [8].

As will be discussed in more detail subsequently, ASPP2 also binds polarity protein Par3, and the transcriptional co-activators Yes-associated protein (YAP) and Transcriptional co-activator with PDZ-binding motif (TAZ), and to PP1 [9]–[11]. Through these binding partners, ASPP2 plays an important role in cell proliferation and differentiation in the mouse embryo (Figure 1.1).

1.1.2 ASPP2 and the Hippo pathway

The Hippo pathway is a conserved signalling pathway that acts as a major regulator of tissue growth and organ size, controlling transcriptional events involved in both cell proliferation and apoptosis [12]–[15]. In mammalian cells, Mammalian sterile 20–like kinase 1 and 2 (MST1 and MST2; homologs of Hippo in *Drosophila*) bind to Salvador 1 (SAV1) (Figure 1.2). This activates the kinase activity of MST1/2, which then phosphorylates Lats1/2.

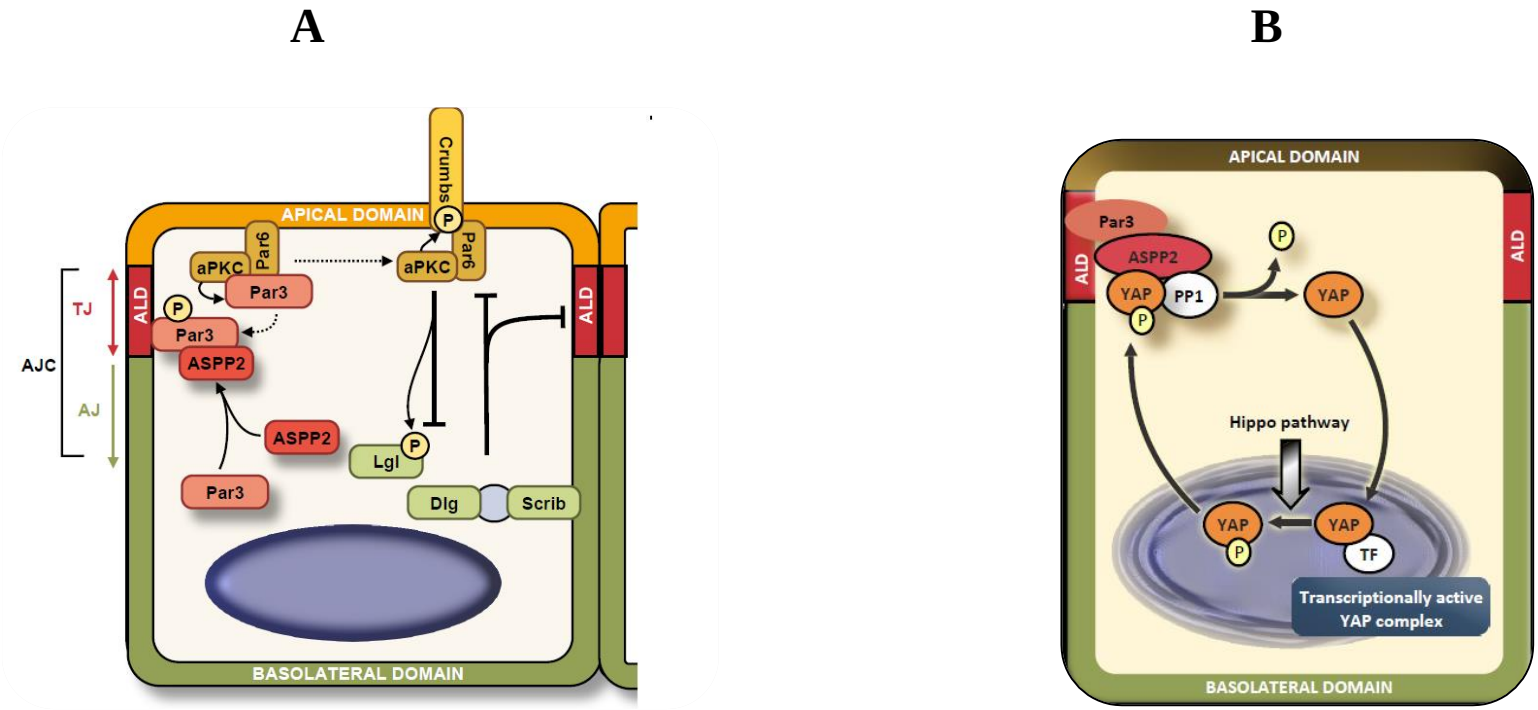

Figure 1.1. ASPP2 and associated polarity components involved in the maintenance of apicobasal polarity in epithelial cells and the establishment of membrane domain identity. A) ASPP2 forms a complex at tight junctions through its interactions with PAR3. PAR3 in turn interacts with many other polarity proteins including aPKC and PAR6. B) ASPP2 acts as a scaffold at tight junctions for PP1 and YAP. PP1 is able to dephosphorylate and thus activate YAP. AJC, adherens junction complex; ALD, apicolateral domain; ALJ, apicolateral junction; TJ, tight junctions.

Figure adapted from Royer & Lu, 2011 [16] and Royer et al, 2014 [11]

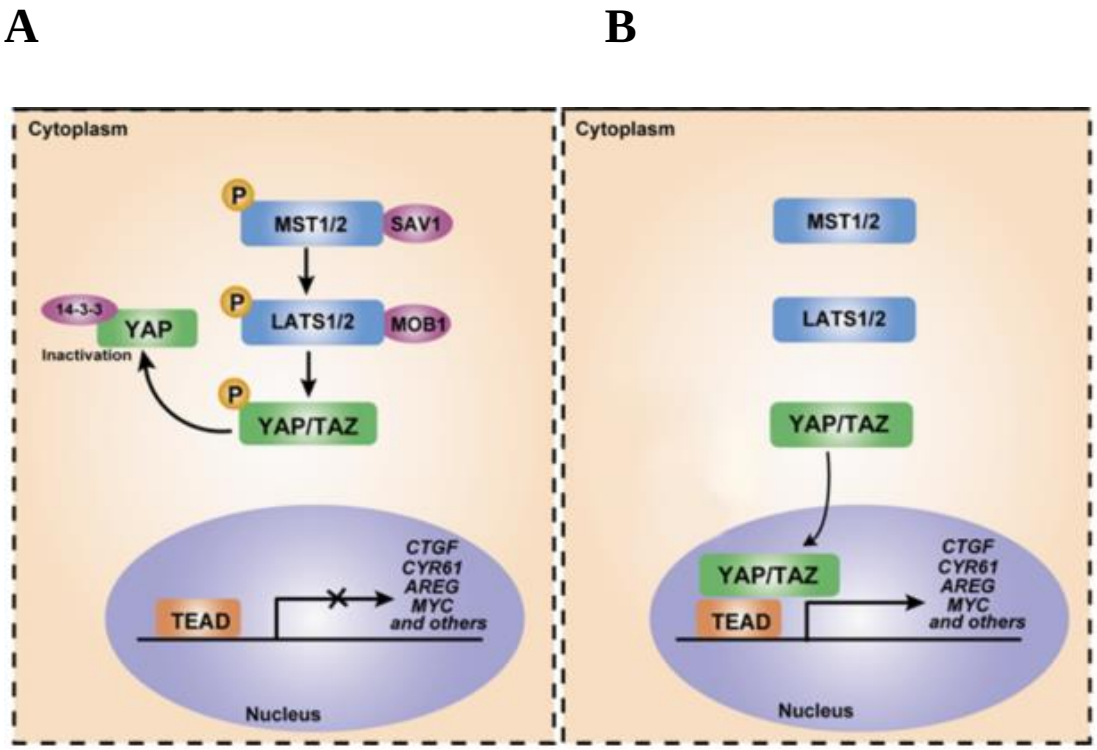

Figure 1.2. Hippo signalling pathway in mammals. A) When Hippo signalling is on, MST1/2 (supported by scaffold protein SAV1) activates LATS1/2 phosphorylation. LATS1/2 forms a complex with MOB1, which also contributes to LATS1/2 activation. The activated LATS1/2 phosphorylates YAP/TAZ, promoting it binding to 14-3-3 protein and leading to cytoplasmic sequestration. This inactivates YAP. B) When the Hippo signalling is off, YAP/TAZ are dephosphorylated and located into the nucleus. Activated YAP/TAZ induce the expression of downstream effectors (e.g. CTGF, CYR61, AREG, MYC) by interaction with transcriptional coactivator TEAD.

Figure adapted from Li et al, 2016 [153]

TEAD drives the expression of a multitude of genes, including pro-growth, pro-migratory and anti-apoptotic genes [17]–[19]. In addition to this role in cell survival, one of the key functions of YAP/TAZ and TEAD in the mouse embryo is the control of cell differentiation, particularly in the first cell fate choice where cells either become TE or ICM (as described further in section 1.2.1 Pre-implantation embryogenesis).

Protein phosphatase 1 (PP1) dephosphorylates YAP/TAZ to promote its nuclear translocation and disrupts YAP/TAZ binding to E3 ubiquitin ligase to inhibit its degradation [10]. ASPP2 assists this by forming an apicolateral complex at tight junctions (TJs) in in polarised epithelial cells, acting as a scaffold for PP1 and YAP (Figure 1.1) [10], [11], [20]. ASPP2 and YAP have similarly been shown to co-localise at TJs in VE of early (E5.5) post-implantation embryos (Figure 1.3) [Unpublished, C. Royer & Srinivas group]. Therefore, ASPP2 may link apicobasal polarity with YAP activity and the Hippo pathway in the mouse embryo.

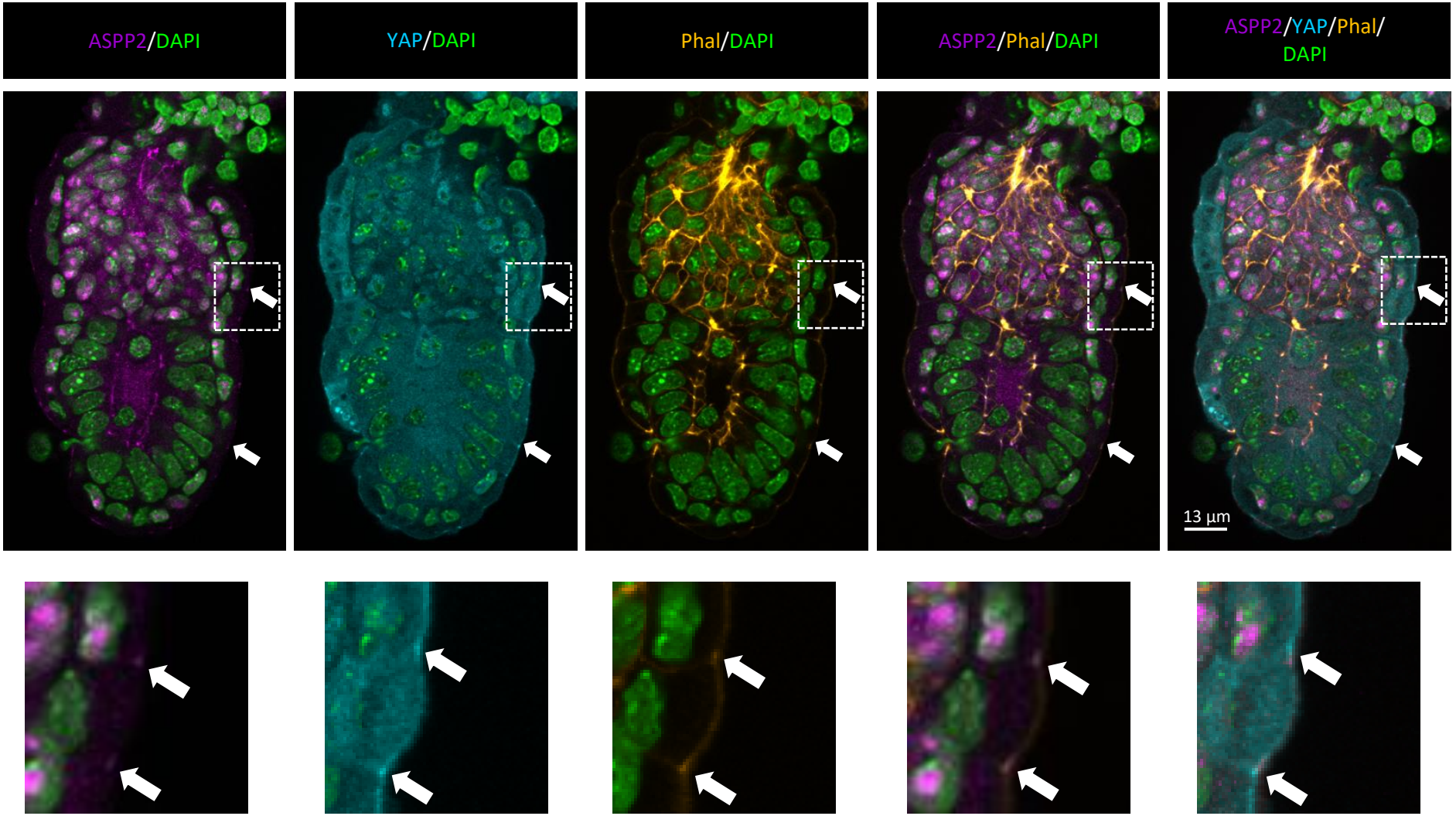

Figure 1.3. E5.5 wildtype embryos. Immunostainings for ASPP2 (magenta), YAP (cyan), DAPI (green), Phalloidin (yellow). Note how ASPP2 and YAP co-localise at tight junctions (white arrows). Imaged at 40X using confocal microscopy with the LSM 880 Zeiss microscope, as detailed in Section 2.6. Data and images from C. Royer & Srinivas group [unpublished]

1.1.3 ASPP2 and polarity

As mentioned previously, ASPP2 plays a role in apicobasal polarity. Polarity is defined as an asymmetry in the spatial distribution of cellular components, structure and functions. Establishment and maintenance of polarity is essential for development and homoeostasis in all metazoans. There are several types of polarity, including planar polarity and apicobasal polarity. The former refers to polarity oriented within the plane of the tissue whereas apicobasal polarity describes the polarization of cells perpendicular to this plane.

Apicobasal polarization results in the generation of two distinct plasma membrane domains, termed the apical and the basolateral domains. These biochemically and structurally different domains are separated by the presence of apicolateral junctional complexes (AJCs), which are comprised of adherens junctions (AJs) and tight junctions (TJs) [21]. TJs are composed of three families of transmembrane proteins (occludin, claudins and junctional adhesion molecules (JAM)), which form a selective barrier regulating diffusion of molecules into the paracellular space, and between the apical and lateral surfaces. AJs are composed of components including nectins, nectin-like molecules and cadherins. AJs form just below the apical surface, encircling the epithelial cell basally to the tight junctions.

The initiation of polarity begins with cell-cell contact and attachment between adjacent cells via the interaction of their E-cadherin molecules in a Ca^{2+} dependent manner [22]. Integrin and extracellular matrix interactions, in addition to nectins and nectin-like molecules, are also thought to play a role in this initial cell-cell contact. This contact acts as a spatial cue for apicobasal polarity and leads to the formation of nascent adherens junctions at the contact sites [23].

The initiation of cell polarization also leads to the recruitment of TJ components, such as zonula occludens 1 (ZO-1), to the apical domain. ZO-1, ZO-2 and ZO-3 there act as scaffolds to recruit

further TJ components, including claudins and occludin, thus directing the formation of TJs [24], [25].

The establishment and maintenance of polarity in epithelial cells is controlled by three groups of proteins, highly conserved from yeast to mammalian cells: the PAR system, the Crumbs CRB/PALS1/PATJ complex and the Scribble SCRIB/DLG/LGL complex [22]. The PAR system is thus named because it was first identified in a screen of *partitioning-defective (PAR)* mutations in *C.elegans*.

The E-cadherin-mediated cell-cell attachment activates Cdc42 from its GDP-bound inactive state to its GTP-bound active form [26]. When Cdc42 and Rac1, both members of the Rho family of small GTPases, are activated, they are able to bind PAR6 [27]. This induces a conformational change in PAR6, meaning that it is able to bind aPKC [28].

The PAR6-aPKC complex can then interact with LGL, which is phosphorylated by aPKC at specific residues [29]. The phosphorylated LGL dissociates from this complex and localizes to the basolateral membrane, where it interacts with DLG/SCRIB and acts together with these proteins to restrict apical components to the apical domain [22], [30]. When LGL is released from the PAR6-aPKC complex, aPKC is then able to bind PAR3, allowing for the active PAR complex to form and localize to the apical TJs [31]. The Crumbs complex binds with the PAR complex via several interactions (e.g. PAR6 and CRB) and acts to maintain the stability of polarity [32]. CRB and PAR3 also redundantly function to restrict LGL to the basal domain [33], [34].

When components of these conserved polarity complexes are knocked down or overexpressed, there are defects in polarity and in junctional formation. For example, when PATJ is downregulated in epithelial cells, ZO-1, ZO-3 and Occludin no longer localize to and assemble tight junctions [35], [36]. Likewise, cells that lack PAR3 have a profound disruption in tight junction formation [37].

ASPP2 is linked to cell polarity through its aforementioned ability to form complexes at tight junctions. ASPP2 binds PAR3 and controls its apical/junctional localization in an interdependent manner: depletion of either one causes a defect in the localization of the other [7], [38]. Depletion of ASPP2 or disruption of the interaction between ASPP2 and PAR3 in epithelial cells causes defects in cell polarity, disrupting the formation of tight junctions and the maintenance and development of apical membrane domains. Thus ASPP2 plays a crucial role in controlling cell polarity. This is important in embryogenesis as polarity directs key developmental processes such as cell fate specification and tissue organisation, as will be discussed in the following sections on early mouse embryogenesis.

1.2 Early mouse embryogenesis

The mouse embryo begins as one cell – a fertilized egg – and proliferates to become a gastrulating embryo. As development proceeds, body axes are generated and cells divide, migrate and differentiate to create an increasingly sophisticated embryo. The heart and somites are among the first of the more complicated embryonic structures to form. As ASPP2 is important in epithelial cell polarity and cell polarity is essential for the formation and structuring of embryonic tissues and their features, I hypothesised that ASPP2 would play a critical role in early embryogenesis.

1.2.1 Pre-implantation embryogenesis

Within 24 hours of fertilization, the single-celled zygote divides to give rise to the 2-cell embryo. At intervals of approximately 12 hours, the embryo undergoes two further divisions to produce an 8-cell embryo made up of blastomeres that are non-polarized and symmetrical.

Before the next cell division occurs, the embryo undergoes a Ca^{2+}-dependent compaction leading to an increase in cell-cell contact. This promotes cell adhesion and thus initiates the generation of apicobasal cell polarity in each of the blastomeres [39], [40]. Factors including atypical protein kinase C (aPKC) and PAR3 and PAR6 localize asymmetrically to the apical side of the blastomeres of the compacted embryo and establish tight junctions. Other proteins, including PAR1, Lethal giant larvae 2 (Lgl2) and E-cadherin, are found at the basolateral membrane of blastomeres [41]–[43]. Thus apicobasal polarity is acquired at E2.5 (embryonic day 2.5).

Subsequently, the blastomeres undergo two rounds of cell division, taking the embryo from 8 to 16 cells (resulting in the generation of the morula) and then from 16 to 32 cells. At this stage, two distinct populations of cells arise: polar 'outside' cells, with the apical side exposed to the outside of the embryo, and apolar 'inside' cells, which are surrounded completely by outside cells. These outside and inside cells give rise to the trophectoderm (TE) and inner cell mass (ICM), respectively (Figure 1.4).

TEAD4 and downstream effectors of the Hippo pathway YAP and TAZ act to interpret the positional information of a cell to restrict expression of Cdx2 and TE fates to outside cells [44], [45]. In outer cells, Hippo signalling remains inactive and YAP/TAZ are thus located in the nucleus (Figure 1.4). Here, they bind TEAD4, resulting in the expression of TE-specific transcription factors including CDX2 and GATA3 [44]. In inner cells, the Hippo pathway is activated, leading to the exclusion of YAP/TAZ from the nucleus. The inner cells thus adopt ICM fate. As previously discussed, ASPP2 is also able to bind YAP/TAZ and may thus play an important role in cell fate decisions through this interaction.

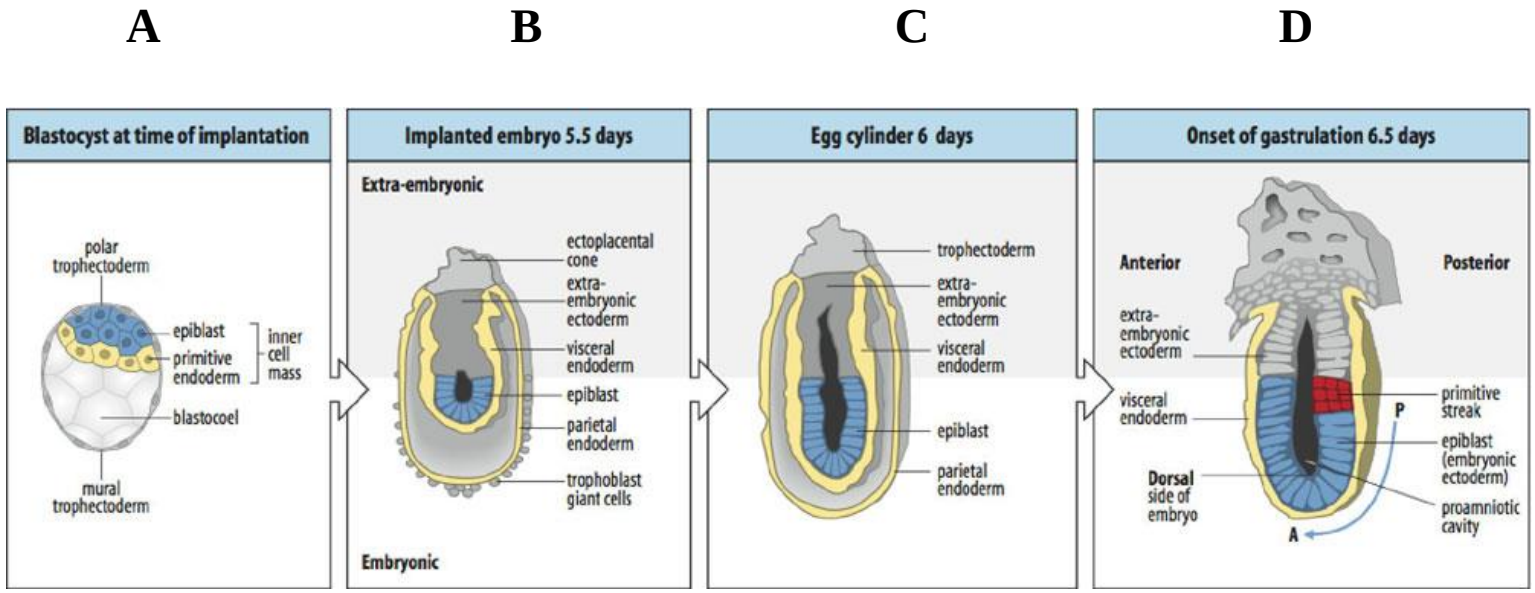

Figure 1.4. Early development of the mouse embryo. A) Preimplantation late stage blastocyst at 4.5 days post-fertilization. The trophectoderm forms the outer layer of the blastocyst. The inner cell mass, made up of the epiblast and primitive endoderm, forms the inside of the blastocyst, along with a fluid-filled cavity termed the blastocoel. B) Peri-implantation egg cylinder at 5.5 days post-fertilization. The trophectoderm invades the maternal endometrium during the process of implantation. The mural trophectoderm gives rise to polyploid trophoblast giant cells and the rest of trophectoderm becomes the ectoplacental cone. The epiblast divides further to produce the extraembryonic ectoderm and the epiblast (embryonic ectoderm). The primitive endoderm migrates to cover inner surface of mural trophectoderm to become the parietal endoderm, and to cover epiblast to become the visceral endoderm. C) Post-implantation egg cylinder at 6 days post-fertilization. By this stage, the embryo has developed further and is cup-shaped, with the epiblast positioned distally in the embryo. D) Gastrulating embryo. Gastrulation takes place with the formation of the primitive streak.

Figure adapted from Wolpert - Principles of Developmental Biology' 5th edition [46]

A crucial role of the TE is the formation of the blastocoel. As the TE matures, its epithelium polarizes and epithelial AJCs are generated, which create an intercellular permeability seal [47], [48]. Cavitation is then initiated around the 32-cell stage by the transport of water across osmotic gradients through aquaporins on the apical and basolateral sides of TE cells [49], [50]. With the formation of this blastocoel, the embryo is now termed a blastocyst.

The formation of the blastocoel directs the generation of the embryonic-abembryonic axis in the early embryo. The ICM cells are positioned on one side of the blastocyst with the blastocoel cavity opposite, giving rise to embryonic (ICM side)-abembryonic (blastocoel side) polarity. The embryonic-abembryonic axis corresponds to the long axis (the proximal-distal axis) of the embryo at pre-gastrulating E5.5 stage, which in turn corresponds to the dorsal-ventral axis.

After the ICM and the TE regions of the embryo have been established, a second differentiation event must take place, segregating the ICM into primitive endoderm (PrE) and the epiblast. The former contributes to the visceral endoderm (VE) and parietal endoderm (PE) of the post-implantation embryo, whereas the latter gives rise to the three germ layers (endoderm, mesoderm and ectoderm) at gastrulation and thus generates the somatic tissues and the germ cells of the fetus.

Nanog, which is associated with maintaining pluripotency, is initially uniformly expressed in the ICM. However, at E3.5, expression becomes restricted to one of two subpopulations of cells found within the ICM in a ‘salt-and-pepper’ pattern [12]. The other subpopulation of cells expresses Gata6. Knockdown studies have shown that Nanog is necessary for epiblast formation and Gata6 is required for PrE formation [13]–[15]. The ‘salt-and-pepper’ pattern of expression at E3.5 suggests that by this stage the ICM cells have already been determined to PrE or epiblast fate, with FGF/ERK signaling likely being the mechanism behind this [51].

By E4.5, the ICM has clearly segregated into the two cell types – the PrE and the epiblast. The cells of the PrE are positioned in a layer on the surface of the ICM, separating the epiblast cells

from the blastocoel cavity, while the epiblast cells are positive for Nanog and Oct3/4. Thus by E4.5, mutually exclusive positions and markers are firmly established and the blastocyst is ready for implantation.

1.2.2 Peri-implantation development

When the epiblast, PrE and TE cell lineages have been segregated, the blastocyst hatches from the zona pellucida. In the mouse embryo, the now-exposed mural TE (that surrounds the blastocyst cavity) makes the first contact with endometrial epithelium and terminally differentiates into primary trophoblastic giant cells (TGCs). The TE interacts with and adheres to the uterine luminal epithelium, triggering the apoptosis of the latter and thus allowing the penetration of the TE into the endometrial stroma [52], [53]. Promoted by factors secreted by the TGCs, the stromal cells then differentiate into decidual cells, which support the development of the growing embryo [54].

Contrary to the terminal differentiation fate of the mural TE cells, the polar TE (that surrounds the outer surface of the ICM) is the source of multipotent trophoblastic stem cells (TSC). After implantation, the polar TE proliferates and differentiates into the extraembryonic ectoderm (ExE). At the proximal tip of the ExE, furthest from the epiblast, the cells differentiate into the ectoplacental cone (EPC). These cell populations build the proximal half of the egg cylinder and later give rise to the placenta.

At E4.5, the PrE gives rise to the PE and the VE (Figure 1.4). The PE migrates from the epiblast to contact the inner surface of the TE where, together with TGCs, they secrete basement membrane proteins to form the Reichert's membrane [55]. From this, a transient parietal yolk sac develops but is degraded following the establishment of the chorioallantoic placenta. The VE is an epithelial sheet that remains in contact with the embryo and will later develop into the endoderm of the visceral yolk sac.

During peri-implantation, the epiblast reorganizes from a ball of non-polarized cells to a polarized cup-shaped epithelium, positioned distally within the embryo (Figure 1.4). The columnar epithelium surrounds the proamniotic cavity, which forms the hollow of the egg cylinder. Apoptosis was previously thought to be the mechanism by which this cavity forms, however, more recent studies have indicated that cell death is in fact not required [56]. Instead, cavity formation may occur as the epiblast reorganises into a rosette-like structure, with the basement membrane transmitting polarisation cues through integrin signalling. Lumenogenesis then occurs as the apical domain constricts. A lumen also forms in the ExE via a similar mechanism, and both lumens merge at E5.5-E5.75 to form the mature pro-amniotic cavity [56], [57].

1.2.3 Patterning early post-implantation embryo

By E6.5, anterior-posterior (AP) polarity is firmly established with the formation of the anterior visceral endoderm (AVE) on the future anterior side of the embryo.

There are two waves of Lefty1 expression; the first begins in a subset of blastomeres in the ICM at E3.5 [58]. The biological relevance of these cells is currently unknown – it may be required to initiate the second wave of Lefty1 expression. The second wave takes place in Gata6-positive cells between E3.75 to E4.0 and produces cells that contribute to the DVE [59]. These Lefty1-positive cells become asymmetrically located at the upper side of the PrE soon after E4.0, where they maintain Lefty1 expression. At E5.5, the DVE-fated cells change from cuboidal to columnar and begin expressing other DVE markers (such as Cer1 and Hhex) until E5.5 [60]. Once these cells are fully differentiated into DVE, they begin to migrate proximally, towards the future anterior side of the embryo. However, upon reaching the embryonic/extra-embryonic junction at E6.0, they migrate laterally and rapidly lose expression of DVE markers [59].

The extra-embryonic ectoderm has been found to play an important role in regulating the formation of the AVE, expressing signals such as Bone morphogenic protein (BMP) that inhibit AVE formation [61]. VE cells at the distal tip are furthest from the inhibitory signals, and can therefore start to express AVE markers. Differentiated AVE cells at the distal end then migrate towards the proximal side, while new AVE cells continue to be generated at the distal tip. By E6.5, the AVE is fully formed at the future anterior side) of the embryo. When these early cells are genetically ablated, the later AVE is able to be generate but unable to migrate [59].

At the future anterior side, Nodal inhibitors (including Lefty1 and Cer1) and Wnt inhibitors (such as Dkk1) are expressed and act on the adjacent epiblast cells to specify them as the future head of the embryo, repressing posterior markers such as T/Brachury and Cripto. The opposite region of the epiblast is furthest from these signals and is thus specified as the future tail [62].

1.2.4 Gastrulation

Gastrulation is the process by which the three germ layers (endoderm, mesoderm and ectoderm) are generated. It is initiated at the primitive streak, which forms in the epiblast at the extraembryonic-embryonic boundary opposite the AVE at E6.5 (Figure 1.5). Wnt3 acts to induce streak formation; it is initially expressed in the proximal region of the epiblast and the adjacent VE at E5.5 [63]. At E6.0, it becomes restricted to the future posterior side of the embryo and Eomes, which was previously expressed only in the extraembryonic ectoderm, is induced in the posterior side. Nodal is necessary for the activation of both these genes [64]. Wnt3 and Eomes initiate the expression of genes such as fibroblast growth factor 8 (Fgf8) and Brachyury/T in the proximal posterior region of early primitive streak embryos [65], [66].

As gastrulation initiates, cells of the epiblast migrate through the streak and generate two cell types: the mesoderm, which is mesenchymal, and the definitive endoderm, which is epithelial. This epithelial-to-mesenchymal transition (EMT) involves the columnar epithelial cells of the

primitive streak ingressing by elongating and acquiring a bottle-shaped morphology. In order for the cells to do this, apically constriction is key [67]. Subsequently, the cells lose their apicobasal polarity and downregulate junctional and basement membrane proteins, enabling them to be able to migrate away from the streak, forming a new mesenchymal, mesoderm cell layer. Fgf receptor 1 (Fgfr1) and Fgf8 are not required for initiation of EMT but are necessary for migration away from the streak and maintenance of the mesenchymal state [68], [69]. However, the exact mechanisms for this are still unknown. The cell layer that does not ingress into the primitive streak is referred as ectoderm and becomes restricted to the epidermal and neural lineage by the end of gastrulation. The events at this stage and the following steps of gastrulation are summarized in Figure 1.6.

The primitive streak elongates distally until it reaches the tip of the embryo at E7.5 and the different lineages arise from different regions of the streak, beginning with the most posterior end [70] (Figure 1.7). At this region in the early streak stage, the extraembryonic mesoderm is generated, which later gives rise to the mesoderm of the yolk sac, chorion and blood islands. BMP4, expressed from the ExE, plays a role in the development and patterning of the extraembryonic mesoderm [71]. Cells from middle and middle-anterior regions of the streak in the late gastrula stage embryo then ingress and give rise firstly to the rostral structures such as heart and forebrain mesoderm, then to the rest of the cranial mesoderm and lastly to the paraxial and lateral mesoderm of the trunk [72]. Finally, the last cell population emerges at the anterior primitive streak and gives rise to the node and the definitive endoderm, which forms the internal mucosal lining of the embryonic gut and its associated organs.

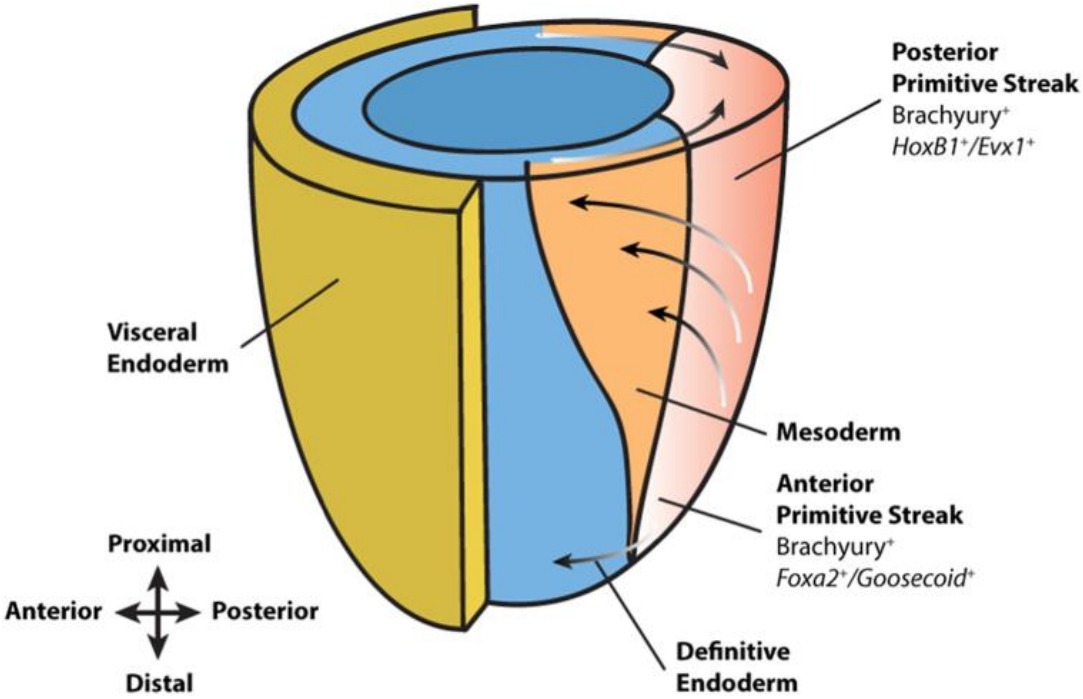

Figure 1.5. Mouse gastrulation. The primitive streak forms at E6 and coexpresses transcription factors including Brachyury in the posterior region and Brachyury and Foxa2 in the anterior region. Epiblast cells enter the proximal primitive streak (black arrows at the top of the embryo) and move through the streak, spreading forward and laterally between the ectoderm and the visceral endoderm to form the mesoderm. The primitive streak elongates distally until it reaches the tip of the embryo at E7.5.

Figure from Murray et al, 2009 [154]

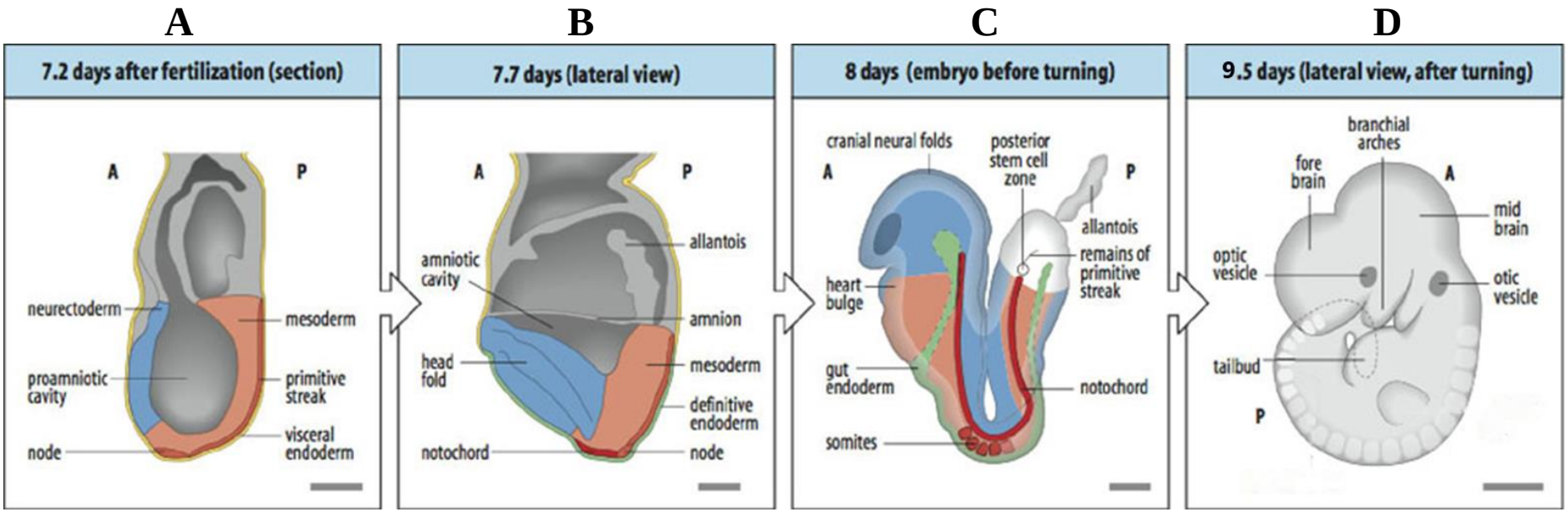

Figure 1.6. Post-implantation and post-gastrulation mouse embryogenesis. A) At E7.2, the primitive steak has elongated and the node has formed at its anterior tip. B) By E7.7, the notochord has formed anterior to the node and head folds have formed. C) By E8.0, neural folds have formed and the embryonic endoderm internalizes to form the gut. D) Between E8.5 and E9.5, the mouse embryo undergoes a large-scale complex conformational change ('turning') to bring the endoderm to the inside of the embryo and the ectoderm to the outside. The embryo becomes completely enclosed in the protective amnion and amniotic fluid.

Figure adapted from Staveley, Memorial University of Newfoundland [73]

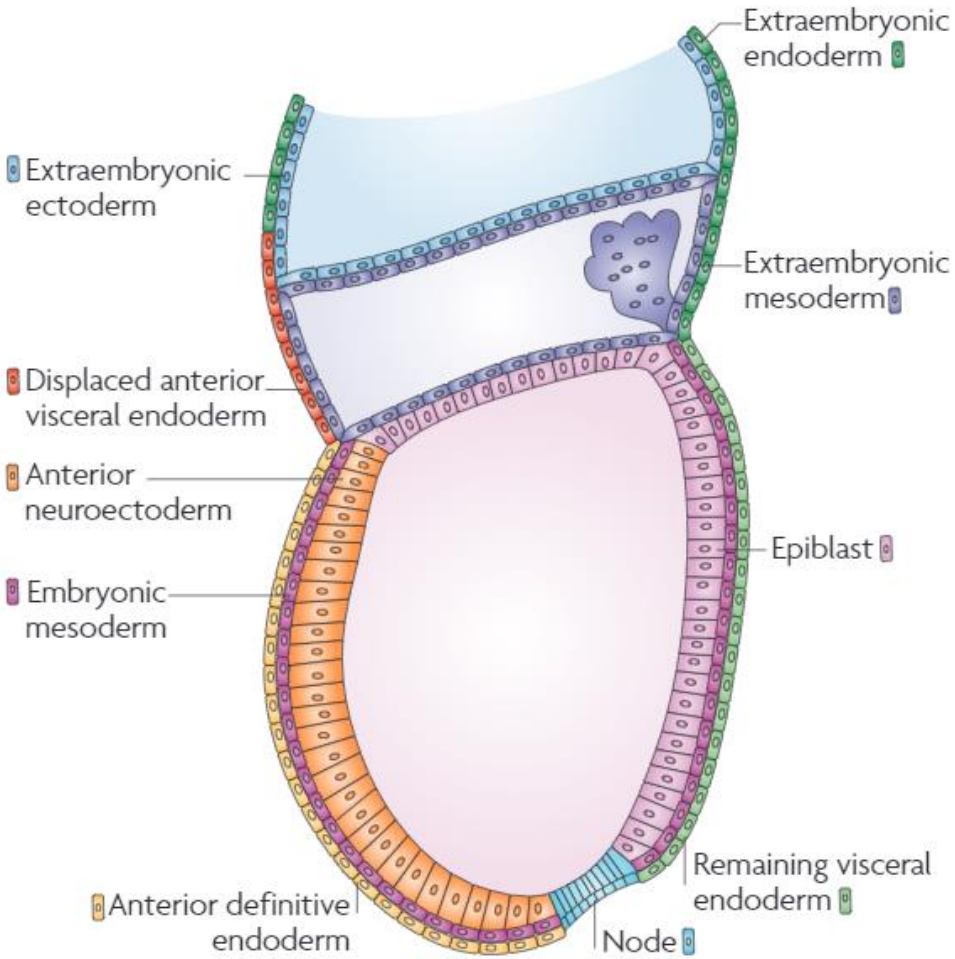

Figure 1.7. Gastrulation occurs at the opposite posterior proximal pole of the embryo to the site of the anterior visceral endoderm (red). Cells of the epiblast (pink) converge towards the posterior of the embryo and ingress at the primitive streak to form the nascent embryonic mesoderm (violet) and extraembryonic mesoderm (purple). As the primitive streak expands to the distal tip of the embryo, cells that are present in the anterior primitive streak give rise to the definitive endoderm (yellow), which emerges on the surface of the embryo and gradually replaces cells of the visceral endoderm (light green). Cells that remain in the epiblast cell layer by the end of gastrulation constitute the neuroectoderm (orange). A specialized population of cells at the anterior tip of the primitive streak form the node (light blue), an important signalling centre for embryonic patterning.

Figure from Arnold et al, 2009 [74]

The prospective definitive endoderm cells must undergo EMT to enable migration but then transition back to epithelial cells after egression from the primitive streak. They are then incorporated into the pre-existing VE epithelial cell layer [75], [76]. The population of definitive endoderm expands anteriorly and laterally from the site of integration, mixed with cells of the VE [77].

Cells ingress from the node to form the axial mesoderm, which later develops into the notochordal plate - a precursor to the notochord. The notochord is the source of inductive signals that specify and pattern the neurons, somites and gut. The node and notochord express many genes that are involved in this organizer activity. For example, several of the genes expressed bind and block specific ligands of the Wnt and transforming growth factor β (TGFβ) signalling pathways [78]. These ligands are expressed in extraembryonic tissues, the proximal ectoderm and the primitive streak. Thus blocking their signalling activity creates gradients that may direct cells to adopt distinct developmental fates.

Along with the generation of the three germ layers, gastrulation involves large-scale changes in the structure of the mouse embryo. The embryo initially develops `inside-out', with the ectoderm being formed internally, surrounded by the mesendoderm [79]. After gastrulation, the germ layers must invert to bring the ectoderm to the outside of the embryo, with the endoderm on the inside and the mesoderm between these two layers. At around the 7-somite stage (approx. E8.5), turning is initiated in the head and tail folds, with the clockwise rotation of each around its long axis. This converts the embryo from a lordotic to a fetal conformation by E9.0 (Figure 1.6).

1.2.5 Early cardiac development

Cardiac precursors are found in the splanchnic mesoderm shortly after gastrulation, with the cardiac mesoderm first occupying the area between the head folds and the extraembryonic

region (Figure 1.8) [80]. At E7.5, the outermost rim of the cardiac mesoderm, closest to the extra-embryonic region, differentiates into cardiomyocytes, with contractile sarcomeric machinery assembled in these cells, and the cardiac crescent of the first heart field is formed [80], [81]. The rest of the cardiac precursors, positioned posteromedially and adjacent to the cardiac crescent, are known as the second heart field and remain undifferentiated at this stage [82].

As the embryo turns, the cardiac region becomes placed in position posterior and ventral to the head folds. The first heart field gives rise to the primitive heart tube, which initially remains open at the dorsal side but by E8.25, the heart tube has lengthened and closed as the two sides of the cardiac crescent fuse together (Figure 1.9) [82]. This in turn gives rise mainly to the left ventricle and part of the atria, whereas the second heart field progressively contributes cardiac precursor cells to the poles of the heart tube, from which the right ventricle, the majority of the atria, the outflow and the inflow tracts are derived [82]–[84]. As the heart tube lengthens, heart looping occurs from E8.5, where the cardiac tube undergoes morphological changes to bring the right ventricle primordium and left ventricle to their definitive positions.

Maintaining an equilibrium between undifferentiated cells and cardiac precursors from the secondary heart field is crucial for proper heart formation. A negative feedback loop between Nkx2-5 and BMP2/Smad1 has been found to be involved in controlling cardiac induction and progenitor proliferation [85]. In the cardiac precursor cells, BMP acts to initiate expression of Hopx, which then inhibits the Wnt pathway and so promotes cardiomyogenesis [86].

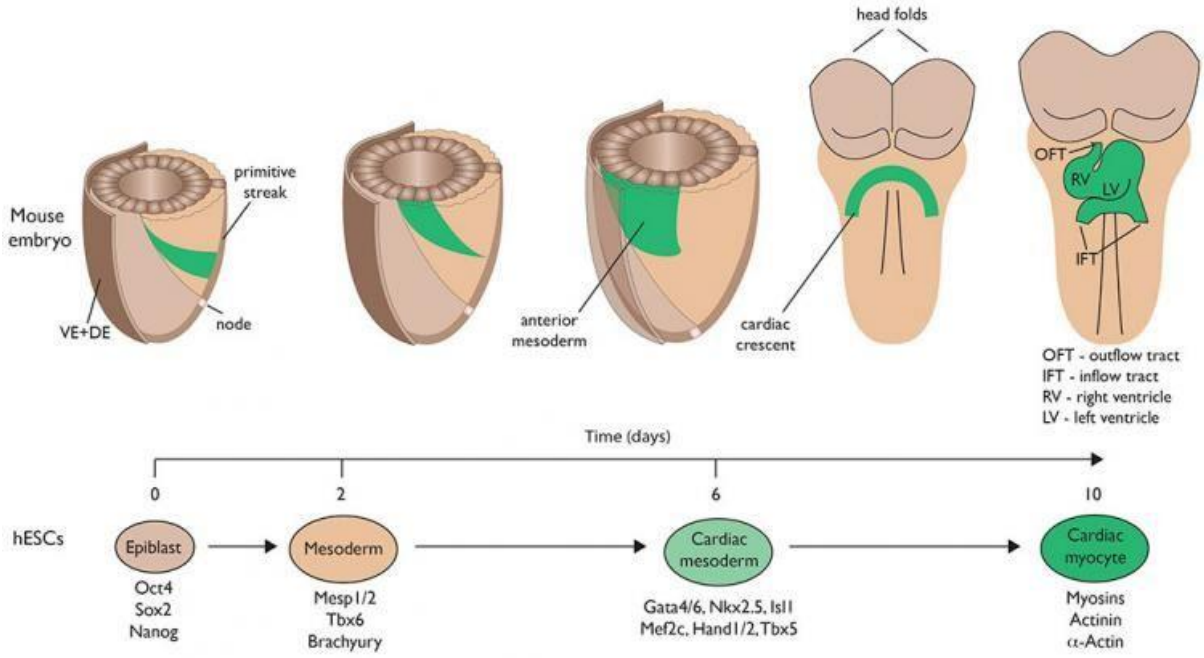

Figure 1.8. Upper panel: diagram depicting the development of the mouse heart. Cells, which give rise to the heart, are in green. Bottom panel: diagram depicting the differentiation steps that heart embryonic stem cells undertake to become beating cardiomyocytes.

Figure from Bernado et al, 2014 [87].

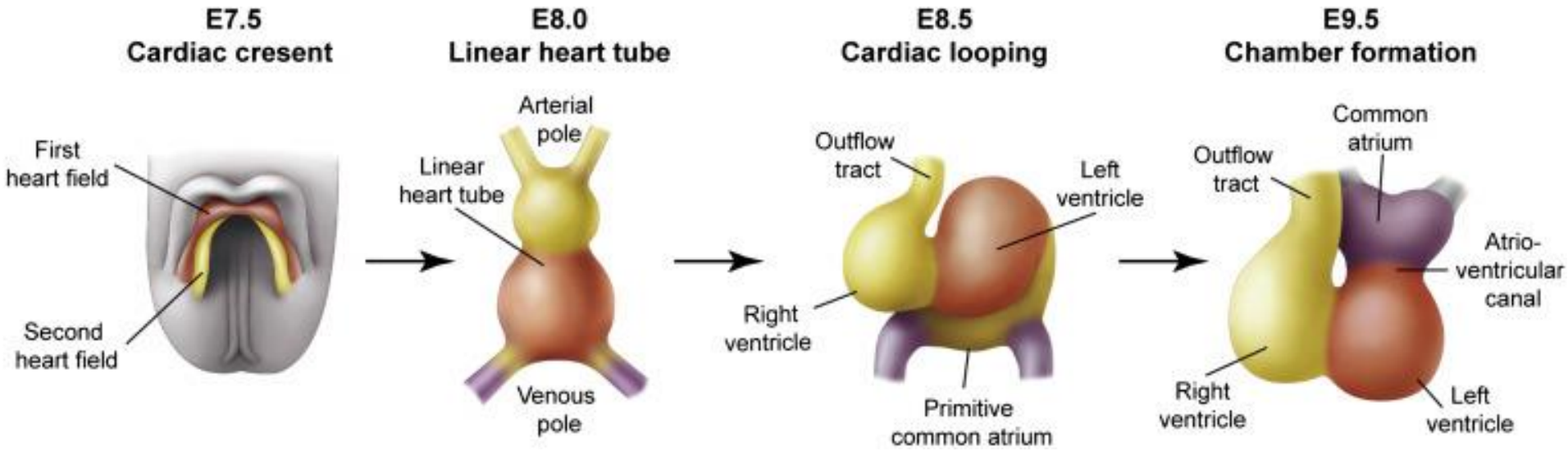

Figure 1.9. Early cardiogenesis in the mouse embryo. During gastrulation, cardiac progenitors migrate to the splanchnic mesoderm to form the cardiac crescent. At E7.5, the cardiac crescent can be divided into two heart fields – the first heart field (red) and the second heart field (yellow) – based on the gene they express and their subsequent contribution to heart. At E8.0, the primitive linear heart tube has formed from the first heart field. This gives rise later to the left ventricle. The second heart field contributes primarily to the poles of the heart, from which the right ventricle, the majority of atria and the outflow and inflow tracts develop. Cardiac looping occurs from E8.5, along with the formation of the primitive atrium. This looping is associated with uneven growth of cardiac chambers By E9.5, the common atrium has moved superior to the ventricles and is separated by a distinct atrio-ventricular canal.

Figure adapted from Epstein et al, 2015 [88]

By E9.5, several segments can be observed, including a common atrial chamber, the primitive left ventricle and the primitive right ventricle [89]. An atrioventricular canal connects the common atrial chamber and the primitive left ventricle. The future right and left ventricles are connected via the bulboventricular canal and the outflow tract connects the future right ventricle to the aortic sac. The beating heart can be clearly observed by this stage.

1.2.6 Somitogenesis

Segmentation is initiated in the mouse embryo with the formation of somites, which begins at E8.0 and ends at E13.0. The paraxial or presomitic mesoderm is divided up into segments of bilaterally symmetrical blocks of epithelial cells to form somites, in an anterior-to-posterior direction. This occurs in a periodic manner, with oscillating signals driving the segmentation process. The model suggested to be responsible for this has been described as a 'clock and wavefront' model (Figure 1.9) [90]. The clock determines the time at which somites form and the wavefront determines where segmentation is initiated.

Segmentation clock genes *Hairy and enhancer of split 1 (Hes1)* and *Hes7* are expressed periodically at the posterior end of the mouse embryo, which is cooperatively regulated by Fgf and Notch signalling [91]–[93]. Fgf signalling is required to initiate Hes expression and both signalling pathways are necessary for the maintenance of Hes propagation [92]. Notch signalling also activates another Notch target Lunatic fringe (Lfng), a modulator of Notch receptors [94].

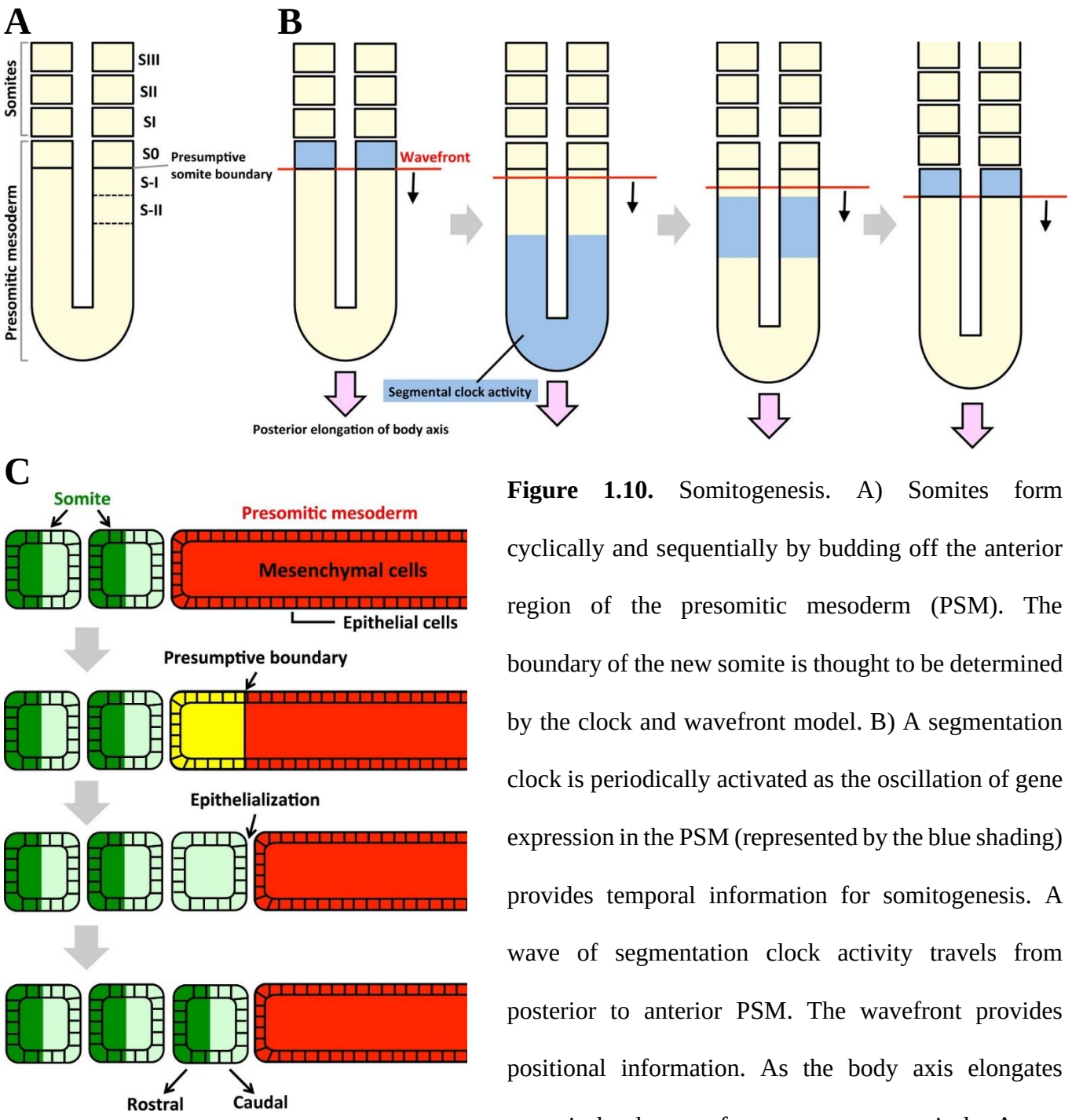

Figure 1.10. Somitogenesis. A) Somites form cyclically and sequentially by budding off the anterior region of the presomitic mesoderm (PSM). The boundary of the new somite is thought to be determined by the clock and wavefront model. B) A segmentation clock is periodically activated as the oscillation of gene expression in the PSM (represented by the blue shading) provides temporal information for somitogenesis. A wave of segmentation clock activity travels from posterior to anterior PSM. The wavefront provides positional information. As the body axis elongates posteriorly, the wavefront regresses posteriorly. A new somite is generated at the anterior PSM after exiting the wavefront.

Figure adapted from Yabe & Takada, 2016 [155]

In addition, Notch activity is crucial for synchronising oscillations between neighbouring cells [95]. Expression of Hes and Lfng then propagates anteriorly. Hes represses its own and Lfng expression, resulting in oscillations in the expression of the two proteins [91], [93], [96]. Lfng acts on Notch receptors to inhibit Notch activity, leading to oscillation of Notch activity [94]. Together, these inhibitory interactions are thought to establish a negative feedback loop that results in stable oscillatory expression of the clock genes.

Many other genes are also thought to be involved in controlling the clock; evidence suggests there is a highly complex oscillatory network [97]. For example, Wnt signalling components, such as Wnt3a, oscillate and are strongly expressed in somite precursor cells [98]. *Wnt3a* is required for maintaining oscillatory activity of genes including *Notch*.

Presomitic mesodermal cells are maintained in an immature state, until the maturation wavefront passes through. Upon exiting the wavefront, they undergo a mesenchymal-to-epithelial transition to mature as somitic cells at the anterior end of the presomitic mesoderm. Posterior-to-anterior gradients of Fgf8 and nuclear β-catenin are opposed by an anterior-to-posterior gradient of retinoic acid (RA) [99]–[101]. Together, these gradients intersect to form a transition point, known as the 'determination front', where the signalling pulse from the oscillating clock is translated into the spatial periodic pattern of segments.

Fgf8 acts posterior to the determination front to maintain cells in their immature state through its inhibition of Mesoderm posterior 2 (Mesp2) [102], [103]. Mesp2 expression is periodically activated by Notch signalling from the clock in a Tbx6-dependent manner just anterior to the determination front. Transcription factor Tbx6 defines the anterior border of the somite [103]–[105]. During the segmentation cycle, Mesp2 is maximally expressed in a one-somite-length fashion. Mesp2 then activates downstream target effector Ripply2, which degrades Tbx6, thus

preventing further expression of Mesp2 [105]. The degradation results in a new anterior border (more posterior in position that the previous border) of Tbx6, which marks the next anterior somitic boundary for the next wave of Mesp2 expression. Mesp2 also activates expression of mastermind-like 1 (MamL1) which represses Notch activity, forming a negative feedback loop [103]. In the newly forming somite, Mesp2 is gradually restricted to the rostral half before finally disappearing and Notch activity is maintained in the caudal half via a positive feedback loop [104], [106].

At the rostral tip of the new somite, Mesp2 plays a crucial role in boundary formation. The Eph family of receptor tyrosine kinases and their Ephrin ligands are expressed in a Notch signalling-dependent pattern in the rostral presomitic mesoderm [107]. Mesp2 upregulates expression of Eph activity at the rostral border of the new somite, which activates Ephrin in the anteriorly juxtaposed cells [108]. The Ephrin reverse signal induces cell epithelialization and the formation of a furrow [109]. This Ephrin-dependent process involves the acquisition of columnar morphology, the formation of apical adherens junctions and the clustering of integrins at the somite boundary. This in turn binds to fibronectin, which recruits other extracellular matrix proteins to the forming border [110].

Newly formed somites consist of an outer shell of polarised epithelial cells surrounding an inner cavity, the somitocoel, that is filled with mesenchymal cells [111]. The epithelial cells have a bottle-like morphology, with necks that extend to the somitocoel, where they form the apical surface of the epithelium. Somites exhibit a phenomenon termed interkinetic nuclear migration [112]. This is where interphase nuclei may be observed throughout the epithelium but mitotic cells are found only at the apical surface, because the nuclei undergo division at the apical surface but migrate basally during interphase. The somites eventually differentiate to form the dermatome

(dermis), myotome (skeletal muscle) and sclerotome (axial skeleton, ribs and vertebrae), with the somitocoel cells contribute to the sclerotome.

1.3 Research aims

My research aims to elucidate the role of ASPP2 in post-implantation embryos. Through its ability to bind many factors, ASPP2 has the potential to link cell polarity, proliferation and differentiation. These processes are essential for embryogenesis. Previous studies have indicated that ASPP2 plays an essential role in embryogenesis, however, little research has been carried out on this. My research thus aims to develop a deeper understanding of the function that ASPP2 has in development.

In order to do this, I aimed to create gene knockout mouse models with both full deletions and conditional deletions of ASPP2 in mouse embryos. The creation of these mouse lines is described in detail in Chapter 3. Following from the creation of these mouse models, I analysed post-implantation embryos containing these gene knockouts to deduce the role that ASPP2 may play in development. These analyses are detailed fully in Chapter 4. Together, these results should shed light on the importance of ASPP2 in development and the embryonic processes that ASPP2 may be involved in.

Chapter 2: Materials and methods

2.1 Mouse husbandry

The work undertaken using mice during this project was undertaken in accordance with the Animals Scientific Procedures Act, 1986. All mice were held under the project license 30/3420. All regulated procedures were carried out under the PIL I505DCE16 (Christophe Royer) and the PIL IA5F65F26 (Elizabeth Sandham).

Mice were maintained on a 7am-7pm light-dark cycle and housed in sterile, temperature-controlled conditions. Mice were weaned at 3 weeks of age and bred from 6 weeks of age. Mice in breeding pairs were checked daily for plugs; if a plug was observed at 1pm, this would be designated as 0.5 days post-coitum and thus the embryo would be staged accordingly as E0.5. All mice, including pregnant females to be dissected for embryo collection, were culled by cervical dislocation or carbon dioxide inhalation (Schedule 1 of the Animals Scientific Procedures Act). A second schedule 1 method was used to confirm death.

2.2 Mouse lines

The following mouse lines were used:

ASPP2$^{+/+}$	Wildtype mice with no mutation in the *ASPP2* gene were used for breeding.
ASPP2$^{+/flox}$	Mice that were heterozygous for floxed *ASPP2* exon 4 were used for conditional gene knockout experiments and for the creation of *ASPP2*-null embryos, as described in Chapter 3.

ASPP2$^{+/+}$, *Tg*$^{Sox2\text{-}Cre/\ Sox2\text{-}Cre}$	Mice that did not contain a mutation in the *ASPP2* gene but did contain the *Sox2-Cre* transgene were used to target gene knockout in tissues expressing *Sox2-Cre*.
ASPP2$^{+/+}$, *Tg*$^{+/Mesp1\text{-}Cre}$	Mice that did not contain a mutation in the *ASPP2* gene but did contain the *Mesp1-Cre* transgene were used to target gene knockout in tissues expressing *Mesp1-Cre*.

2.3 Genotyping

DNA for genotyping adult mice was obtained from ear biopsies. Both the ear biopsies and embryo samples were lysed to prepare the DNA for genotyping following a crude lysis protocol.

2.3.1 DNA preparation by crude lysis

The crude lysis protocol for ear biopsies is as follows:

Ear biopsies were lysed in 150µL lysis buffer supplemented with 0.5µL Proteinase K (Sigma Aldrich) at 55°C for a minimum of 3 hours. These were centrifuged at 14000 rpm for 1 minute and then incubated the lysate at 95°C for 15 minutes to heat inactivate the Proteinase K. Subsequently, these were centrifuged again at 14000 rpm for 1 minute. The lysate was stored at -20°C.

For embryos, the quantity of lysis buffer and Proteinase K used depended on the size/stage of the embryo. For E9.5 and E8.5 embryos, 10µL of lysis buffer and 0.035µL Proteinase K were used. Embryo lysates were incubated at 55°C for 1 hour instead of 3 hours, then at 95°C for 5 minutes instead of 15 minutes. For E3.5 embryos, 5µL of lysis buffer and 0.015µL Proteinase K were used.

Lysis buffer:	Stock	Quantity
50mM Tris HCl (pH8-8.5)	1M	5mL
1mM EDTA	0.5M	200µL
0.5% Tween 20		500µL
H_2O		94.3mL
	Total	100mL

After preparing the lysis buffer, the buffer was syringe filtered and stored at -20°C.

2.3.2 Genotyping using polymerase chain reaction (PCR)

MegaMix (Microzone) was used for PCR reactions. MegaMix contains Taq polymerase (recombinant) in 1.1x reaction buffer (2.75 mM MgCl2) with 220 µM dNTPs & stabiliser. A standard PCR reaction used 14.1µL MegaMix, 0.3µL DNA, 0.3µL Primer 1 and 0.3µL Primer 2 (primers from a 10µM stock). If necessary, this was adjusted depending on the reaction and number of primers to improve sensitivity. The full list of appropriate primer and reaction conditions can be found in the table below.

A nested PCR was used to improve sensitivity when genotyping embryos for the *ASPP2* mutation as the small amount of DNA present in these lysates proved a challenge for the non-nested PCR to amplify sufficiently to detect both the *ASPP2* wildtype and the *ASPP2*-null alleles simultaneously.

Table 2.1. PCR genotyping primer and reaction conditions

Gene targeted for genotyping	**Primers used**	**Primer reagent quantities**	**PCR conditions**	**PCR product**
ASPP2 (adult mice)	Primer A (common forward primer): 5'-TCTACCCTGTGGGTCCATGA-3' Primer B (ASPP2-floxed/wildtype reverse primer): 5'-GCTCGAGTCACTCAACAATGG-3' Primer C (*ASPP2*-null reverse primer): 5¹-TTTCCTGGAACTTGCCAAAC-3'	14.1µL MegaMix 0.3µL Primer A 0.3µL Primer B 0.3µL Primer C 0.1uL DNA	3 mins at 94°C, 35 cycles of 30 seconds at 94°C, 30 seconds at 61°C, 30 seconds at 72°C 7 mins at 72°C	Primers A and B form a 304bp band indicating wildtype *ASPP2* allele or a 470bp band indicating floxed *ASPP2* allele. Primers A and C form a 400bp product indicating *ASPP2*-null allele.

ASPP2 (embryos)	Primers A, B and C as detailed above. Primer D (common forward primer): 5'-ATCTCCACATAGCCCACGC-3' Primer E (wildtype reverse primer): 5'-ACTGCTGTTTGATACTTGGGT-3' Primer F (*ASPP2*-null reverse primer): 5'-TGGGCTCTGAAAAGAACACCT-3'	Ran as a nested PCR. Reaction 1: 14.1µL MegaMix 0.3µL Primer D 0.3µL Primer E 0.3µL Primer F 0.1uL DNA Reaction 2: 14.1µL MegaMix 0.3µL Primer A 0.3µL Primer B 0.3µL Primer C 0.1uL of primary reaction product	Reaction 1: 3 mins at 94°C, 25 cycles of 30 seconds at 94°C, 30 seconds at 60°C, 30 seconds at 72°C 7 mins at 72°C. Reaction 2: 3 mins at 94°C, 35 cycles of 30 seconds at 94°C, 30 seconds at 61°C, 30 seconds at 72°C 7 mins at 72°C	Reaction 1: Primers D and E form a 625bp product. Primers D and F form a 719bp product. Reaction 2: Primers A, B and C form the products indicated above.
FLP	Primer G (FLP forward primer): 5'-CACCACCTAAGGTGCTTGTTC-3'	14.1µL MegaMix 0.3µL Primer G	3 mins at 94°C,	Primers G and H form a 372bp product

	Primer H (FLP reverse primer): 5'-TCTACCCTGTGGGTCCATGA-3'	0.3µL Primer H 0.3uL DNA	35 cycles of 30 seconds at 94°C, 30 seconds at 64°C, 30 seconds at 72°C 7 mins at 72°C	if the *FLP* transgene is present.
CRE	Primer I (CRE forward primer): 5'-GTTCGCAAGAACCTGATGGACA-3' Primer J (CRE reverse primer): 5'-CTAGAGCCTGTTTTGCACGTTC-3'	14.1µL MegaMix 0.3µL Primer I 0.3µL Primer J 0.3uL DNA	3 mins at 94°C, 32 cycles of 30 seconds at 94°C, 30 seconds at 65°C, 30 seconds at 72°C 7 mins at 72°C	Primers I and J form a 300bp product when the *CRE* transgene is present.
Crb1/Rd8	Primer K (Rd8 forward primer): 5'-GCCCCTGTTTGCATGGAGGAAACTTGGAAGACAGCTACAGTTCTTCTG-3' Primer L (Rd8 reverse primer): 5'-GTGAAGACAGCTACAGTTCTGATC-3'	14.1µL MegaMix 0.3µL Primer K 0.3µL Primer L 0.3uL DNA	3 mins at 94°C, 35 cycles of 30 seconds at 94°C, 30 seconds at 64°C, 30 seconds at 72°C 7 mins at 72°C	Primers K and L form a 244bp product when the *Crb1/Rd8* mutation is present.

2.3.3 Genotyping by qPCR

As described in Chapter 3, the mouse line containing the *Sox2-Cre* transgene was interbred to produce a homozygous line ($Tg^{Sox2\text{-}Cre/\ Sox2\text{-}Cre}$). In order to confirm this, quantitative PCR (qPCR) was employed, with Gusb as a control.

The qPCR protocol is as follows:

Cre forward primer: GCG GTC TGG CAG TAA AAA CTA TC

Cre reverse primer: GTG AAA CAG CAT TGC TGT CAC TT

Gusb forward primer: AGCTAAGGCTGGCCTTGAATTCCT

Gusb reverse primer: TGTGAGAGAGCACACTGCAATCCT

Each single 20µL reaction contained 10µL SYBR green, 0.4µL forward primer, 0.4µL reverse primer (primers from a 10µL stock) and 4.2µL H_2O. 16µL of this was pipetted into each qPCR plate well, followed by 4µL of DNA lysate, resulting in a total of 20µL in each well. The plate was then sealed and centrifuged briefly. The samples were run in a StepOne™ (Thermo Fisher Scientific) machine using the following settings: 95°C for 20 seconds, followed by 40 cycles of 95°C for 3 seconds, 60°C for 30 seconds. This was succeeded by a melting curve stage where the samples are held at 95°C for 15 seconds, 60°C for 1 minute and then 95°C for 15 seconds, after which the programme stopped and held at this temperature.

2.4 Embryo collection

In order to collect their embryos, pregnant mice were euthanized by cervical dislocation and the abdominal cavity was cut open. The uterine horns were cut out and placed in a dish containing M2 medium. From this point, embryo collection was carried out under a bright-field microscope. For E3.5 embryos (pre-implantation), a 27G needle was inserted into each of the

uterine horns and M2 media was flushed through each horn to release the E3.5 embryos into the medium. A mouth pipette was then used to collect the E3.5 embryos and place in a new dish of fresh M2 media. For the collection of E8.5 and E9.5 embryos (post-implantation), the decidua were dissected out of the uterine horns. Each deciduum was then teased apart with fine forceps to release the embryo inside. The Reichert's membrane was then mechanically removed using fine tungsten needles. A full detailed pictorial guide of the dissection of post-implantation egg-cylinder stage embryos was published by Srinivas, 2010 [113].

2.5 Immunohistochemistry and staining of embryos

2.5.1 Antibody staining protocol

After collection, E8.5 and E9.5 embryos were fixed in 4% paraformaldehyde (PFA) at room temperature for 40 minutes to 1 hour (depending on the size of the embryo). The embryos were then washed three times for 15 minutes in 0.1% Triton X-100 in phosphate-buffered saline solution (PBS), then permeabilized for 40 minutes to 1 hour in 0.25% PBS-Triton-X100. Following this, the embryos were washed again three times for 15 minutes in 0.1% PBS-Tween 20 (PBS containing 0.1% Tween 20). The embryos were incubated in blocking buffer for around 24 hours at 4°C.

Blocking solution:

0.1% PBS-Tween 20

3% BSA

2.5% Horse serum

Following incubation in blocking buffer, the embryos were incubated in primary antibody at a concentration of 1:100 in blocking buffer for 24 hours at 4°C. The unbound primary antibody was subsequently washed away by washing three times for 15 minutes in 0.1% PBS-Tween 20.

The embryos were then incubated in secondary antibody at a concentration of 1:100 in blocking buffer for 24 hours at 4°C. If required, Atto-conjugated Phalloidin (Sigma Aldrich) was added at this stage. Following the incubation, unbound secondary antibodies (plus Phalloidin) were washed away by subjecting the embryos to three washes for 15 minutes in 0.1% PBS-Tween 20.

The embryos were subsequently incubated in Vectashield containing 4',6-diamidino-2-phenylindole, dihydrochloride (DAPI) mounting medium for a minimum of 24 hours at 4°C.

2.5.2 Antibodies and conjugated dyes

Table 2.2. Primary antibodies

Antibody	**Source**		**Host**
ASPP2	Sigma	HPA021603	Rabbit
FoxC2	Santa Cruz	sc515234	Mouse
Sox2	Santa Cruz	sc17320	Goat
Sarcomeric α-actinin	Abcam	ab68167	Rabbit

Table 2.3. Secondary antibodies and conjugated dyes

Antibody	Source	Emission Spectra
Donkey anti-rabbit IgG	Invitrogen A-21206	Alexa Fluor 488
Donkey anti-goat IgG	Invitrogen A-21082	Alexa Fluor 633
Donkey-anti-mouse IgG	Invitrogen A-31570	Alexa Fluor 555
Phalloidin	Sigma 65906	Atto 647

2.6 Confocal microscopy of fixed embryos

Following the incubation of fixed and stained embryos for a minimum of 24 hours in DAPI-Vectashield (Vectashield containing DAPI), embryos were mounted individually on glass slides in a small quantity (around 3µL) of DAPI-Vectashield. To prevent the three-dimensional structure of the embryos from being disturbed by the weight of the coverslip, standard laboratory tape was used as a spacer between the slide and the coverslip. The coverslips were sealed used nail varnish.

The stained embryos were imaged used a LSM 880 Zeiss microscope. The 5X (0.16NA) and 10X (0.3NA) objectives were used for locating the embryos and taking low-resolution images of the whole embryo whereas the 20X (0.6NA) and 40X (1.2NA) objectives were used to take detailed, high-resolution images of the embryo and specific areas of the embryo. The 405nm, 488nm, 561nm and 633nm lasers were used to excite the fluorophores within the stained embryo. Image stacks of the entire embryo were taken at 2 µm axial resolution. The Zeiss 880 confocal settings were adjusted for each embryo to ensure the best image quality – this included alterations in the laser power, gain and digital offset to ensure no pixels were saturated. When

imaging embryos from the same litter in order to compare mutant and wildtype embryos, all embryos of that litter were imaged using the same settings. When capturing large, detailed images of the embryo, tiling was used.

2.7 Image analysis

Image acquisition, including tile scan stitching, was carried out using Zen software. Image analysis was carried out using Volocity software (Improvision). FIJI was also used to process and analyse images.

To calculate embryo size along the rostral-caudal axis, I used the middle image from the Z-stack taken of the entire embryo. This image was analysed in FIJI using the outline function to find and then calculate the cross-sectional area of the embryo at its largest point. The size of the somites and the size of the somitocoel in the embryos was calculated in the same manner.

To calculate the anterior:posterior ratio of the embryos, the point at which the most rostral somite was visible was used as the boundary between the anterior and posterior regions. FIJI was used to outline and calculate the cross-sectional areas in reference to this region.

2.8 Statistical analysis

Statistical analyses were performed using the two-tailed Student's t-test with unequal variance using R software. Statistical significance was calculated using $p<0.05$ as the significance level (* $p < 0.05$, ** $p < 0.01$, *** $p < 0.001$).

Chapter 3: Generating the mouse transgenic tools required to study ASPP2 function during embryogenesis

3.1 Introduction

ASPP2 plays an essential role in embryogenesis due to its ability to link cell polarity, proliferation and differentiation. However, there have been relatively few studies on this subject, especially at early stages of development. In this chapter, I discuss my generation of mouse lines that can be used to elucidate the function of ASPP2 during early development.

I am using a knockout approach to study gene function. The principle behind this is to inactivate a gene to identify its role in development and deduce its function in normal physiological homeostasis. To take this a step further, tissue-specific knockout can be carried out, where the gene is deleted in a particular tissue rather than the entire embryo. This allows the study of gene function in one specific organ, tissue or cell type. By analysing results from various different tissue-specific knockouts, a more detailed overview of the role of a gene can be gathered.

Many tissue-specific models rely on the Cre-Lox system. In this system, the allele of the target gene has been edited so that it is flanked by LoxP sites. These mice can then be crossed to a line that is heterozygous or homozygous for a *Cre* recombinase gene under the control of the tissue-specific promoter. In the resulting offspring, Cre directs the LoxP sites to recombine and thus excise the target gene [114], [115]. However, it can only do this in cells where it is expressed, meaning that cells that do not express the particular promoter are heterozygous for the gene deletion.

3.1.1 Previous studies of ASPP2 in embryogenesis

In order to investigate the role of ASPP2 in post-implantation embryogenesis, I utilised mouse lines in which exon 4 of *ASPP2* has been deleted. These differ from the two previously

published lines that have aimed to characterise the function of ASPP2 in development in that this mutation was designed to create a large-scale frameshift upon deletion of exon 4.

Vives et al. first generated *ASPP2*-null embryos in 2006 where exon 3 and a 2kb upstream region were replaced by a neomycin resistance (neoR) cassette to form allele tm1a (the targeted trap allele in EUCOMM (European Conditional Mouse Mutagenesis Program) ES cells, that has been generated by targeting yet functions as a gene-trap knockout) [116]. However, the deletion of exon 3 meant that the sequence of exon 4 was in-frame with exon 2. Thus, this is not a full knockout and is in fact more akin to a hypomorphic allele.

Homozygous deletion of exon 3 ($ASPP2^{\Delta 3}$) was found to be lethal in a pure C57BL/6J background as no such pups were born. In a mixed 129SvxC57BL/6J background, only around 6.4% of pups were homozygous for the mutant allele – far less than the expected Mendelian segregation of 25%. All these pups died before weaning, due to severe defects in the central nervous system (CNS) including hydrocephalus. Timed-mating experiments showed that at E18.5, $ASPP2^{\Delta 3}$ embryos were found in the expected percentage of 25%, suggesting they die shortly before birth. Interestingly, in a Balb/c background, $ASPP2^{\Delta 3}$ pups were born at the expected Mendelian ratios, with the majority surviving after weaning, although they also exhibited severe CNS defects [7].

Kampa et al. generated an alternative *ASPP2*-null mouse line in 2009, where exons 10-17 where replaced with a *neoR* gene [117]. This disrupted the binding domains of many proteins, including p53. Western blot analysis showed there was an approximate 2-fold reduction in ASPP2 protein levels in heterozygous mice. However, $ASPP2^{\Delta 10\text{-}17}$ mice are not viable due to an uncharacterized early embryonic lethal event. $ASPP2^{\Delta 10\text{-}17}$ homozygous embryos were not found as early as E6.5. $ASPP2^{\Delta 10\text{-}17}$ homozygous embryos could not be generated in a Balb/c background. This is particularly surprising since previous work had shown that *ASPP2* mutations result in less severe phenotypes in a Balb/c background [7]. The $ASPP2^{\Delta 10\text{-}17}$ does

not disrupt the first 9 exons, thus it is possible that some short isoforms of *ASPP2* are produced. Furthermore, the addition of the neoR cassette may have off-target effects on development.

The *ASPP2*$^{\Delta 10\text{-}17}$ line was originally intended to be used by the Srinivas group for studying the role of ASPP2 in mouse embryogenesis. It was deposited at Jax laboratories, from where our group received it. After carrying out some initial experiments with this line, it was found that the line we had received was in fact not the correct line and instead contained another mutation rather than the intended *ASPP2* gene disruption. Therefore this mouse line was not available for study in any case.

The mouse lines I used were designed to create a large frameshift in the sequence of *ASPP2* while adding minimal excess nucleotides.

A

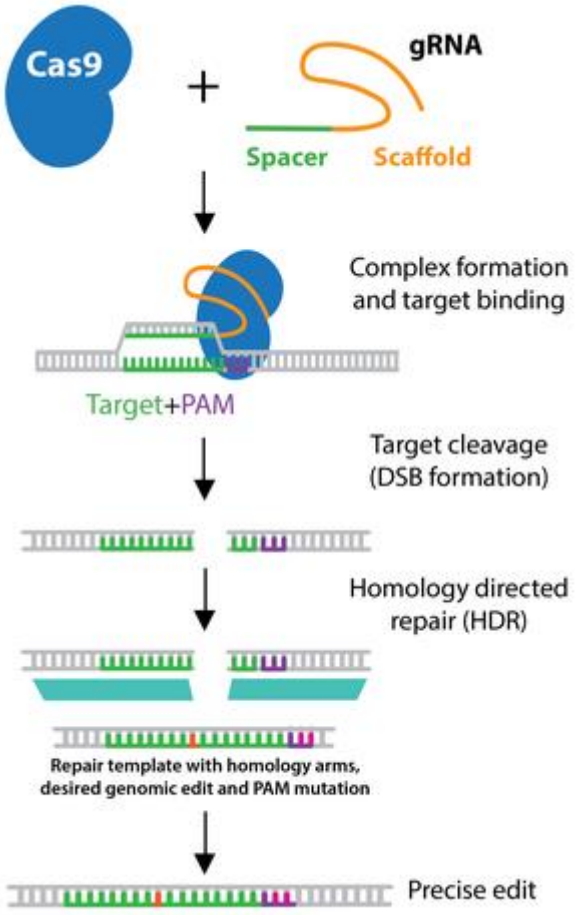

Figure 3.1. CRISPR-Cas 9 method for gene knockout. A) The CRISPR-Cas9 complex is delivered to the target sequence using guide RNA (gRNA). Cas9 binds to PAM adjacent to the target site and initiates cleavage at the target site. This results in a double-stranded break (DSB). The DSB is repaired by homology-directed repair. B) Repair by HDR involves a repair template containing the desired insertion. Homologous regions in the template and the target DNA recombine, resulting in the incorporation of the cassette into the genome.

Figure adapted from Addgene.com [121]

B

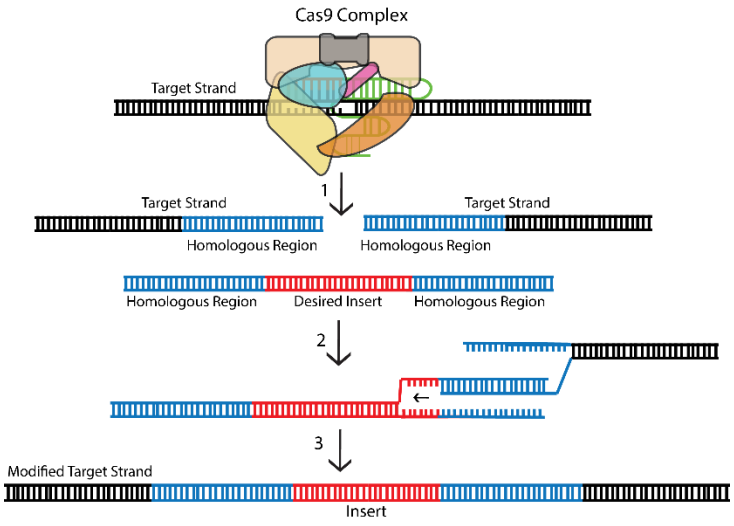

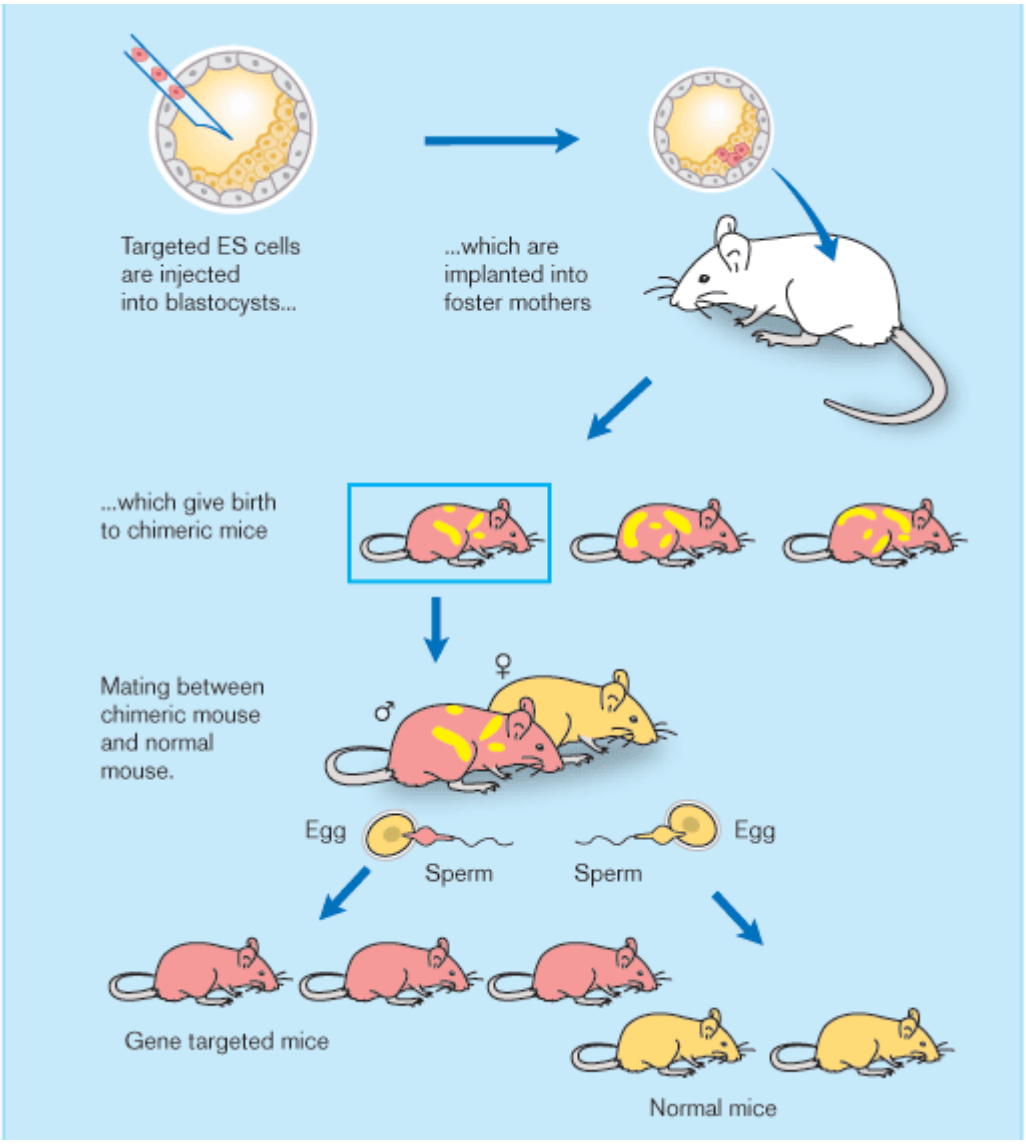

Figure 3.2. Edited ESCs are injected into blastocysts, which are injected into 'foster mothers' to generate chimeric mice (with red representing the edited allele and yellow representing the wildtype allele in the figure) that are able to transmit the mutated gene to their progeny. Figure adapted from Cappuchi et al [118]

3.1.2 General mouse gene targeting strategy

The EUCOMM and Knockout Mouse Program (KOMP) are founder members of the International Knockout Mouse Consortium (IKMC). THE IKMC aims to produce a collection of mouse ESC lines that in total (over this entire collection) include a knockout of every gene in the mouse genome. The broad strategy of IKMC involves editing the genes of mouse ESC using the CRISPR/Cas9 system.

CRISPR delivers nuclease Cas9 complexed with a synthetic guide RNA (gRNA) to the desired location in the genome (Figure 3.1) [119], [120]. The CRISPR-Cas9 with its guide RNA are delivered to mouse ESC by microinjection or electroporation. The genomic target can be any DNA sequence of around 20 nucleotides that meets two conditions: The sequence must be unique so that other sections of the genome are not targeted and the target is present immediately adjacent to a Protospacer Adjacent Motif (PAM). PAM is a short sequence of 2-6 nucleotides that serves as a binding signal for Cas9 [119]–[121].

Cas9 nuclease acts as a pair of genetic scissors and opens both strands of the targeted sequence of DNA to introduce the modification [119]–[121]. In this case, knock-in mutations were generated that incorporate exogenous DNA by using it as a repair template, facilitated by homology directed repair (HDR). In the case of IKMC-generated edited ESCs, a cassette containing the target exon flanked by loxP sites, as well as encoding the *lacZ* gene, *neoR* (neomycin resistant) gene and FRT sites is incorporated into the genome by HDR (Figure 3.3). The alternative method of DNA repair involves knock-out mutations that repair the double-stranded break by means of non-homologous end joining (NHEJ) (Figure 3.1). NHEJ does not require a template. Instead, the single-stranded overhangs on the ends of the double-stranded breaks caused by Cas9 recombine in an imperfect manner. This frequently leads to random nucleotide deletions but may cause insertions (and sometimes even translocations). Therefore gene functionality is deleted or disrupted.

Edited ESC can be selected using the lacZ and neoR genes in the cassette as only edited cells will express lacZ and be resistant to neomycin. When the edited ESC have been developed and selected, chimera are created using these ESC by injecting the edited cells into a blastocyst-stage mouse embryo (Figure 3.2). The blastocysts are injected into a 'foster mother' mouse to permit the full development and birth of mice carrying the edited allele. The first generation of mice will be chimeric for the allele. Mice carrying this edited allele are then bred to homozygosity.

3.1.3 Generation of initial mouse line

Cre/loxP technology was employed to generate *ASPP2*-null mice. Derived from the P1 bacteriophage, Cre recombinase recombines a short pair of target sequences; the loxP sites [114], [115]. This system can be utilised to excise any region of DNA placed between the sites. The loxP sites can thus be placed around a target exon in a gene, resulting in mice that contain the floxed (flanked by loxP sites) allele but are phenotypically wildtype until they undergo recombination upon induction by Cre.

ESC from a C57BL/6N background were engineered at Harwell (from the EUCOMM/KOMP resource) in the manner described previously in which exon 4 of the *ASPP2* gene was floxed. The targeting cassette also contained elements encoding the *lacZ* gene, *neoR* gene and FRT sites (Figure 3.3). As detailed in Table 3.1, the only known structured domains encoded by exons 1 to 3 of the *ASPP2* gene are a Ubiquitin-like domain and a hypothetical alpha-helix domain; therefore, even if the initial part of this protein can be produced following the deletion of exon 4 and resulting frameshift of the remainder of the *ASPP2* gene, it is highly unlikely that this would be able to carry out any of the usual functions of ASPP2.

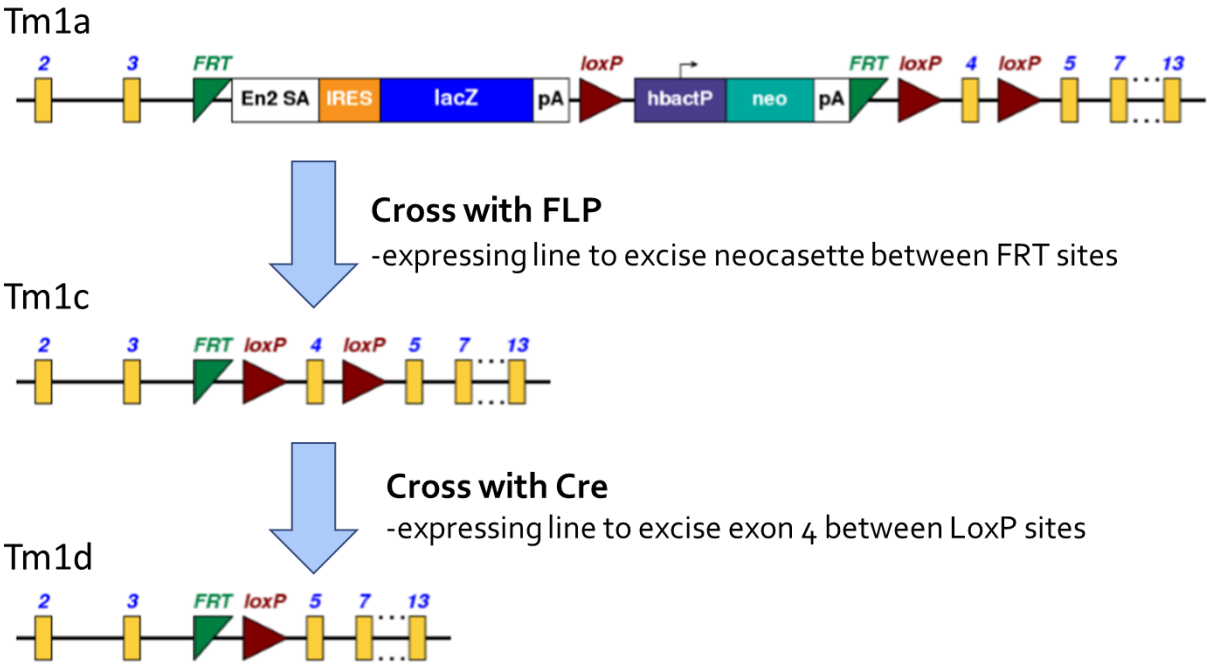

Figure 3.3. The tm1a allele contains FRT sites and loxP sites. Crossing this to a line expressing FLP will result in recombination between the FRT sites, excising this section and leaving behind one FRT site. This produces the tm1c allele. The tm1c allele does not contain *lacZ* and *neoR* genes but exon 4 of *ASPP2* remains intact, flanked by loxP sites. Crossing the tm1c allele to mice expressing Cre will lead to recombination between the loxP sites, excising the targeted exon and thus preventing the expression of *ASPP2*. This produces the tm1d allele. The tm1d allele does not contain the targeted exon 4 but does contain one FRT and one loxP site.

Table 3.1. Known domains and exons of ASPP2

Domain/exon	Amino acid start	Amino acid end	Source
Phosphatidylinositol 3-kinase Catalytic Subunit (Ubiquitin-like fold)	4	89	Gene3d (3.10.20.90)
Exon 1	1	9	NCBI
Conserved lysine K48 (lysine involved in chain linkage in ubiquitin)	10	89	Conserved Domains Database (cd17225)
Ubiquitin-like domain	10	91	SuperFamily (SSF54236)
Exon 2	10	49	NCBI
Exon 3	50	96	NCBI
Exon 4	97	124	NCBI
Exon 5	125	158	NCBI
Exon 6	159	217	NCBI
Exon 7	218	277	NCBI
Exon 8	278	332	NCBI
Exon 9	333	409	NCBI
Exon 10	410	445	NCBI
Exon 11	446	494	NCBI
Exon 12	495	649	NCBI
Exon 13	650	908	NCBI
Exon 14	909	954	NCBI
Ankyrin repeat-containing domain superfamily	910	1134	Gene3D (1.25.40.20)
Ankyrin repeat-containing domain superfamily	936	1058	SuperFamily (SSF48403)
Anykrin-repeat region	942	1022	Pfam (PF12796)
Exon 15	955	999	NCBI
Anykrin-repeat region	964	993	Smart (SM00248)
Anykrin-repeat region	964	995	Prosite profiles (PS50297)

Anykrin-repeat region	964	996	Prosite profiles (PS50088)
Anykrin-repeat region	997	1024	Prosite profiles (PS50297)
Anykrin-repeat region	997	1026	Smart (SM00248)
Anykrin-repeat region	997	1026	Prosite profiles (PS50088)
Exon 16	1000	1055	NCBI
Exon 17	1056	1121	NCBI
Exon 18	1122	1134	NCBI
SH3 domain	1063	1123	Prosite profiles (PS50002)
SH3 domain	1065	1125	SuperFamily (SSF50044)
SH3 domain	1066	1124	Smart (SM00326)
SH3 domain	1070	1118	Pfam (PF14604)

Chimera were generated using the genetically engineered, *ASPP2*-floxed ESC and the edited allele was able to be transmitted to the germline. The resulting mice can be crossed to a line expressing FLP recombinase to excise the tm1a allele and create the tm1c allele (Figure 3.3). FLP directs recombination between the FRT sites, thus excising this section and leaving behind one FRT site. The tm1c allele has deletions of the *lacZ* and *neoR* genes but exon 4 of *ASPP2* remains intact, flanked by loxP sites. Thus, the tm1c allele is suitable for conditional mutagenesis upon excision by Cre. Crossing mice expressing the tm1c allele to mice expressing Cre will lead to recombination between the loxP sites. This removes the targeted exon, deleting *ASPP2*, and creates a tm1d allele with only one FRT and one loxP site remaining.

The mouse line initially produced was heterozygous for the tm1a allele. The sperm from these mice were used in IVF and crossed to ova expressing a FLP-recombinase, which causes recombination between the FRT sites and excision of the *lacZ/neo* cassette. These resulting mice were heterozygous for the tm1c allele and were my start point for generating mouse lines in which exon 4 of *ASPP2* is deleted.

As aforementioned, the mice received from Harwell were engineered in a C57BL/6N background. The mouse lines that I used in crosses for conditional deletion of *ASPP2* had a C57BL/6J background. These mice are both derived from the same inbred strain of mice. An inbred strain is defined as a population of mice resulting from at least 20 consecutive generations of brother–sister matings, producing animals that are almost clones of each other, with very limited genetic variability. It has become clear that the strain may influence the phenotype of mutant embryos, as seen in $ASPP2^{\Delta 3}$ embryos [7], [116]. However, a comprehensive genomic and phenotypic comparison between these two mouse substrains has recently revealed a range of sequence variation and significant phenotypic differences, despite the fact that they belong to the same overall strain [122].

One of the major differences between the two strains is that a single nucleotide deletion, creating a frameshift mutation, in the *Crb1* gene on chromosome 1 is present in homozygous form in all C57BL/6N substrains, but not in the C57BL/6J mouse lines [123]. This mutation, termed the *retinal degeneration 8* or *rd8* mutation due to the retinal defects mice homozygous for this mutation develop, leads to a premature stop codon that truncates the transmembrane and cytoplasmic portion of CRB1 [124]. CRB1, one of three mammalian homologues of the *Drosophila* Crumbs protein, has been shown to regulate apical–basal polarity in complex with other proteins, such as Pals1/Patj and Par3/Par6/aPKC [125], [126]. In addition, it has been found that deficiency in CRB2, another Crumbs homologue, leads to disrupted polarity of the epiblast cells at the primitive streak, leading to defects in gastrulation and thus in mesoderm and endoderm formation, resulting in embryonic lethality by E12.5 [127].

As ASPP2 plays a role in apical-basal polarity (as described in Introduction section 1.2.3, ASPP2 and polarity), it is possible that the *rd8* mutation in *CRB1* could have a compounding effect on the phenotype, exaggerating any phenotypic variation.

3.1.3 Aims of this chapter

The broad aim of this thesis is to study the function of ASPP2 in different embryonic germ layers. In order to do this, I needed to generate several mouse lines. The aims of this chapter were:

- To generate a reasonably congenic *ASPP2* conditional line (that does not contain the *Rd8* mutation or *FLP* transgene)
- To homozygose this line to facilitate tissue-specific experiments
- To generate a line heterozygous for the *ASPP2*-null mutation and homozygous for a epiblast-specific Cre (Sox2-Cre), in order to produce epiblast-specific null embryos

- To generate a line heterozygous for the *ASPP2*-null mutation and heterozygous for Cre specific to mesoderm including cardiac progenitors (*Mesp1-Cre*), in order to produce cardiac mesoderm-specific null embryos in crosses with ASPP2 conditional mice.

3.2 Results

3.2.1 Generation of uniform genetic background

As mentioned previously, the mice that I received from Harwell (F0) were from a C57BL/6N substrain and the mice I was to be carrying out breeding experiments with were from the C57BL/6J substrain. Present in homozygous form on chromosome 1 of all C57BL/6N substrains, but not found in the C57BL/6J mouse lines, is the *rd8* mutation. In addition to this mutation, the F0 mice received from Harwell differed in other genetic aspects to the C57BL/6J mice lines. The floxed mouse line was originally designed with a *lacZ-neoR* cassette flanked by FRT sites. At Jax laboratories, IVF was carried out to cross this mouse line with a mouse line expressing FLP to drive recombination between the FRT sites and excise the lacZ-neo cassette. Thus, the floxed F0 mouse line I initially began working with contained both an FRT site and FLP.

In order to make the genetic background more uniform and reduce the possibility of the genetic variance influencing the phenotype of the *ASPP2* mutant embryos, I bred the mice received from Harwell into a C57BL/6J background for 4 generations (from F0 to F4). Females received from Harwell ($ASPP2^{+/flox}$, $Crb1^{rd8/rd8}$, Tg^{FLP}) in the C57BL/6N background were bred with wildtype males ($ASPP2^{+/+}$) in the C57BL/6J background to produce mice that were heterozygous for the floxed *ASPP2* mutation ($ASPP2^{+/flox}$) in the C57BL/6J background. I chose to cross the floxed females with wildtype males because there is some evidence that recombination occurs more frequently in females [128]. Thus I hoped that the *Crb1* mutation,

the transgene and the C57BL6/N background would be bred out more quickly through the use of females being crossed into wildtype males.

I bred out the *FLP* transgene from the mouse line by breeding mice in generations F1, F2 and F3 that were heterozygous for the floxed mutation (tm1c allele) but did not contain the *FLP* transgene (where possible). This selection was done using a genotyping via polymerase chain reaction (PCR) to identify the presence (or absence) of the floxed allele (Figure 3.4) and *FLP* gene (Figure 3.5). Breeding out the *rd8* mutation was more difficult due to the fact that both *CRB1* and *ASPP2* are found on chromosome 1 (24.06 centimorgans apart). I assayed for segregation in the same manner as that for FLP: using genotyping via PCR to identify the presence or absence of the *rd8* mutation (Figure 3.6). After a further 4 generations (from F4 to F8), I succeeded in segregating out the *rd8* mutation and thus generated a reasonably congenic mouse line, ready for conditional experiments.

3.2.2 Generation of heterozygous *ASPP2*-null line

After carrying out the backcrosses detailed above, I crossed the F8 $ASPP2^{+/flox}$ mice, now in a C57BL/6J background, to a mouse line expressing Cre under the control of a Sox2 promoter ($ASPP2^{+/+}$, $Tg^{Sox2\text{-}Cre/\ Sox2\text{-}Cre}$) also in a C57BL/6J background which led to recombination between the loxP sites and excision of exon 4. Therefore the floxed gene becomes a null gene in the presence of tissues expressing Cre ($ASPP2^{+/flox}$ becomes $ASPP2^{+/-}$). As Sox2 is expressed in the entire epiblast, including the germline cells, the mice produced from this cross will have exon 4 deleted in all their tissues. Thus the subsequent generation (F9) contains mice that are heterozygous for the *ASPP2*-null mutation (tm1d allele) and for the *Sox2-Cre* transgene ($ASPP2^{+/-}$, $Tg^{+/Sox2\text{-}Cre}$) in the epiblast tissue. The identification of mice that were heterozygous for the null mutation was done using PCR genotyping (Figure 3.4). I subsequently backcrossed

this line to wildtype C57BL/6J mice for 1 generation (to F10) to segregate out the *Sox2-Cre* transgene, resulting in mice heterozygous for *ASPP2*-null and without the *Sox2-Cre* transgene. This was assayed, as before, using PCR genotyping to establish the presence or absence of Cre (Figure 3.7). The resulting heterozygous F10 $ASPP2^{+/-}$ mice can then be interbred to produce $ASPP2^{-/-}$ embryos.

3.2.3 Generation of homozygously floxed ASPP2

To facilitate the conditional excision experiments, in which *ASPP2* is knocked out in various tissues of the mouse, I interbred the heterozygous $ASPP2^{+/flox}$ (F8) mice to produce homozygous $ASPP2^{flox/flox}$ mice. These mice were assessed via genotyping as seen in Figure 3.4. Unlike the $ASPP2^{+/flox}$ mice, these mice do not contain the wildtype band, only the tm1c allele.

Figure 3.4A. PCR genotyping of the *ASPP2*-floxed tm1c allele [figure legend on next page]

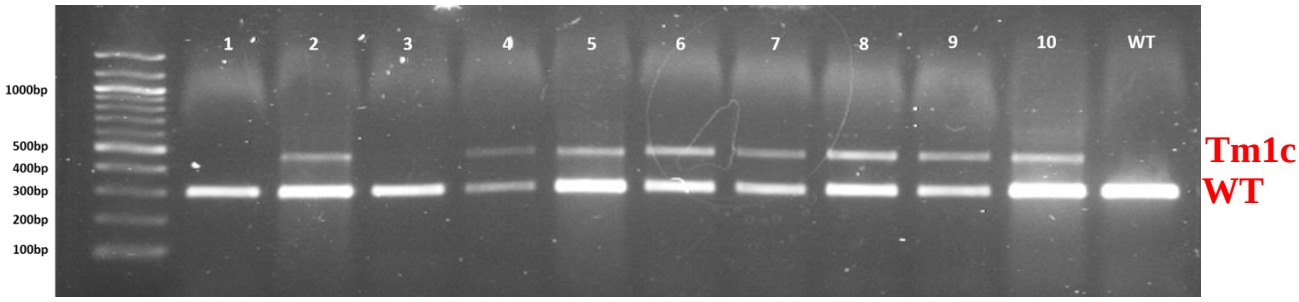

Figure 3.4B. PCR genotyping of the *ASPP2*-null tm1d allele [figure legend on next page]

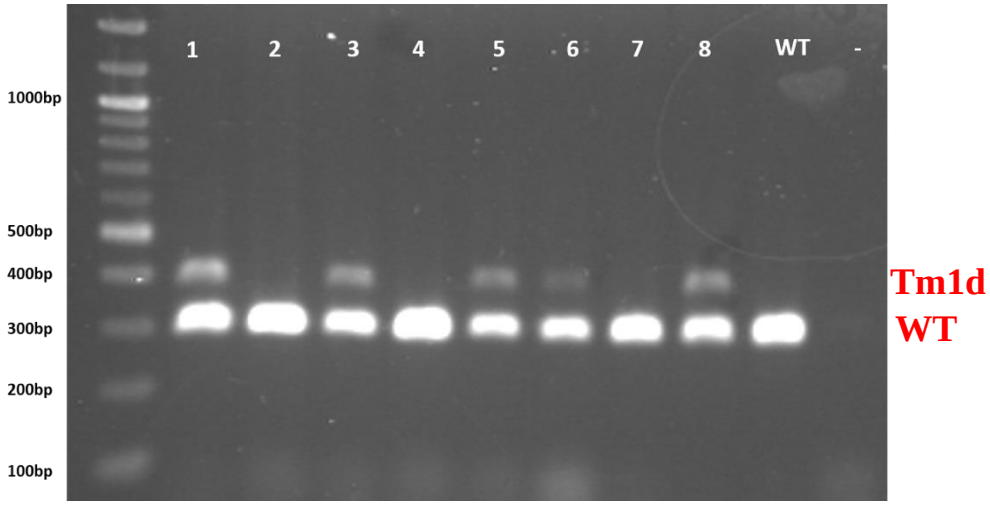

Figure 3.4C. PCR genotyping of the *ASPP2*-floxed tm1c and the *ASPP2*-null tm1d alleles on same gel [figure legend on next page]

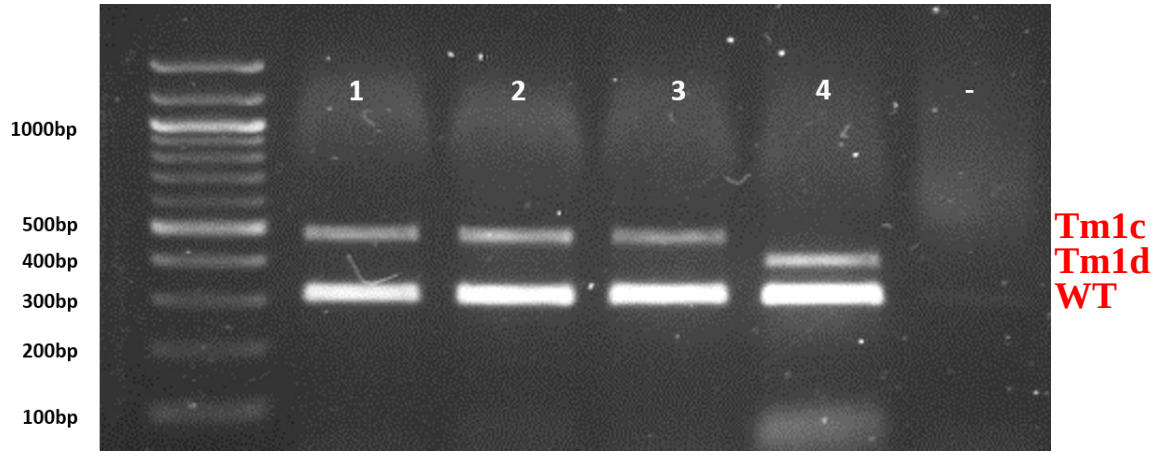

Figure 3.4. Genotyping of the *ASPP2*-floxed tm1c allele and the *ASPP2*-null tm1d allele. The floxed tm1c allele produces a 470 bp (base pair) product in comparison to the 304bp product of the wildtype (WT) allele (examples labelled at the right-hand side of the gel). It can be seen in Figure 3.4A that many of the mice contain both of these bands, indicating that they are heterozygous for the floxed allele. The mice containing only the smaller band are wildtype. The *ASPP2*-null tm1d allele produces a 400 bp product (examples labelled at the right-hand side of the gel). Figure 3.4B shows that around half of the mice genotyped here contain both of these bands, indicating that they are heterozygous for the null allele. The mice containing only the smaller band are wildtype. Figure 3.4C demonstrates the size difference between the tm1c and tm1d bands; mice 1-3 are heterozygous for the floxed tm1c allele and mice 4 is heterozygous for the slightly smaller *ASPP2*-null tm1d allele. All mice contain the wildtype band. The negative control (labelled -) contained lysis buffer in the place of a DNA sample.

Figure 3.5A. Genotyping via PCR of parental F0 mice from Harwell for FLP

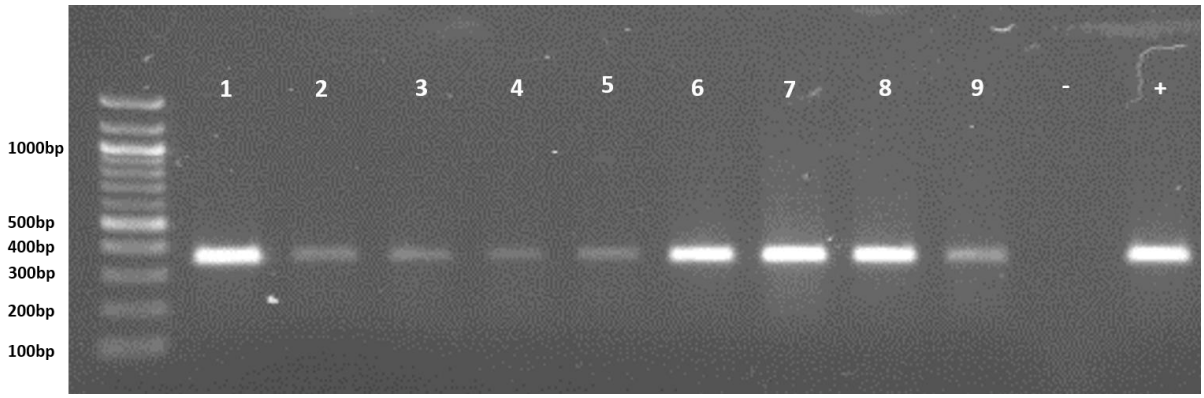

Figure 3.5B. Genotyping via PCR of F2 generation mice for FLP

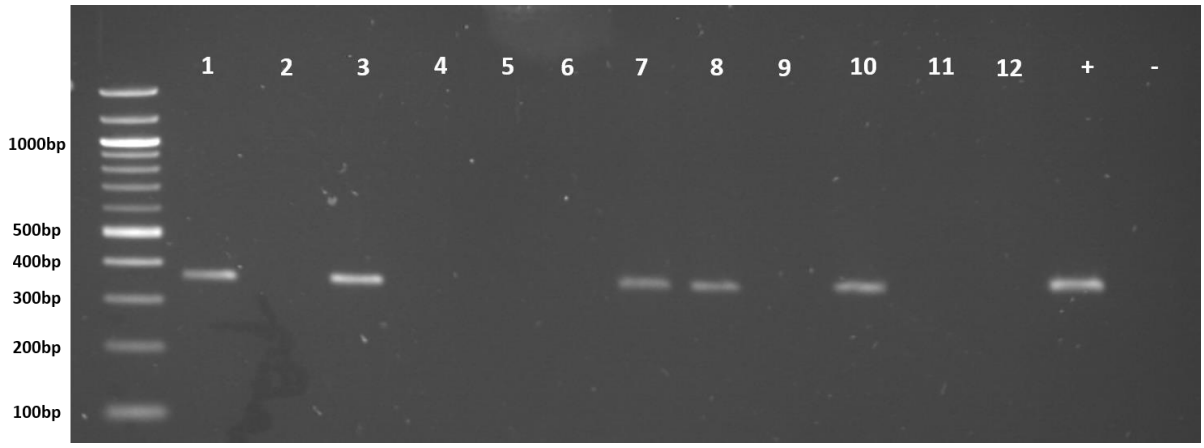

Figure 3.5. Genotyping for the FLP transgene. 3.5A) The parental F0 generation mice from Harwell all contained the *FLP* transgene and thus all 9 mice genotyped were positive for *FLP* when they underwent genotyping via PCR. 3.fB) The F2 generation mice had undergone two generations of breeding in the process to remove the *FLP* transgene. By this generation, the *FLP* transgene was still present but over half (7) of the 12 mice no longer contained the transgene, facilitating future breeding out of the transgene over the subsequent generations. The positive control (labelled +) contained a DNA sample known to contain the *FLP* transgene and the negative control (labelled -) contained lysis buffer in the place of a DNA sample.

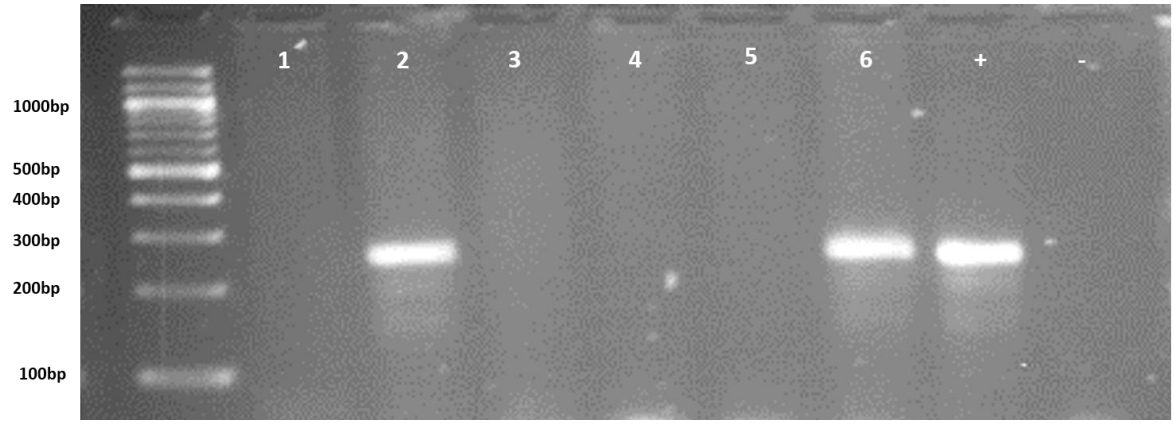

Figure 3.6. Genotyping for the *rd8* mutation. The *rd8* mutation was initially present in all of the F0 mice received from Harwell. As this PCR gel shows, after 5 generations of breeding (F5), two of the six mice in this generation still contain the *rd8* mutation. This is an improvement but shows that at this stage, further breeding was required to segregate out this mutation. The positive control (labelled +) contained a DNA sample known to contain the *rd8* mutation and the negative control (labelled -) contained lysis buffer in the place of a DNA sample.

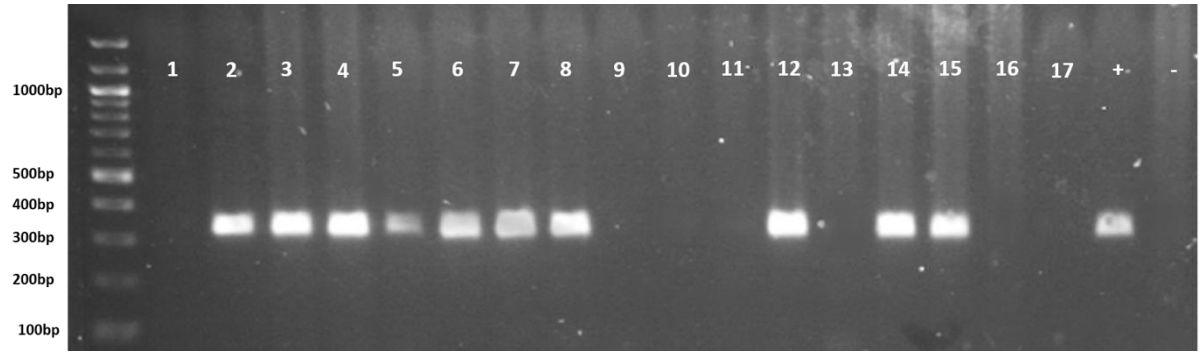

Figure 3.7. Genotyping for *Cre*. This shows the PCR gel for *Cre* from the F10 generation of mice. The previous F9 generation was heterozygous for the *Sox2-Cre* transgene. Breeding to wildtype mice generated the F10 mice, which were either heterozygous for the transgene or null for the transgene. The positive control (labelled +) contained a DNA sample known to contain the *FLP* transgene and the negative control (labelled -) contained lysis buffer in the place of a DNA sample.

3.2.4 Deletion of ASPP2 in Mesp1-positive mesoderm progenitor cells

I used a mouse line expressing Cre under the control of a Mesp1 promoter to wanted to investigate the role of ASPP2 in tissues derived from MESP1-positive mesoderm cells, including the heart. Mesp1 is expressed in almost all precursors of the cardiovascular system and plays an essential role in cardiac morphogenesis [129], [130]. Expression begins at E6.5 and at E7.5, it is expressed in the extraembryonic mesoderm and cranial-cardiac embryonic mesoderm. By E9.5, Mesp1 is strongly expressed in the heart.

For use in these *Mesp1*-positive *ASPP2* knockout experiments, I crossed the aforementioned F10 heterozygous *ASPP2*-null ($ASPP2^{+/-}$) mice to a mouse line expressing *Mesp1-Cre* to generate compound heterozygotes. These $ASPP2^{+/-}$, $Tg^{+/Mesp1\text{-}Cre}$ mice were then crossed to the $ASPP2^{flox/flox}$ mice described in Section 3.2.3, resulting in excision of exon 4 solely in the region in which Mesp1 is expressed: namely the cardiac tissue. Thus this allowed me to investigate the tissue-specific requirement of ASPP2 in the early cardiac lineage.

3.2.5 Generation of epiblast-specific ASPP2 knockouts

Sox2-Cre is expressed in both the epiblast as well as the extra-embryonic visceral endoderm [131], [132]. To study the role of ASPP2 in the epiblast, *ASPP2* can be specifically knocked out in the epiblast using the Sox2-Cre mouse line.

Mice from the F9 cross that were heterozygous for *ASPP2*-null and for the *Sox2-Cre* transgene ($ASPP2^{+/-}$, $Tg^{+/Sox2\text{-}Cre}$) were crossed with mice that were homozygous for the *Sox2-Cre* transgene and wildtype for *ASPP2* ($ASPP2^{+/+}$, $Tg^{Sox2\text{-}Cre/\ Sox2\text{-}Cre}$) to produce F10 mice that were heterozygous for the *ASPP2*-null mutation and homozygous for the *Sox2-Cre* transgene ($ASPP2^{+/-}$, $Tg^{Sox2\text{-}Cre/Sox2\text{-}Cre}$). I confirmed homozygosity for *Sox2-Cre* using quantitative PCR (qPCR), as shown in Figure 3.8. These mice could then be crossed to the $ASPP2^{flox/flox}$ mice described in Section 3.2.3. As Cre is expressed under control of the Sox2 promoter in the

epiblast, it is here that recombination and excision of exon 4 will occur. Thus in epiblast-specific knockouts, the epiblast will be *ASPP2*$^{-/-}$ but the majority of extra-embryonic tissues will be *ASPP2*$^{-/flox}$.

3.3 Discussion

3.3.1 *ASPP2*-null embryos

The generation of the heterozygous mouse line *ASPP2*$^{+/-}$ will permit the characterisation of *ASPP2*-null embryos, thus allowing us to study the requirement for ASPP2 in development.

As discussed previously, the *ASPP2*-null mutation is embryonically lethal when homozygous. However, this characterisation took place in a pure C57BL/6J background. Studies on *ASPP2*$^{\Delta 3}$ have found that the background affects the severity of the phenotype, being embryonically lethal in a pure C57BL/6J background but with pups surviving post-weaning in a Balb/c background [7], [116]. Thus, it is conceivable that the background could also affect the phenotype with this exon 4 deletion mutation. The C57BL/6J *ASPP2*$^{+/-}$ mouse line could therefore be crossed to a different background to see if the mutation still results in embryonic lethality. If it does not, or if the embryos are less severely affected and survive until a later stage, this would allow the analysis of ASPP2 during later embryogenesis – perhaps including late organogenesis (E12-E14).

Thus, it is clear from experiments already carried out that there is an absolute requirement for ASPP2 in embryogenesis as *ASPP2*-null embryos undergo an early embryonic lethality event. However, much characterisation remains to be done to find out when ASPP2 is required and the function it has in development.

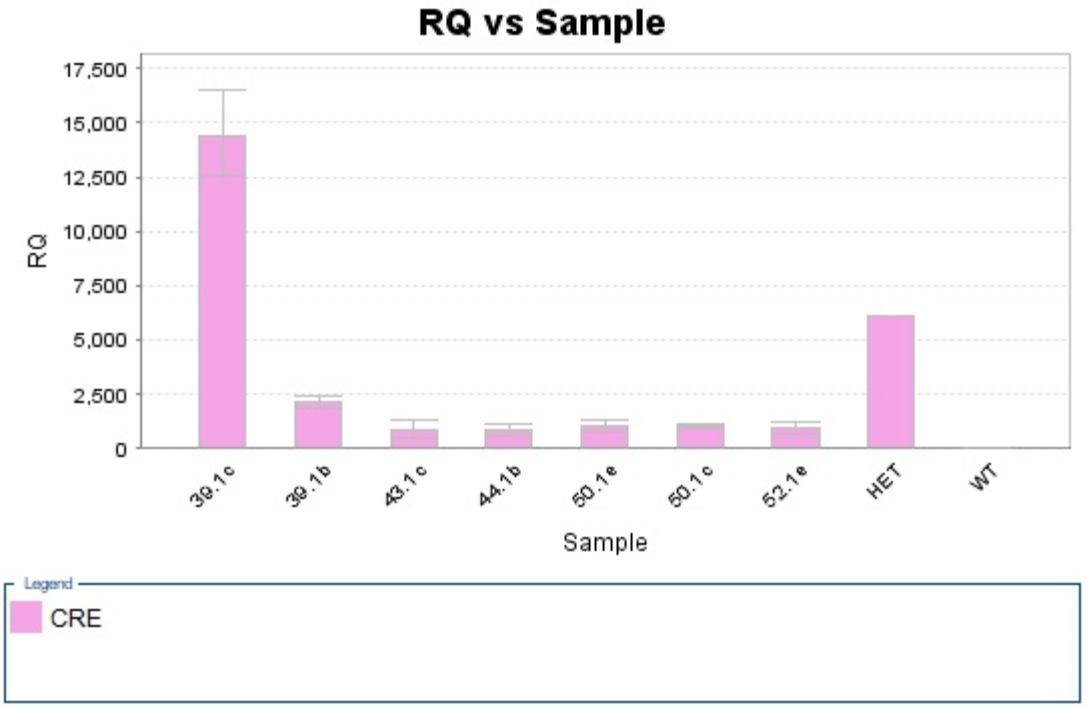

Figure 3.8. Quantitative PCR of *Cre*. This shows qPCR results from the F10 generation of mice resulting from a cross of mice that were heterozygous for *ASPP2*-null and for the *Sox2-Cre* transgene (*ASPP2*$^{+/-}$, *Tg*$^{+/Sox2\text{-}Cre}$) and mice that were homozygous for the *Sox2-Cre* transgene and wildtype for *ASPP2* (*ASPP2*$^{+/+}$, *Tg*$^{Sox2\text{-}Cre/\ Sox2\text{-}Cre}$). Although this example shows less than exact results (less *Cre* expression than expected in most of the samples), it is clear that the first mouse genotyped is homozygous for *Sox2-Cre* as it contains over double the quantity of *Cre* expression as the heterozygous control. A sample known to be heterozygous (HET) and a sample known to be wildtype (WT) were used as controls.

3.3.2 Epiblast-specific knockout experiments

The epiblast-specific knockouts rely on expression of Cre from a Sox2 promoter to delete ASPP2 in the epiblast region of the embryo. Sox2 is expressed in all epiblast cells at E6.5 with little or no activity in extraembryonic cells at this time [132]. Analysis of Sox2-Cre expression with a lacZ reporter showed that all epiblast cells were lacZ-positive at E6.5, but there were no lacZ-positive cells in the VE or the ExE. At E7.5, all three epiblast-derived germ layers were lacZ-positive and lacZ-positive cells were also observed in the epiblast-derived extraembryonic membranes; the amnion, allantois, and mesoderm of the yolk sac and chorion. A low level of lacZ positive cells were observed in non-epiblast derived chorion cells. However, this only occurred in around 3% of cells, meaning that Sox2-Cre acts as an effective tool for removal of target gene expression in the early epiblast. It is unlikely that the small amount of chorion cells that may be negative for ASPP2 expression will affect the overall phenotype of the epiblast-specific knockout.

At this stage of my research, the epiblast-specific knockout was yet to be characterised. It is probable that it will exhibit a similar phenotype to the *ASPP2*-null embryos. Due to the potential function of ASPP2 in linking cell polarity, proliferation and differentiation, deleting its expression in the epiblast will likely lead to similar severe defects seen in the full null embryos. As discussed further in Chapter 4, *ASPP2*$^{-/-}$ embryos exhibit defects in yolk sac formation, with the embryo forming outside the yolk sac instead of being surrounded by it. As the yolk sac is formed from both a VE layer and an epiblast-derived extra-embryonic mesoderm layer, it will be interesting to see if defects in the yolk sac still exist when *ASPP2* is knocked out solely in the epiblast and its derivatives.

3.3.3 Further conditional experiments

The generation of the *ASPP2*$^{flox/flox}$ mouse line permits the carrying out of conditional experiments (including the aforementioned epiblast-specific knockouts), where Cre under control of tissue-specific promoters can be used to analyse the requirement for ASPP2 in that tissue.

As discussed previously, I have generated a compound heterozygote *ASPP2, Mesp1-Cre* mouse line for use in Mesp1 progenitor knockout experiments. Characterisation of this will be discussed in Chapter 4.

The Cre and *ASPP2*$^{flox/flox}$ system is highly flexible, meaning that Cre can be expressed under the control of a wide variety of promoters to examine the function of ASPP2 in a large range of tissues. Thus, it is not only the epiblast and the cardiac region that can be analysed. For example, future conditional experiments could include using Cre under the control of a Transthyretin (Ttr) promoter. Reporter systems have shown that Ttr is expressed throughout the VE in early (E5.5) embryos and in the visceral yolk sac and fetal liver of later stage (E9.5) embryos [77]. Thus, using this experimental technique, the requirement for ASPP2 in the VE could be investigated.

In addition to tissue-specific deletion, conditional knockouts can consist of temporal inactivation of the target gene, under the control of ligand-dependent chimeric Cre recombinases [133]. These are comprised of Cre fused to mutated hormone-binding domains of the estrogen receptor (ER) and are so known as CreER recombinases. The CreER recombinases are inactive but can be activated by ER ligand tamoxifen, thus meaning Cre activity is temporally controllable.

Recent work from our laboratory has shown that *ASPP2*$^{-/-}$ embryos die at a relatively early stage and exhibit severe defects by E8.5 [134]. Thus, temporal gene inactivation would allow us to study the requirement for ASPP2 later in development. CreER could be expressed from

a ubiquitous promoter such as Rosa26 to elucidate the function of ASPP2 at a given timepoint in the entire embryo. Further, CreER could also be expressed from tissue-specific promoters to look at the role of ASPP2 in those developing tissues at specific timepoints.

3.3.4 Embryoid body experiments

Embryoid bodies (EBs) are derived from embryonic stem cells (ESCs), when ESCs aggregate together and differentiate to form a three-dimensional structure, mimicking post-implantation embryonic tissues [135]. EBs present similarities to post-implantation egg-cylinder stage embryos, exhibiting a single layer of outside endoderm cells and an inside epiblast-like inner cell layer [136], [137]. They retain many of the same lineage specific differentiation programmes and patterns of gene expression as that those seen in early embryogenesis [135]. Therefore, EBs are a good model for studies into early embryonic development as they circumvent the difficulties of carrying out experiments on early stage embryos (such as the inaccessibility of the embryos, and the time-consuming and technically challenging nature of experiments using *in vivo* embryos as opposed to this *in vitro* model). They also provide sufficient material to allow biochemical approaches that are not feasible using early post-implantation embryos.

ESCs can be derived from *ASPP2*$^{flox/flox}$ blastocysts. Cre can then be used to induce recombination in this cell line to produce a line of *ASPP2*$^{-/-}$ cells, from which EBs can subsequently be generated. Immunostaining, Western blots and qRT-PCR can be carried out to see if the gene expression profiles of these EBs differ to EBs generated from control lines. Comparisons of protein-protein interaction studies can be carried out to identify possible novel binding partners. Similarly, as a change in phosphorylation status normally indicates a change in protein activity, phosphoproteomic experiments can be carried out on the EBs. Together, these interaction profiles may reveal previously unidentified downstream targets of ASPP2.

Various molecular inhibitors may then be used to attempt to disrupt the interaction in control EBs and the resulting phenotype can be analysed to study the importance of this interaction.

Chapter 4: A preliminary characterisation of the role of ASPP2 in the embryo

4.1 Introduction

The function of a protein cannot usually be fully determined by analysing amino acid motifs or analysing the role of similar proteins in similar organisms. Gene inactivation is the best method of elucidating the role of a protein. In this chapter, I discuss preliminary characterisations of the function of ASPP2 in embryogenesis as determined from gene knockout experiments.

4.1.1 Knocking out ASPP2 in mouse embryos

As discussed in more detail in Chapter 3, I have produced mouse lines in which exon 4 of *ASPP2* is deleted or is floxed and thus ready for deletion upon crossing with a Cre-expressing line. This mutation causes a frameshift downstream and eliminates expression of *ASPP2*. This permits characterisation of the role of ASPP2 during embryogenesis.

Although other mouse models for *ASPP2* deletion exist, its function in development has not previously been fully characterised. The $ASPP2^{\Delta 10\text{-}17}$ experiments were unable to find any *ASPP2*-null embryos even as early as E6.5 and therefore characterisation could not be carried out (although stages earlier than E5.5 were not investigated) [117].

The $ASPP2^{\Delta 3}$ studies carried out in a Balb/c background resulted in pups that survived post-weaning. Experiments on these embryos at E13.5 showed morphological abnormalities in the retina and brain, with cells losing their normal orientation (indicating a loss of polarity), being less organized than their wildtype counterparts and exhibiting deregulated growth [7]. However, as discussed previously, $ASPP2^{\Delta 3}$ is a hypomorphic mutation rather than a full mutation.

Therefore, characterisation of my exon 4 deletion model of *ASPP2*-null embryos will be the first full mutation of *ASPP2* examined during embryogenesis.

4.1.2 Distribution of ASPP2 in mouse embryos

ASPP2 acts as a scaffold by binding to many other proteins, including polarity protein PAR3. It binds to PAR3 at tight junctions where it is able to interact with many other factors such as PP1 and YAP/TAZ. Protein phosphatase 1 (PP1) dephosphorylates YAP/TAZ to promote its nuclear translocation and activation [10]. YAP/TAZ has a wide range of functions during embryogenesis, including the promotion of cell growth and proliferation and the attenuation of apoptosis [138]–[140]. ASPP2 and YAP have been shown to co-localise at TJs in VE of early (E5.5) post-implantation embryos (Figure 1.9) [Unpublished, C. Royer & Srinivas group]. However due to the broad functions of ASPP2 and its large range of binding partners [2], [3] [4], [5] [6][7], [8], it is expected that ASPP2 would have a broad expression and localization pattern within embryos.

4.1.3 Preliminary experiments of *ASPP2*-null in mouse embryos

The *ASPP2*-null mutation described in this thesis is embryonically lethal. Preliminary experiments at Harwell found that no homozygous mutants are born and there is a 2:1 ratio of heterozygotes to wildtype, instead of the expected Mendelian percentages of 50% and 25% respectively (unpublished work).

At E3.5, *ASPP2*-null embryos can be detected at the expected frequency (25% from heterozygous crosses described in Chapter 3) and these embryos have no obvious defects in development. Thus ASPP2 may not be required during pre-implantation embryogenesis. However, it is likely that it is required during the later stages of peri-implantation and in early

postimplantation. Exactly when this requirement begins will require further characterisation. Here, I begin to characterise its requirements in early post-implantation mouse embryos.

Preliminary results by C. Royer have indicated that *ASPP2*$^{-/-}$ embryos at E6.5 have disrupted development, including a thickened, disorganized posterior side of the embryo (possibly due to over-proliferation, disruption of cell junctions and/or dysregulation of cell division) [Unpublished, C. Royer & Srinivas group]. Thus ASPP2 plays an important role at the very early stages of post-implantation development. However, these embryos still appear to be largely normal, with no major defects. Thus I have characterised a later stage to see how development progresses and gain more information on the possible role of ASPP2 in early post-implantation mouse embryos.

4.1.4 Overall morphology of *ASPP2*-null embryos

In my preliminary experiments, I began by imaging wildtype embryos to form an overview of how ASPP2 is distributed in the embryo and how E8.5 and E9.5 embryos are structed. I found that ASPP2 localises at tight junctions in E8.5 and E9.5 embryos, although it is found throughout the entire embryo (Figure 4.1). ASPP2 is most clearly observed at the apical surfaces of epithelial cells, where ASPP2 localisation appears as distinct puncta (Figure 4.1, Figure 4.2). This is particularly obvious at the apical surface of the somite epithelial cells that form the lumen of the somite (Figure 4.2, Figure 4.3).

I have carried out preliminary characterisations of *ASPP2*$^{-/-}$ embryos at E8.5 and E9.5. At both these stages, the null embryos exhibit gross abnormalities in morphology. One major defect that can be observed clearly in mutant embryos at E8.5 (Figure 4.4, Figure 4.5) and in some of the E9.5 mutants (Figure 4.8, Figure 4.9) is the unusual way in which these embryos protrude from the yolk sac. In wildtype E8.5 (Figure 4.6, Figure 4.7) and E9.5 embryos (Figure 4.10, Figure 4.11), the yolk sac surrounds the embryo proper. However, in the *ASPP2*$^{-/-}$ embryos, the embryo proper is positioned outside of the yolk sac. This is presumably the result of a defect in rostral folding, but further experiments at earlier stages will likely be needed to verify if this is the case.

Some E9.5 mutants exhibit this yolk sac defect, but others are so disturbed in morphology that even distinguishing between the various types of embryonic tissue is a challenge (Figure 4.12, Figure 4.13). These embryos were clearly advanced in the process of resorption, with the majority of the fetal tissue being ectoplacental cone and a minimal amount being fetal membrane tissue [141]. In addition, although the allantois is visible in *ASPP2*-null embryos, the amnion is not present in these embryos.

ASPP2-null embryos also have a clear difference in size in comparison to wildtype embryos. Comparisons of the cross-sectional area of the embryo proper of *ASPP2*$^{-/-}$ and wildtype embryos at both E8.5 and E9.5 show that the former are smaller than the latter (Figure 4.14). Some of this size discrepancy may be due to the noticeably smaller anterior portion of the embryos. The anterior half of the embryo is far less developed in *ASPP2*-null embryos, as indicated by analysis that revealed that the proportion of anterior:posterior in these mutant embryos is far lower (Figure 4.15). This is more clearly seen at E8.5 than E9.5 because the *ASPP2*-null embryos at E9.5 are generally too disturbed to permit proper analysis of tissue morphology. The mutant embryos at E8.5 lack obvious cardiac (as will be discussed in more detail later) and foregut regions, and have greatly reduced head and midgut regions.

Figure 4.1. ASPP2 distribution in wildtype E9.5 embryos

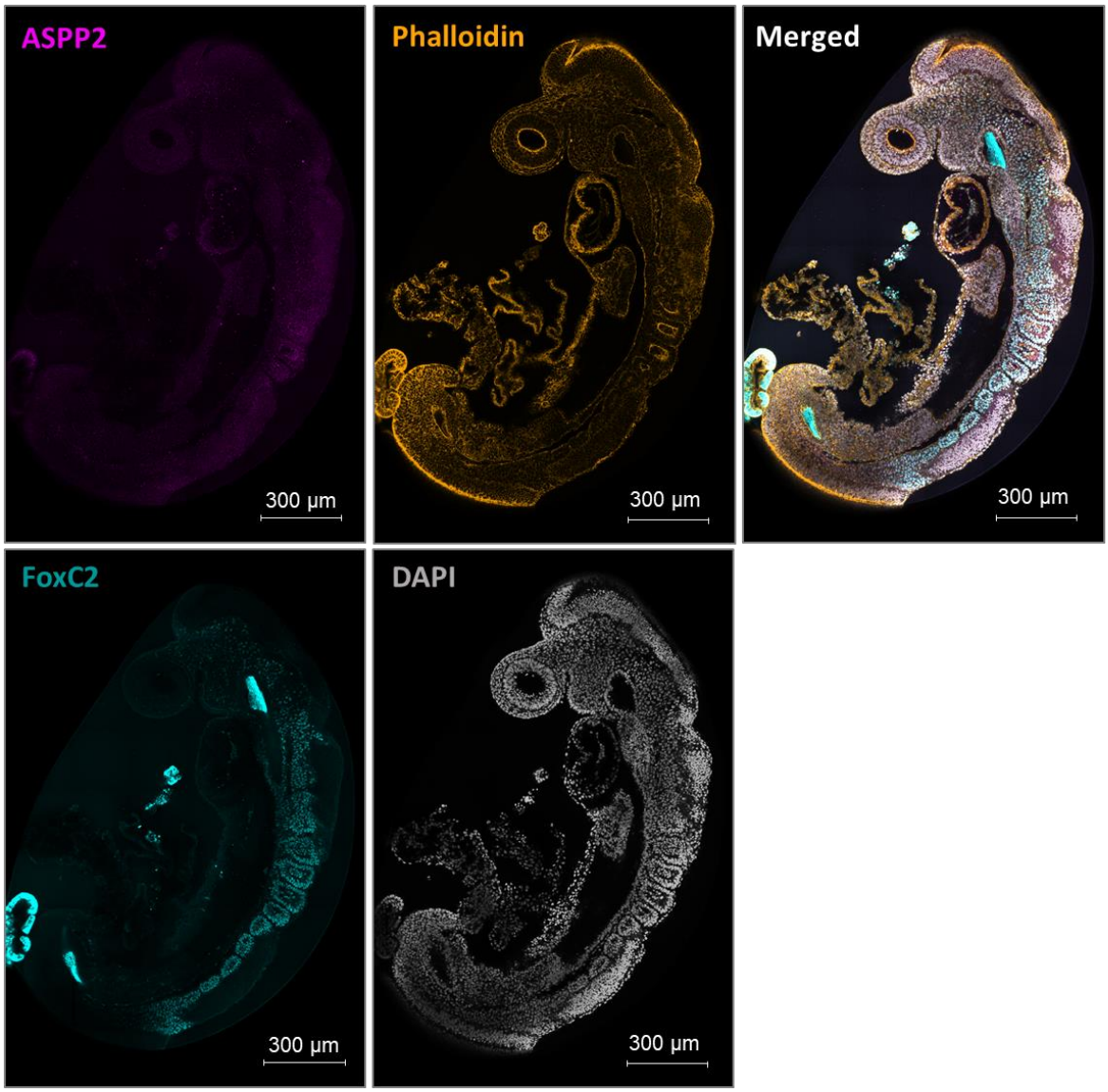

Figure 4.1. ASPP2 is distributed throughout wildtype embryos, as seen in Figure 4.1A. It is particularly concentrated in puncta at apical membranes. Immunostaining for ASPP2 (magenta), somite marker FoxC2 (cyan), nuclear marker DAPI (grayscale) and actin marker Phalloidin (gold). Scale bars = 300 µm.

Figure 4.2. ASPP2 distribution in wildtype E9.5 embryo somites

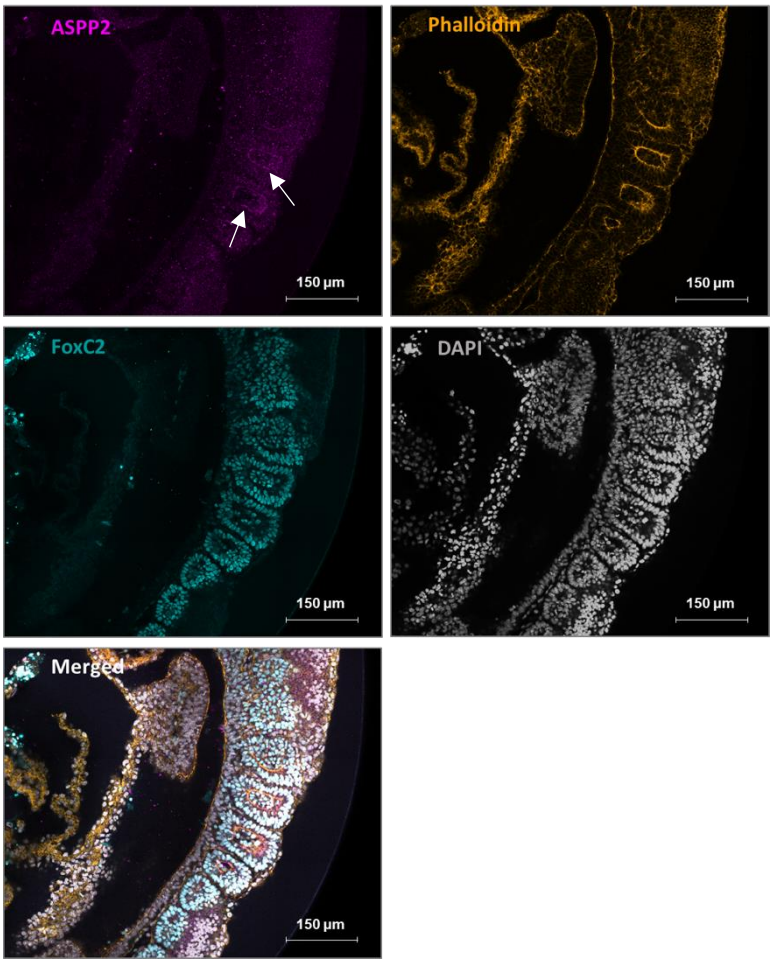

Figure 4.2. ASPP2 is particularly concentrated in puncta at apical membranes in E9.5 embryos, which can be seen most clearly in the somites (examples are demonstrated with white arrows). Immunostaining for ASPP2 (magenta), somite marker FoxC2 (cyan), nuclear marker DAPI (grayscale) and actin marker Phalloidin (gold). Scale bars = 150 µm.

Figure 4.3. Examples of ASPP2 puncta at the apical surface of the lumen of somites in wildtype E9.5 embryos

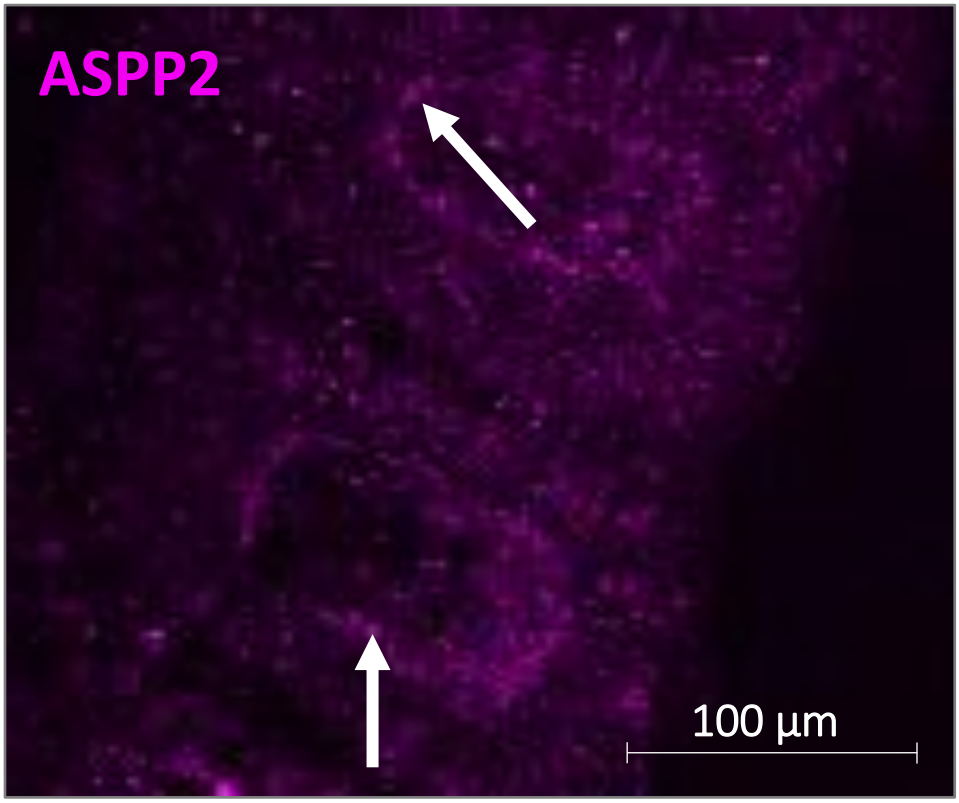

Figure 4.3. The concentration of ASPP2 in puncta at apical membranes is most clearly in the somites. This figure shows a close-up of somites in a wildtype E9.5 ASPP2 embryo. White arrows mark out examples of where ASPP2 is found in distinct puncta. Immunostaining for ASPP2 (magenta). Scale bar = 100 µm.

Figure 4.4. *ASPP2*-null embryo at E8.5 (split channels)

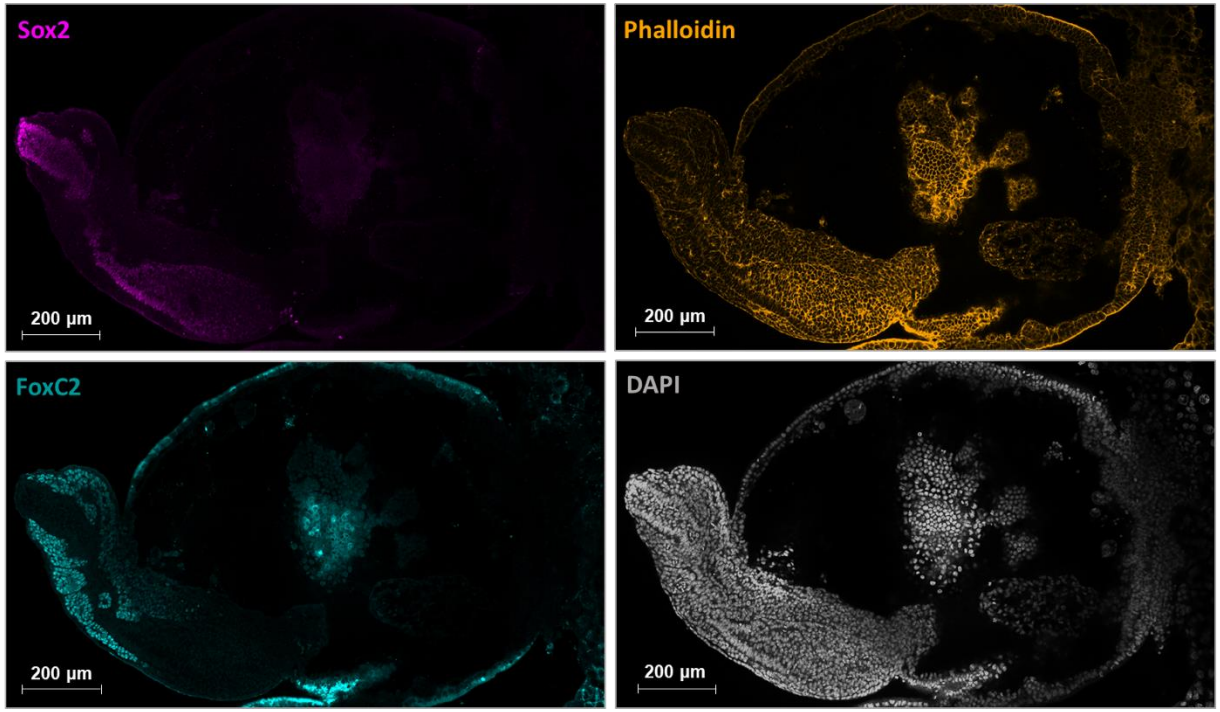

Figure 4.4. This figure depicts an *ASPP2*-null at E8.5, with separate microscope channels. The *ASPP2*-null embryo is developing outside of the yolk sack (YS) and is noticeably deformed. It has fewer somites that the wildtype embryo and these somites are disrupted in structure. The *ASPP2*-null embryo also has a majorly disturbed anterior region and no discernible heart. Immunostainings for Sox2 (magenta), paraxial and somitic mesoderm marker FoxC2 (cyan), nuclear marker DAPI (grayscale) and F-actin marker Phalloidin (gold). Scale bars = 200 µm.

Figure 4.5. *ASPP2*-null embyro at E8.5 (merged channels)

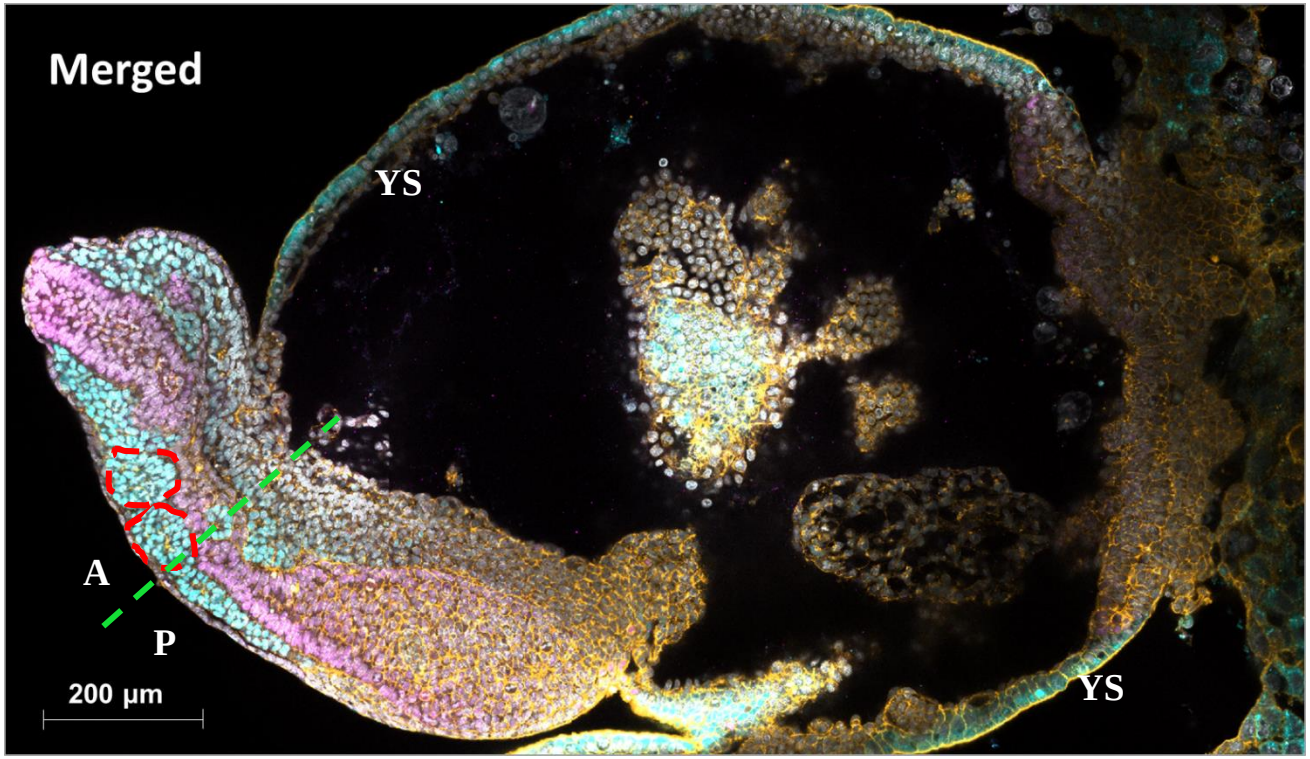

Figure 4.5. This figure depicts an *ASPP2*-null at E8.5, with merged channels. The *ASPP2*-null embryo is developing outside of the yolk sack (YS) and is noticeably deformed. It has fewer somites (examples of somites were outlined in red) that the wildtype embryo and these somites are disrupted in structure. The *ASPP2*-null embryo also has a majorly disturbed anterior region (anterior, A and posterior, P, halves separated by green dotted line) and no discernible heart (H). Immunostainings for Sox2 (magenta), paraxial and somitic mesoderm marker FoxC2 (cyan), nuclear marker DAPI (grayscale) and F-actin marker Phalloidin (gold). Scale bars = 200 µm.

Figure 4.6. Wildtpye embryo at E8.5 (split channels)

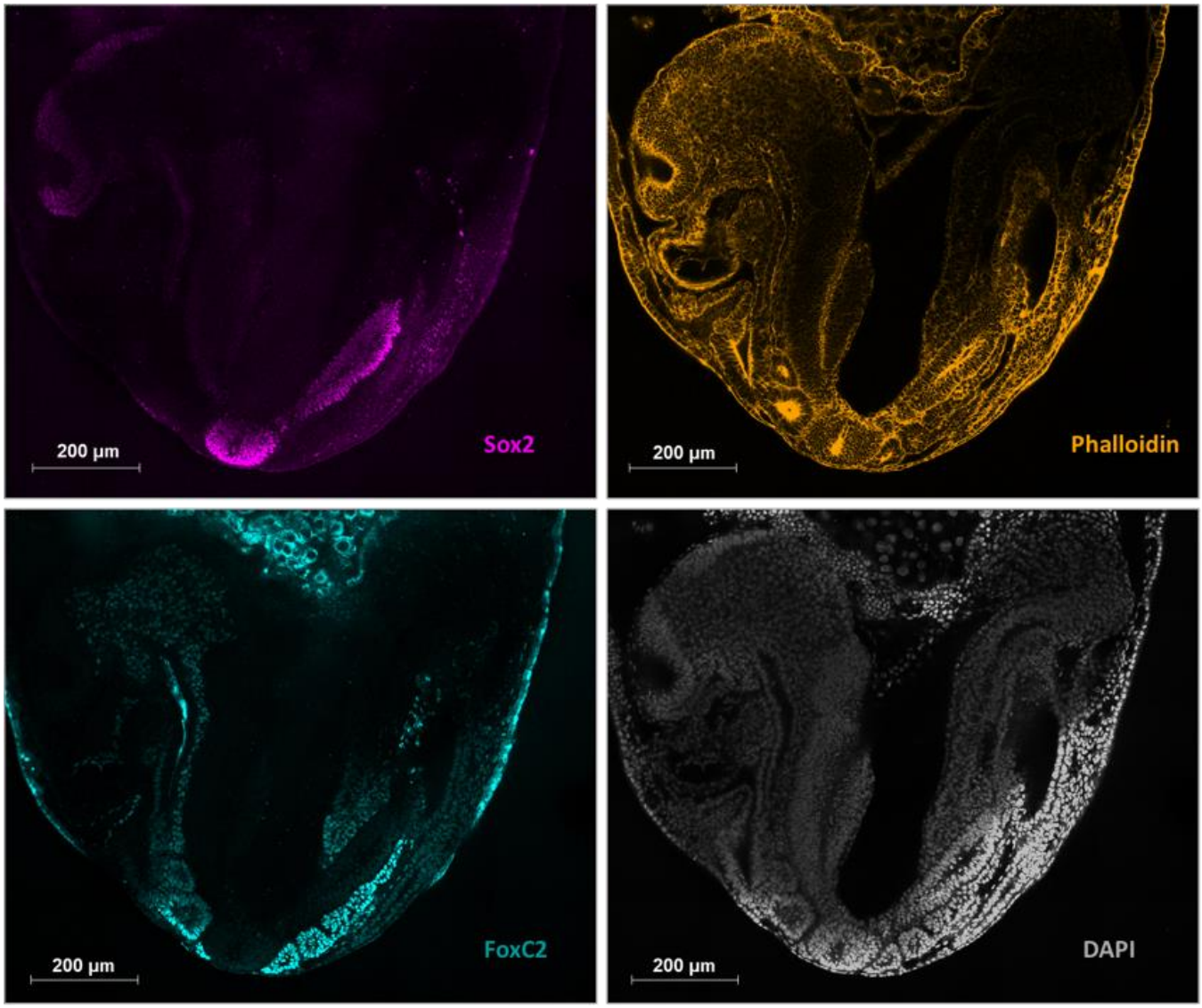

Figure 4.6. This figure depicts wildtype embryo at E8.5, with split channels. Here, the somites, heart structure, anterior and posterior regions have all formed as normal. Immunostainings for Sox2 (magenta), paraxial and somitic mesoderm marker FoxC2 (cyan), nuclear marker DAPI (grayscale) and F-actin marker Phalloidin (gold). Scale bars = 200 µm.

Figure 4.7. Wildtype embryo at E8.5 (merged channels)

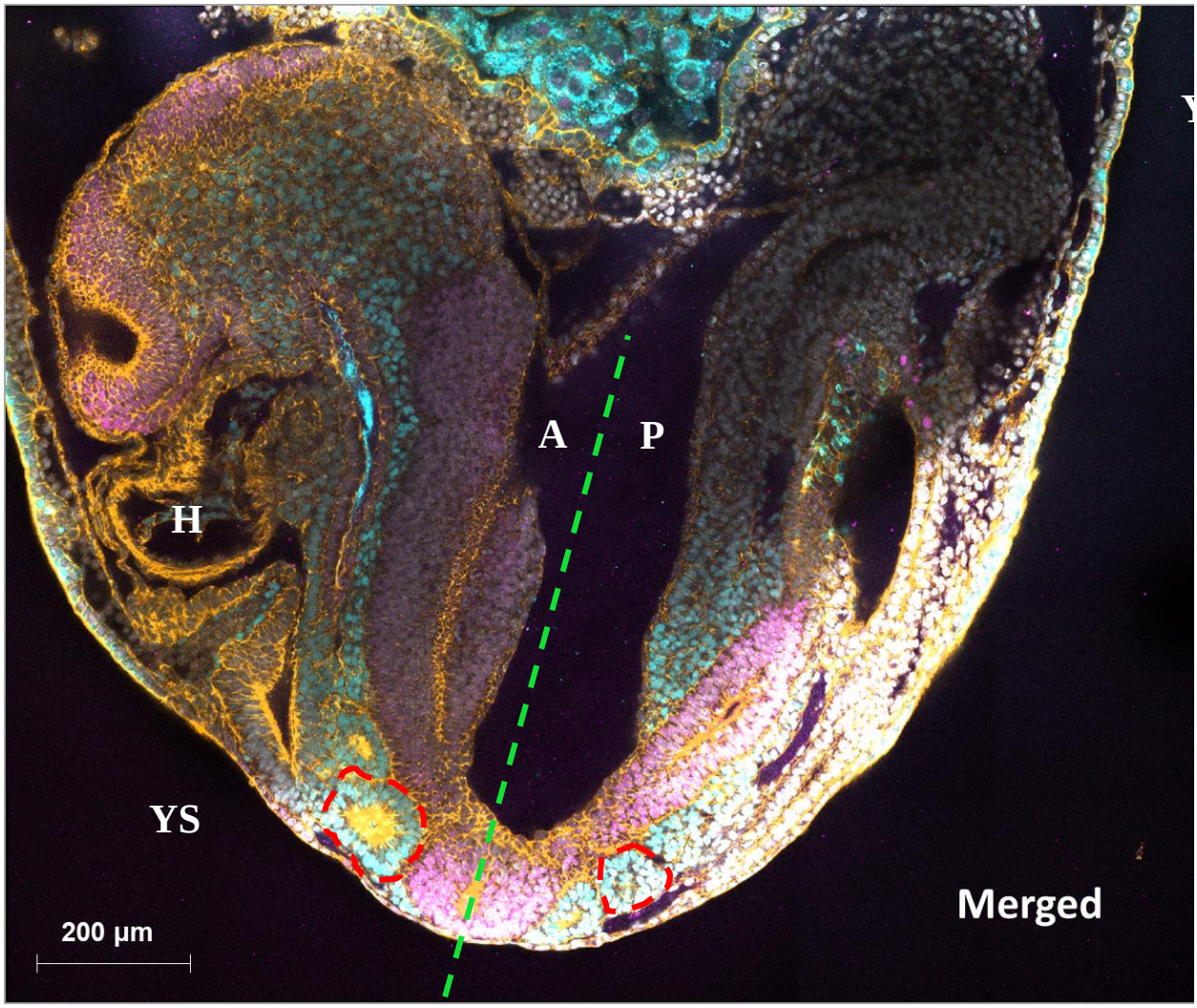

Figure 4.7. This figure depicts wildtype embryo at E8.5, with merged channels. Here, the somites (outlined in red), heart structure (H), yolk sac (YS), anterior (A) and posterior (P) regions have all formed as normal. Immunostainings for Sox2 (magenta), paraxial and somitic mesoderm marker FoxC2 (cyan), nuclear marker DAPI (grayscale) and F-actin marker Phalloidin (gold). Scale bars = 200 µm.

Figure 4.8. *ASPP2*-null embryo at E9.5 (split channels)

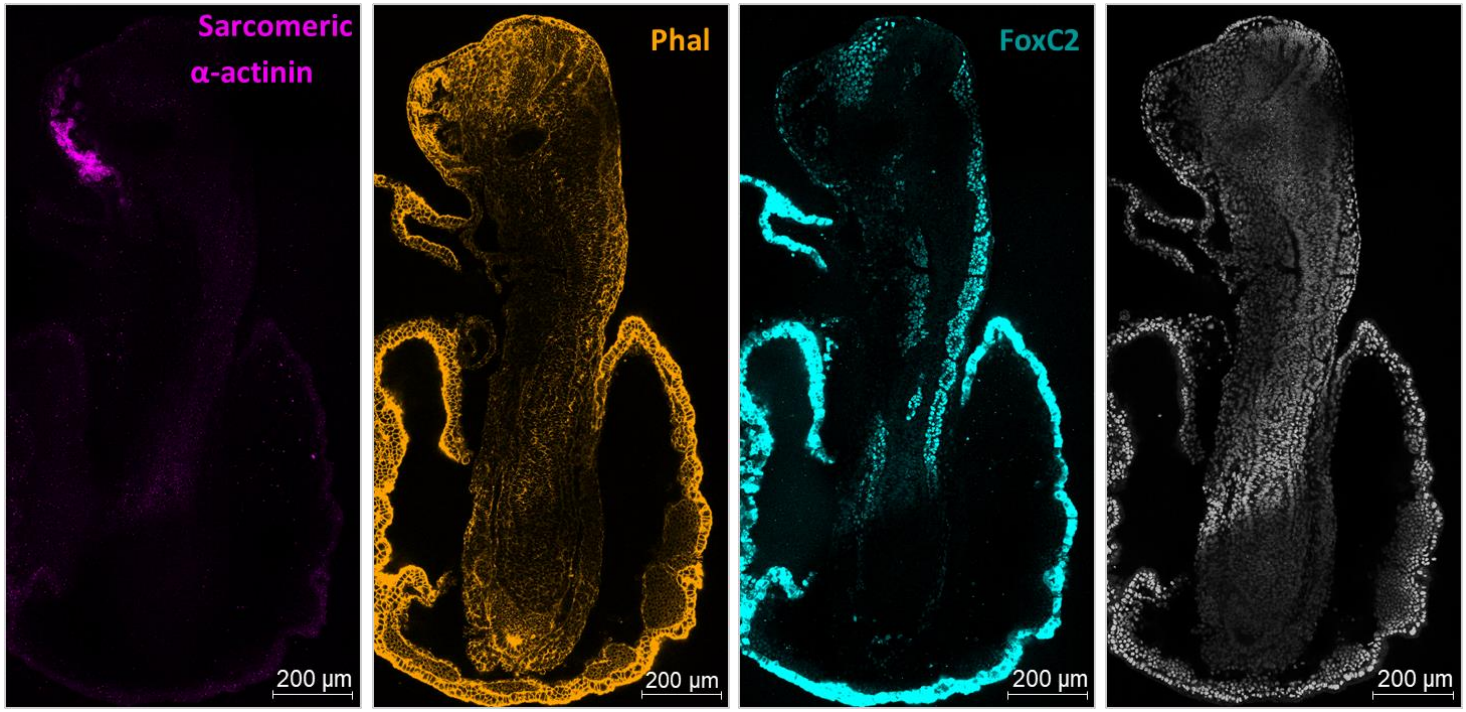

Figure 4.8. This figure depicts an *ASPP2*-null embryo at E9.5, with split channels. The *ASPP2*-null embryo is developing outside of the yolk sack, as is typical for *ASPP2*-null embryos, although this embryo is partially contained within the yolk sac. The *ASPP2*-null embryo exhibits severely disturbed morphology; it has far fewer somites than the wildtype embryo and the somites it does have are abnormal. The *ASPP2*-null embryo also has a majorly disturbed anterior region and no discernible heart, although there is a small region staining positive for cardiac marker Sarcomeric α-actinin. The fact that features are still able to be analysed and somites still form means that this is one of the more advanced examples of *ASPP2*-null embryos at E9.5; other *ASPP2*-null embryos at E9.5 have already started to undergo resorption. Immunostainings for cardiac marker Sarcomeric α-actinin (magenta), somite marker FoxC2 (cyan), nuclear marker DAPI (grayscale) and F-actin marker Phalloidin (gold). Scale bars = 200 µm.

Figure 4.9. *ASPP2*-null embyro at E9.5 (merged channels)

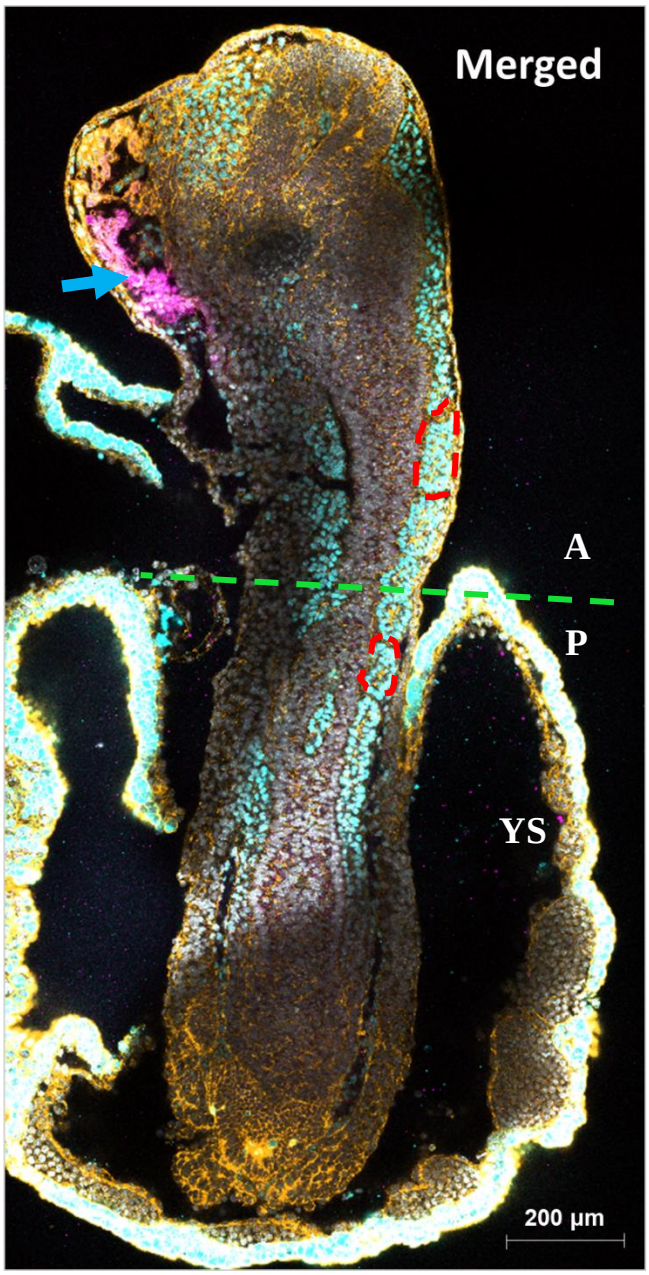

Figure 4.9. This figure depicts an *ASPP2*-null embryo at E9.5, with merged microscope channels. The *ASPP2*-null embryo is developing outside of the yolk sack (YS), as is typical for *ASPP2*-null embryos, although this embryo is partially contained within the yolk sac. The *ASPP2*-null embryo exhibits severely disturbed morphology; it has far fewer somites (examples outlined with a dashed red line) than the wildtype embryo and the somites it does have are abnormal. The *ASPP2*-null embryo also has a majorly disturbed anterior region (anterior, A and posterior, P, halves marked by green dotted line) and no discernible heart, although there is a small region (marked with blue arrow) staining positive for cardiac marker Sarcomeric α-actinin. The fact that features are still able to be analysed and somites still form means that this is one of the more advanced examples of *ASPP2*-null embryos at E9.5; other *ASPP2*-null embryos at E9.5 have already started to undergo resorption. Immunostainings for cardiac marker Sarcomeric α-actinin (magenta), somite marker FoxC2 (cyan), nuclear marker DAPI (grayscale) and F-actin marker Phalloidin (gold). Scale bars = 200 µm.

Figure 4.10. Wildtpye embryo at E9.5 (split channels)

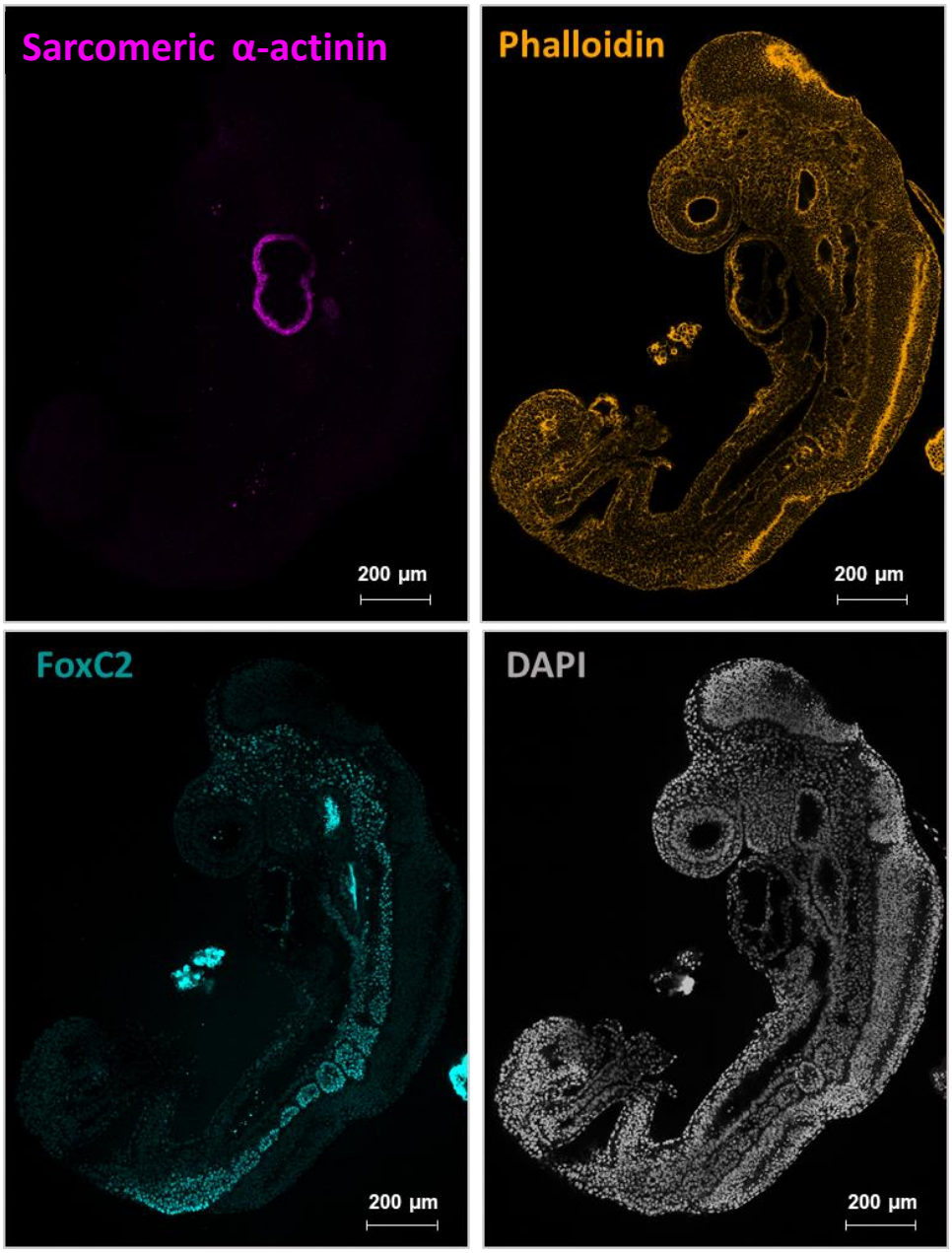

Figure 4.10. This figure depicts wildtype embryo at E9.5, with split channels. The wildtype embryo has been dissected from its yolk sac to facilitate staining. Here, the somites, heart structure, yolk sac, anterior and posterior regions have all formed as normal. Immunostainings for cardiac marker Sarcomeric α-actinin (magenta), paraxial and somitic mesoderm marker FoxC2 (cyan), nuclear marker DAPI (grayscale) and F-actin marker Phalloidin (gold). Scale bars = 200µm.

Figure 4.11. Wildtype embryo at E9.5 (merged channels)

Figure 4.11. This figure depicts wildtype embryo at E8.5, with merged channels. The wildtype embryo has been dissected from its yolk sac to facilitate staining. Here, the somites (outlined in red), heart structure (H), yolk sac (YS), anterior (A) and posterior (P) regions have all formed as normal. Immunostainings for Sox2 (magenta), paraxial and somitic mesoderm marker FoxC2 (cyan), nuclear marker DAPI (grayscale) and F-actin marker Phalloidin (gold). Scale bars = 200 µm.

Figure 4.12. *ASPP2*-null E9.5 embryo in the early stage of resorption

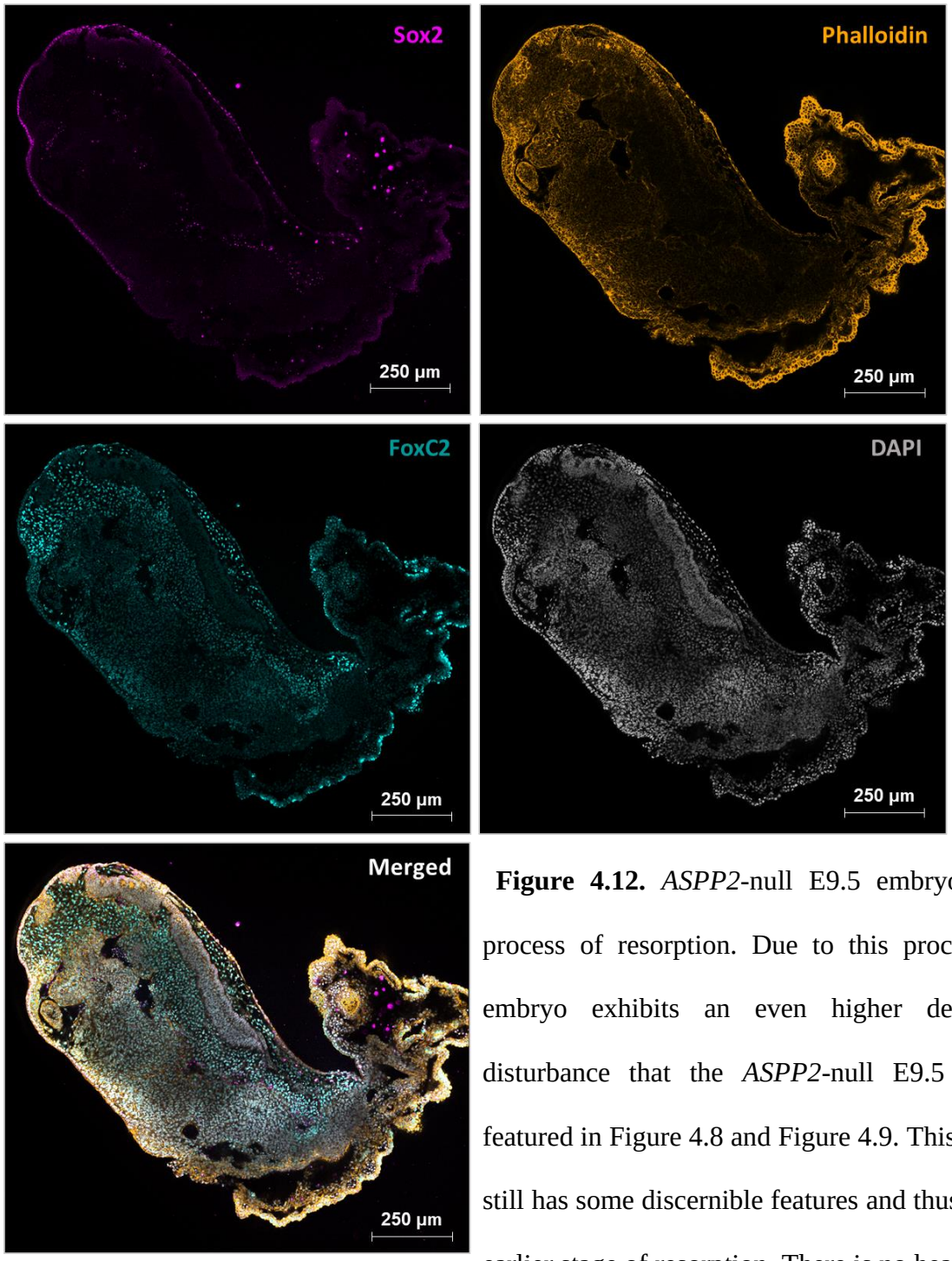

Figure 4.12. *ASPP2*-null E9.5 embryo in the process of resorption. Due to this process, this embryo exhibits an even higher degree of disturbance that the *ASPP2*-null E9.5 embryo featured in Figure 4.8 and Figure 4.9. This embryo still has some discernible features and thus is in an earlier stage of resorption. There is no heart region or somites but an anterior region (a rough anterior (A)/posterior (P) boundary is marked in the merged image with a green dashed line) can still be identified. Immunostainings for endoderm marker Sox2 (magenta), somite marker FoxC2 (cyan), nuclear marker DAPI (grayscale) and F-actin marker Phalloidin (gold). Scale bars = 250 µm.

Figure 4.13. *ASPP2*-null E9.5 embryo in the later stage of resorption

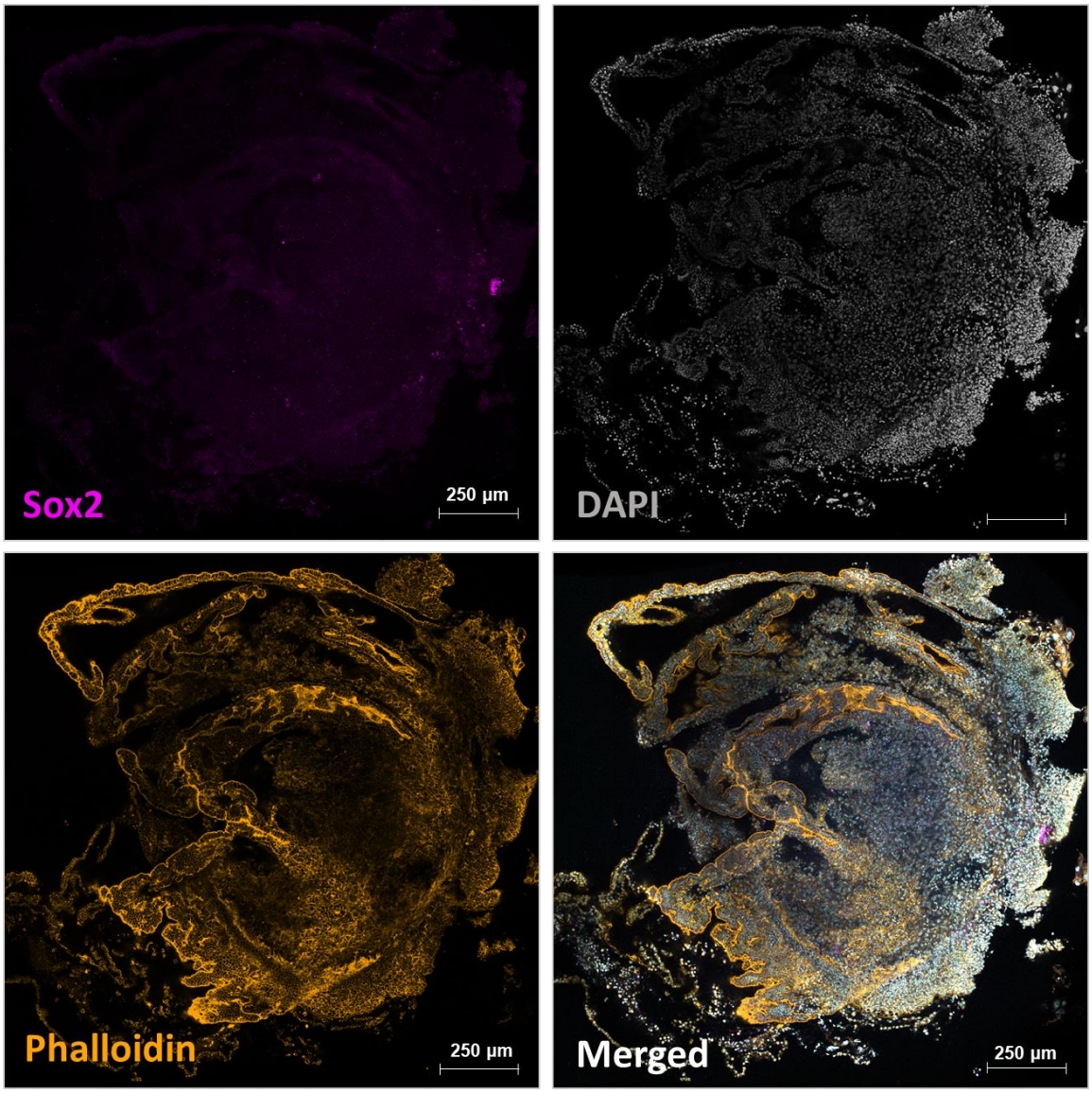

Figure 4.13. *ASPP2*-null E9.5 embryo in the process of resorption. This example of resorption is further along than that depicted in Figure 4.12, with no discernible features. Instead, it appears as an unorganised mass of fetal membranes. Immunostainings for endoderm marker Sox2 (pink), nuclear marker DAPI (white) and actin marker Phalloidin (gold). Scale bars = 250 µm.

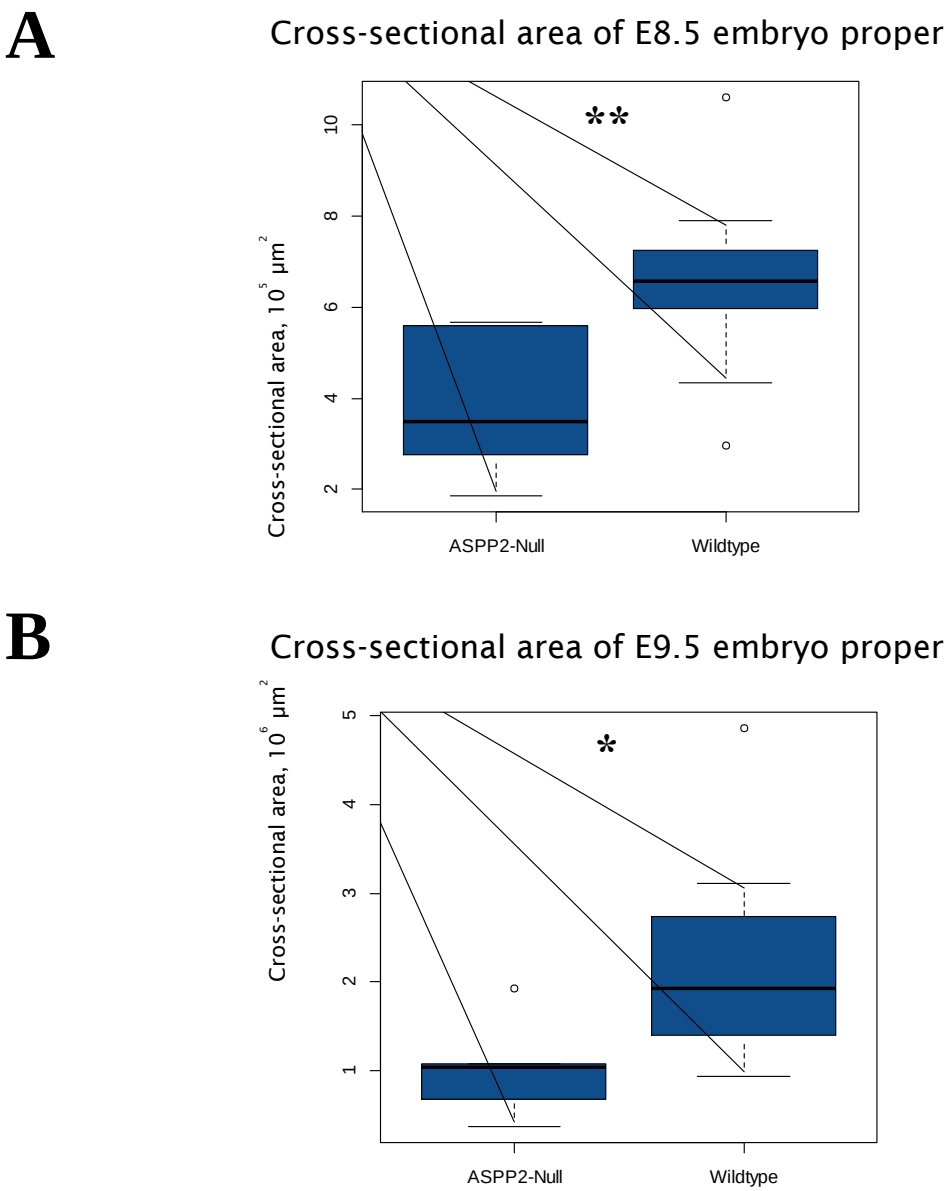

Figure 4.14. *ASPP2*-null embryos are smaller than wildtype embryos

Comparisons of the cross-sectional area of the embryo proper at E8.5 and E9.5 revealed that *ASPP2*-null embryos are smaller at both stages (t-test, $p<0.01$ at E8.5 (*ASPP2*-null n=6, wildtype n=11), $p<0.05$ at E9.5 (*ASPP2*-null n=5, wildtype n=14)).

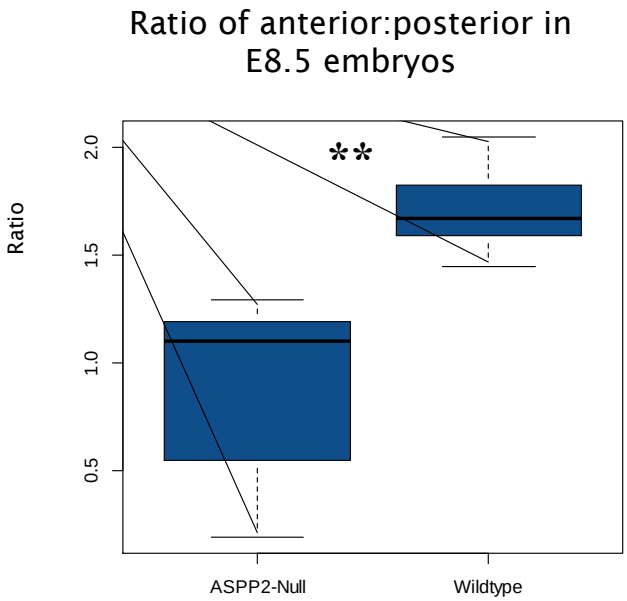

Figure 4.15. *ASPP2*-null embryos have a significantly lower anterior:posterior ratio

Comparisons of ratio of anterior:posterior between *ASPP2*-null and wildtype embryos showed that the former have a much lower ratio. This is due to the anterior region being far less developed and highly disturbed in *ASPP2*-null embryos (t-test, $p<0.005$ (*ASPP2*-null n=6, wildtype n=8)).

4.1.5 Somites in *ASPP2*-null embryos

Somites of wildtype embryos are comprised of an outer layer of epithelial cells with a bottle-like morphology that surround the somitocoel, which is filled with mesenchymal cells [111]. One major phenotype of the *ASPP2*$^{-/-}$ embryos is a disruption to somite formation and morphology.

Firstly, the number of somites in *ASPP2*-null compared with wildtype embryos is greatly reduced at E9.5. There is an average of 18.9 somites in wildtype embryos at this stage, compared to 3.4 in mutant embryos (Figure 4.16). Many of these embryos are undergoing resorption, where the fetus has died and the fetal tissue is being degenerated and resorbed. Although somites can be found in some *ASPP2*-null embryos at E9.5, the resorption process means that in other embryos have already begun to break down and thus somites cannot be identified in these.

On the other hand, there is no significant difference in number of somites between wildtype and *ASPP2*-null embryos at E8.5, with the former having an average of 5.9 per embryo and the latter having an average of 6 (Figure 4.16). Thus, somitogenesis may be initiated correctly.

However, even though the number of somites does not differ significantly at E8.5, the morphology of the somites does. Somites at this stage are significantly smaller (Figure 4.17). In *ASPP2*-null that do possess somites at E9.5, a similarly large difference in size exists (Figure 4.17).

In addition to being smaller, the somites of *ASPP2*$^{-/-}$ embryos exhibit gross abnormalities in structure. The somites of these embryos are often highly disrupted (Figure 4.18), rather than having an organised layer of epithelial cells around a central cavity as observed in wildtype embryos (Figure 4.19). Instead of a single layer of cells, the epithelial cells are multi-layered, with some having the classic bottle-shaped morphology but others lacking this. Furthermore, many of the somites have an abnormal shape, being less spherical than their wildtype

counterparts, and are also less clearly delineated from the surrounding tissue. The proportion of abnormal somites, characterised here by a large, observable disruption in shape and epithelial integrity, is far higher in *ASPP2*-null embryos than wildtype embryos (Figure 4.20). *ASPP2*-null somites are also more likely to lack the central cavity (Figure 4.21). In the somites that have cavitated, the size of the cavity between wildtype and *ASPP2*-null embryos is significantly different (Figure 4.22). The somites that can be identified in E9.5 *ASPP2*-null embryos exhibit the same defects as those observed in E8.5 *ASPP2*-null embryos (Figure 4.23). For comparison, examples of E9.5 wildtype somites are shown in Figure 4.24.

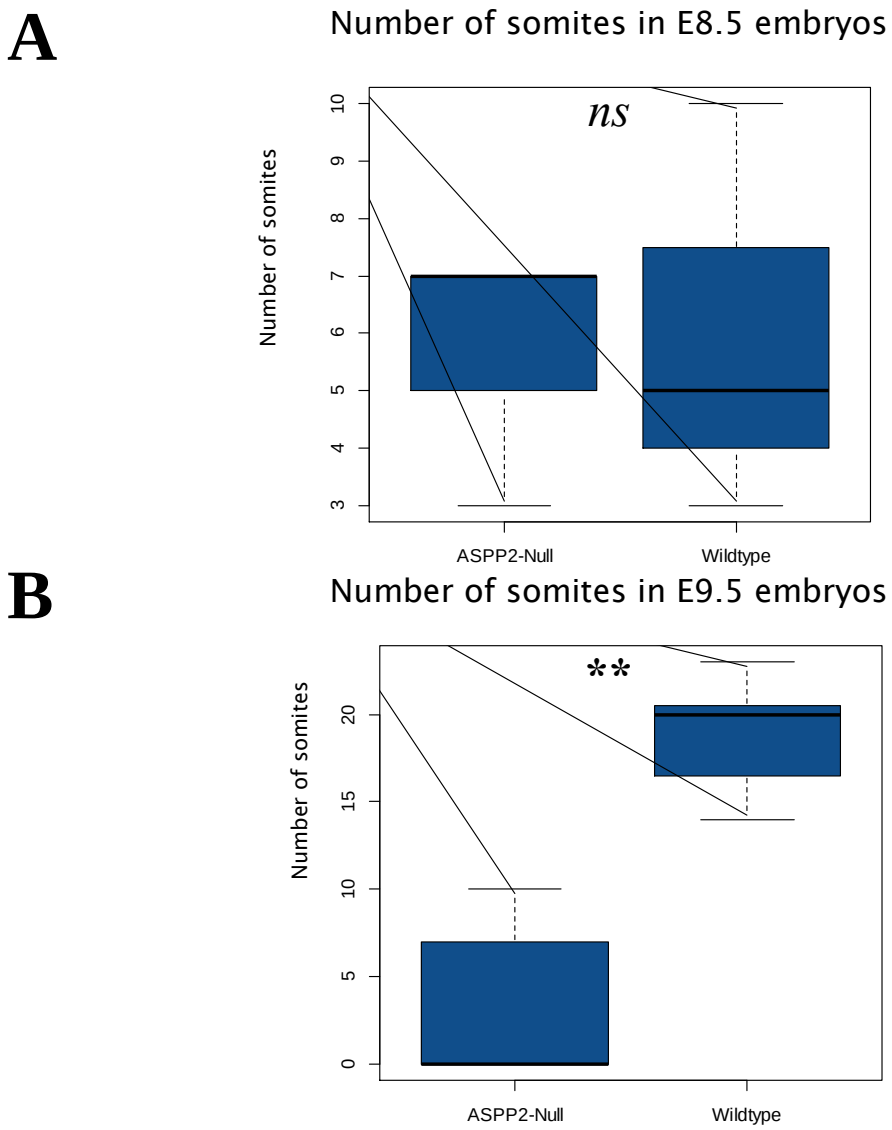

Figure 4.16. *ASPP2*-Null embryos at E9.5 have a greatly reduced number of somites

Comparisons of the number of somites at E8.5 found no significant difference between *ASPP2*-null embryos and wildtype embryos (t-test, p>0.5 (*ASPP2*-null n=6, wildtype n=11)). However, at E9.5, there was a significant difference, with wildtype embryos having many more somites than the mutant embryos (t-test, p<0.005 (*ASPP2*-null n=5, wildtype n=11)).

A

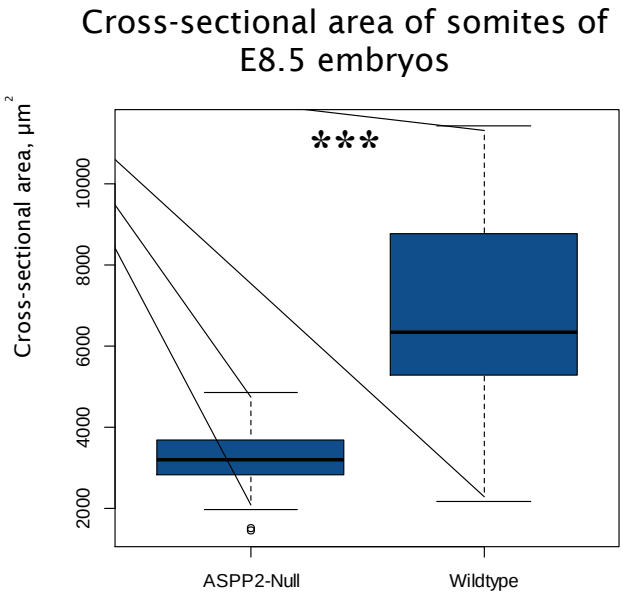

B

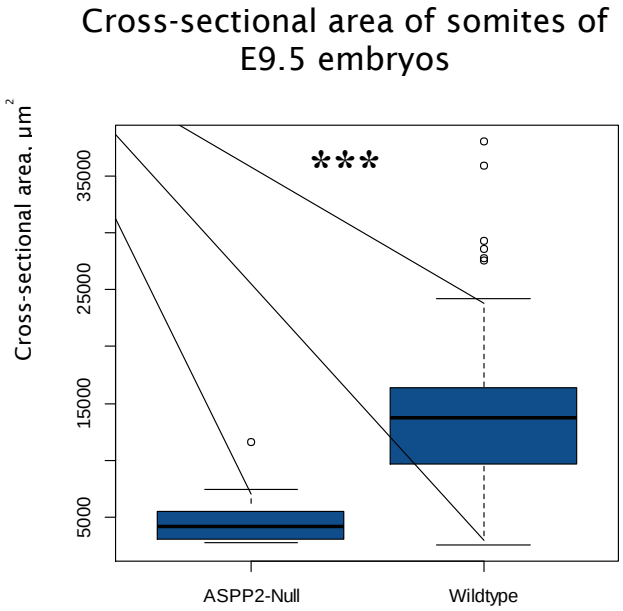

Figure 4.17. The somites of *ASPP2*-Null embryos are significantly smaller

Comparisons of the cross-sectional area of somites at E8.5 found a significant difference between *ASPP2*-null embryos and wildtype embryos at E8.5 ($p<1x10^{15}$ (*ASPP2*-null n=34 somites from n=6 embryos, wildtype n=58 somites from n=10 embryos)). A similarly large difference was also observed at E9.5 ($p<1x10^{6}$ (*ASPP2*-null n=15 somites from n=2 embryos, wildtype n=217 somites from n=14 embryos)).

Figure 4.18. Somites of *ASPP2*-null E8.5 embryo

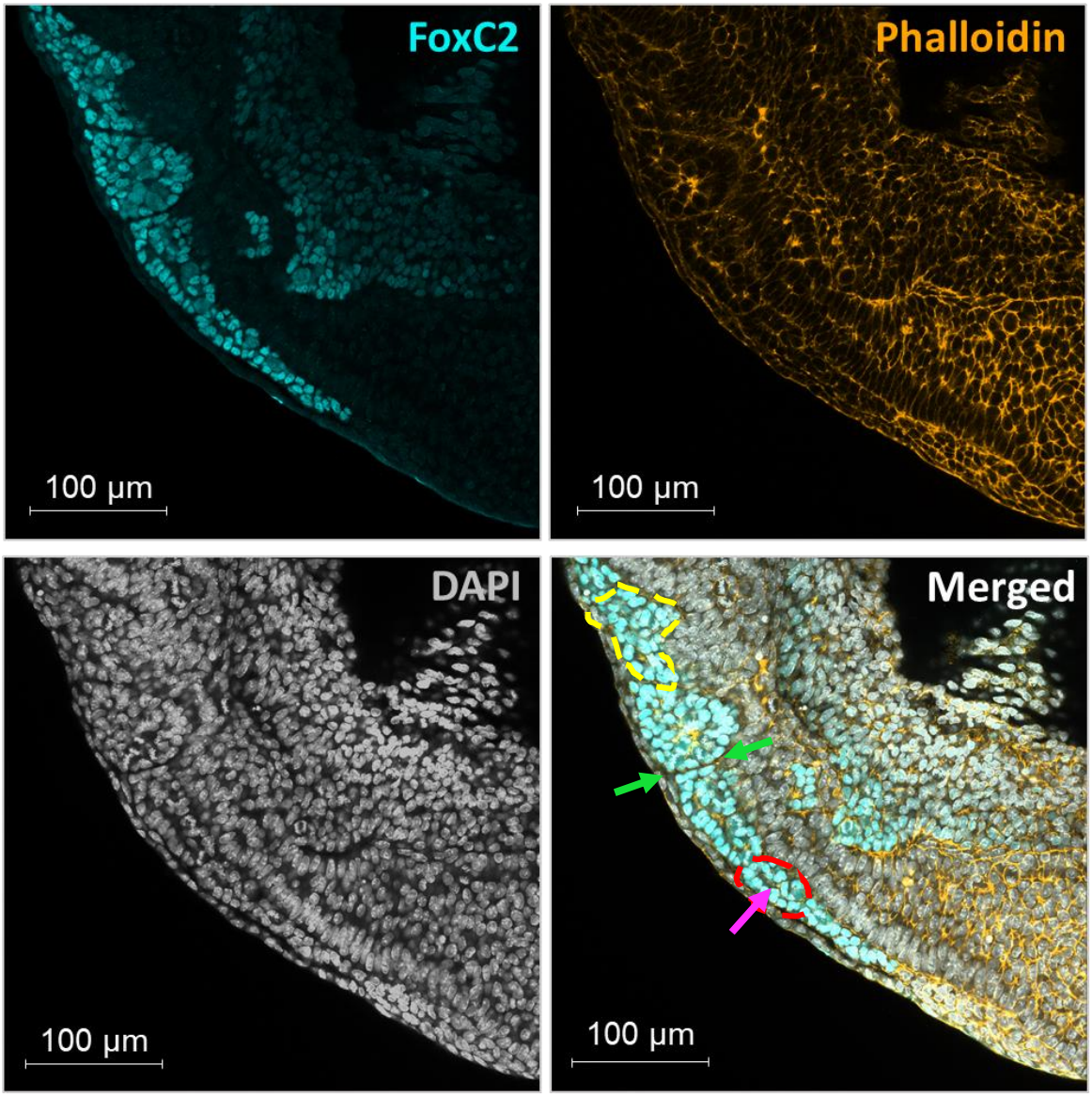

Figure 4.18. This figure depicts the somites of an *ASPP2*-null embryo at E8.5. Some *ASPP2*-null somites develop normally - an example of this is outlined with a dashed red line. These somites have a central somitocoel (example marked with a pink arrow) surrounded by a monolayer of epithelial cells. However, others lose this organisation (an example is outlined with a dashed yellow line). In addition, the boundaries between the somites (example marked with green arrow) are less distinct and the somites have a less uniform shape. Immunostainings for somite marker FoxC2 (cyan), nuclear marker DAPI (grayscale) and actin marker Phalloidin (gold). Scale bars = 100 µm.

Figure 4.19. Somites of wildtype E8.5 embryo

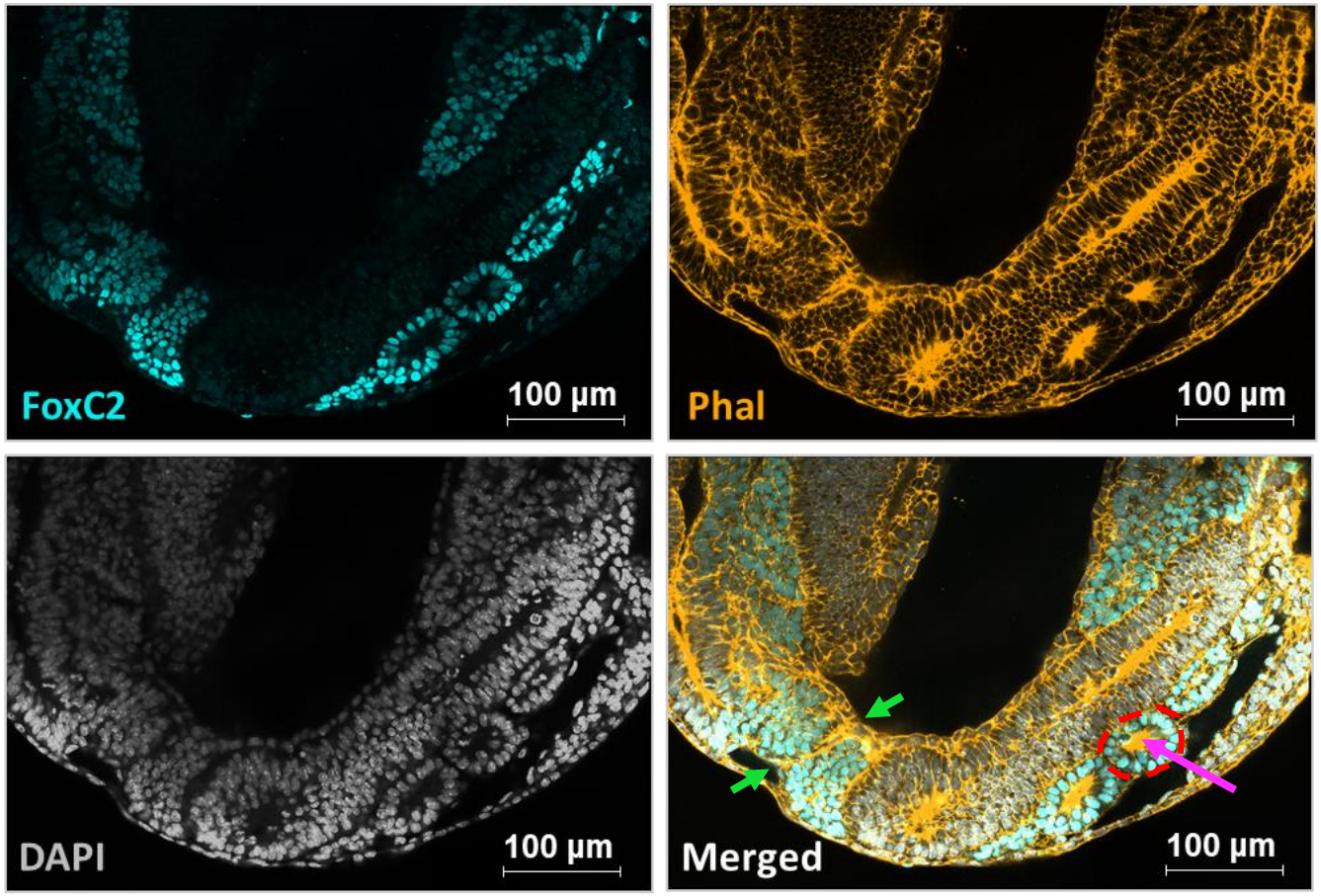

Figure 4.19. This figure depicts the somites of a wildtype embryo at E8.5. An example of a normal somite example outlined in dashed red with the central somitocoel with a pink arrow, surrounded by a monolayer of epithelial cells. The boundaries between the somites (example marked with green arrow) are distinct and the somites have a uniform shape. Stained for somite marker FoxC2 (cyan), nuclear marker DAPI (grayscale) and actin marker Phalloidin (gold). Scale bars = 100 µm.

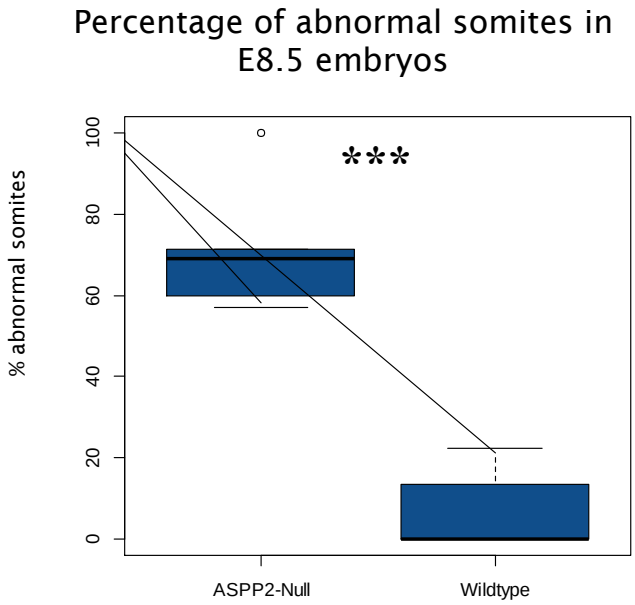

Figure 4.20. A large proportion of the somites of *ASPP2*-Null embryos are disturbed

The percentages of abnormal somites, characterised by a large, observable disruption in shape and epithelial integrity, were compared between *ASPP2*-null embryos and wildtype embryos at E8.5. *ASPP2*-null embryos have a much higher proportion of disrupted somites ($p<0.001$ (*ASPP2*-null n=6 embryos, wildtype n=11 embryos)).

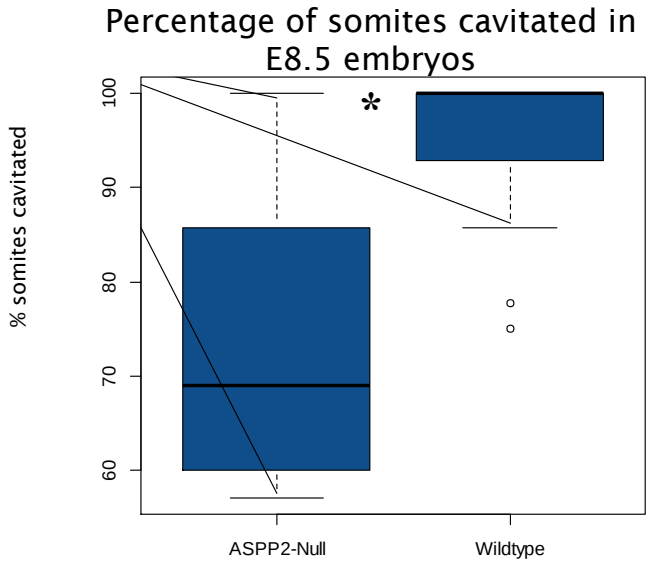

Figure 4.21. A lower proportion of the somites of *ASPP2*-Null embryos form a somitocoel

The percentages of somites that had formed a somitocoel were compared between *ASPP2*-null embryos and wildtype embryos at E8.5. *ASPP2*-null embryos have a lower proportion of cavitated somites ($p<0.05$ (*ASPP2*-null n=6 embryos, wildtype n=11 embryos)).

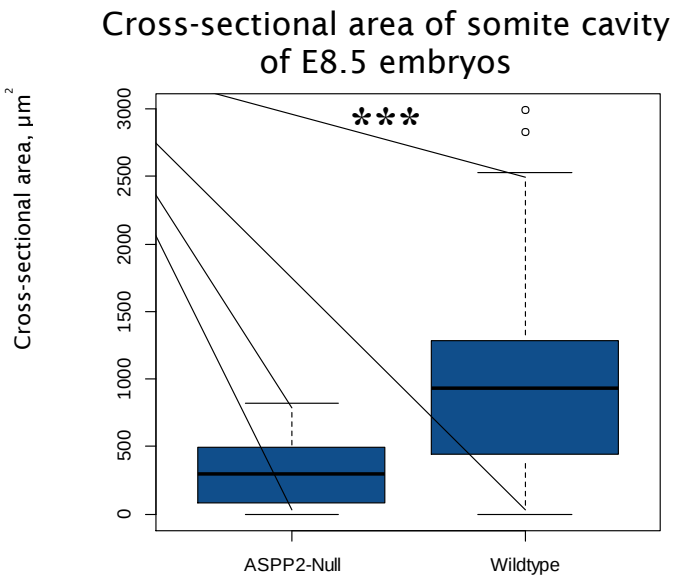

Figure 4.22. The somitocoels of *ASPP2*-Null embryos are smaller

The cross-sectional area of the somitocoels in somites of *ASPP2*-null and wildtype embryos at E8.5 were compared. *ASPP2*-null embryos have smaller somitocoels ($p<1x10^6$ (*ASPP2*-null n=34 somites from n=6 embryos, wildtype n=58 somites from n=10 embryos)).

Figure 4.23. Somites of *ASPP2*-null E9.5 embryo

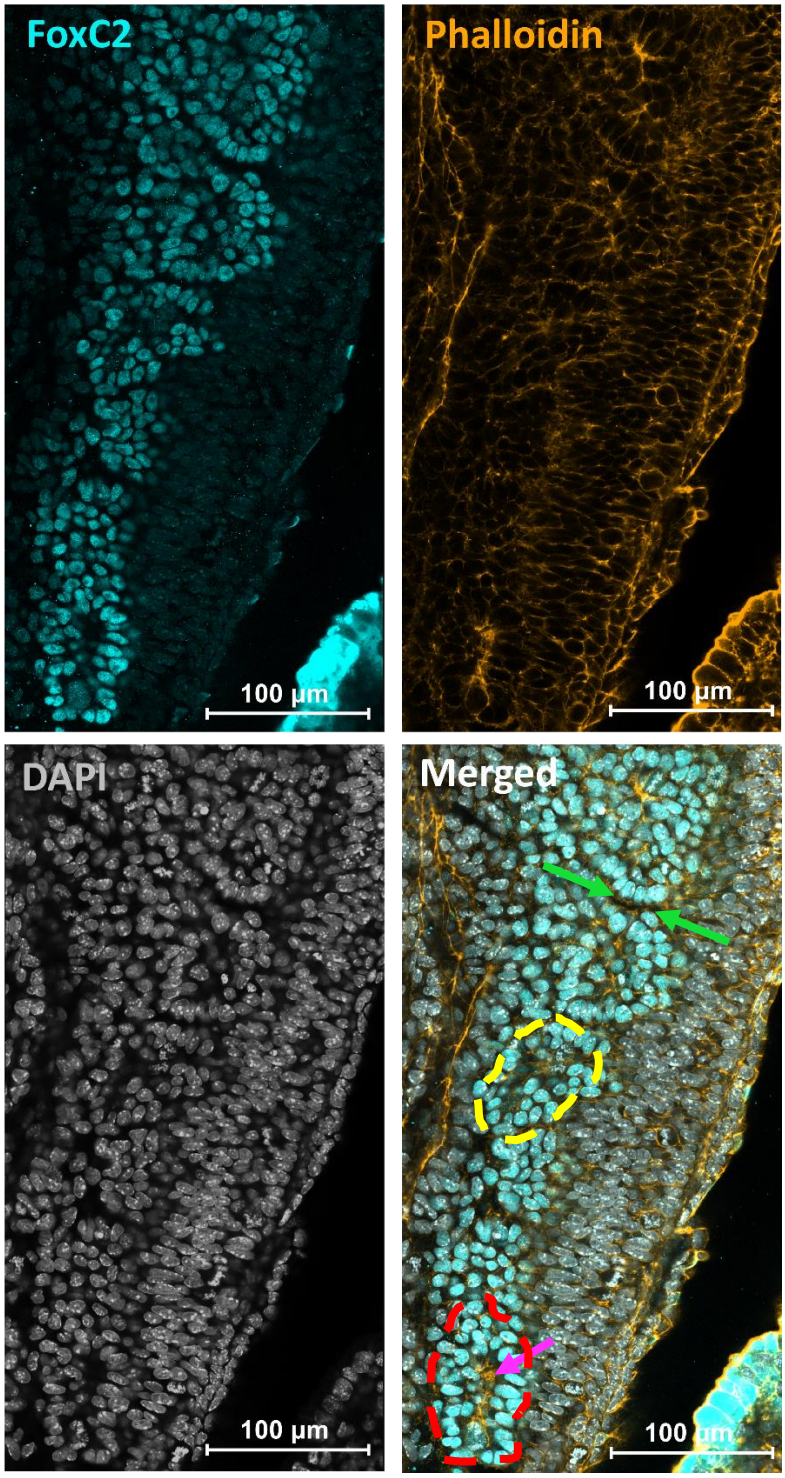

Figure 4.23. This figure depicts the somites of an *ASPP2*-null embryo at E9.5. Only some *ASPP2*-null embryos at E9.5 have somites that are distinguishable. One or two of these may develop normally - an example of this is outlined with a dashed red line. These somites have a central somitocoel (example marked with a pink arrow) surrounded by a monolayer of epithelial cells. Most somites distinguishable in *ASPP2*-null E9.5 embryos have lost this organisation (an example is outlined with a dashed yellow line). In addition, the boundaries between the somites (example marked with green arrow) are less distinct and the somites have a less uniform shape. Immunostaining for somite marker FoxC2 (cyan), nuclear marker DAPI (grayscale) and F-actin marker Phalloidin (gold). Scale bars = 100 µm.

Figure 4.24. Somites of wildtype E9.5 embryo

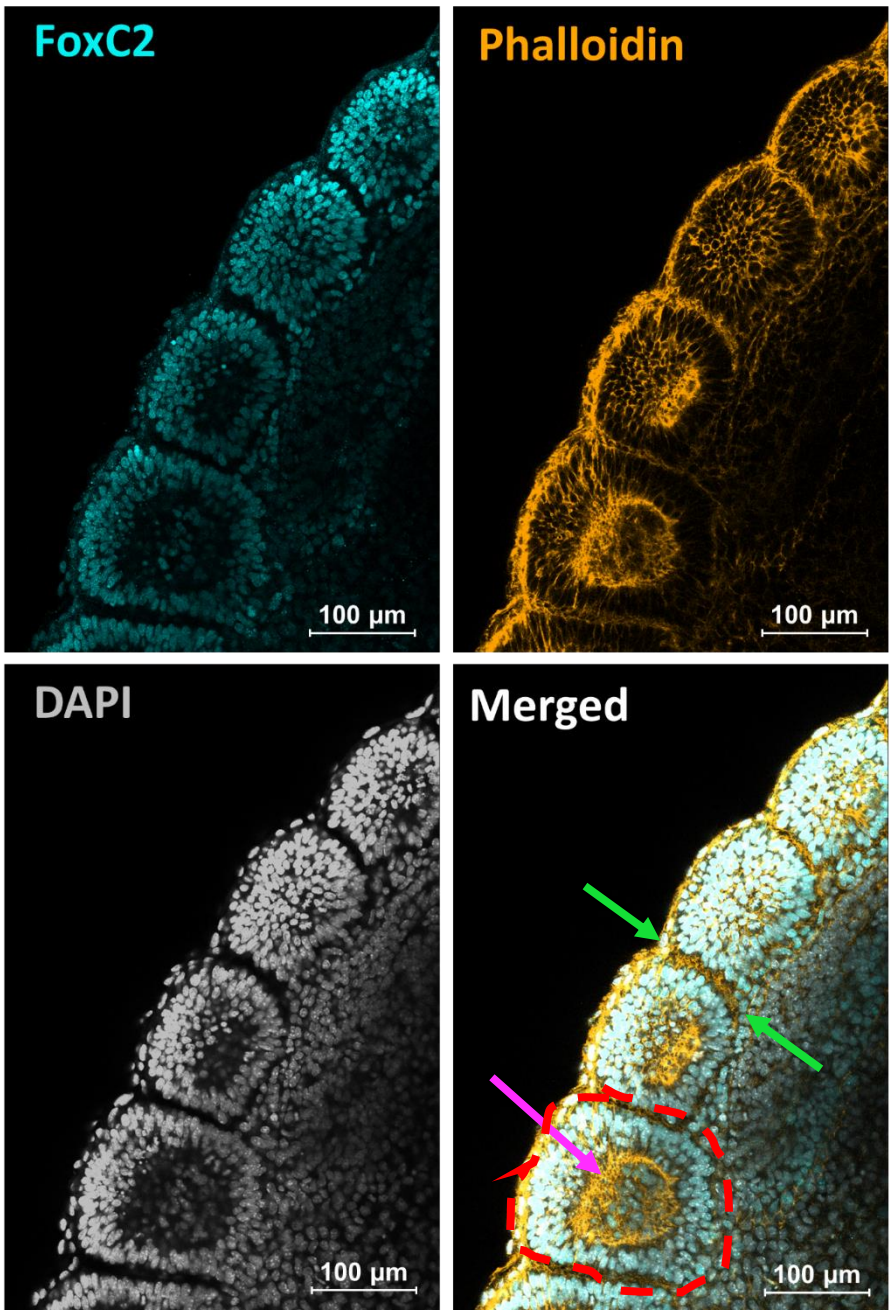

Figure 4.24. This figure depicts the somites of a wildtype embryo at E9.5. An example of a normal somite is outlined in dashed red, with the central somitocoel (marked with a pink arrow) surrounded by a monolayer of epithelial cells. The boundaries between the somites (example marked with green arrow) are distinct and the somites have a uniform shape. Immunostainings for somite marker FoxC2 (cyan), nuclear marker DAPI (grayscale) and F-actin marker Phalloidin (gold). Scale bars = 100 µm.

4.1.6 Cardiac development in *ASPP2*-null embryos

A noticeable feature of *ASPP2*$^{-/-}$ embryos is that they lack a heart structure. No heart tube structures can be observed in these embryos, despite being an obvious feature of wildtype embryos. There was little staining with cardiac marker sarcomeric alpha-actinin observed in these embryos at E9.5 (Figure 4.8, Figure 4.9). However, some sarcomeric organization does seem to be present in the mutant, suggesting that cardiomyocytes can differentiate despite the lack of tissue structure.

To investigate the cause of this absence of cardiac region, I generated knockout embryos with a deletion of *ASPP2* in Mesp1-positive mesoderm progenitor cells. As discussed in Chapter 3, I crossed *ASPP2*$^{+/-}$, *Tg*$^{+/Mesp1\text{-}Cre}$ mice to the *ASPP2*$^{flox/flox}$ mice to knock out ASPP2 expression in the cardiac tissue. Mesp1 is expressed in almost all cardiovascular precursors at E6.5, in the extraembryonic mesoderm and cranial-cardiac embryonic mesoderm at E7.5, and in the entire heart by E9.5 [129], [130]. It drives expression of Cre and therefore the excision of exon 4 of *ASPP2* in these regions.

Interestingly and unexpectedly, the embryos that are *ASPP2*-null in the cardiac lineage appear to be morphologically normal at E9.5 (Figure 4.25). Like wildtype embryos, they have a heart and also stain strongly for sarcomeric alpha-actinin. There are no obvious defects in these embryos.

Figure 4.25. Embryo (E9.5) that is *ASPP2*-null in the cardiac lineage from Mesp1

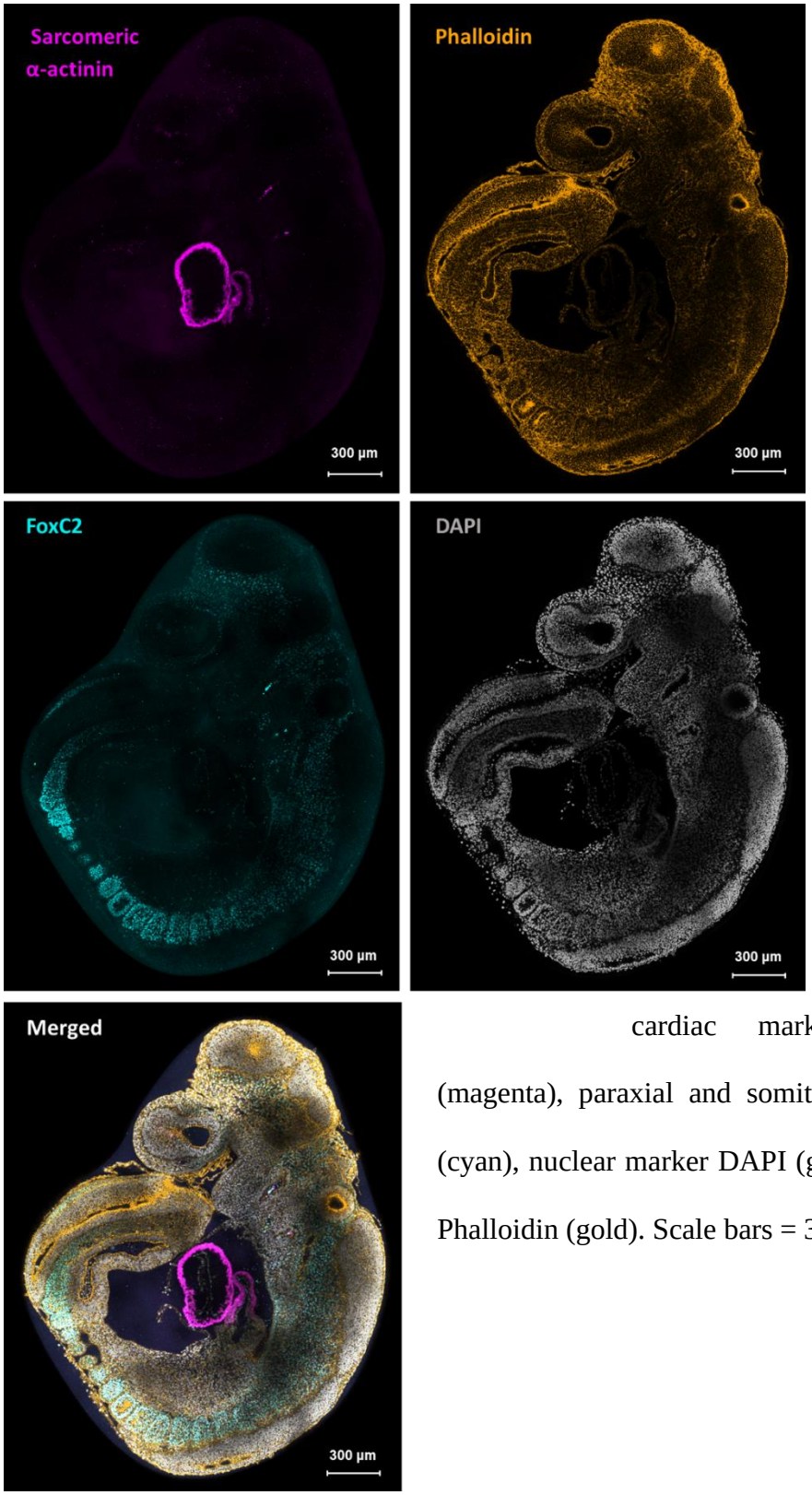

Figure 4.25. Example of a E9.5 embryo that is *ASPP2*-null in the cardiac lineage resulting from the expression of Cre in Mesp1-positive mesodermal cells. There are no noticeable defects, even in the heart, which appears to be normal. The embryo is indistinguishable morphologically from wildtype E9.5 embryos (as seen in Figure 4.25). Immunostainings for cardiac marker Sarcomeric α-actinin (magenta), paraxial and somitic mesoderm marker FoxC2 (cyan), nuclear marker DAPI (grayscale) and F-actin marker Phalloidin (gold). Scale bars = 300 µm.

Figure 4.26. Wildtype E9.5 embryo

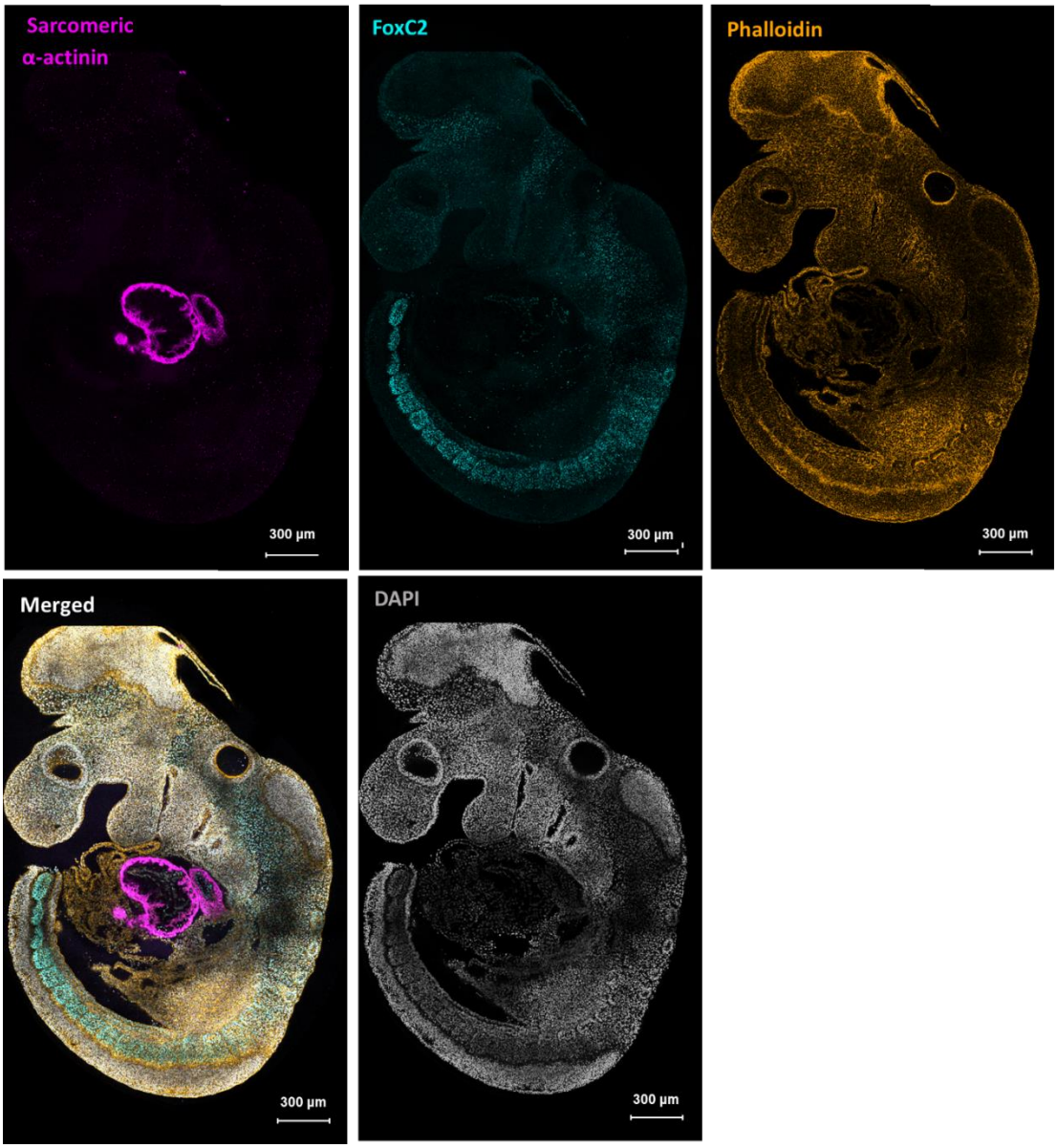

Figure 4.26. Example of a wildtype E9.5 embryo for comparison with the example that is *ASPP2*-null in the cardiac lineage from Mesp1 shown in Figure 4.25. Immunostainings for cardiac marker Sarcomeric α-actinin (magenta), paraxial and somitic mesoderm marker FoxC2 (cyan), nuclear marker DAPI (grayscale) and F-actin marker Phalloidin (gold). Scale bars = 300 µm.

4.3 Discussion

4.3.1 Gross abnormalities in embryo proper of *ASPP2*-null embryos

Major defects in the embryo proper of *ASPP2*-null embryos include the disruption of body axis elongation and an overall reduction in size when compared to wildtype embryos at E8.5. Given the many downstream effectors of ASPP2, a large variety of factors likely contribute to this phenotype.

For example, it is probable that the function of ASPP2 in controlling YAP plays a role in the small size of the *ASPP2*$^{-/-}$ embryos. ASPP2 induces the dephosphorylation and activation of YAP at tight junctions by forming a complex with PP1 [10], [11]. After activation, nuclear YAP has a wide range of important functions in the developing embryo, including the promotion of cell growth and proliferation and the attenuation of apoptosis [138]–[140]. Thus, ASPP2 may indirectly control these processes through its role in activating YAP.

When *ASPP2* expression is knocked out, activated YAP levels are predicted to be lower. *ASPP2*$^{-/-}$ embryos may therefore have a similar phenotype to *YAP*$^{-/-}$ embryos. As YAP has such a crucial role in growth of tissues, it is unsurprising that *YAP*$^{-/-}$ embryos are significantly smaller than wildtype embryos at E7.5 and later stages [142]. This size defect was also observed in E8.5 and E9.5 *ASPP2*$^{-/-}$ embryos, so it is conceivable that ASPP2's function in YAP activation may be an explanation (at least in part) for this abnormality.

Interestingly, *YAP*$^{-/-}$ embryos also exhibit defects in body axis elongation but, conversely to *ASPP2*$^{-/-}$ embryos, it is the caudal region rather than the rostral region that is most affected. In the *YAP*-null embryos, although the anterior portion of the embryo is still disrupted, the tail end is much shorter due to the failure to maintain a posterior epiblast-like epithelium. The *ASPP2*-null embryos, on the other hand, show severe anterior defects, with a very shortened rostral region.

Partial knock-out *ASPP2*$^{\Delta 3}$ embryos show over-proliferation in neural progenitors and do not exhibit the shortened anterior phenotype [7]. Overexpression of *ASPP2* in zebrafish embryos results in a shortened body but a normal size head [143]. This contrasts to my results, which demonstrate shortened anterior regions and an overall reduction in size upon deletion of ASPP2. Thus, there is some conflict with the current literature that makes the phenotype difficult to fully explain. However, the common factor of these phenotypes is that ASPP2 plays a crucial role in regulating tissue growth, resulting in disrupted growth when overexpressed or knocked out. In addition to binding growth-promoting factor YAP, ASPP2 also binds pro-apoptotic factors, including p53 [2]. Therefore, when *ASPP2* is knocked out, the resulting phenotype may be a balance of the reduced apoptosis and the reduced activation of pro-growth YAP. The partial knockout *ASPP2*$^{\Delta 3}$ model favour the pro-growth function of ASPP2, possibly by still allowing some binding to YAP. My model may knockout both the pro-growth and anti-apoptotic function of ASPP2, meaning that the CNS and anterior region of the embryo is majorly reduced in size rather than having an over-proliferation of cells.

Furthermore, some *YAP*-null at E8.5 are able to develop anterior somites and others are not. However, the somites that do form look similar to wildtype somites and do not exhibit the defects seen in the somites of *ASPP2*-null embryos. Some *YAP*-null embryos at E8.5 have initiated heart development similar to wildtype embryos. Others appear similar to *ASPP2*$^{-/-}$ embryos and have no cardiac structures.

4.3.2 Gross abnormalities in extra-embryonic membranes of *ASPP2*-null embryos

A major defect of the *ASPP2*-null embryos is the highly disrupted yolk sac that develops with the embryo growing outside the yolk sac rather than being surrounded by it. This abnormality appears

to be highly unusual; it might be the result of a defect in rostral folding, an idea supported by a roughly similar phenotype in BMP2 mutants [144]. *YAP*$^{-/-}$ embryos have yolk sac defects, but this is a very different phenotype, with the embryos instead having a distinctive rippled yolk sac appearance, coupled with the failure of yolk sac vasculogenesis [142].

Abnormal or absent yolk sacs are associated with spontaneous abortions in both mice and humans [142], [145], [146]. It is thus unsurprising that the *ASPP2*$^{-/-}$ mutation is embryonically lethal. At earlier stages, I did not observe any mesoderm migration defects and so the extraembryonic layer should be able to form.

Spontaneous regression of the yolk sac (and embryonic death) has been observed in humans. One case report found the presence of a yolk sac at 8 weeks 3 days into the pregnancy but by 10 weeks 5 days, the yolk sac was absent [147]. It is also conceivable that the yolk sac defects observed in the *ASPP2*-null mice could also be incidences of spontaneous yolk sac regression. The mouse yolk sac differs anatomically from human yolk sacs. In human development, the yolk sac is attached to, but does not envelop, the embryo. Therefore, it is difficult to compare abnormalities of the two structures. If the yolk sac did envelop the human embryo and then underwent this regression, it is possible that this would resemble the defect seen in *ASPP2*-null embryos, with the embryo proper located outside the yolk sac.

The yolk sac in E9.5 mutant embryos persists at least in small portions even when the embryo proper is highly disrupted and the embryo is clearly in the process of resorption. It could be the case that the yolk sac defect adds to the severity of the defect in the embryo, perhaps triggering the breakdown of other embryonic tissues as they become exposed and no longer surrounded by the yolk sac. In a study of spontaneous embryo resorption in mice, one particular case at E9.0 observed the resorbing embryo still surrounded by its amniotic membrane but located outside the

yolk sac [148]. Additionally, in several embryonic resorption cases at both E8.0 and E9.0, embryonic membranes including the yolk sac were absent. Therefore, it is possible that the yolk sac may begin to breakdown, and thus allow the embryo proper to burst through, as part of the resorption process.

4.3.3 Disruption of somitogenesis

Somitogenesis is another process that is clearly disturbed in *ASPP2*-null embryos. This process appears to be initiated correctly because at E8.5, there is no significant difference in the number of anterior somites between *ASPP2*-null and wildtype embryos. On the other hand, at E9.5, somitogenesis has progressed caudally in the wildtype embryos but *ASPP2*-null embryos exhibit very few to no somites. This may be due to the broad morphogenetic defects that seem to occur in *ASPP2*-null embryos at this stage. However, it may also be due to a halting in the process of somitogenesis. A possible mechanism linking ASPP2 and somitogenesis lies in β-catenin.

ASPP2 binds to β-catenin, preventing it from entering the nucleus and activating gene expression [8]. ASPP2 carries out this function by forming a complex of β-catenin–E-cadherin, which anchors β-catenin at cell-cell junctions. ASPP2 may also acts indirectly, potentiating RAS signalling, thus inhibiting β-catenin N-terminal phosphorylation [3], [8]. Knockdown of ASPP2 leads to higher levels of nuclear β-catenin and Wnt signalling.

A posterior-to-anterior gradient of nuclear β-catenin is crucial for defining the spatial periodic pattern of segments [99]. The expression of β-catenin can be stabilized in the presomitic mesoderm, by deleting the sequence recognized by complexes that targets β-catenin for degradation. This results in elevated nuclear β-catenin throughout the presomitic mesoderm (PSM). In these mutant embryos, only up to four irregular somites form in the most anterior part

of the paraxial mesoderm. However, in most cases, no somites form at all and there is no morphological boundary formation along the PSM. The anterior PSM shows signs of maturation, with expression of somite markers such as *Raldh2*, but this expression lower than that of wildtype embryos. The accumulation of nuclear β-catenin also leads to an anterior shift of the determination front and delays the activation of *Mesp2* expression, preventing expression of downstream targets of Mesp2. The requirement of a downregulation of nuclear β-catenin in order to activate Mesp2 downstream targets may explain the absence of morphological boundary formation in mutant embryos.

Thus, this may explain the somitogenesis phenotype observed in the *ASPP2*-null embryos, as ASPP2 knockdown leads to higher levels of nuclear β-catenin so it can be deduced that ASPP2 deletion will also cause nuclear β-catenin accumulation. The phenotype observed in the *ASPP2*-null embryos was very similar to that observed in the overexpressed β-catenin mutants, with some irregular anterior somites forming and boundary formation appearing to be disturbed. The β-catenin mutants have a stronger somite phenotype, likely due to functional redundancy in its upstream targets compensating for the loss of *ASPP2* in the *ASPP2*-null mutants.

4.3.4 Morphological abnormalities of somites in *ASPP2*-null embryos

Some of the morphological abnormalities of somites in *ASPP2*$^{-/-}$ embryos could be attributed to the defects resulting from nuclear β-catenin accumulation as described above. The small number of irregularly shaped somites with unclearly defined boundaries is a phenotype also seen in the overexpressed β-catenin mutants [99].

The maturation of somitic cells involves a mesenchymal-to-epithelial transition. *ASPP2*-null somites exhibit defects in epithelial organisation, with many epithelial cells lacking the classic

bottle-shape morphology and the cells forming a multi-layered structure rather than a single layer organised around the somitocoel, which is filled with mesenchymal cells.

ASPP2 plays a role in MET, also through a nuclear β-catenin pathway. By reducing its nuclear accumulation, ASPP2 prevents β-catenin from activating the zinc finger E-box binding homeobox 1 protein (ZEB1) [8]. When ASPP2 is knocked down, ZEB1 levels are increased and E-cadherin is reduced, and EMT rather than MET is promoted. The somite morphology phenotype observed in *ASPP2*$^{-/-}$ embryos may be due in part to this failure to properly execute MET. MET is important for establishing cell shape and organisation and thus this may be a contributing factor to the disrupted somites.

Providing more support for this theory is the evidence from *paraxis* mutants. Paraxis is a basic helix-loop-helix transcription factor, expressed in the PSM and somites. *Paraxis*-null mice are unable to form epithelia [149]. This phenotype is stronger than that observed when ASPP2 is deleted or knocked down. In the latter, EMT may be promoted but epithelia is still able to form [8]. Interestingly, in the *Paraxis*-null mutants, no epithelial somites form but the embryo is still able to segment into loose mesenchymal sections with approximately the correct size and periodicity of somites [149]. The fact that the somite-like sections are still roughly the same size and have boundaries forming in the correct location (albeit less sharply demarcated) indicates that disrupted MET is not behind the somitogenesis phenotype observed in *ASPP2*$^{-/-}$ embryos. However, the somites of the *Paraxis*-null embryos do resemble the somites of *ASPP2*-null embryos in that there is a loose bunch of cells, rather than an organised single layer, and the somitocoel is absent.

The *Paraxis*-null somites are more disrupted than the *ASPP2*-null somites: in *ASPP2*-null embryos, the somitocoel is absent in some somites but does form in others, although it is smaller

than that of wildtype somites. In addition, there is still some polarisation in the somite cells of *ASPP2*-null embryos. Although the cells may be arranged in a multi-layered fashion and often lack a bottle-shaped morphology, they are generally still focused around a central point. On the other hand, the somite cells of *Paraxis*-null embryos have no organisation and exist as a loose sphere of cells [149].

Therefore, the disruption, but not complete failure, of MET may be behind the abnormalities in somite and somite cell morphology in *ASPP2*-null embryos.

4.3.5 The role of ASPP2 in cardiac development

ASPP2 is critical in cardiac development as *ASPP2*-null embryos do not develop a heart. However, when *ASPP2* was deleted in the lineage resulting from the Mesp1-expressing early cardiac progenitors, these embryos developed normal hearts at E8.5 and E9.5. This implies that the perturbation in cardiac development is a secondary defect, likely caused by disturbances to the surrounding tissues meaning that the cardiac progenitors do not receive the signals they require to continue developing.

Once again, it is possible that β-catenin plays a role in this phenotype. When β-catenin is deleted in the definitive endoderm, multiple hearts form all along the anterior-posterior axis of the embryo [150]. This indicates that deletion of β-catenin changes cell fate from endodermal to precardiac mesoderm fate. Knockdown of ASPP2 causes accumulation of nuclear β-catenin, driving target gene expression [8]. Thus, *ASPP2*-null embryos likely have higher levels of β-catenin throughout the embryo. This may cause expansion of the endoderm at the cost of the precardiac mesoderm.

Cardiac mesoderm formation is thought to be promoted by signals from the anterior endoderm; when precardiac mesoderm from chick embryos is cultured in the absence of anterior endoderm,

cardiomyocytes fail to differentiate [151]. Also in chick embryos, it was found that Wnt inhibitor Crescent is present in the anterior endoderm [152]. These results suggest that cardiogenesis is induced in the precardiac mesoderm at a region of high BMP and low Wnt activity [152]. Knocking down ASPP2 leads to higher levels of Wnt signalling [8]. Deleting *ASPP2* may therefore prevent cardiogenesis by increasing Wnt activity.

The *ASPP2*$^{-/-}$, *Tg*$^{+/Mesp1\text{-}Cre}$ mice are *ASPP2*-null in the cardiac lineage but *ASPP2*-positive in the endoderm. In these mice, the endoderm should be specified normally and have normal levels of β-catenin and Wnt signalling, whilst the cardiac lineage may have higher levels of nuclear β-catenin and Wnt signalling due to the *ASPP2* knockout. In *ASPP2*-null embryos, the ubiquitously higher levels of nuclear β-catenin and Wnt signalling may prevent there from being a region of low Wnt activity to induce cardiogenesis. However, in the cardiac progenitor knockouts, the anterior endoderm will still be lower in Wnt activity and therefore, although the precardiac mesoderm has higher Wnt activity than usual, the high BMP/low Wnt region that is necessary for the induction of heart formation will still be present and so the heart will still form.

Therefore, Wnt inhibitors, such as Crescent, that are present in the anterior endoderm may be the critical factor of this phenotype. In *ASPP2*$^{-/-}$ embryos, higher levels of Wnt signalling in the anterior endoderm may mean that, although inhibitors are still produced, the inhibitors are depleted in the anterior endoderm. Thus, Wnt signalling in the precardiac mesoderm remains high and cardiogenesis cannot occur. However, in *ASPP2*$^{-/-}$, *Tg*$^{+/Mesp1\text{-}Cre}$ embryos, Wnt signalling is normal in the anterior endoderm and so the inhibitors produced here can instead act on the neighbouring precardiac mesoderm, reducing Wnt in the precardiac mesoderm and therefore inducing heart formation.

Conclusions

My research focused on elucidating the role of ASPP2 in post-implantation mouse embryogenesis. In order to do this, my project had two main aims. The first was to create mouse lines that would enable full and conditional gene knockouts of *ASPP2* in mouse embryos. The second was to analyse the embryos produced by these mouse lines to deduce the effect of deleting *ASPP2* expression as a whole and in individual tissues. By doing this, the importance of ASPP2 and the potential functions that it may have in embryogenesis could be deduced.

I produced several mouse lines to complete the first aim of my project. I then used these lines to perform initial characterisations of the role of ASPP2 in the post-implantation embryo. My results suggest that ASPP2 does not play a major role in gastrulation as all three germ layers are able to form correctly, however, it is likely that ASPP2 is important in patterning the mesoderm and regulating its epithelial architecture. When *ASPP2* was knocked out and the resulting E8.5 and E9.5 embryos were analysed, I found that the somites did not form correctly, being smaller than their wildtype counterparts and lacking the organised structure of a monolayer of cells surrounding the somitocoel. Heart formation was also perturbed, with the mutant embryos lacking a heart structure. Overall, development appeared to become progressively more disordered as it proceeded, resulting in embryonic lethality by E9.5.

Recently, Royer, myself and the Srinivas lab have shared a manuscript (titled *ASPP2/PP1 complexes maintain the integrity of pseudostratified epithelia undergoing remodelling during morphogenesis*, available at bioXriv doi:10.1101/2020.11.03.366906, shown at the end of this thesis) on our work analysing the role of ASPP2, as well as its binding partner PP1, in embryogenesis. This paper supports the findings shown in my thesis, as it demonstrates that the

ASPP2/PP1 complex is essential for post-implantation embryogenesis, in particularly during gastrulation in the primitive streak, in somites and in the head fold region, as was observed in the embryos analysed in this thesis. The results from my thesis and this manuscript suggest that there is a requirement for the ASPP2/PP1 complex in maintaining pseudostratified epithelial integrity during morphogenetic events characterised by intense tissue remodelling and high cell proliferation. Further investigations showed that the ASPP2/PP1 complex achieves this via its function in maintaining the integrity and organising the F-actin cytoskeleton at apical surfaces of dividing cells.

Overall, my results demonstrate clearly that ASPP2 is vital for embryogenesis in post-gastrulation mouse embryogenesis. This is likely because of its functions in maintaining apicobasal polarity and epithelial structure. There is still much work to be done to fully understand the functions that ASPP2 may have in embryogenesis. The mouse lines I produced will aid with this as they may be utilized in further conditional knockout experiments under the control of different tissue-specific promoters, or at different embryonic stages (such as E6.5 and E7.5). This would enable the investigation into exactly when embryogenesis appears to be perturbed. We could also deduce in what regions of the embryo and what developmental processes ASPP2 is essential for. Therefore, there is plenty that remains to be done to gain further insight into the role of ASPP2 in embryogenesis.

References

[1] K. Iwabuchi, P. L. Bartel, B. I. N. Lit, R. Marraccino, and S. F. I, "Two cellular proteins that bind to wild-type but not mutant p53," *Proc Natl Acad Sci USA*, vol. 91, no. 13, pp. 6098–6102, 1994.

[2] Y. Samuels-Lev *et al.*, "ASPP Proteins Specifically Stimulate the Apoptotic Function of p53," *Mol. Cell*, vol. 8, no. 4, pp. 781–794, 2001.

[3] Y. Wang, N. Godin-Heymann, X. Dan Wang, D. Bergamaschi, S. Llanos, and X. Lu, "ASPP1 and ASPP2 bind active RAS, potentiate RAS signalling and enhance p53 activity in cancer cells," *Cell Death Differ.*, vol. 20, no. 4, pp. 525–534, 2013, doi: 10.1038/cdd.2013.3.

[4] J. Yang, M. Hori, N. Takahashi, T. Kawabe, H. Kato, and T. Okamoto, "NF-k B subunit p65 binds to 53BP2 and inhibits cell death induced by 53BP2," *Oncogene*, vol. 18, no. 37, pp. 5177–5186, 1999.

[5] L. Naumovski and M. L. Cleary, "The p53-Binding Protein 53BP2 Also Interacts with Bcl2 and Impedes Cell Cycle Progression at G 2 / M," *Mol. Cell. Biol.*, vol. 16, no. 7, pp. 3884–3892, 1996.

[6] H. Nakagawa, K. Koyama, Y. Murata, M. Morito, T. Akiyama, and Y. Nakamura, "APCL, a central nervous system-specific homologue of adenomatous polyposis coli tumor suppressor, binds to p53-binding protein 2 and translocates it to the perinucleus," *Cancer Res.*, vol. 60, no. 1, pp. 101–105, 2000.

[7] R. Sottocornola *et al.*, "ASPP2 Binds Par-3 and Controls the Polarity and Proliferation of Neural Progenitors during CNS Development," *Dev. Cell*, vol. 19, no. 1, pp. 126–137, 2010, doi: 10.1016/j.devcel.2010.06.003.

[8] Y. Wang *et al.*, “ASPP2 controls epithelial plasticity and inhibits metastasis through β 2-catenin-dependent regulation of ZEB1,” *Nat. Cell Biol.*, vol. 16, no. 11, pp. 1092–1104, 2014, doi: 10.1038/ncb3050.

[9] N. R. Helps, H. M. Barker, S. J. Elledge, and P. T. W. Cohen, “Protein phosphatase 1 interacts with p53BP2, a protein which binds to the tumour suppressor p53,” *FEBS Lett.*, vol. 377, pp. 295–300, 1995.

[10] C. Y. Liu *et al.*, “PP1 cooperates with ASPP2 to dephosphorylate and activate TAZ,” *J. Biol. Chem.*, vol. 286, no. 7, pp. 5558–5566, 2011, doi: 10.1074/jbc.M110.194019.

[11] C. Royer *et al.*, “ASPP2 Links the Apical Lateral Polarity Complex to the Regulation of YAP Activity in Epithelial Cells,” *PLoS One*, vol. 9, no. 10, 2014.

[12] K. F. Harvey, C. M. Pfleger, and I. K. Hariharan, “The Drosophila Mst Ortholog, hippo, Restricts Growth and Cell Proliferation and Promotes Apoptosis,” *Cell*, vol. 114, pp. 457–467, 2003.

[13] S. Pantalacci, N. Tapon, and P. Léopold, “The Salvador partner Hippo promotes apoptosis and cell-cycle exit in Drosophila,” *Nat. Cell Biol.*, vol. 5, no. 10, 2003, doi: 10.1038/ncb1051.

[14] S. Wu, J. Huang, J. Dong, and D. Pan, “Hippo Encodes a Ste-20 Family Protein Kinase that Restricts Cell Proliferation and Promotes Apoptosis in Conjunction with salvador and warts,” *Cell*, vol. 114, pp. 445–456, 2003.

[15] R. W. Justice, D. F. Woods, and P. J. Bryant, “The Drosophila tumor suppressor gene warts encodes a homolog o-f human myotonic dystrophy kinase and is required for the control of cell shape and proliferation,” *Genes Dev.*, pp. 534–546, 1995.

[16] C. Royer and X. Lu, “Epithelial cell polarity: a major gatekeeper against cancer?,” *Cell*

Death Differ., vol. 18, no. 9, p. 1470-1477, 2011.

[17] B. Zhao *et al.*, "Inactivation of YAP oncoprotein by the Hippo pathway is involved in cell contact inhibition and tissue growth control," *Genes Dev.*, vol. 21, pp. 2747–2761, 2007, doi: 10.1101/gad.1602907.Hpo/Sav.

[18] S. Wu, Y. Liu, Y. Zheng, J. Dong, and D. Pan, "The TEAD / TEF Family Protein Scalloped Mediates Transcriptional Output of the Hippo Growth-Regulatory Pathway," *Dev. Cell*, vol. 14, no. March, pp. 388–398, 2008, doi: 10.1016/j.devcel.2008.01.007.

[19] X. Varelas, "The Hippo pathway effectors TAZ and YAP in development, homeostasis and disease," *Development*, vol. 141, no. 8, pp. 1614–1626, 2014, doi: 10.1242/dev.102376.

[20] X. Espanel and M. Sudol, "Yes-associated Protein and p53-binding Protein-2 Interact through Their WW and SH3 Domains," *J. Biol. Chem.*, vol. 276, no. 17, pp. 14514–14523, 2001, doi: 10.1074/jbc.M008568200.

[21] N. Sabherwal and N. Papalopulu, "Apicobasal polarity and cell proliferation during development," *Essays Biochem.*, vol. 53, pp. 95–109, 2012, doi: 10.1042/BSE0530095.

[22] E. Assémat, E. Bazellières, E. Pallesi-pocachard, A. Le Bivic, and D. Massey-harroche, "Polarity complex proteins," *Biochim. Biophys. Acta - Biomembr.*, vol. 1778, no. 3, pp. 614–630, 2008, doi: 10.1016/j.bbamem.2007.08.029.

[23] W. Meng and M. Takeichi, "Adherens Junction: Molecular Architecture and Regulation," *Cold Spring Harb. Perspect. Med.*, vol. 1, no. 6, 2009, doi: 10.1098/rstb.1989.0070.

[24] M. A. Odenwald *et al.*, "ZO-1 interactions with F-actin and occludin direct epithelial polarization and single lumen specification in 3D culture," *J. Cell Sci.*, vol. 130, no. 1, pp. 243–259, 2017, doi: 10.1242/jcs.188185.

[25] K. Umeda *et al.*, "ZO-1 and ZO-2 Independently Determine Where Claudins Are

Polymerized in Tight-Junction Strand Formation," *Cell*, vol. 126, no. 4, pp. 741–754, 2006, doi: 10.1016/j.cell.2006.06.043.

[26] S. H. Kim, Z. Li, and D. B. Sacks, "E-cadherin-mediated Cell-Cell Attachment Activates Cdc42," *J. Biol. Chem.*, vol. 275, no. 47, pp. 36999–37005, 2000, doi: 10.1074/jbc.M003430200.

[27] S. K. Kim, "Cell polarity: new PARtners for Cdc42 and Rac," *Nat. Cell Biol.*, vol. 2, no. August, pp. 143–145, 2000.

[28] S. M. Garrard, C. T. Capaldo, L. Gao, M. K. Rosen, I. G. Macara, and D. R. Tomchick, "Structure of Cdc42 in a complex with the GTPase-binding domain of the cell polarity protein, Par6," *EMBO J.*, vol. 22, no. 5, pp. 1125–1133, 2003.

[29] J. Betschinger, K. Mechtler, and J. A. Knoblich, "The Par complex directs asymmetric cell division by phosphorylating the cytoskeletal protein Lgl," *Nature*, vol. 422, pp. 326–330, 2003, doi: 10.1038/nature01440.1.

[30] T. Yamanaka, Y. Horikoshi, N. Izumi, A. Suzuki, K. Mizuno, and S. Ohno, "Lgl mediates apical domain disassembly by suppressing the PAR-3 – aPKC – PAR-6 complex to orient apical membrane polarity," *J. Cell Sci.*, vol. 119, no. 10, pp. 2107–2118, 2006, doi: 10.1242/jcs.02938.

[31] Y. Izumi *et al.*, "An Atypical PKC Directly Associates and Colocalizes at the Epithelial Tight Junction with ASIP, a Mammalian Homologue of Caenorhabditis elegans Polarity Protein PAR-3," *J. Cell Biol.*, vol. 143, pp. 95–106, 1998.

[32] K. Campbell, E. Knust, and H. Skaer, "Crumbs stabilises epithelial polarity during tissue remodelling," *J. Cell Sci.*, vol. 122, no. 15, pp. 2604–2612, 2009.

[33] G. Tanentzapf and U. Tepass, "Interactions between the crumbs, lethal giant larvae and

bazooka pathways in epithelial polarization," *Nat. Cell Biol.*, vol. 5, no. 1, pp. 46–52, 2003, doi: 10.1038/ncb896.

[34] E. Morais-de-Sá, V. Mirouse, and D. St Johnston, "aPKC Phosphorylation of Bazooka Defines the Apical/Lateral Border in Drosophila Epithelial Cells," *Cell*, vol. 141, no. 3, pp. 509–523., 2010.

[35] D. Michel, J. Arsanto, D. Massey-Harroche, C. Béclin, J. Wijnholds, and A. Le Bivic, "PATJ connects and stabilizes apical and lateral components of tight junctions in human intestinal cells," *J. Cell Sci.*, vol. 118, pp. 4049–4057, 2005, doi: 10.1242/jcs.02528.

[36] K. Shin, S. Straight, and B. Margolis, "PATJ regulates tight junction formation and polarity in mammalian epithelial cells," *J. Cell Biol.*, vol. 168, no. 5, pp. 705–711, 2005, doi: 10.1083/jcb.200408064.

[37] X. Chen and I. G. Macara, "Par-3 controls tight junction assembly through the Rac exchange factor Tiam1," *Nat. Cell Biol.*, vol. 7, no. 3, pp. 262–269, 2005, doi: 10.1038/ncb1226.

[38] W. Cong *et al.*, "ASPP2 regulates epithelial cell polarity through the PAR complex," *Curr. Biol.*, vol. 20, no. 15, pp. 1408–1414, 2010, doi: 10.1016/j.cub.2010.06.024.

[39] R. Pey, C. Vial, G. Schatten, and M. Hafner, "Increase of intracellular Ca2+ and relocation of E-cadherin during experimental decompaction of mouse embryos," *Proc. Natl. Acad. Sci.*, vol. 95, no. 22, pp. 12977–12982, 2002, doi: 10.1073/pnas.95.22.12977.

[40] M. Zhu, C. Y. Leung, M. N. Shahbazi, and M. Zernicka-Goetz, "Actomyosin polarisation through PLC-PKC triggers symmetry breaking of the mouse embryo," *Nat. Commun.*, vol. 8, no. 1, 2017, doi: 10.1038/s41467-017-00977-8.

[41] C. M. Pauken and D. G. Capco, "The expression and stage-specific localization of protein kinase C isotypes during mouse preimplantation development," *Dev. Biol.*, vol. 223, no. 2,

pp. 411–421, 2000, doi: 10.1006/dbio.2000.9763.

[42] B. Plusa *et al.*, “Downregulation of Par3 and aPKC function directs cells towards the ICM in the preimplantation mouse embryo,” *J. Cell Sci.*, vol. 118, no. 3, pp. 505–515, 2005, doi: 10.1242/jcs.01666.

[43] S. Vinot, T. Le, S. Ohno, T. Pawson, B. Maro, and S. Louvet-Valle, “Asymmetric distribution of PAR proteins in the mouse embryo begins at the 8-cell stage during compaction,” *Dev. Biol.*, vol. 282, no. 2, pp. 307–319, 2005, doi: 10.1016/j.ydbio.2005.03.001.

[44] N. Nishioka *et al.*, “Tead4 is required for specification of trophectoderm in pre-implantation mouse embryos,” *Mech. Dev.*, vol. 125, pp. 270–283, 2008, doi: 10.1016/j.mod.2007.11.002.

[45] N. Nishioka *et al.*, “The Hippo Signaling Pathway Components Lats and Yap Pattern Tead4 Activity to Distinguish Mouse Trophectoderm from Inner Cell Mass,” *Dev. Cell*, vol. 16, no. 3, pp. 398–410, 2009, doi: 10.1016/j.devcel.2009.02.003.

[46] L. Wolpert, *Principles of Development, 5th Edition*. Oxford: OU Press, 2015.

[47] B. Sheth *et al.*, “Differentiation of the epithelial apical junctional complex during mouse preimplantation development: a role for rab13 in the early maturation of the tight junction,” *Mech. Dev.*, vol. 97, no. 1–2, pp. 93–104, 2002, doi: 10.1016/s0925-4773(00)00416-0.

[48] L. Larue, M. Ohsugi, J. Hirchenhain, and R. Kemler, “E-cadherin null mutant embryos fail to form a trophectoderm epithelium,” *Proc. Natl. Acad. Sci.*, vol. 91, no. 17, pp. 8263–7, 1994, [Online]. Available: http://www.ncbi.nlm.nih.gov/pubmed/8058792%0Ahttp://www.pubmedcentral.nih.gov/articlerender.fcgi?artid=PMC44586.

[49] L. C. Barcroft, H. Offenberg, P. Thomsen, and A. J. Watson, “Aquaporin proteins in murine trophectoderm mediate transepithelial water movements during cavitation,” *Dev. Biol.*, vol. 256, no. 2, pp. 342–354, 2003, doi: 10.1016/S0012-1606(02)00127-6.

[50] A. J. Watson and G. M. Kidder, “Immunofluorescence assessment of the timing of appearance and cellular distribution of Na/K-ATPase during mouse embryogenesis,” *Dev. Biol.*, vol. 126, no. 1, pp. 80–90, 1988, doi: 10.1016/0012-1606(88)90241-2.

[51] C. Simon, S. Rahman, D. Raina, C. Schröter, and A. Hadjantonakis, “Live Visualization of ERK Activity in the Mouse Blastocyst Reveals Lineage-Specific Signaling Dynamics,” *Dev. Cell*, vol. 53, no. 5, pp. 341–353, 2020.

[52] E. L. Parr, H. N. Tung, and M. B. Parr, “Apoptosis as the Mode of Uterine Epithelial Cell Death during Embryo Implantation in Mice and Rats,” *Biol. Reprod.*, vol. 36, no. 1, pp. 211–225, 2005, doi: 10.1095/biolreprod36.1.211.

[53] A. Joswig, H.-D. Gabriel, M. Kibschulll, and E. Winterhager, “Apoptosis in uterine epithelium and decidua in response to implantation: evidence for two difrerent pathways,” *Reprod. Biol. Endocrinol.*, vol. 9, pp. 1–9, 2003.

[54] B. M. Bany and J. C. Cross, “Post-implantation mouse conceptuses produce paracrine signals that regulate the uterine endometrium undergoing decidualization,” *Dev. Biol.*, vol. 294, no. 2, pp. 445–456, 2006, doi: 10.1016/j.ydbio.2006.03.006.

[55] B. L. M. Hogan, A. R. Cooper, and M. Kurkinen, “Incorporation into Reichert’s membrane of laminin-like extracellular proteins synthesized by parietal endoderm cells of the mouse embryo,” *Dev. Biol.*, vol. 80, no. 2, pp. 289–300, 1980, doi: 10.1016/0012-1606(80)90405-4.

[56] I. Bedzhov and M. Zernicka-Goetz, “Self-organizing properties of mouse pluripotent cells

initiate morphogenesis upon implantation," *Cell*, vol. 156, no. 5, pp. 1032–1044, 2014, doi: 10.1016/j.cell.2014.01.023.

[57] N. Christodoulou *et al.*, "Sequential formation and resolution of multiple rosettes drive embryo remodelling after implantation," *Nat. Cell Biol.*, vol. 20, pp. 1278–1289, 2018.

[58] K. Takaoka *et al.*, "The mouse embryo autonomously acquires anterior-posterior polarity at implantation," *Dev. Cell*, vol. 10, no. 4, pp. 451–459, 2006, doi: 10.1016/j.devcel.2006.02.017.

[59] K. Takaoka, M. Yamamoto, and H. Hamada, "Origin and role of distal visceral endoderm , a group of cells that determines anterior – posterior polarity of the mouse embryo," *Nat. Publ. Gr.*, vol. 13, no. 7, pp. 743–752, 2011, doi: 10.1038/ncb2251.

[60] D. Mesnard, M. Guzman-Ayala, and D. B. Constam, "Nodal specifies embryonic visceral endoderm and sustains pluripotent cells in the epiblast before overt axial patterning," *Development*, vol. 4, no. May, 2006, doi: 10.1242/dev.02413.

[61] M. Yamamoto *et al.*, "Antagonism between Smad1 and Smad2 signaling determines the site of distal visceral endoderm formation in the mouse embryo," *J. Cell Biol.*, vol. 184, no. 2, pp. 323–334, 2009, doi: 10.1083/jcb.200808044.

[62] C. Kimura, K. Yoshinaga, E. Tian, M. Suzuki, S. Aizawa, and I. Matsuo, "Visceral endoderm mediates forebrain development by suppressing posteriorizing signals," *Dev. Biol.*, vol. 225, no. 2, pp. 304–321, 2000, doi: 10.1006/dbio.2000.9835.

[63] P. Liu, M. Wakamiya, M. J. Shea, U. Albrecht, R. R. Behringer, and A. Bradley, "Requirement for Wnt3 in vertebrate axis formation," *Nat. Genet.*, vol. 22, no. 4, pp. 361–365, 1999, doi: 10.1038/11932.

[64] J. Brennan, C. C. Lu, D. P. Norris, T. A. Rodriguez, R. S. P. Beddington, and E. J.

Robertson, “Nodal signalling in the epiblast patterns the early mouse embryo,” *Nature*, vol. 411, no. 6840, pp. 965–969, 2001, doi: 10.1038/35082103.

[65] P. H. Crossley and G. R. Martin, “The mouse Fgf8 gene encodes a family of polypeptides and is expressed in regions that direct outgrowth and patterning in the developing embryo,” *Development*, vol. 121, no. 2, pp. 439–451, 1995.

[66] B. Herrmann, “Expression pattern of the Brachyury gene in whole-mount TWis/TWis mutant embryos,” *Development*, vol. 113, no. 3, pp. 913–917, 1991.

[67] M. Williams, C. Burdsal, A. Periasamy, M. Lewandoski, and A. Sutherland, “The mouse primitive streak forms in situ by initiation of epithelial to mesenchymal transition without migration of a cell population,” *Dev. Dyn.*, vol. 241, no. 2, pp. 270–283, 2012.

[68] X. Sun, E. N. Meyers, M. Lewandoski, and G. R. Martin, “Targeted disruption of Fgf8 causes failure of cell migration in the gastrulating mouse embryo,” *Genes Dev.*, vol. 13, no. 14, pp. 1834–1846, 1999, doi: 10.1101/gad.13.14.1834.

[69] B. Ciruna and J. Rossant, “FGF Signaling Regulates Mesoderm Cell Fate Specification and Morphogenetic Movement at the Primitive Streak,” *Dev. Cell*, vol. 1, no. 1, pp. 37–49, 2001, doi: 10.1016/S1534-5807(01)00017-X.

[70] S. Nowotschin and A. K. Hadjantonakis, “Cellular dynamics in the early mouse embryo: from axisformation to gastrulation,” *Curr Opin Genet Dev*, vol. 71, no. 2, pp. 233–236, 2013, doi: 10.1038/mp.2011.182.doi.

[71] G. Winnier, M. Blessing, P. A. Labosky, and B. L. M. Hogan, “Bone morphogenetic protein-4 is required for mesoderm formation and patterning in the mouse,” *Genes Dev.*, vol. 9, no. 17, pp. 2105–2116, 1995, doi: 10.1101/gad.9.17.2105.

[72] S. J. Kinder, T. E. Tsang, G. A. Quinlan, A. K. Hadjantonakis, A. Nagy, and P. P. Tam,

"The orderly allocation of mesodermal cells to the extraembryonic structures and the anteroposterior axis during gastrulation of the mouse embryo.," *Development*, vol. 126, no. 21, pp. 4691–701, 1999, [Online]. Available: http://www.ncbi.nlm.nih.gov/pubmed/10518487.

[73] B. Staveley, "Molecular & Developmental Biology (BIOL3530)," *Memorial University of Newfoundland*. http://www.mun.ca/biology/desmid/brian/BIOL3530/DB_03/DBNVert1.html (accessed May 10, 2020).

[74] S. J. Arnold and E. J. Robertson, "Making a commitment: Cell lineage allocation and axis patterning in the early mouse embryo," *Nat. Rev. Mol. Cell Biol.*, vol. 10, no. 2, pp. 91–103, 2009, doi: 10.1038/nrm2618.

[75] P. P. Tam and R. S. Beddington, "Establishment and organization of germ layers in the gastrulating mouse embryo," *Ciba Found Symp.*, vol. 165, pp. 25–49, 1992.

[76] M. Viotti, S. Nowotschin, and A. Hadjantonakis, "SOX17 links gut endoderm morphogenesis and germ layer segregation," *Nat. Cell Biol.*, vol. 16, pp. 1146–1156, 2014.

[77] G. S. Kwon and A. K. Hadjantonakis, "Transthyretin mouse transgenes direct RFP expression or Cre-mediated recombination throughout the visceral endoderm," *Genesis*, vol. 47, no. 7, pp. 447–455, 2009, doi: 10.1002/dvg.20522.

[78] B. P. Davidson and P. P. L. Tam, "The node of the mouse embryo," *Curr. Biol.*, vol. 10, no. 17, pp. R617–R619, 2000, doi: 10.1016/s0960-9822(00)00675-8.

[79] M. Fujinaga, "Development of sidedness of asymmetric bodyexpression of theTGFb-family memberleftyin mouse embryos.structures in vertebrates," *Int. J. Dev. Biol.*, vol. 41, pp. 153–186, 1997.

[80] R. C. Tyser, A. M. Miranda, C. Chen, S. M. Davidson, S. Srinivas, and P. R. Riley, "Calcium handling precedes cardiac differentiation to initiate the first heartbeat," *Elife*, vol. 5, pp. 1–25, 2016, doi: 10.7554/elife.17113.

[81] M. Buckingham, S. Meilhac, and S. Zaffran, "Building the mammalian heart from two sources of myocardial cells," *Nat. Rev. Genet.*, vol. 6, no. 11, pp. 826–835, 2005, doi: 10.1038/nrg1710.

[82] R. G. Kelly, M. E. Buckingham, and A. F. Moorman, "Heart fields and cardiac morphogenesis," *Cold Spring Harb. Perspect. Med.*, vol. 4, no. 10, pp. 1–11, 2014, doi: 10.1101/cshperspect.a015750.

[83] D. Galli, J. N. Dominguez, S. Zaffran, A. Munk, N. A. Brown, and M. E. Buckingham, "Atrial myocardium derives from the posterior region of the second heart field, which acquires left-right identity as Pitx2c is expressed," *Development*, vol. 135, no. 6, pp. 1157–1167, 2008, doi: 10.1242/dev.014563.

[84] C. H. Mjaatvedt *et al.*, "The outflow tract of the heart is recruited from a novel heart-forming field," *Dev. Biol.*, vol. 238, no. 1, pp. 97–109, 2001, doi: 10.1006/dbio.2001.0409.

[85] O. W. J. Prall *et al.*, "An Nkx2-5/Bmp2/Smad1 negative feedback loop controls second heart field progenitor specification and proliferation," *Cell*, vol. 128, no. 5, pp. 947–959, 2010.

[86] R. Jain *et al.*, "Integration of Bmp and Wnt signaling by Hopx specifies commitment of cardiomyoblasts," *Science (80-.).*, vol. 348, pp. 1–8, 2015, doi: 10.4172/2157-7633.1000305.Improved.

[87] A. Bernardo *et al.*, "BRACHYURY and CDX2 mediate BMP-induced differentiation of human and mouse pluripotent stem cells into embryonic and extraembryonic lineages," *Cell*

Stem Cell, vol. 9, no. 2, pp. 144–155, 2011.

[88] J. Epstein, H. Aghajanian, and M. Singh, "Semaphorin signaling in cardiovascular development," *Cell Metab.*, vol. 21, no. 2, pp. 163–173, 2015.

[89] S. Savolainen, J. F. Foley, and S. A. Elmore, "Histology Atlas of the Developing Mouse Heart," *Toxicol. Pathol.*, vol. 37, no. 4, pp. 395–414, 2009, doi: 10.1177/0192623309335060.Histology.

[90] J. Cooke and E. C. Zeeman, "A clock and wavefront model for control of the number of repeated structures during animal morphogenesis," *J. Theor. Biol.*, vol. 58, no. 2, pp. 455–476, 1976, doi: 10.1016/S0022-5193(76)80131-2.

[91] H. Hirata *et al.*, "Instability of Hes7 protein is crucial for the somite segmentation clock," *Nat. Genet.*, vol. 36, no. 7, pp. 750–754, 2004, doi: 10.1038/ng1372.

[92] Y. Niwa, Y. Masamizu, T. Liu, R. Nakayama, C. X. Deng, and R. Kageyama, "The Initiation and Propagation of Hes7 Oscillation Are Cooperatively Regulated by Fgf and Notch Signaling in the Somite Segmentation Clock," *Dev. Cell*, vol. 13, no. 2, pp. 298–304, 2007, doi: 10.1016/j.devcel.2007.07.013.

[93] Y. Bessho, R. Sakata, S. Komatsu, K. Shiota, S. Yamada, and R. Kageyama, "Dynamic expression and essential functions of," *Genes Dev.*, pp. 2642–2647, 2001, doi: 10.1101/gad.930601.2642.

[94] J. K. Dale, M. Maroto, M.-L. Dequeant, P. Malapert, M. McGrew, and O. Pourquie, "Periodic Notch inhibition by Lunatic Fringe underlies the chick segmentation clock," *Nature*, vol. 421, no. 6920, pp. 275–278, 2003, doi: 10.1038/nature01244.

[95] L. Herrgen, S. Ares, L. G. Morelli, C. Schröter, F. Jülicher, and A. C. Oates, "Intercellular coupling regulates the period of the segmentation clock," *Curr. Biol.*, vol. 20, no. 14, pp.

1244–1253, 2010, doi: 10.1016/j.cub.2010.06.034.

[96] Y. Bessho, H. Hirata, Y. Masamizu, and R. Kageyama, “Periodic repression by the bHLH factor Hes7 is an essential mechanism for the somite segmentation clock,” *Genes Dev.*, vol. 17, no. 12, pp. 1451–1456, 2003, doi: 10.1101/gad.1092303.

[97] M.-L. Dequéant, “A Complex Oscillating Network of Signaling Genes Underlies the Mouse Segmentation Clock Mary-Lee Dequéant,” *Science (80-.).*, vol. 1595, no. 2006, pp. 1595–1599, 2013, doi: 10.1126/science.1133141.

[98] A. Aulehla *et al.*, “Wnt3a plays a major role in the segmentation clock controlling somitogenesis,” *Dev. Cell*, vol. 4, no. 3, pp. 395–406, 2003, doi: 10.1016/S1534-5807(03)00055-8.

[99] A. Aulehla *et al.*, “A β-catenin gradient links the clock and wavefront systems in mouse embryo segmentation,” *Nat. Cell Biol.*, vol. 10, p. 186, Dec. 2007, [Online]. Available: https://doi.org/10.1038/ncb1679.

[100] A. Sawada, M. Shinya, Y. J. Jiang, A. Kawakami, A. Kuroiwa, and H. Takeda, “Fgf/MAPK signalling is a crucial positional cue in somite boundary formation.,” *Development*, vol. 128, no. 23, pp. 4873–80, 2001, [Online]. Available: http://www.ncbi.nlm.nih.gov/pubmed/11731466.

[101] R. D. Del Corral and K. G. Storey, “Opposing FGF and retinoid pathways: A signalling switch that controls differentiation and patterning onset in the extending vertebrate body axis,” *BioEssays*, vol. 26, no. 8, pp. 857–869, 2004, doi: 10.1002/bies.20080.

[102] J. Dubrulle, M. J. Mcgrew, O. Pourquie, C. De Luminy, and M. Cedex, “and Regulates Segmentation Clock Control of Spatiotemporal Hox Gene Activation,” *Cell*, vol. 106, pp. 219–232, 2001.

[103] N. Sasaki, M. Kiso, M. Kitagawa, and Y. Saga, “The repression of Notch signaling occurs via the destabilization of mastermind-like 1 by Mesp2 and is essential for somitogenesis,” *Development*, vol. 138, no. 1, pp. 55–64, 2011, doi: 10.1242/dev.055533.

[104] Y. Saga, “Segmental border is defined by the key transcription factor Mesp2, by means of the suppression of Notch activity,” *Dev. Dyn.*, vol. 236, no. 6, pp. 1450–1455, 2007, doi: 10.1002/dvdy.21143.

[105] M. Oginuma, Y. Niwa, D. L. Chapman, and Y. Saga, “Mesp2 and Tbx6 cooperatively create periodic patterns coupled with the clock machinery during mouse somitogenesis,” *Development*, vol. 135, no. 15, pp. 2555–2562, 2008, doi: 10.1242/dev.019877.

[106] J. Takahashi *et al.*, “Analysis of Ripply1/2-deficient mouse embryos reveals a mechanism underlying the rostro-caudal patterning within a somite,” *Dev. Biol.*, vol. 342, no. 2, pp. 134–145, 2010, doi: 10.1016/j.ydbio.2010.03.015.

[107] I. Del Barco Barrantes *et al.*, “Interaction between Notch signalling and Lunatic fringe during somite boundary formation in the mouse,” *Curr. Biol.*, vol. 9, no. 9, pp. 470–480, 1999, doi: 10.1016/S0960-9822(99)80212-7.

[108] A. Barrios, R. J. Poole, L. Durbin, C. Brennan, N. Holde, and S. W. Wilson, “Eph/Ephrin Signaling Regulates the Mesenchymal-to-Epithelial Transition of the Paraxial Mesodermduring Somite Morphogenesis,” *Curr. Biol.*, vol. 13, pp. 1571–1582, 2003.

[109] T. Watanabe, Y. Sato, D. Saito, R. Tadokoro, and Y. Takahashi, “EphrinB2 coordinates the formation of a morphological boundary and cell epithelialization during somite segmentation,” *Proc. Natl. Acad. Sci.*, vol. 106, no. 18, pp. 7467–7472, 2009, doi: 10.1073/pnas.0902859106.

[110] A. Girós, K. Grgur, A. Gossler, and M. Costell, “α5β1 Integrin-Mediated Adhesion to

Fibronectin Is Required for Axis Elongation and Somitogenesis in Mice," *PLoS One*, vol. 6, no. 11, 2011.

[111] B. Christ, R. Huang, and M. Scaal, "Amniote somite derivatives," *Dev. Dyn.*, vol. 236, no. 9, pp. 2382–2396, 2007, doi: 10.1002/dvdy.21189.

[112] P. C. Spear and C. A. Erickson, "Interkinetic Nuclear Migration: A Mysterious Process in Search of a Function," *Dev Growth Differ.*, vol. 54, no. 3, pp. 306–316, 2012.

[113] S. Srinivas, "Imaging cell movements in egg-cylinder stage mouse embryos," *Cold Spring Harb. Protoc.*, vol. 5, no. 12, pp. 1386–1394, 2010, doi: 10.1101/pdb.prot5539.

[114] B. Sauer and N. Henderson, "Site-specific DNA recombination in mammalian cells by the Cre recombinase of bacteriophage P1," *PNAS*, vol. 85, pp. 5166–5170, 2011, [Online]. Available: papers3://publication/uuid/F3833F0A-D564-4C62-BE97-744A709E3AA5.

[115] N. Sternberg and D. Hamilton, "Bacteriophage P1 site-specific recombination," *J. Mol. Biol.*, vol. 150, pp. 467–486, 2004, doi: 10.1016/0022-2836(81)90384-3.

[116] V. Vives *et al.*, "ASPP2 is a haploinsufficient tumor suppressor that cooperates with p53 to suppress tumor growth," *Genes Dev.*, vol. 20, no. 10, pp. 1262–1267, 2006, doi: 10.1101/gad.374006.

[117] K. M. Kampa *et al.*, "Apoptosis-stimulating protein of p53 (ASPP2) heterozygous mice are tumor-prone and have attenuated cellular damage-response thresholds," *PNAS*, vol. 106, no. 11, pp. 4390–4395, 2009.

[118] M. R. Capecchi, M. J. Evans, and O. Smithies, "Gene Modification in Mice." https://www.nobelprize.org/prizes/medicine/2007/advanced-information/.

[119] R. M. Quadros, D. W. Harms, M. Ohtsuka, and C. B. Gurumurthy, "Insertion of sequences at the original provirus integration site of mouse ROSA26 locus using the CRISPR/Cas9

system," *FEBS Open Bio.*, vol. 5, pp. 191–197, 2015.

[120] H. Wang *et al.*, "One-step generation of mice carrying mutations in multiple genes by CRISPR/Cas-mediated genome engineering," *Cell*, vol. 153, no. 4, pp. 910–918, 2013.

[121] Addgene, "Addgene CRISPR guide," *Addgene*. https://www.addgene.org/guides/crispr/.

[122] M. M. Simon *et al.*, "A comparative phenotypic and genomic analysis of C57BL/6J and C57BL/6N mouse strains," *Genome Biol.*, vol. 14, no. 7, pp. 1–22, 2013, doi: 10.1186/gb-2013-14-7-r82.

[123] M. J. Mattapallil *et al.*, "The Rd8 mutation of the Crb1 gene is present in vendor lines of C57BL/6N mice and embryonic stem cells, and confounds ocular induced mutant phenotypes.," *Invest. Ophthalmol. Vis. Sci.*, vol. 53, no. 6, pp. 2921–2927, 2012, doi: 10.1167/iovs.12-9662.

[124] A. K. Mehalow *et al.*, "CRB1 is essential for external limiting membrane integrity and photoreceptor morphogenesis in the mammalian retina," *Hum. Mol. Genet.*, vol. 12, no. 17, pp. 2179–2190, 2003, doi: 10.1093/hmg/ddg232.

[125] M. H. Roh *et al.*, "The Maguk protein, Pals1, functions as an adapter, linking mammalian homologues of Crumbs and Discs Lost," *J. Cell Biol.*, vol. 157, no. 1, pp. 161–172, 1999, doi: 10.1083/jcb.200109010.

[126] S. A. Van De Pavert, A. Kantardzhieva, A. Malysheva, J. Meuleman, I. Versteeg, and J. Wijnholds, "Crumbs homologue 1 is required for maintenance of photoreceptor cell polarization and adhesion during light exposure," *J. Cell Sci.*, vol. 117, no. 18, pp. 4169–4177, 2004, doi: 10.1242/jcs.01301.

[127] Z. Xiao *et al.*, "Deficiency in Crumbs Homolog 2 (Crb2) Affects Gastrulation and Results in Embryonic Lethality in Mice," *Dev. Dyn.*, vol. 240, pp. 2646–2656, 2011, doi:

10.1002/dvdy.22778.

[128] M. Davisson, T. H. Roderick, and D. Doolittle, “Recombination percentages and chromosomal assignments,” in *Mouse Genetic Variants and Strains of the Laboratory*, M. F. Lyon and A. Searle, Eds. Oxford: Oxford University Press, 1989, pp. 432–505.

[129] Y. Saga, S. Kitajima, and S. Miyagawa-Tomita, “Mesp1 expression is the earliest sign of cardiovascular development,” *Trends Cardiovasc. Med.*, vol. 10, no. 8, pp. 345–352, 2000, doi: 10.1016/S1050-1738(01)00069-X.

[130] Y. Saga, N. Hata, and S. Kobayashi, “MesP1: a novel basic helix-loop-helix protein expressed in the nascent mesodermal cells during mouse gastrulation,” …, vol. 2778, pp. 2769–2778, 1996, [Online]. Available: http://dev.biologists.org/content/122/9/2769.short.

[131] A. Avilion, S. Nicolis, L. Pevny, L. Perez, N. Vivian, and R. Lovell-Badge, “Multipotent cell lineages in early mouse development depend on SOX2 function,” *Genes Dev.*, vol. 17, no. 1, pp. 126–140, 2003, doi: 10.1101/gad.224503.derm.

[132] S. Hayashi, P. Lewis, L. Pevny, and A. P. McMahon, “Efficient gene modulation in mouse epiblast using a Sox2Cre transgenic mouse strain,” *Mech. Dev.*, vol. 5, pp. 97–101, 2002.

[133] S. Feil, N. Valtcheva, and R. Feil, “Inducible Cre Mice,” in *Gene Knockout Protocols: Second Edition*, W. Wurst and R. Kühn, Eds. Totowa, NJ: Humana Press, 2009, pp. 343–363.

[134] C. Royer *et al.*, “ASPP2/PP1 complexes maintain the integrity of pseudostratified epithelia undergoing remodelling during morphogenesis,” *bioRxiv*, pp. 1–23, 2020, [Online]. Available: https://doi.org/10.1101/2020.11.03.366906.

[135] I. Desbaillets, U. Ziegler, P. Groscurth, and M. Gassmann, “Gene Manipulation and Integrative Physiology Embryoid bodies : an in vitro model of mouse embryogenesis,” *Exp.*

phyisology, vol. 85, no. 6, pp. 645–651, 2000.

[136] M. M. Shen and P. Leder, “Leukemia inhibitory factor is expressed by the preimplantation uterus and selectively blocks primitive ectoderm formation in vitro.,” *Proc. Natl. Acad. Sci.*, vol. 89, no. 17, pp. 8240–8244, 2006, doi: 10.1073/pnas.89.17.8240.

[137] T. C. Doetschman, H. Eistetter, M. Katz, W. Schmidt, and R. Kemler, “The in vitro development of blastocyst-derived embryonic stem cell lines: formation of visceral yolk sac, blood islands and myocardium.,” *J. Embryol. Exp. Morphol.*, vol. 87, pp. 27–45, 1985, [Online]. Available: http://www.ncbi.nlm.nih.gov/pubmed/3897439.

[138] C. G. Hansen, Y. L. D. Ng, W. L. M. Lam, S. W. Plouffe, and K. L. Guan, “The Hippo pathway effectors YAP and TAZ promote cell growth by modulating amino acid signaling to mTORC1,” *Cell Res.*, vol. 25, no. 12, pp. 1299–1313, 2015, doi: 10.1038/cr.2015.140.

[139] J. Dong *et al.*, “Elucidation of a Universal Size-Control Mechanism in Drosophila and Mammals,” *Cell*, vol. 130, no. 6, pp. 1120–1133, 2007, doi: 10.1016/j.cell.2007.07.019.

[140] S. Strano *et al.*, “Physical Interaction with Yes-associated Protein Enhances p73 Transcriptional Activity,” *J. Biol. Chem.*, vol. 276, no. 18, pp. 15164–15173, 2001, doi: 10.1074/jbc.M010484200.

[141] Y. Tao and X. J. Liu, “The majority of resorptions in old mice are euploid,” *PLoS One*, vol. 10, no. 12, pp. 1–9, 2015, doi: 10.1371/journal.pone.0143360.

[142] E. M. Morin-Kensicki *et al.*, “Defects in Yolk Sac Vasculogenesis , Chorioallantoic Fusion and Embryonic Axis Elongation in Mice with Targeted Disruption of Yap65,” *Mol. Cell. Biol.*, vol. 26, no. 1, pp. 77–87, 2006, doi: 10.1128/MCB.26.1.77.

[143] C. Liu *et al.*, “Aspp2 negatively regulates body growth but not developmental timing by modulating IRS signaling in zebrafish embryos,” *Gen. Comp. Endocrinol.*, vol. 197, pp. 82–

91, 2014, doi: 10.1016/j.ygcen.2013.12.006.

[144] M. Madabhushi and E. Lacy, “Anterior visceral endoderm directs ventral morphogenesis and placement of head and heart via BMP2 expression,” *Dev. Cell*, vol. 21, no. 5, pp. 907–919, 2011, doi: 10.1016/j.devcel.2011.08.027.

[145] F. N. Cho, S. N. Chen, M. H. Tai, and T. L. Yang, “The quality and size of yolk sac in early pregnancy loss,” *Aust. New Zeal. J. Obstet. Gynaecol.*, vol. 46, no. 5, pp. 413–418, 2006, doi: 10.1111/j.1479-828X.2006.00627.x.

[146] S. Moradan and M. Forouzeshfar, “Are abnormal yolk sac characteristics important factors in abortion rates?,” *Int. J. Fertil. Steril.*, vol. 6, no. 2, pp. 127–130, 2012.

[147] E. Mara and G. S. Foster, “Spontaneous regression of a yolk sac associated with embryonic death,” *J. Ultrasound Med.*, vol. 19, no. 9, pp. 655–656, 2000, doi: 10.7863/jum.2000.19.9.655.

[148] L. E. Flores, T. B. Hildebrandt, A. A. Kühl, and B. Drews, “Early detection and staging of spontaneous embryo resorption by ultrasound biomicroscopy in murine pregnancy,” *Reprod. Biol. Endocrinol.*, vol. 12, no. 1, pp. 1–12, 2014, doi: 10.1186/1477-7827-12-38.

[149] R. Burgess, A. Rawls, D. Brown, A. Bradley, and E. N. Olson, “Requirement of the paraxis gene for somite formation and musculoskeletal patterning,” *Nature*, vol. 384, pp. 570–573, 1996.

[150] H. Lickert, S. Kutsch, Y. Tamai, M. M. Taketo, and R. Kemler, “Formation of Multiple Hearts in Mice followingDeletion of Beta-cateninin the Embryonic Endoderm,” *Dev. Cell*, vol. 3, pp. 171–181, 2002.

[151] Y. Sugi and J. Lough, “Anterior endoderm is a specific effector of terminal cardiac myocyte differentiation of cells from the embryonic heart forming region,” *Dev. Dyn.*, vol. 200, no.

2, pp. 155–162, 1994, doi: 10.1002/aja.1002000207.

[152] M. J. Marvin, G. Di Rocco, A. Gardiner, S. M. Bush, and A. B. Lassar, “Inhibition of Wnt activity induces heart formation from posterior mesoderm,” *Genes Dev.*, vol. 15, no. 3, pp. 316–327, 2001, doi: 10.1101/gad.855501.

[153] N. Li, C. Xie, and N. Lu, “Crosstalk between Hippo signalling and miRNAs in tumour progression,” *Febs J.*, vol. 284, no. 7, pp. 1045–1055, 2016.

[154] C. E. Murry and G. Keller, “Differentiation of Embryonic Stem Cells to Clinically Relevant Populations: Lessons from Embryonic Development,” *Cell*, vol. 132, no. 4, pp. 661–680, 2008, doi: 10.1016/j.cell.2008.02.008.

[155] T. Yabe and S. Takada, “Molecular mechanism for cyclic generation of somites: Lessons from mice and zebrafish,” *Dev Growth Differ.*, vol. 58, pp. 31–42, 2016

ASPP2/PP1 complexes maintain the integrity of pseudostratified epithelia undergoing remodelling during morphogenesis

Christophe Royer[1]*, Elizabeth Sandham[1], Elizabeth Slee[2], Jonathan Godwin[1,3], Nisha Veits[1], Holly Hathrell[1], Felix Zhou[2], Karolis Leonavicius[1,4], Jemma Garratt[1,5], Tanaya Narendra[1,5], Anna Vincent[5], Celine Jones[6], Tim Child[5,6], Kevin Coward[6], Chris Graham[6], Xin Lu[2] and Shankar Srinivas[1]*

[1]Department of Physiology, Anatomy and Genetics, University of Oxford, Oxford OX1 3QX, United Kingdom.

[2]Ludwig Institute for Cancer Research, Nuffield Department of Medicine, University of Oxford, Oxford OX3 7DQ, United Kingdom.

[3]Department of Biochemistry, University of Oxford, South Parks Road, Oxford OX1 3QU, United Kingdom.

[4]Current address: Institute of Biotechnology, Vilnius University, Vilnius, Lithuania.

[5]Oxford Fertility, Institute of Reproductive Sciences, Oxford Business Park North, Oxford, OX4 2HW, United Kingdom.

[6]Nuffield Department of Women's and Reproductive Health, University of Oxford, Level 3, Women's Centre, John Radcliffe Hospital, Headington, Oxford, OX3 9DU, United Kingdom.

*e-mail: christophe.royer@dpag.ox.ac.uk; shankar.srinivas@dpag.ox.ac.uk

ABSTRACT

During development, pseudostratified epithelia undergo large scale morphogenetic events associated with increased mechanical stress. The molecular mechanisms that maintain tissue integrity in this context are poorly understood. Using a variety of genetic and imaging approaches, we uncover that the ASPP2/PP1 complex ensures proper epiblast and proamniotic cavity architecture via a mechanism that specifically prevents the most apical daughter cells from delaminating apically following cell division events. The ASPP2/PP1 complex achieves this by maintaining the integrity and organisation of the F-actin cytoskeleton at the apical surface of dividing cells. ASPP2/PP1 is also essential during gastrulation in the primitive streak, in somites and in the head fold region, suggesting that this complex is required across a wide range of pseudostratified epithelia during morphogenetic events that are accompanied by intense tissue remodelling and high cell proliferation. Finally, our study also suggests that the interaction between ASPP2 and PP1 is essential to the tumour suppressor function of ASPP2 which may be particularly relevant in the context of tissues that are subject to increased mechanical stress.

INTRODUCTION

Pseudostratified epithelia are common building blocks and organ precursors throughout embryonic development in a wide array of organisms[1]. As in other epithelia, their cells establish and maintain apical-basal polarity. However, their high nuclear density, high proliferation rate and nuclei movement during interkinetic nuclear migration (IKNM) make them unique. As IKNM proceeds, mitotic cells round up at the apical surface of the epithelium before dividing. During this process, mitotic cells generate enough force to locally distort the shape of the epithelium[2] or accelerate invagination[3]. During development, pseudostratified epithelia are also subject to large scale morphogenetic events that dramatically affect their shape and organisation. This is particularly true during gastrulation when cells apically constrict in the primitive streak as they push their cell body basally to eventually delaminate into the underlying mesoderm cell layer[4–7] or when the ectoderm is reshaped to form the head folds. The combined mechanical strains due to IKNM and morphogenetic events poses an incredible challenge for pseudostratified epithelia to maintain tissue integrity during development. However, the molecular mechanisms that allow them to cope with increased mechanical stress are poorly defined.

During these morphogenetic events, epithelial cells continually rely on apical constrictions involving specific F-actin cytoskeleton organisation and actomyosin contractility to modify tissue shape and organisation[8,9]. As cells apically constrict, the coupling of apical junctions to the actomyosin network is essential in transmitting forces across tissues[10]. Reciprocally, as apical constrictions reshape the apical domain of epithelial cells, apical junctions must be able to withstand the forces generated to maintain tissue integrity. Apical-basal polarity components, such as Par3, are vital for apical constrictions[11] and the integrity of apical junctions[12]. However, it remains unknown how components of the apical-basal polarity machinery maintain tissue integrity in conditions of increased mechanical stress as morphogenetic events occur.

ASPP2 is a Par3 interactor and component of the apical junctions[13,14]. Here, using a variety of genetic and imaging approaches, we show that during morphogenetic events crucial for the normal development of the early post-implantation embryo, ASPP2 maintains epithelial integrity in pseudostratified epithelia under increased mechanical stress. ASPP2 is required for proamniotic cavity formation, the maintenance of primitive streak architecture, somite structure and head fold formation. In the proamniotic cavity, ASPP2 maintains epithelial architecture by preventing apical daughter cells from escaping the epiblast. Mechanistically, we show that this is achieved via the ability of ASPP2 to directly recruit protein phosphatase 1 and through its essential role in maintaining F-actin cytoskeleton organisation at the apical junctions. Our results show that ASPP2 is an essential component of a system that maintains tissue integrity under conditions of increased mechanical stress in a broad range of tissues.

RESULTS

The phosphatase and polarity function of ASPP2 are not required for trophectoderm development

ASPP2 can regulate both apical-basal cell polarity and the phosphorylation status of YAP/TAZ through its interaction with Par3[13,14] and PP1[15,16] respectively. Both cell polarity and the phosphorylation of YAP and TAZ are crucial to trophectoderm (TE) development[17–21]. We therefore started with the hypothesis that ASPP2 may be important for outside cell polarisation and TE fate determination during preimplantation development. In support of this, we found that ASPP2 could start to be detected as early as E2.5 at cell-cell junctions (Figure S1A). As seen in other examples of polarised epithelia[13,14,16,22], ASPP2 was strongly localised to the apical junction in the TE from the 32-cell stage onwards (Figure 1A). This localisation pattern was similar in human blastocysts, suggesting that ASPP2 behaves in a similar way across mammals (Figure S1B).

A Previous study revealed that ASPP2 may play a role during early embryogenesis, as ASPP2-mutant embryos in which exons 10-17 were deleted could not be recovered at E6.5[23]. However, the phenotype of these embryos was not described, and earlier stages were not examined. To investigate the role of ASPP2 during preimplantation development we generated *ASPP2*-null embryos in which exon 4 was deleted (*ASPP2*$^{\Delta E4/\Delta E4}$) resulting in a frameshift and early stop codons. To be able to distinguish between phenotypes relating to ASPP2's PP1 regulatory function and other functions, we also generated embryos homozygous for a mutant form of ASPP2 that was specifically unable to associate with PP1 (*ASPP2*$^{RAKA/RAKA}$)[24]. *ASPP2*$^{\Delta E4/\Delta E4}$ and *ASPP2*$^{RAKA/RAKA}$ blastocysts appeared to be morphologically normal with properly formed blastocyst cavities (Figure 1B and S1C). YAP was clearly nuclear in the TE and cytoplasmic in the inner cell mass (ICM) suggesting that the ICM and TE lineage

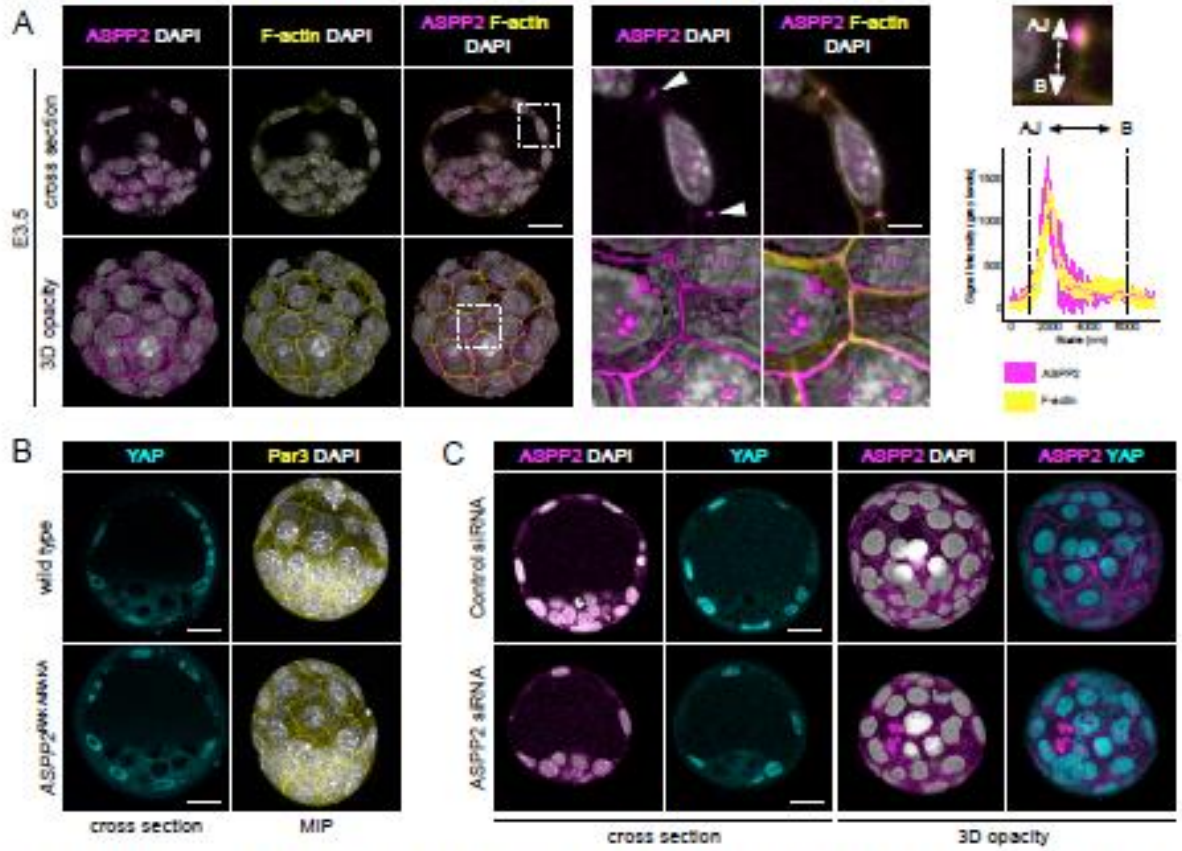

Figure 1: The ASPP2/PP1 complex is not required during preimplantation development. A. ASPP2 was detected by indirect immunofluorescence in E3.5 embryos at the early blastocyst stage to analyse its localisation pattern. A cross section through the equatorial plane of a representative embryo is shown (top row), as well as a 3D opacity rendering of the same embryo (bottom row). The F-actin cytoskeleton and nuclei were visualised using Phalloidin and DAPI respectively. A magnified image of the dashed area is shown on the right. Note how ASPP2 colocalises with F-actin at the apical junctions in cells of the trophectoderm (TE) (white arrowheads). This is quantified in the juxtaposed graph showing ASPP2 and F-actin signal intensity along the apical-basal axis of cell-cell junctions. AJ: apical junction; B: base of the trophectoderm. Scale bars: 20 µm and 5 µm (for the magnification). B. The localisation pattern of YAP and Par3 were analysed in wild type and *ASPP2*$^{RAKA/RAKA}$ embryos by indirect immunofluorescence. A cross section of representative embryos through the equatorial plane shows the localisation of YAP in the nuclei of the TE in both wild type and *ASPP2*$^{RAKA/RAKA}$ embryos. Maximum intensity projections of these embryos show the localisation of Par3 at the level of apical junctions in the TE. Scale bar: 20 µm. C. ASPP2 knockdown in E3.5 embryos using siRNA against ASPP2 mRNA. ASPP2 knockdown was confirmed by indirect immunofluorescence. Note how signal at the apical junctions is specific to ASPP2. Note how YAP is normally localised to the nuclei of TE cells in ASPP2-depleted embryos. Scale bar: 20 µm.

were properly allocated (Figure 1B). The polarity protein Par3 (Figure 1B) and F-actin cables (Figure S1C) were strongly localised at the apical junctions, suggesting that polarity and overall cell architecture were normal. It was sometimes possible to see some residual ASPP2 protein at the apical junction in early *ASPP2*$^{\Delta E4/\Delta E4}$ blastocysts, potentially due to residual maternal ASPP2 expression. To eliminate the possibility that perdurance of maternally encoded ASPP2 compensates for the zygotic mutations, we microinjected 1-cell embryo with siRNA against ASPP2 and cultured them to the blastocyst stage. Control and ASPP2-depleted embryos were morphologically indistinguishable. The localisation of YAP was similar between control and ASPP2-depleted embryos (Figure 1C). YAP phosphorylation at Serine 127 was stronger in the cytoplasm of ICM cells in comparison to the TE in both controls and ASPP2-depleted embryos (Figure S1D). Taken together, these results show that neither ASPP2's polarity function nor its PP1 regulatory function are required during preimplantation development.

ASPP2/PP1 interaction is required for proamniotic cavity architecture

Since it has previously been shown that deletion of ASPP2 may be embryonic lethal around E6.5[23], we next investigated whether ASPP2 was required at early post-implantation stages. To test this, we generated *ASPP2*$^{\Delta E4/\Delta E4}$ embryos at different stages and examined the localisation of Par6 and F-actin to assess apical-basal polarity and overall tissue organisation, respectively. At E5.5, *ASPP2*$^{\Delta E4/\Delta E4}$ embryos did not exhibit obvious morphological defects in comparison to wild type and heterozygous litter mates. Polarised Par6 could be detected at the apical membrane in the visceral endoderm (VE) and the epiblast, suggesting that both cell layers properly polarised (Figure S2A). In contrast, E6.5 *ASPP2*$^{\Delta E4/\Delta E4}$ embryos exhibited strong morphological defects in comparison to wild type and heterozygous litter mates. The proamniotic cavity either entirely failed to form (6 embryos out of 10 mutants) or was greatly reduced in size at E6.5 (4 embryos out of 10 mutants) (Figure 2A) and always absent at E7.5 (Figure S2B). In embryos lacking a proamniotic cavity, the epiblast was disorganised, and instead of being a pseudostratified epithelium, appeared multi-layered. This seemed to be the result of an ectopic accumulation of cells from the epiblast in place of the proamniotic cavity. The ectopic cells in the centre of the embryo exhibited a complete lack of polarised Par6 and in embryos with reduced cavity size, the accumulated cells showed reduced apical Par6 (Figure 2B). This suggested that the ectopic accumulation of cells where the proamniotic cavity ought to be was accompanied by a progressive loss of cell polarity in the epiblast. F-actin localisation was also profoundly abnormal in these cells (Figure 2B). In wild type embryos, F-actin was enriched at apical junctions, whereas in *ASPP2*$^{\Delta E4/\Delta E4}$ embryos it was distributed more uniformly across the apical surface (Figure 2C). This suggests that ASPP2 is required for organising the F-actin cytoskeleton at the apical junctions.

Because signals from the basement membrane are believed to be essential for proamniotic cavity formation[25], we examined the localisation of laminin and found it unaltered in *ASPP2*$^{\Delta E4/\Delta E4}$ embryos. This suggested that the loss of cell polarity and ectopic accumulation of cells was not accompanied by, or due to, breakage in the basement membrane (Figure 2D and 2E). Finally, when we examined the basolateral membrane marker SCRIB, we observed that its basolateral localisation was unaffected in *ASPP2*$^{\Delta E4/\Delta E4}$ embryos. However, SCRIB was also strongly expressed at the apical junctions in the epiblast of wild type embryos. This particular localisation pattern was intermittently disrupted in *ASPP2*$^{\Delta E4/\Delta E4}$ embryos, specifically at the interface between cells of the epiblast and cells ectopically accumulating in the proamniotic cavity (Figure 2F and 2G). Together, these results suggest that the apparent loss of apical cell polarity seen is *ASPP2*$^{\Delta E4/\Delta E4}$ embryos originates from defects specific to the apical junctions rather than at the level of the basolateral or basement membranes.

The outside VE monolayer epithelium also normally expresses ASPP2 (Figure 5A and S5A and B) but was intact and exhibited apical Par6 in *ASPP2*$^{\Delta E4/\Delta E4}$ mutants (Figure 2A), suggesting that its epithelial architecture and integrity was maintained and that ASPP2 is required specifically in the epiblast at this stage. To verify that an epiblast specific requirement for ASPP2 led to the failure of proamniotic cavity formation in *ASPP2*$^{\Delta E4/\Delta E4}$ embryos, we conditionally ablated ASPP2 expression in just the epiblast (*ASPP2*$^{epi\Delta E4/\Delta E4}$ embryos) (Figure S2C). These embryos phenocopied *ASPP2*$^{\Delta E4/\Delta E4}$ embryos, demonstrating that at this stage, ASPP2 is required only in the epiblast.

To test whether this requirement for ASPP2 is rooted in its ability to recruit and regulate PP1, we analysed *ASPP2*$^{RAKA/RAKA}$ embryos at E6.5. We found that *ASPP2*$^{RAKA/RAKA}$ embryos, similarly to *ASPP2*$^{\Delta E4/\Delta E4}$ embryos, exhibit either reduced proamniotic cavity size or no cavity at all. This was again accompanied by a reduced apical Par6 in the epiblast when the proamniotic cavity was of reduced size and absence of apical Par6 when no cavity was present (Figure 2H and 2I). The basolateral localisation of SCRIB once again was not affected, whereas its localisation at apical junctions was severely disrupted in *ASPP2*$^{RAKA/RAKA}$ embryos (Figure S2D and S2E). This shows that at E6.5, *ASPP2*$^{RAKA/RAKA}$ mutant embryos have an identical phenotype to *ASPP2*$^{\Delta E4/\Delta E4}$ mutant embryos, demonstrating the key role of the ASPP2/PP1 interaction in regulating epiblast and proamniotic cavity architecture.

ASPP2 controls apical daughter cell reincorporation into the epiblast.

Our results so far show that ASPP2 is essential for the architecture of the epiblast and the formation of the proamniotic cavity. When ASPP2's function is impaired, apolar cells accumulate ectopically in place of the proamniotic cavity. However, it remained unclear how this occurred and what biological process ASPP2 actually controls in the epiblast. Amongst possible explanations is that the phenotype was the consequence of epiblast cells delaminating apically into the proamniotic cavity because of a drastic shift in the proportion of orthogonal cells divisions, a breakdown of the apical junction domain, a failure of daughter

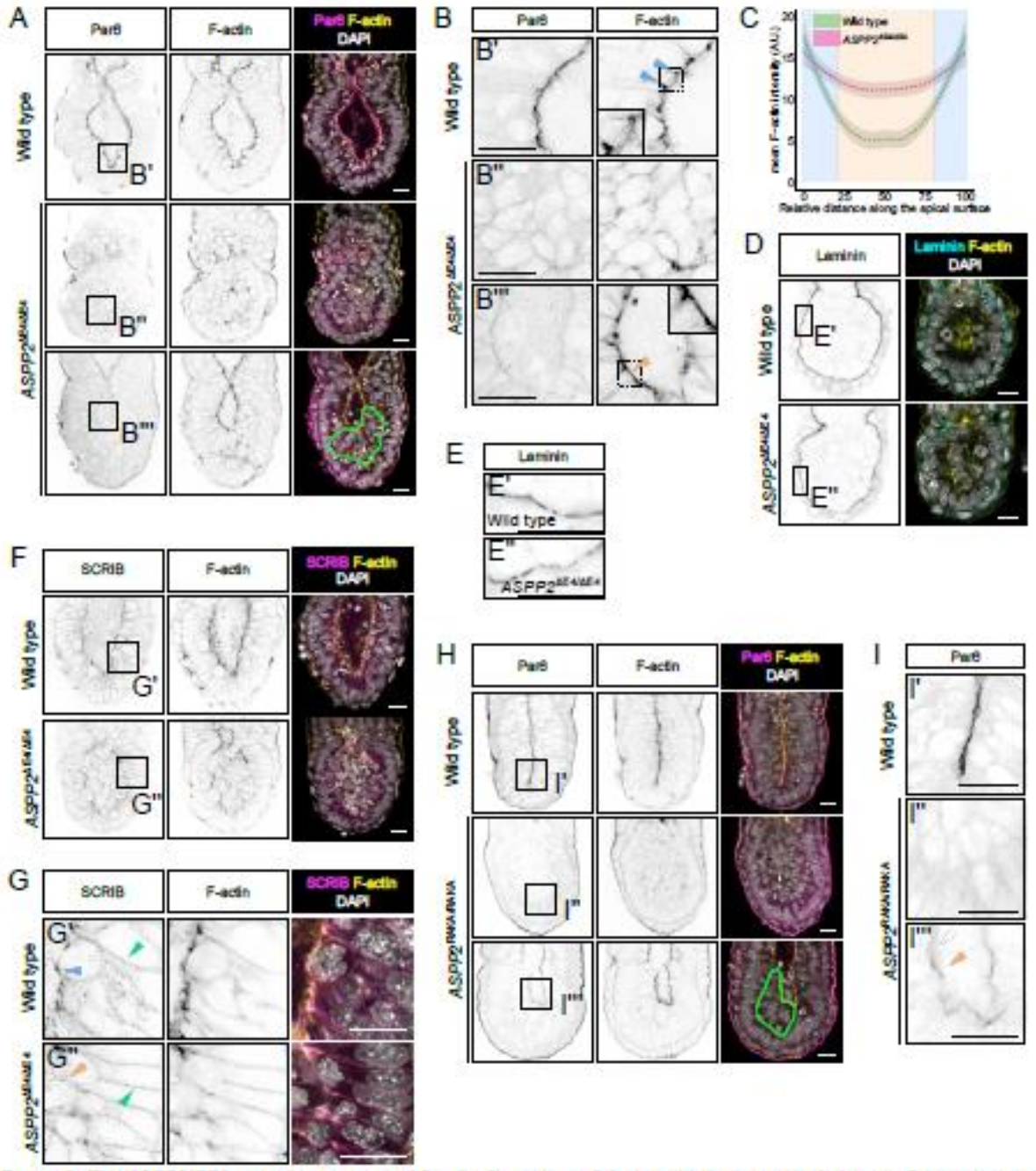

Figure 2: The ASPP2/PP1 complex is required for the formation of the proamniotic cavity. A. Immunofluorescence of wild type and *ASPP2*$^{\Delta E4/\Delta E4}$ E6.5 embryos using an anti-Par6 antibody. The phenotypic variability of *ASPP2*$^{\Delta E4/\Delta E4}$ embryos is illustrated, with embryos either lacking cavities (middle row) or exhibiting smaller cavities (bottom row). The green dashed line highlights the ectopic accumulation of cells in the epiblast of *ASPP2*$^{\Delta E4/\Delta E4}$ embryos. B. Magnification of the corresponding regions shown in panel A. Blue arrowheads highlight the enrichment of F-actin at apical junctions in the epiblast. Note how F-actin is not enriched at apical junctions but is instead more homogenously distributed across the apical surface of epiblast cells in *ASPP2*$^{\Delta E4/\Delta E4}$ embryos (orange arrowhead). The insets within images are 2x magnifications of the corresponding dashed areas. C. Quantification of F-actin signal intensity along the apical surface of epiblast cells of wild type (n=3 embryos, 5 measurements per embryo) and *ASPP2*$^{\Delta E4/\Delta E4}$ embryos (n=3 embryos, 5 measurements per embryo). Measurements were made on cross sections along the apical domain of individual epiblast cells from apical junction to apical junction (represented with a blue background in the graph). See material and methods for details. D. Immunofluorescence of wild type and *ASPP2*$^{\Delta E4/\Delta E4}$ E5.5 embryos using an anti-Laminin antibody. E. Magnification of the corresponding dashed areas in panel D. F. Immunofluorescence of wild type and *ASPP2*$^{\Delta E4/\Delta E4}$ E6.5 embryos using an anti-SCRIB antibody. G. Magnification of the corresponding dashed areas in panel F. Green arrowheads highlight basolateral SCRIB. Note the enrichment of SCRIB at the apical junctions in the epiblast of wild type embryos (blue arrowhead) and its absence in the corresponding localisation in *ASPP2*$^{\Delta E4/\Delta E4}$ embryos (orange arrowhead). H. Immunofluorescence of wild type and *ASPP2*$^{RAKA/RAKA}$ E6.5 embryos using an anti-Par6 antibody. The green dashed line highlights the ectopic accumulation of cells in the epiblast of *ASPP2*$^{RAKA/RAKA}$ embryos. I. Magnification of the corresponding dashed regions in H. Note the reduced amount of Par6 along the apical domain of epiblast cells in *ASPP2*$^{RAKA/RAKA}$ embryos (orange arrowhead). Nuclei and the F-actin cytoskeleton were visualised with DAPI and Phalloidin respectively. Scale bars: 20 µm.

cells reincorporating basally following cell divisions or a combination of these. To answer this question, we generated *ASPP2*$^{\Delta E4/\Delta E4}$ embryos with fluorescently labelled membranes, which enabled us to follow the movement of epiblast cells in these embryos by time-lapse confocal microscopy (Figure 3A and Movie 1). In wild type and heterozygous embryos, we could observe the movement of cell bodies along the apical-basal axis during interkinetic nuclear migration (IKNM), with mitotic cells rounding up at the apical surface of the epiblast before dividing as previously described[26].

We first analysed the orientation of cell divisions but could not detect differences in overall cell division angle in *ASPP2*$^{\Delta E4/\Delta E4}$ embryos in comparison to controls (Figure S3A), even when division events were binned into categories as "orthogonal", "parallel" or "oblique". To determine if there was a defect in IKNM, we also analysed the distance at which cell divisions occurred from the basement membrane of the epiblast. Again, there was no notable difference between *ASPP2*$^{\Delta E4/\Delta E4}$ and wild type embryos, suggesting that even in the absence of apical-basal polarity and the proamniotic

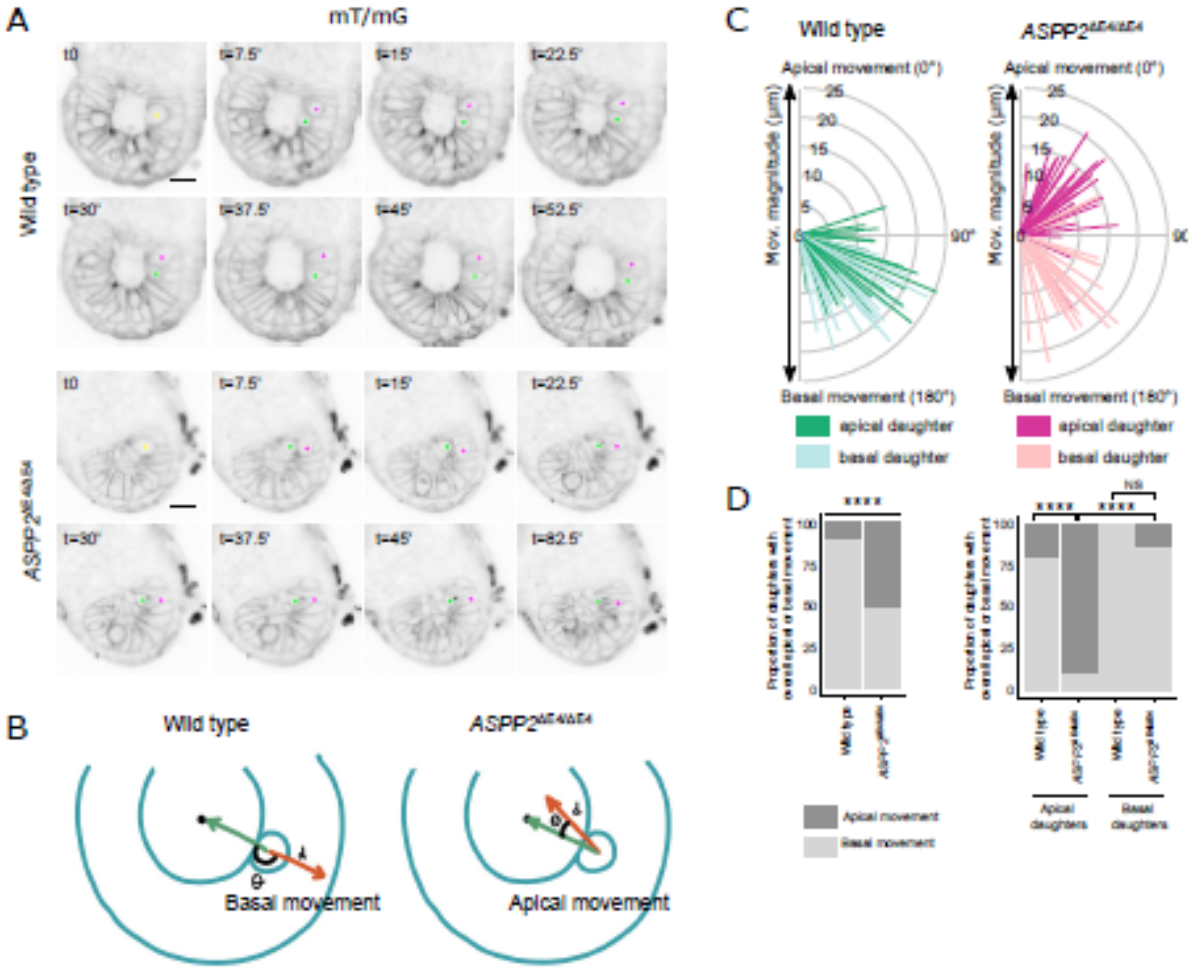

Figure 3: ASPP2 is required for apical daughter cell reincorporation into the epiblast following cell division events. A. Time lapse imaging of wild type and *ASPP2*$^{\Delta E4/\Delta E4}$ embryos. mT/mG-labelled cell membranes were used to manually track cell movement. Yellow dots highlight mother cells at the apical surface of the epiblast immediately prior to a cell division event. Green and magenta dots identify the resulting daughter cells. Note how both daughters reintegrate the epiblast in the wild type whereas one of the two daughters fails to do so in the absence of ASPP2 even after a prolonged period of time (t=82.5'). B. Diagram illustrating the method used to quantify daughter cell movement following cell divisions. Daughter cell movement was characterised by both the distance travelled (d) and the direction of travel (θ) expressed as the angle between the reference vector (the green vector starting from the initial position of the mother cell prior to the division event to the centre of the embryonic region) and the vector characterising absolute daughter cell movement (the red vector starting from the initial position of the mother cell prior to the division event to the final position of the daughter cell). The left panel illustrates the case of a daughter moving basally to reincorporate the epiblast and the right panel describes abnormal daughter cell movement towards the centre of the embryonic region such as seen in *ASPP2*$^{\Delta E4/\Delta E4}$ embryos. C. Graph quantifying cell movement in wild type (n=3 embryos, 56 cells) and *ASPP2*$^{\Delta E4/\Delta E4}$ embryos (n=3 embryos, 66 cells). For a given pair of daughter cells, each daughter was defined as "apical" or "basal" depending on their respective position relative to the centre of the embryonic region immediately after a cell division event. D. Proportion of daughter cells with an overall apical or basal movement in wild type and *ASPP2*$^{\Delta E4/\Delta E4}$ embryos. Left panel: Quantification of the proportion of daughter cells with an overall apical (θ from 0° to 90°) or basal movement (θ from 90° to 180°) in wild type and *ASPP2*$^{\Delta E4/\Delta E4}$ embryos. Right panel: quantification of the proportion of apical and basal daughters with an overall apical (θ from 0° to 90°) or basal movement (θ from 90° to 180°) in wild type and *ASPP2*$^{\Delta E4/\Delta E4}$ embryos. **** p<0.0001, NS: non-significant (Fisher's exact test of independence).

cavity, cells of the epiblast were able to proceed with IKNM (Figure S3B).

We next looked at the behaviour of daughter cells after cytokinesis. In wild type embryos, following cell divisions, the cell body of both daughters moved basally so that they came to span the entire height of the epithelium along the apical-basal extent of the epiblast. In contrast, in *ASPP2*$^{\Delta E4/\Delta E4}$ embryos, dividing cells moved towards the embryonic centre as normal, but upon division, daughter cells delaminated apically towards the centre of mass of the embryonic region (Figure 3A). This suggested that ASPP2 may be specifically required for the retention of daughter cells within the epiblast. To further characterise this failure of dividing cells to reintegrate into the epiblast epithelium, we quantified the movement of daughter cells from the initial point of cell division (Figure 3B-D). We found that in wild type and heterozygous embryos, this movement was almost always basal for both daughters (51/56, 91.1%). In contrast, in mutant embryos, for half the daughter cells (33/66, 50%) the movement was apical (Figure 3C and 3D). We found that in the majority of cases (29/33, 87.9%), it was the daughter that was relatively more apically positioned with respect to its sister that abnormally moved apically following cell divisions (Figure 3D). This suggests that ASPP2 is involved in a novel mechanism specifically required for apical daughter cell reintegration into the pseudostratified epiblast following cell division, which is crucial in maintaining the architecture of the epiblast and proamniotic cavity.

ASPP2/PP1 complexes maintain epithelial integrity in regions of high mechanical stress.

Our results all point to an important role for ASPP2 in regulating tissue architecture, possibly via the regulation of F-actin organisation at the apical junction. However, this was difficult to study in *ASPP2*$^{\Delta E4/\Delta E4}$ and *ASPP2*$^{RAKA/RAKA}$ embryos on a C57BL/6 background because of the relative severity of the defect. We therefore bred *ASPP2*$^{RAKA/RAKA}$ mutation into a BALB/c background, to take advantage of the fact that ASPP2 phenotypes are often not as dramatic in this background[14]. Consistent with this, BALB/c *ASPP2*$^{RAKA/RAKA}$ homozygous embryos completely bypassed the phenotype at E6.5 observed in C57BL/6 *ASPP2*$^{RAKA/RAKA}$ embryos. Instead, the phenotype of these embryos was milder, and they were only grossly different from wild type and heterozygous embryos one day later, at E7.5. *ASPP2*$^{RAKA/RAKA}$ embryos exhibited two distinct phenotypes. The majority (34/41, 82.9%), that we termed type I embryos, exhibited a strong accumulation of cells in their posterior, suggestive of a defect in the primitive streak (Figure S4A and 4A). A minority (7/41, 17.1%), that we termed type II embryos, were developmentally delayed but did not exhibit any structural defects.

Given that *ASPP2*$^{\Delta E4/\Delta E4}$ and *ASPP2*$^{RAKA/RAKA}$ in a BI/6 background showed striking abnormalities in the localisation of F-actin, we examined the localisation of F-actin in the posterior of type I *ASPP2*$^{RAKA/RAKA}$ embryos at E7.5 (Figure 4B and Figure S4C). In wild type embryos, we were able to clearly identify cells apically constricting and pushing their cell body basally towards the nascent mesodermal cell layer. This is characteristic of cells in the primitive streak in the process of delaminating basally[4]. It was also evident that F-actin was enriched at the apical junctions in these cells (Figure 4C). In contrast, *ASPP2*$^{RAKA/RAKA}$ embryos exhibited a clear ectopic accumulation of cells apical to the primitive streak as visualised by T expression (Figure 4B). In these cells, F-actin was abnormally uniformly disturbed along the apical surface, with no clear apical-junction enrichment (Figure 4C). To investigate this further, we performed Airyscan super-resolution imaging of these embryos (Figure 4D-F).This revealed that the mesh-like structure normally formed by F-actin at the apical junctions in cells of the epiblast was severely disrupted in the posterior of *ASPP2*$^{RAKA/RAKA}$ embryos. Instead, F-actin appeared to form spike-like structures at the surface of cells in this region (Movie 2) (figure 4E and 4F). This profound disruption of F-actin localisation indicates that the PP1 regulatory function of ASPP2 is required for F-actin organisation in the cells of the primitive streak.

The epiblast specific requirement for ASPP2 despite its broad expression (Figure 1A and 6A-C) and the localisation of the phenotype primarily to the posterior region of the epiblast in the BALB/c background suggest that specific epithelia or epithelial regions are more sensitive to ASPP2 deficiency than others. We hypothesised therefore that ASPP2 may be important particularly for dividing cells to reintegrate within epithelia subject to increased mechanical stress at the apical junction, for example during the apical curving required to form a cavity. In support of this hypothesis, phospho-myosin levels were higher in dividing cells in the epiblast, in particular at the apical junctions. This shows that actomyosin contractility increases at the apical junctions of dividing cells, which might result in increased mechanical stress (Figure 5A). One prediction of this hypothesis is that increasing the mechanical stress in Type I *ASPP2*$^{RAKA/RAKA}$ embryos in a BALB/c background might induce an earlier or more severe phenotype reminiscent to that seen in the C57BL/6 background. To test this prediction, we cultured E6.5 BALB/c wild type and mutant embryos (a day before any phenotype is evident in mutants) within the confines of cylindrical cavities made of biocompatible hydrogels, in order to alter their shape[27] and subject the epiblast epithelium to higher levels of mechanical stress (Figure 5B). Wild type embryos elongated without showing any sign of disrupted tissue integrity (0 out of 4 embryos). Conversely, *ASPP2*$^{RAKA/RAKA}$ embryos showed reduced cavity size with a clear accumulation of cells (2 out of 2 embryos), phenocopying *ASPP2*$^{\Delta E4/\Delta E4}$ and *ASPP2*$^{RAKA/RAKA}$ mutant embryos in a C57BL/6 background (Figure 5C). Interestingly, F-actin and Myosin were abnormally distributed at the apical surface of cells accumulating ectopically in *ASPP2*$^{RAKA/RAKA}$ mutant embryos, suggesting that actomyosin contractility was disrupted. Together, This indicates that although *ASPP2*$^{RAKA/RAKA}$ mutants in a BALB/c background can bypass the proamniotic cavity phenotype, increasing mechanical stress is sufficient to make them again susceptible to it and suggests that ASPP2 may be required in response to increased mechanical stress to maintain epithelial tissue integrity.

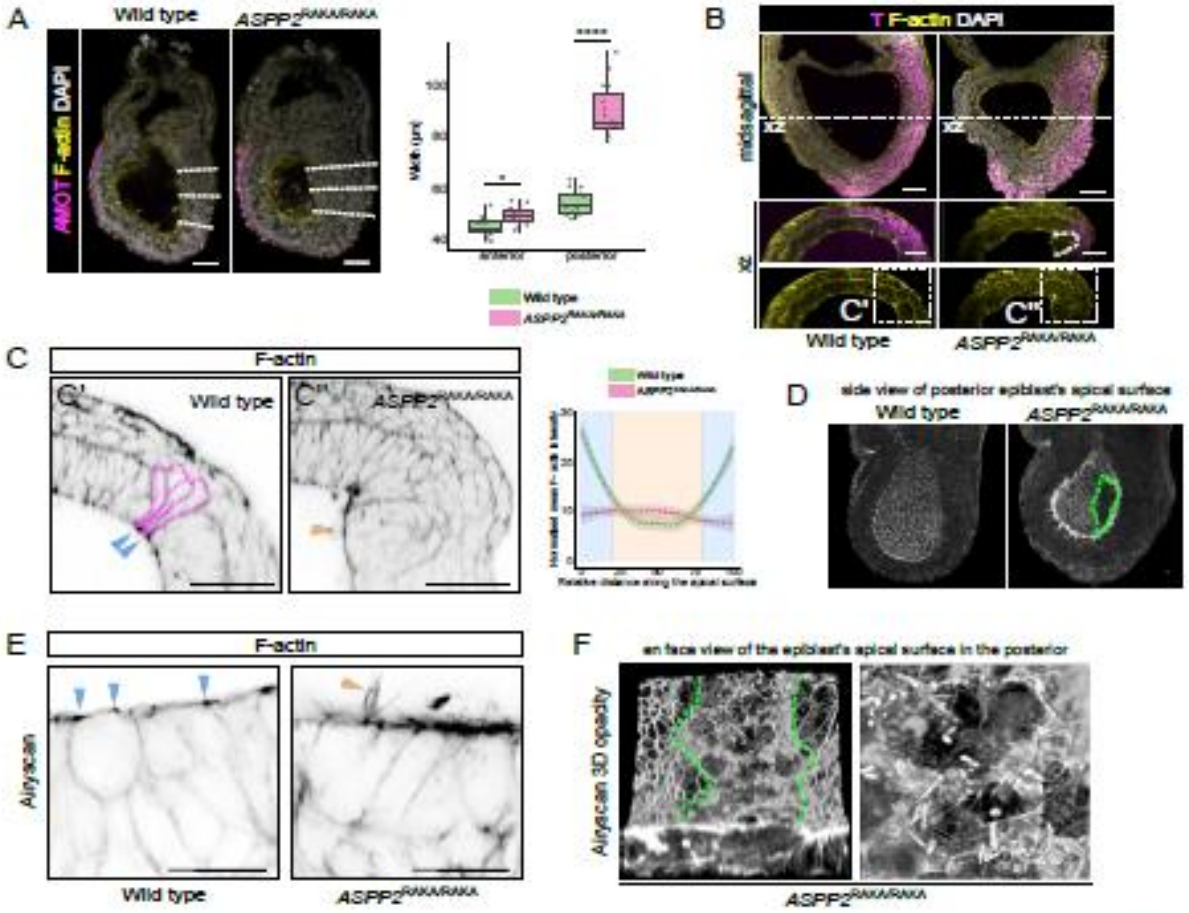

Figure 4: ASPP2 is required for epithelial integrity in the primitive streak. A. Posterior thickening in E7.5 *ASPP2*$^{RAKA/RAKA}$ embryos in a BALB/C background. Left panel: the anteroposterior axis was defined using AMOT localisation pattern. Right panel: comparison of tissue thickness in the anterior (3 measurements per embryo) and the posterior (3 measurements per embryo) of wild type (n=5 embryos) and *ASPP2*$^{RAKA/RAKA}$ embryos (n=5 embryos). * p<0.05, ****p<0.0001 (nested ANOVA). B. Cells accumulate in the primitive streak region of *ASPP2*$^{RAKA/RAKA}$ embryos. Immunofluorescence of E7.5 wild type and *ASPP2*$^{RAKA/RAKA}$ embryos using a T (Brachyury) antibody. C. Cells ectopically accumulating in the primitive streak region are unable to apically constrict and do not have enriched F-actin at the apical junctions (orange arrowhead) in comparison to wild type (blue arrow heads). Magenta dotted lines highlight cells apically constricting to push their cell bodies basally towards the underlying mesoderm cell layer. Right panel: quantification of F-actin signal intensity along the apical surface of epiblast cells in the primitive streak region of wild type (n=3 embryos, 5 cells per embryo) and *ASPP2*$^{RAKA/RAKA}$ embryos (n=3 embryos, 5 cells per embryo). Measurements were made on cross sections along the apical domain of individual epiblast cells from apical junction to apical junction (represented with a blue background in the graph). D-F. Airyscan imaging reveals the extent of F-actin disorganisation at the surface of cells accumulating ectopically in the primitive streak region of *ASPP2*$^{RAKA/RAKA}$embryos. D. 3D opacity rendering of embryo optical halves, enabling visualisation of the apical surface of epiblast cells in the proamniotic cavity. Note the absence of the typical F-actin mesh pattern at the apical surface of cells in the posterior of *ASPP2*$^{RAKA/RAKA}$ embryos (green dotted line). E. F-actin localisation pattern in the primitive streak region of wild type and *ASPP2*$^{RAKA/RAKA}$ embryos. F-actin was enriched at the apical junctions of wild type embryos (blue arrowheads). Orange arrowheads highlight the formation of F-actin spike-like structures at the contact-free surface of *ASPP2*$^{RAKA/RAKA}$ embryos. F. En face view of the epiblast's apical surface in the posterior of an *ASPP2*$^{RAKA/RAKA}$ embryo. Green dotted lines demarcate the disorganised apical region of the posterior and the more organised lateral regions of the epiblast. Right panel: magnification of the epiblast's apical surface in the posterior of an *ASPP2*$^{RAKA/RAKA}$ embryo showing F-actin forming spike-like structures. Nuclei and the F-actin cytoskeleton were visualised with DAPI and Phalloidin respectively. Scale bars: 20 µm.

ASPP2 maintains the architecture of the F-actin cytoskeleton during cell division events via its PP1 regulatory function.

To understand how the absence of ASPP2 specifically regulates apical daughter cell reintegration into the epiblast, we analysed in detail its localisation pattern. ASPP2 was localised at the apical junctions in the VE (Figure 6A and Figure S5A and B) and the epiblast (Figure 6B and see Fig S2C for antibody specificity). In the former, ASPP2 was uniformly distributed along the apical junctions forming a regular mesh at the surface of the embryo (Figure 6A and Figure S5A and B). In the epiblast however, ASPP2 appeared enriched at specific locations along the apical junctions (Figure 6B). The high curvature of the inner apical surface of the epiblast makes it difficult to examine from standard confocal volumes. We therefore computationally 'unwrapped'[28] the apical surfaces of the VE and epiblast so that we

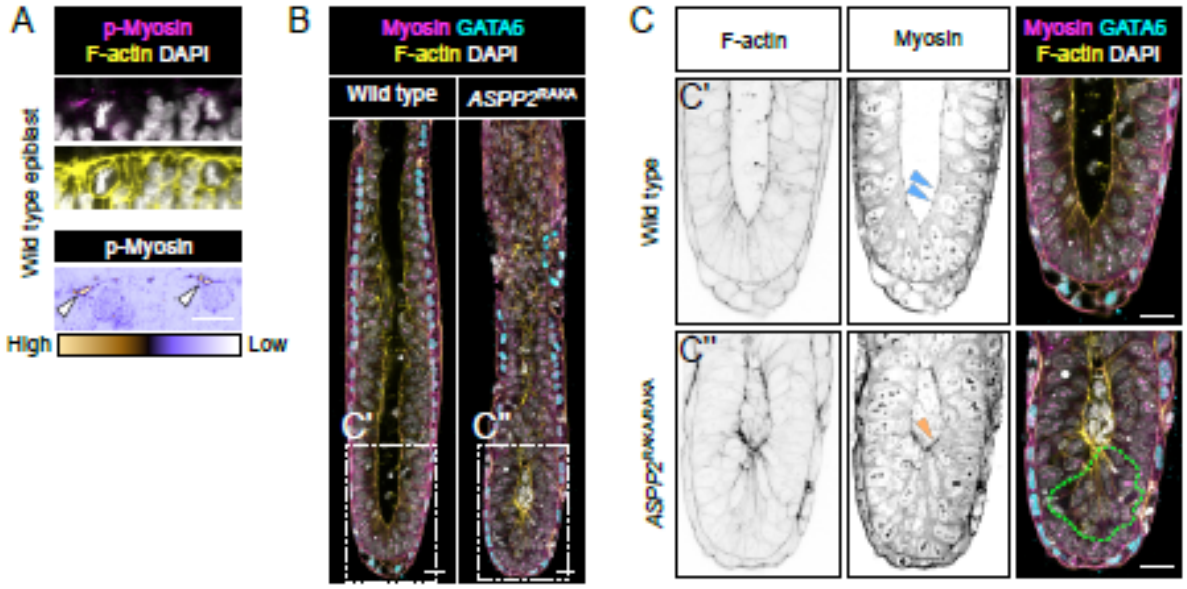

Figure 5: ASPP2$^{RAKA/RAKA}$ embryo are more susceptible to mechanical stress. A. Phospho-myosin levels are higher at the apical junctions of dividing cells in the epiblast (white arrowheads). B. wild type (n=3) and *ASPP2*$^{RAKA/RAKA}$ (n=2) embryos were grown for 30' in cylindrical cavities made of biocompatible hydrogels. The localisation pattern of GATA6 and Myosin was then analysed by immunofluorescence. C. Magnification of the embryos shown in E. The green dotted line highlights the ectopic accumulation of cells seen in *ASPP2*$^{RAKA/RAKA}$ embryos. The orange arrowhead points to the abnormal distribution of Myosin at the apical surface of these cells. Nuclei and the F-actin cytoskeleton were visualised with DAPI and Phalloidin respectively. Scale bars: 20 µm.

could more directly compare them (Figure 6C). This revealed that, although ASPP2 was uniform in its distribution along all junctions in the VE, in the epiblast, it was enriched specifically at F-actin-rich tricellular junctions.

The enrichment of ASPP2 in regions of high F-actin and the disruption of F-actin localisation in mutants suggests that ASPP2 may somehow be linked to the F-actin cytoskeleton. Because ASPP2 does not possess any known F-actin binding domain, we looked if previously identified ASPP2 binding partners could provide this link. Interestingly, ASPP2 has been found to interact with Afadin in a number of proteomic studies[29,30]. Afadin is an F-actin-binding protein that has previously been shown to not only be enriched at tricellular junctions but to also regulate their architecture[31]. Moreover, at E7.5, *Afadin*-null embryos display a phenotype reminiscent of the phenotype observed in E7.5 *ASPP2*$^{\Delta E4/\Delta E4}$ embryos (Figure S2B) with cells accumulating in the proamniotic cavity[32], suggesting that Afadin and ASPP2 have overlapping functions. To confirm that ASPP2 and Afadin can be found within the same protein complex, we immunoprecipitated endogenous Afadin in Caco-2 cells, a colorectal cancer cell line with strong epithelial characteristics that retains the ability to polarise. ASPP2 co-immunoprecipitated with Afadin, indicating that they are indeed found in the same protein complex (Figure 6D). To further investigate where this complex might form, we analysed the localisation of endogenous ASPP2 and Afadin in Caco-2 and MDCK cells using super-resolution Airyscan microscopy. We found the proteins colocalised primarily at tricellular junctions, where F-actin was also enriched, including in dividing cells in metaphase (Figure 6E and S5C). Their expression pattern also partially overlapped at bicellular junctions (Figure S5C). Interestingly, Afadin was also found at the mitotic spindles (Figure 6E) and cleavage furrow (Figure S5D), where ASPP2 was juxtaposed with Afadin. In E6.5 embryos, Afadin showed a similar localisation pattern to ASPP2, at the apical junction of cells in the epiblast and VE (Figure 6F and S5E). In the epiblast, similarly to ASPP2, it was more abundant at the F-actin-rich tricellular junctions.

Together, these results highlight the importance of the localisation pattern of ASPP2 in the epiblast, suggesting that it may be able to interact with F-actin at the apical junctions via its interaction with Afadin. They also suggest that this interaction might be important in dividing cells. To test this possibility, we generated *ASPP2*$^{RAKA/RAKA}$ embryos in a C57BL/6 background carrying a LifeAct-GFP transgene[33] that allowed us to visualise F-actin in living embryos with time-lapse confocal microscopy (Figure 6G and H and Figure S5F). During cell division events, following mitotic rounding, apical F-actin localisation was disrupted in *ASPP2*$^{RAKA/RAKA}$ embryos whereas it was maintained in wild type embryos (Figure 6G). This was followed by an ectopic accumulation of cells at the apical surface of the epiblast, reducing the size of the proamniotic cavity (Figure 6H). These results suggest that the PP1 regulatory function of ASPP2 is required to maintain the architecture of apical F-actin, particularly during cell division events in the epiblast.

ASPP2 supports tissue integrity across a variety of pseudostratified epithelia

Next, we investigated whether ASPP2 was only required in the epiblast or whether it also functioned in other tissues undergoing morphogenesis. To this end,

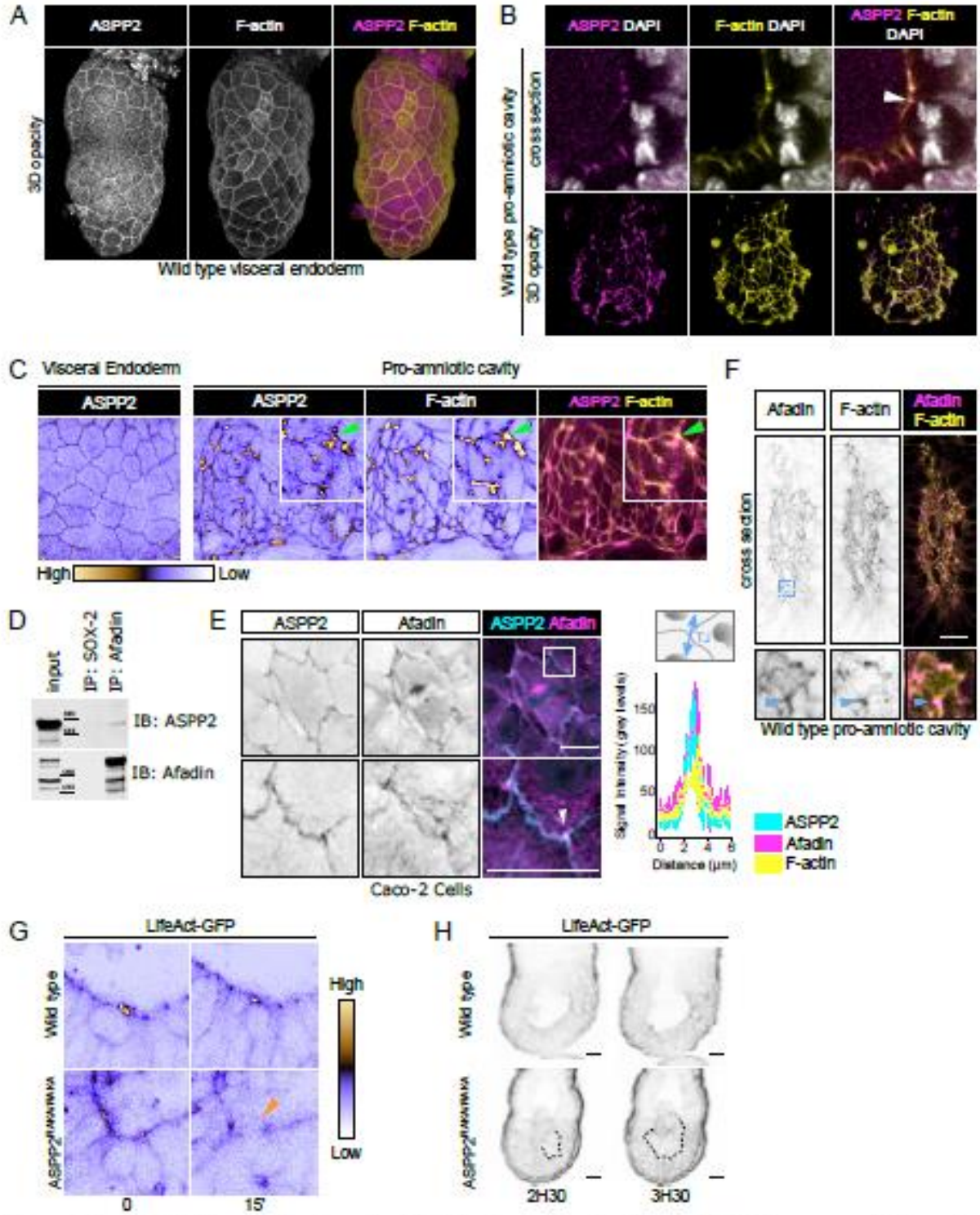

Figure 6: the ASPP2/PP1 complex is required for F-actin organisation during cell division events. A. 3D opacity rendering showing the localisation of ASPP2 in E5.5 wild type embryos at the apical junctions of the visceral endoderm where it colocalises with F-actin. B. Cross section (top row) and 3D opacity rendering (bottom row) of the proamniotic cavity showing the localisation pattern of ASPP2 and F-actin at the apical junctions (white arrowhead). C. The outer surface of the VE and apical surface of the epiblast were computationally 'unwrapped', revealing the enrichment of ASPP2 and F-actin at tricellular junctions in the epiblast (green arrowheads). D. The interaction between endogenous ASPP2 and the F-actin-binding protein Afadin was examined in Caco-2 cells by co-immunoprecipitation. E. The localisation pattern of endogenous ASPP2 and Afadin in Caco-2 cells was examined by immunofluorescence. The bottom row represents the magnified region highlighted by a dotted box and shows the enrichment of ASPP2 and Afadin at tricellular junctions. ASPP2, Afadin and F-actin signal intensity was quantified across tricellular junctions (graph on the right). F. The localisation pattern of Afadin in the proamniotic cavity was analysed by immunofluorescence in E6.5 wild type embryos. Afadin colocalised strongly with F-actin at tricellular junctions (blue arrowhead). G. The localisation pattern of F-actin was analysed by time-lapse microscopy in wild type and *ASPP2*^{RAKARAKA} LifeAct-GFP positive embryos. Note how apical F-actin is disrupted in *ASPP2*^{RAKARAKA} LifeAct-GFP positive

embryos following a cell division event (orange arrowhead). H. At later time points, the ectopic accumulation of cells in the epiblast of *ASPP2*$^{RAKA/RAKA}$ LifeAct-GFP positive embryos was evident (dotted line). Nuclei and the F-actin cytoskeleton were visualised with DAPI and Phalloidin respectively. Scale bars: 20 µm.

we examined *ASPP2*$^{\Delta E4/\Delta E4}$ embryos at later stages of development around the time of gastrulation. At E7.5, during late primitive streak stages, mesoderm formation (marked by expression of T) and migration were broadly comparable between *ASPP2*$^{\Delta E4/\Delta E4}$ embryos and wild type littermates, despite the absence of a proamniotic cavity and the dramatic accumulation of cells now filling the entirety of the space inside the embryos (Figure 7A, Movie 3). Furthermore, there was no difference in the velocity, directionality and distance travelled by mesoderm cells migrating from wild type and *ASPP2*$^{\Delta E4/\Delta E4}$ mesoderm explants (Figure S6A and Movie 4). This suggested that ASPP2 was not required for mesoderm specification or migration.

To test whether further patterning of the mesoderm occurred in the absence of ASPP2, we examined *ASPP2*$^{\Delta E4/\Delta E4}$ embryos at E8.5. Morphologically, these embryos were severely disrupted, shorter along the anterior-posterior axis and without head folds (Figure 7B). However, using the cardiac progenitor marker NKX2.5, we found that this population of cells was able to migrate rostrally despite the dramatic morphological defects present in *ASPP2*$^{\Delta E4/\Delta E4}$ embryos (Figure 7B). At E9.5, some cells in the anterior of these embryos were also positive for alpha sarcomeric α-actinin, suggesting that the NKX2-5 positive cells could differentiate into cardiomyocytes (Figure 7C and S6B). Next, we analysed whether the mesoderm could go on to form structurally normal somites. Using FOXC2 as a marker of somitic mesoderm, we were able to identify distinct somite-like structures in *ASPP2*$^{\Delta E4/\Delta E4}$ embryos (Figure 7D and S6B). However, we found that these somites were smaller than normal (Figure 7E). Compared to wild-type control somites, a large proportion of mutant somites exhibited disrupted epithelial organisation (Figure 7D and 7F) and a reduced proportion formed cavities (Figure 6D and 6G). The relative size of the somitocoel in *ASPP2*$^{\Delta E4/\Delta E4}$ embryos was also significantly reduced in comparison to wild type controls (Figure 7H). Importantly, somites with disrupted epithelial organisation and lacking cavities had features reminiscent of *ASPP2*$^{\Delta E4/\Delta E4}$ epiblasts: cells could be seen accumulating in the centre resulting in the obliteration of the somitocoel (Figure 7D). These cells also displayed a lack of apical Par6, suggesting that as in the epiblast, in the forming somites, apical-basal polarity was disrupted (Figure 7I).

These results suggest that ASPP2 is required not only in the epiblast, but more generally in pseudostratified epithelia[14]. To investigate this further, we tested the requirement for ASPP2 in lumen formation during cystogenesis. We derived embryonic stem cells (ESC) from embryos with exon 4 of *ASPP2* flanked by two LoxP sites. To generate *ASPP2*$^{\Delta E4/\Delta E4}$ ESC, they were infected with a CRE-recombinase-expressing adenovirus. When grown in Matrigel, we found that the majority of *ASPP2*$^{\Delta E4/\Delta E4}$ ESC-derived cysts failed to form lumens in comparison to control cysts (Figure S6C). Similarly, ESC derived from *ASPP2*$^{RAKA/RAKA}$ embryos failed to form lumens in comparison to wild type ESC, suggesting that the formation of lumens during cystogenesis requires ASPP2/PP1 interaction (Figure S6D).

Since our data suggests that ASPP2 is required in regions undergoing increased mechanical stress (Figure 5A and B), we wanted to examine further the potential importance of ASPP2 during head fold formation. We took advantage of the *ASPP2*$^{RAKA/RAKA}$ embryos in a BALB/c background as their phenotype is milder and they develop a proamniotic cavity (Figure 4A), reducing the likelihood that phenotypes observed in the head fold region are secondary defects due to overall tissue disorganisation. At E8.5, wild type embryos exhibited fully formed head folds (Figure 7J). In contrast, *ASPP2*$^{RAKA/RAKA}$ embryos failed to form head folds in the rostral region of the ectoderm. In this region, the epithelium buckled locally, without being able to fully complete head fold morphogenesis. Interestingly, this was accompanied by a loss of organisation of F-actin at the apical junction, similarly to what was observed in the proamniotic cavity of *ASPP2*$^{\Delta E4/\Delta E4}$ embryos and in the primitive streak of *ASPP2*$^{RAKA/RAKA}$ embryos in a BALB/C background (Figure 7J). These results strongly suggest that ASPP2 is required to maintain tissue integrity by regulating F-actin organisation at the apical junctions as tensions increase in the rostral region of the ectoderm during head fold formation. Together, these results also reinforce the idea that ASPP2, and its interaction with PP1, are required during morphogenetic events that result in increased tensions at the level of apical junctions in epithelial tissues.

DISCUSSION

Our study unveils a central role for ASPP2 in maintaining pseudostratified epithelial integrity under increased mechanical stress during major morphogenetic events: in the formation of the proamniotic cavity, the primitive streak during gastrulation, somite formation and in the head fold region.

Strikingly, ASPP2 controls proamniotic cavity formation via a mechanism that, following cell divisions, specifically prevents the most apical daughter cells from delaminating apically. ASPP2 achieves this by maintaining the integrity and organisation of the F-actin cytoskeleton at the apical surface of dividing cells. This mechanism is consistent with ASPP2 playing a role in maintaining epithelial integrity under increased mechanical stress considering that mitotic rounding results in forces sufficient to contract the epithelium in the apical-basal axis and mechanically contribute to expansion of the lumen[2]. However, it remains unclear why it is only the more apically localised daughter cells that are affected in ASPP2 mutant embryos. One possibility is that these daughters do not inherit the basal process that tethers cells to the basement

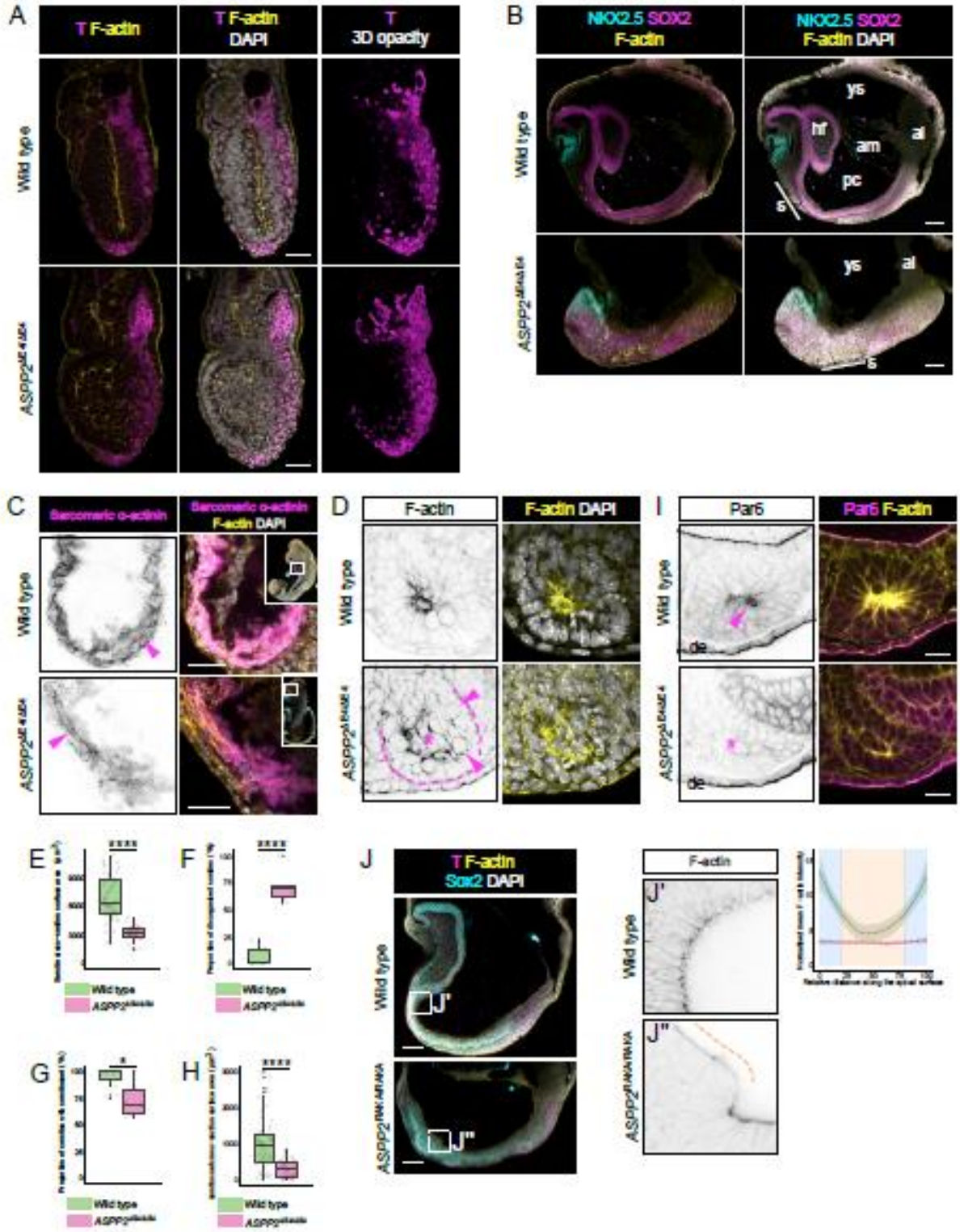

Figure 7: The ASPP2/PP1 complex is required for tissue integrity across a variety of highly proliferative pseudostratified epithelia. A. The primitive streak expands comparatively in E7.5 wild type and *ASPP2*$^{\Delta E4/\Delta E4}$ embryos. Mesoderm cells were labelled by immunofluorescence using an antibody against Brachyury (T). B. Patterning proceeds normally in the absence of ASPP2. The ectoderm and cardiac progenitors were labelled in E8.5 wild type and *ASPP2*$^{\Delta E4/\Delta E4}$ embryos with antibodies against SOX2 and NKX2.5 respectively. ys: yolk sack, al: allantois, s: somites, hf: head fold, am: amnion, pc: proamniotic cavity. C. Cardiac progenitors can differentiate into cardiomyocytes in E9.5 *ASPP2*$^{\Delta E4/\Delta E4}$ embryos. The presence of the contractile machinery (magenta arrowheads) was assessed in wild type and *ASPP2*$^{\Delta E4/\Delta E4}$ embryos using an antibody against sarcomeric α-actinin. D. Somite architecture is disrupted in *ASPP2*$^{\Delta E4/\Delta E4}$ embryos. The dotted line highlights the contour of a somite in an *ASPP2*$^{\Delta E4/\Delta E4}$ embryo. The star indicates the ectopic accumulation of cells in the centre of this somite. Arrowheads point to mitotic figures. E-H. Quantification of somite characteristics in wild type (n=10 embryos, 58 somites) and *ASPP2*$^{\Delta E4/\Delta E4}$ (n=6 embryos, 35 somites) embryos at E8.5. * p<0.05, ****p<0.0001

(Student's T-test). I. Apical-basal polarity is defective in the somites of *ASPP2*$^{\Delta E4/\Delta E4}$ embryos. Par6 localised apically in wild type somites (arrowhead) whereas it was absent in *ASPP2*$^{\Delta E4/\Delta E4}$ embryos (star). de: definitive endoderm. J. Head fold formation is defective in *ASPP2*$^{RAKA/RAKA}$ embryos. The organisation of apical F-actin was disorganised locally in the anterior ectoderm of *ASPP2*$^{RAKA/RAKA}$ embryos (orange dotted line). F-actin signal intensity along the apical surface of ectoderm cells in disrupted areas in *ASPP2*$^{RAKA/RAKA}$ embryos (n=3 embryos, 5 cells per embryo) was compared to wild type cells (n=3 embryos, 5 cells per embryo). Measurements were made on cross sections along the apical domain of individual ectoderm cells from apical junction to apical junction (represented with a blue background in the graph). Nuclei and the F-actin cytoskeleton were visualised with DAPI and Phalloidin respectively. Scale bars: 20 µm (D, I), 50 µm (A, C), 100 µm (B, J).

membrane in pseudostratified epithelia. However, the idea that the basal process is inherited asymmetrically is controversial[34]. Other mechanisms, such as the extent of cell-cell interactions between neighbouring cells and apical daughter cells in comparison to the more basal daughters may be involved.

It has been suggested that the purpose of interkinetic nuclear migration is to ensure that cells divide apically to safeguard the integrity of pseudostratified epithelia[35]. Here we show that this is not sufficient to maintain tissue integrity as, in the absence of ASPP2, the apical-basal movement of nuclei and the position of cell divisions during IKNM proceeds unhindered. Our observations also suggest that the organisation of the F-actin cytoskeleton at the apical junctions is not required for nuclear movement during INKM and that intact basolateral domain and attachment to the basement membrane are sufficient instead.

Given that the ASPP2 interactors Par3[36,37] and Afadin[38–40], tricellular junctions[41], as well as tissue tension[42–45] have all been shown to determine cell division orientation to some extent, it was important to explore whether ASPP2 could play a role in this process. However, our results indicate that ASPP2 does not control the orientation of cell divisions in the epiblast. Similarly to previous work[26], we also find no bias towards cell divisions orientated in the plane of the epithelium, suggesting that, at these early stages of development, planar cell polarity may not play a role in directing cell division orientation. We therefore cannot rule out that, in a different context, ASPP2 might control cell division orientation in conjunction with Afadin. In fact, later in development in E8.5 *ASPP2*$^{RAKA/RAKA}$ embryos, cells sometimes delaminated basally in the anterior regions of the ectoderm, reminiscent of the phenotype observed in SCRIB- and DLG-depleted Drosophila wing discs, where cell divisions are normally orientated in the plane of the epithelium by cell-cell junctions to maintain epithelial integrity[46].

Our results highlight the previously underappreciated localisation of ASPP2 at tricellular junctions in epithelial cells, in particular of the epiblast, and reveal the unknown biological function of ASPP2/PP1 complexes in the regulation of F-actin organisation at the apical junction. Considering that Afadin regulates the architecture of tricellular junctions in response to tensions[31,47], the interaction between Afadin and ASPP2 strongly suggests that ASPP2 may exert its F-actin function at tricellular junctions via Afadin. The role of Afadin in regulating the linkage between F-actin and junctions during apical constrictions48 suggests that ASPP2 may also be important in this process, which may be particularly relevant in the primitive streak. Tricellular junction are emerging as a particularly important aspect of tissue homeostasis, at the intersection between actomyosin contractility and apical-basal organisation in the context of tissue tensions[48]. We therefore suggest that ASPP2 may be directly involved in the response to tissue tension by interacting with Afadin at the level of tricellular junctions to maintain F-actin organisation.

Our study also suggests that the interaction between ASPP2 and PP1 might be essential to the well documented tumour suppressor function of ASPP2[50–52]. Simply abrogating the ability of ASPP2 to recruit PP1 is enough to induce the formation of abnormal discrete clusters of cells in the epiblast reminiscent of tumours. This suggests that mutations in ASPP2 that interfere with its interaction with PP1 might, in conjunction with mechanical stress, lead to tumour development. These mutations could be in the canonical PP1-binding domain of ASPP2, but also in other key domains which have been shown to contribute to the interaction[53]. Recent findings support the idea that ASPP2 mutations could lead to tumorigenesis in the presence of mechanical stress. Using insertional mutagenesis in mice with mammary-specific inactivation of Cdh1, ASPP2 was identified as part of a mutually exclusive group containing three other potential tumour suppressor genes (Myh9, Ppp1r12a and Ppp1r12b), suggesting that these genes target the same process[54]. With our finding that ASPP2 controls the organisation of the F-actin cytoskeleton, it now becomes apparent that, in addition to three of these genes being PP1-regulatory subunits, all four are in fact F-actin regulators. Biological studies to test specific mutations found in ASPP2 in cancer and elucidating the substrates and specific phospho-residues targeted by the ASPP2/PP1 complex will therefore provide new insights into the tumour suppressor role of ASPP2 and might help developing new approaches to cancer treatment.

MATERIALS AND METHODS

Mouse strains and embryo generation

All animal experiments complied with the UK Animals (Scientific Procedures) Act 1986, were approved by the local Biological Services Ethical Review Process and were performed under UK Home Office project licenses PPL 30/3420 and PCB8EF1B4.

All mice were maintained on a 12-hour light, 12-hour dark cycle. Noon on the day of finding a vaginal plug was designated 0.5 dpc. For preimplantation stages, embryos were flushed using M2 medium (Sigma M7167) at the indicated stages. For post-implantation stages, embryos of the appropriate stage were dissected in M2 medium with fine forceps and tungsten needles.

We originally obtained *ASPP2* mutant mice in which exons 10–17 were replaced with a neo-r gene[23] from Jackson Laboratory. After careful characterisation of this mouse line, we found that the Neo cassette was not inserted in the ASPP2 locus. As a consequence, we used a different strategy to generate *ASPP2* mutant mice. C57BL/6N-Trp53bp2<tm1a (EUCOMM) heterozygous sperm (obtained from the Mary Lyon Centre) was initially used to fertilise ACTB:FLPe B6J homozygous oocytes (Jackson Laboratory). This resulted in the removal by the flippase of the LacZ and neo-r region flanked by FRT sites and the generation of heterozygous mice with one allele of ASPP2 in which exon 4 was flanked by LoxP sites. Those mice were bred in a C57BL/6J background for over four generations to breed out the rd8 mutation in the CRB1 gene found in the C57BL/6N background and eliminate the remaining FRT site left behind. They were then crossed to generate mice homozygous for the ASPP2 conditional allele in a C57BL/6J background ($ASPP2^{tm1a/tm1a}$ mice). These mice were also crossed with Sox2Cre mice[95] to generate mice with Exon 4 excised in one allele of *ASPP2* ($ASPP2^{WT/\Delta E4}$ mice). $ASPP2^{WT/\Delta E4}$ mice were subsequently backcrossed into wildtype C57BL/6J mice to segregate out the Sox2Cre transgene.

$ASPP2^{WT/\Delta E4}$ mice were used to generate $ASPP2^{\Delta E4/\Delta E4}$ embryos. To produce epiblast-specific *ASPP2*-null embryos ($ASPP2^{Epi\Delta E4/\Delta E4}$ embryos), $ASPP2^{WT/\Delta E4}$ mice homozygous for the Sox2Cre transgene were crossed with $ASPP2^{tm1a/tm1a}$ mice. To generate $ASPP2^{\Delta E4/\Delta E4}$ embryos with fluorescently labelled membranes, we established $ASPP2^{WT/\Delta E4}$ mice heterozygous for the mT/mG transgene[96] and crossed them with $ASPP2^{WT/\Delta E4}$ mice.

The $ASPP2^{WT/RAKA}$ mice were made by inGenious Targeting Labs (Ronkonkoma, NY). A BAC clone containing exon 14 of the trp53bp2 gene was subcloned into a ~2.4kb backbone vector (pSP72, Promega) containing an ampicillin selection cassette for retransformation of the construct prior to electroporation. A pGK-gb2 FRT Neo cassette was inserted into the gene. In the targeting vector, the wild type GTG AAA TTC was mutated to GCG AAA GCC by overlap extension PCR and introduced into C57BL/6 x 129/SvEv ES cells by electroporation. Inclusion of the mutations in positive ES cell clones was confirmed by PCR, sequencing and Southern blotting. ES cells were microinjected into C57BL/6 blastocysts and resulting chimeras mated with C57BL/6 FLP mice to remove the Neo cassette. The presence of the mutation was confirmed by sequencing. Mice were then back-crossed with BALB/cOlaHsd or C57BL/6J mice for at least eight generations to obtain the RAKA mutation in the respective pure background. $ASPP2^{RAKA/RAKA}$ embryos were generated from heterozygous crosses. To generate LifeAct-GFP-positive $ASPP2^{RAKA/RAKA}$ embryos, we generated $ASPP2^{WT/RAKA}$ mice heterozygous for the LifeAct-GFP transgene[33].

siRNA microinjections

siGENOME RISC-Free Control siRNA (Dharmacon) and Silencer Select Pre-designed siRNAs against mouse ASPP2 (Ambion) were resuspended in nuclease-free sterile water and used at 20 µM. For zygotes, 3 to 4 week old CD-1 females (Charles River UK) were injected intraperitoneally with 5 IU of PMSG (Intervet) and 48 h later with 5 IU of hCG (Intervet), and were paired with C57Bl/6J male mice (in house). Zygotes were retrieved from oviductal ampullae at 20 hours post-hCG. Cumulus-enclosed zygotes were denuded by exposure to 1 mg/mL hyaluronidase (Sigma) in modified mHTF (Life Global) containing 3mg/ml BSA for 3–6 min and cultured in LGGG-020 (life Global) containing 3mg/ml BSA in the presence of 5% CO2 at 37°C. Microinjection of zygotes commenced 2 hours after release from cumulus mass. Zygotes with a normal morphology were microinjected into the cytoplasm in 30µl drops of modified HTF media containing 4mg/ml BSA using a PMM-150FU Piezo impact drive (Primetech) using homemade glass capillaries with 5–10 pL of siRNA. Zygotes were returned to LGGG-020 containing 3mg/ml BSA in the presence of 5% CO2 at 37°C until analysis.

Human embryo collection

Human embryos were donated from patients attending the Oxford Fertility with approval from the Human Fertilization and Embryology Authority (centre 0035, project RO198) and the Oxfordshire Research Ethics Committee (Reference number 14/SC/0011). Informed consent was attained from all patients. Embryos were fixed in 4% paraformaldehyde, washed twice and kept in PBS containing 2% bovine serum albumin (PBS-BSA) at 4°C until they were used for immunohistochemistry.

Wholemount immunohistochemistry

Post-implantation embryos were fixed in 4% paraformaldehyde in phosphate-buffered saline (PBS) at room temperature for 20 to 45 minutes depending on embryo stages. Embryos were washed twice for 10 minutes in 0.1% PBS-Tween (PBS containing 0.1% Tween 20). Embryos were then permeabilized with 0.25% PBS-Triton (PBS containing 0.25 Triton X-100) for 25 minutes to 1 hour depending on embryo stages and then washed twice for 10 minutes in 0.1% PBS-Tween. Embryos were incubated overnight in a blocking solution (3% Bovine serum albumin, 2.5% donkey serum in 0.1% PBS-Tween). The next day, primary antibodies were diluted in blocking solution and added to the embryos overnight. The following day, embryos were washed three times for 15 minutes in 0.1% PBS-Tween and then incubated with secondary antibodies and Phalloidin diluted in blocking solution overnight. Finally, embryos were washed four times in 0.1% PBS-Tween and kept in DAPI-containing VECTASHIELD Antifade Mounting Medium (Vector Laboratories) at 4°C until used for imaging. Short incubation steps were carried out in wells of a 12-well plate on a rocker at room temperature and overnight steps were carried out in 1.5 mL Eppendorf tubes at 4°C.

For preimplantation embryos, fixation and permeabilization times were reduced to 15 minutes and 2% PBS-BSA (PBS containing 2% Bovine serum albumin) was used for washing steps. Blocking and secondary antibody incubation steps were reduced to one hour. Embryos were transferred between solutions by mouth-pipetting. the embryos were mounted in 8-well chambers in droplets consisting of 0.5 µL DAPI-containing VECTASHIELD and 0.5 µL 2% PBS-BSA. After mounting the embryos were kept in the dark at 4°C until they were imaged.

Immunocytochemistry

Caco-2 and MDCK.2 cells were maintained in Dulbecco's modified Eagle's medium containing 10% fetal bovine serum, penicillin, and streptomycin at 37°C in a 5% CO2 atmosphere incubator. In preparation for immunocytochemistry, Caco-2 cells were seeded onto coverslips in 24-well plates with fresh medium. 48 hours later, cells were fixed with 4% paraformaldehyde (in PBS) for 10 minutes, washed twice in PBS, and then permeabilized with 0.1% Triton X-100 in PBS for 4 minutes. Cells were washed twice in PBS and 2% PBS-BSA was then used as a blocking solution for 30 minutes prior to incubation with primary antibodies. Primary antibodies were diluted in 2% PBS-BSA and applied to cells for 40 minutes. Cells were then washed three times with PBS. Secondary antibodies (1:400), DAPI (1:2000, Invitrogen) and Phalloidin (1:400) were diluted in 2% PBS-BSA and applied to cells for 20 minutes. Coverslips were then washed three times with PBS and mounted onto glass slides with a small drop of Fluoromout-G (SouthernBiotech). They were air-dried before being sealed with nail varnish. All incubation steps

were carried out at room temperature on a rocker. Samples were kept in the dark at 4°C until they were imaged.

Antibodies and phalloidin conjugates

The following antibodies were used at the stated dilutions: rabbit anti-ASPP2 (Sigma, HPA021603), 1:100-1:200 (IHC); mouse anti-ASPP2 (Santa Cruz Biotechnologies, sc135818), 1:100 (ICC), 1:1000 (IB); mouse anti-YAP (Santa Cruz Biotechnology, sc-101199), 1:100 (IHC); rabbit anti-pYAP S127 (Cell Signaling, 4911), 1:100 (IHC); rabbit anti-Par3 (Millipore, 07-330), 1:100 (IHC); rabbit anti-Pard6b (Santa Cruz Biotechnology, sc-67393), 1:100 (IHC); rabbit anti-SCRIB (Santa Cruz Biotechnology, sc28737), 1:100 (IHC); goat anti-Brachyury (Santa Cruz Biotechnology, sc17745), 1:100 (IHC); rabbit anti-Sarcomeric α-actinin (Abcam, ab68167), 1:100 (IHC); mouse anti-FOXC2 (Santa Cruz Biotechnology, sc515234), 1:100 (IHC); rabbit anti-SOX-2 (Millipore, AB5603), 2 µL per mg of cell lysate (co-IP), 1:100 (IHC); goat anti-NKX2.5 (Santa Cruz Biotechnology, sc8697), 1:100 (IHC); rabbit anti-Afadin (Sigma, A0224), 2 µL per mg of cell lysate (co-IP), 1:100 (IHC, ICC), 1:1000 (IB); rabbit anti-Laminin (Sigma, L9393), 1:200 (IHC); goat anti-AMOT (Santa Cruz Biotechnologies, sc82491), 1:200 (IHC); goat anti-GATA-6 (R&D Systems, AF1700), 1:100 (IHC); rabbit anti-Myosin IIa (Cell Signaling, #3403), 1:100; rabbit anti-phospho-Myosin light chain 2 (Cell Signaling, #3674), 1:100. The following were used at 1:100 for IHC and 1:400 for ICC: Alexa fluor 555 donkey-anti-mouse (Invitrogen, A-31570), Alexa fluor 647 goat-anti-rat (Invitrogen, A-21247), Alexa fluor 488 donkey-anti-rabbit (Invitrogen, A21206), Phalloidin-Atto 488 (Sigma, 49409), Phalloidin–Atto 647N (Sigma, 65906).

Confocal microscopy, image analysis and quantification

Samples were imaged on a Zeiss Airyscan LSM 880 confocal microscope with a C-Apochromat 40x/1.2 W Korr M27 water immersion objective or a Plan-Apochromat 63x/1.4 OIL DIC M27 objective. For super-resolution imaging, an Airyscan detector was used[57]. Volocity (version 6.3.1, PerkinElmer) and Zen (Zeiss) software were used to produce maximum intensity projections and 3D opacity renderings. Image analysis was performed on optical sections. For signal intensity profiles along the apical-basal axis and across tricellular junctions, the arrow tool in the Zen software was used. Anterior and posterior embryo widths measurements were made using the line tool in Volocity.

For F-actin signal intensity profiles across the apical surface of epiblast or ectoderm cells, Fiji's freehand line tool with a width of "3" was used. Because the size of the apical domain was different for each cell measured, distances were expressed as percentages, with 100% representing the total distance across the apical domain. To account for depth-dependent signal attenuation, F-actin signal intensity at the apical domain was normalized by mean F-actin intensity in the nucleus of the cell measured. In each experiment, for each genotype, three embryos were used for measurements and 5 cells were analysed per embryo. The LOWES method was used to fit a line to the data.

Mouse embryo culture for live imaging and image analysis

To restrain embryo movement during imaging, lanes were constructed inside 8-well Lab-Tek II chamber slide (Nunc), using glass rods made from hand-drawn glass capillaries. Shorter pieces were used as spaces between two rods to create a space slightly wider than an embryo. Silicone grease was used to maintain the rods together. Each well was filled with medium containing 50% phenol red-free CMRL (PAN-Biotech, Germany) supplemented with 10 mM L-glutamine (Sigma-Aldrich) and 50% Knockout Serum Replacement (Life Technologies, England). The chamber was equilibrated at 37°C and an atmosphere of 5% CO_2 for at least 2 h prior to use. Freshly dissected embryos were placed in the lanes between two rods and allowed to settle prior to imaging on a Zeiss LSM 880 confocal microscope equipped with an environmental chamber to maintain conditions of 37°C and 5% CO_2. Embryos were imaged with a C-Apochromat 40x/1.2 W Korr M27 water immersion objective. Using a laser excitation wavelength of 561 nm, embryos labelled with mT/mG were imaged every 7.5 minutes and for each time point, nine z-sections were acquired every 3 µm around the midsagittal plane for up to 10 hours. For LifeAct-positive embryos, a laser excitation wavelength of 488 nm was used, and embryos were imaged every 15 minutes for 6 hours. For each time point, 12 z-sections every 1.5 µm were collected around the midsagittal plane.

Daughter cell movement was quantified using the Fiji plugin TrackMate (v5.2.0). Timepoints were registered using Fiji. Jittering was accounted for by correcting cell coordinates relatively to the centre of the embryonic region. The distance travelled by daughter cells (d) was analysed by calculating the distance between the coordinates of their final position and the coordinates of their respective mother cell immediately prior cell division. The direction of daughter cell movement (θ) was analysed by calculating the angle between the vector describing cell movement (that is the vector originating from the coordinates of the mother cell immediately prior cell division to the coordinates of the daughter cell at its final position) and the vector from the coordinates of the mother cell prior cell division to the coordinates of the embryonic region's centre. To establish the angle of cell division, we first defined a vector starting at the coordinates of one daughter and ending at the coordinates of the other immediately after cell division. We then defined a second vector originating halfway between the two daughters and terminating at the centre of the embryonic region. The angle of cell division was defined as the angle between those two vectors. The relative position of cell divisions was defined as the distance between the position of the mother cell immediately prior to cell division and the base of the epiblast.

Embryo culture in channels

Channels were formed by casting a 5% (which corresponded to approximately 4.2kPa stiffness[58]) acrylamide hydrogel (containing 39:1 bisacrylamide) around 60 µm wires within the confinement of a two-part mould (10x10x1mm). Ammonium persulphate (0.1%) and TEMED (1%) were added to polymerize polyacrylamide. The wires were then removed to form cylindrical cavities within hydrogel pieces. The hydrogels were carefully washed and equilibrated in embryo culture media at 37°C and 5% CO_2. The embryos were then inserted into the channels using a glass capillary with a diameter slightly larger than the embryo itself. It was used to stretch the hydrogel channel before injecting the embryos and letting the channels relax and deform the embryos. Cell viability in channels had previously been assessed without any noticeable difference with control embryos[27]. After 30 minutes, embryos were fixed inside the hydrogels with 4% PFA for 35 minutes. Once fixed, embryos were removed from the hydrogel channels and wholemount immunohistochemistry was performed.

Co-immunoprecipitation and SDS-PAGE/immunoblotting

For immunoprecipitation experiments, Caco-2 cells from confluent 10 cm diameter dishes were washed twice with PBS and then lysed in 500 µL of a buffer containing 50 mM Tris-HCl at pH 8, 150 mM NaCl, 1 mM EDTA, Complete Protease Inhibitor Cocktail (Roche) and 1% Triton X-100. Lysates were left on ice for 30 minutes, briefly sonicated and spun down at 21,000 x g for 30 minutes at 4°C. The supernatant was

transferred to another tube and protein concentration was measured (Bradford, Bio-Rad). 1 mg of protein lysate was used per condition. Lysates were precleared using 20 µL protein G Sepharose 4 fast flow (1:1 in PBS, GE Healthcare) for 30 minutes at 4°C on a shaker. The supernatant was incubated for 30 minutes at 4°C on a shaker with 2 µL of the indicated antibody. 30 µL protein G Sepharose 4 Fast Flow (1:1 in PBS) was added to each condition and samples were incubated overnight at 4°C on a shaker. Samples were washed 5 times with ice cold lysis buffer. 25 µL sample buffer was added and samples were incubated at 95°C for 5 minutes before being subjected to SDS-PAGE/immunoblotting.

Mesoderm explants and mesoderm cell migration

ASPP2$^{WT/RAKA}$ mice heterozygous for the LifeAct-GFP transgene were crossed and E7.5 embryos were dissected in M2. Embryos were then incubated in a 2.5% pancreatin mixture on ice for 20 minutes. Using tungsten needles, the visceral endoderm layer was removed and then the mesodermal wings were separated from the underlying epiblast. Mesodermal tissue was grown in fibronectin-coated 8-well Lab-Tek II chamber slides and cultured in DMEM containing 10% fetal bovine serum, penicillin, and streptomycin at 37°C and 5% $CO2^{59}$. Samples were imaged on a Zeiss LSM 880 confocal microscope equipped with an environmental chamber to maintain conditions of 37°C and 5% CO2. A laser excitation wavelength of 488 nm was used, and explants were imaged every 5 minutes for 5 hours. For each time point, 9 z-section with 1 µm step were collected.

Individual cells migrating away from the explants were tracked using the manual tracking plugin in Fiji. The movement, velocity and directionality of individual cells was analysed. Movement represented the total distance travelled in µm by an individual cell. Velocity represented the average speed in µm/min of a given cell. Directionality was used as a measure of how direct or convoluted a cell's path was and was calculated as the ratio between the total distance travelled and the distance in a straight line between a cell's start and end position[60].

Embryonic stem cell-derived cysts

Using small-molecule inhibitors of Erk and Gsk3 signalling[61], *ASPP2*$^{tE4/tE4}$ and *ASPP2*$^{RAKA/RAKA}$ (and *ASPP2*$^{WT/WT}$ controls) ESC were generated from flushed E2.5 embryos obtained from crosses between *ASPP2*$^{tE4/tE4}$ and *ASPP2*$^{WT/RAKA}$ mice, respectively. Briefly, embryos were grown for two days in organ culture dishes, containing pre-equilibrated preimplantation embryo culture media supplemented with 1 µM PDO325901 and 3 µM CHIR99021 (Sigma-Aldrich). Embryos were grown one more day in NDiff 227 media (Takara) supplemented with 1 µM PDO325901 and 3 µM CHIR99021 (NDiff + 2i). The trophectoderm was removed by immunosurgery and "epiblasts" were grown in gelatinised dishes in the presence of NDiff + 2i and ESGRO (recombinant mouse LIF Protein, Millipore) to establish ESC lines.

ASPP2$^{tE4/tE4}$ ESC were infected with an Ad-CMV-iCre adenovirus (Vector Biolabs) to delete exon 4 of *ASPP2*. Deletion of exon 4 was assessed by PCR. Non-infected *ASPP2*$^{tE4/tE4}$ ESC were used as controls. Wild type ESC derived from litter mates were used as controls for *ASPP2*$^{RAKA/RAKA}$ ESC. To form cysts, 4500 ESC were resuspended in 150 µL Matrigel (354230, Corning) and plated into a well of an 8-well Lab-Tek II chamber slide. The gel was left to set for 10 minutes at 37°C before 300 µL differentiation medium (DMEM supplemented with 15% FCS, 1% Penicillin/Streptomycin, 1% Glutamine, 1% MEM non-essential amino acids, 0.1 mM 2-mercaptoethanol and 1mM sodium pyruvate) was added. ESC were grown for 72 hours at 37°C and 5% CO2 before immunostaining was performed.

ACKNOWLEDGEMENTS

This work was funded by Wellcome Senior Investigator Award 103788/Z/14/Z (SS). We thank Jenny Nichols for advice and protocols for deriving Embryonic Stem Cells.

AUTHOR CONTRIBUTIONS

C.R., and S.S. led the project, conceived, and designed the experiments. C.R., E.Sa., E.Sl., J.Go., N. V., K.L., J.Ga., and T.N. conducted the experiments. C.R. and S.S. analysed the data. C.R. performed the statistical analyses. E.Sl. and X.L. designed and established the *ASPP2*$^{WT/RAKA}$ mouse line. H.H. and F.Z. performed the unwrapping of ASPP2 and F-actin immunostaining in E5.5 embryos. A.V., C.J., T.C., K.C. and C.G. organised the collection of human embryos. C.R. and S.S. wrote the manuscript.

REFERENCES

1. Norden, C. Pseudostratified epithelia - cell biology, diversity and roles in organ formation at a glance. J. Cell Sci. 130, 1859–1863 (2017).

2. Hoijman, E., Rubbini, D., Colombelli, J. & Alsina, B. Mitotic cell rounding and epithelial thinning regulate lumen growth and shape. Nat. Commun. 6, (2015).

3. Kondo, T. & Hayashi, S. Mitotic cell rounding accelerates epithelial invagination. Nature 494, 125–129 (2013).

4. Williams, M., Burdsal, C., Periasamy, A., Lewandoski, M. & Sutherland, A. Mouse primitive streak forms in situ by initiation of epithelial to mesenchymal transition without migration of a cell population. Dev. Dyn. 241, 270–283 (2012).

5. Voiculescu, O., Bodenstein, L., Jun, I. L. & Stern, C. D. Local cell interactions and self-amplifying individual cell ingression drive amniote gastrulation. Elife 2014, 1–26 (2014).

6. Shook, D. & Keller, R. Mechanisms, mechanics and function of epithelial-mesenchymal transitions in early development. Mech. Dev. 120, 1351–1383 (2003).

7. Ramkumar, N. et al. Crumbs2 promotes cell ingression during the epithelial-to-mesenchymal transition at gastrulation. Nat. Cell Biol. 18, 1281–1291 (2016).

8. Martin, A. C. & Goldstein, B. Apical constriction: themes and variations on a cellular mechanism driving morphogenesis. Development 141, 1987–98 (2014).

9. Heisenberg, C.-P. & Bellaiche, Y. Forces in Tissue Morphogenesis and Patterning. Cell 153, 948–962 (2013).

10. Martin, A. C., Gelbart, M., Fernandez-Gonzalez, R., Kaschube, M. & Wieschaus, E. F. Integration of contractile forces during tissue invagination. J. Cell Biol. 188, 735–749 (2010).

11. Ishiuchi, T. & Takeichi, M. Willin and Par3 cooperatively regulate epithelial apical constriction through aPKC-mediated ROCK phosphorylation. Nat. Cell Biol. 13, 860–6 (2011).

12. Chen, X. & Macara, I. G. Par-3 controls tight junction assembly through the Rac exchange factor Tiam1. Nat. Cell Biol. 7, 262–9 (2005).

13. Cong, W. et al. ASPP2 regulates epithelial cell polarity through the PAR complex. Curr. Biol. 20, 1408–14 (2010).

14. Sottocornola, R. et al. ASPP2 binds Par-3 and controls the polarity and proliferation of neural progenitors during CNS development. Dev. Cell 19, 126–37 (2010).

15. Liu, C.-Y. et al. PP1 cooperates with ASPP2 to dephosphorylate and activate TAZ. J. Biol. Chem. 286, 5558–

66 (2011).

16. Royer, C. et al. ASPP2 Links the Apical Lateral Polarity Complex to the Regulation of YAP Activity in Epithelial Cells. PLoS One 9, e111384 (2014).

17. Plusa, B. et al. Downregulation of Par3 and aPKC function directs cells towards the ICM in the preimplantation mouse embryo. J. Cell Sci. 118, 505–15 (2005).

18. Nishioka, N. et al. The Hippo Signaling Pathway Components Lats and Yap Pattern Tead4 Activity to Distinguish Mouse Trophectoderm from Inner Cell Mass. Dev. Cell 16, 398–410 (2009).

19. Hirate, Y. et al. Polarity-dependent distribution of angiomotin localizes hippo signaling in preimplantation embryos. Curr. Biol. 23, 1181–1194 (2013).

20. Leung, C. Y. & Zernicka-Goetz, M. Angiomotin prevents pluripotent lineage differentiation in mouse embryos via Hippo pathway-dependent and -independent mechanisms. Nat. Commun. 4, 2251 (2013).

21. Mamada, H., Sato, T., Ota, M. & Sasaki, H. Cell competition in mouse NIH3T3 embryonic fibroblasts is controlled by the activity of Tead family proteins and Myc. J. Cell Sci. 128, 790–803 (2015).

22. Buti, L. et al. CagA–ASPP2 complex mediates loss of cell polarity and favors H. Pylori colonization of human gastric organoids. Proc. Natl. Acad. Sci. 117, 2645–2655 (2020).

23. Kampa, K. M. et al. heterozygous mice are tumor-prone and have attenuated cellular damage – response thresholds. Proc. Natl. Acad. Sci. 53, (2009).

24. Llanos, S. et al. Inhibitory member of the apoptosis-stimulating proteins of the p53 family (iASPP) interacts with protein phosphatase 1 via a noncanonical binding motif. J. Biol. Chem. 286, 43039–44 (2011).

25. Bedzhov, I. & Zernicka-Goetz, M. Self-organizing properties of mouse pluripotent cells initiate morphogenesis upon implantation. Cell 156, 1032–44 (2014).

26. Ichikawa, T. et al. Live Imaging of Whole Mouse Embryos during Gastrulation: Migration Analyses of Epiblast and Mesodermal Cells. PLoS One 8, e64506 (2013).

27. Leonavicius, K. et al. Mechanics of mouse blastocyst hatching revealed by a hydrogel-based microdeformation assay. Proc. Natl. Acad. Sci. 115, 10375–10380 (2018).

28. Rauzi, M. et al. Embryo-scale tissue mechanics during Drosophila gastrulation movements. Nat. Commun. 6, 8677 (2015).

29. Hennigan, R. F., Fletcher, J. S., Guard, S. & Ratner, N. Proximity biotinylation identifies a set of conformation-specific interactions between Merlin and cell junction proteins. Sci. Signal. 12, (2019).

30. Zhang, P. et al. ASPP1/2-PP1 complexes are required for chromosome segregation and kinetochore-microtubule attachments. Oncotarget 6, 41550–41565 (2015).

31. Choi, W. et al. Remodeling the zonula adherens in response to tension and the role of afadin in this response. J. Cell Biol. 213, 243–260 (2016).

32. Ikeda, W. et al. Afadin: A key molecule essential for structural organization of cell- cell junctions of polarized epithelia during embryogenesis. J. Cell Biol. 146, 1117–1131 (1999).

33. Riedl, J. et al. Lifeact mice for studying F-actin dynamics. Nat. Methods 7, 168–169 (2010).

34. Kosodo, Y. & Huttner, W. B. Basal process and cell divisions of neural progenitors in the developing brain. Dev. Growth Differ. 51, 251–261 (2009).

35. Strzyz, P. J. et al. Interkinetic Nuclear Migration Is Centrosome Independent and Ensures Apical Cell Division to Maintain Tissue Integrity. Dev. Cell 32, 203–219 (2015).

36. Hao, Y. et al. Par3 controls epithelial spindle orientation by aPKC-mediated phosphorylation of apical Pins. Curr. Biol. 20, 1809–18 (2010).

37. Williams, S. E., Ratliff, L. a, Postiglione, M. P., Knoblich, J. a & Fuchs, E. Par3-mInsc and Gαi3 cooperate to promote oriented epidermal cell divisions through LGN. Nat. Cell Biol. 16, (2014).

38. Keder, A. et al. The Hippo pathway core cassette regulates asymmetric cell division. Curr. Biol. 25, 2739–2750 (2015).

39. Gao, L. et al. Afadin orients cell division to position the tubule lumen in developing renal tubules. Development 144, 3511–3520 (2017).

40. Speicher, S., Fischer, A., Knoblich, J. & Carmena, A. The PDZ Protein Canoe Regulates the Asymmetric Division of Drosophila Neuroblasts and Muscle Progenitors. Curr. Biol. 18, 831–837 (2008).

41. Bosveld, F. et al. Epithelial tricellular junctions act as interphase cell shape sensors to orient mitosis. Nature 530, 495–498 (2016).

42. Hart, K. C. et al. E-cadherin and LGN align epithelial cell divisions with tissue tension independently of cell shape. Proc. Natl. Acad. Sci. U. S. A. 114, E5845–E5853 (2017).

43. Tang, Z. et al. Mechanical Forces Program the Orientation of Cell Division during Airway Tube Morphogenesis. Dev. Cell 44, 313-325.e5 (2018).

44. Scarpa, E., Finet, C., Blanchard, G. B. & Sanson, B. Actomyosin-Driven Tension at Compartmental Boundaries Orients Cell Division Independently of Cell Geometry In Vivo. Dev. Cell 47, 727-740.e6 (2018).

45. Finegan, T. M. et al. Tissue tension and not interphase cell shape determines cell division orientation in the Drosophila follicular epithelium . EMBO J. 38, 1–18 (2019).

46. Nakajima, Y.-I., Meyer, E. J., Kroesen, A., McKinney, S. a. & Gibson, M. C. Epithelial junctions maintain tissue architecture by directing planar spindle orientation. Nature 500, 1–5 (2013).

47. Manning, L. A., Perez-Vale, K. Z., Schaefer, K. N., Sewell, M. T. & Peifer, M. The Drosophila Afadin and ZO-1 homologues Canoe and Polychaetoid act in parallel to maintain epithelial integrity when challenged by adherens junction remodeling. Mol. Biol. Cell 30, 1938–1960 (2019).

48. Sawyer, J. K., Harris, N. J., Slep, K. C., Gaul, U. & Peifer, M. The Drosophila afadin homologue Canoe regulates linkage of the actin cytoskeleton to adherens junctions during apical constriction. J. Cell Biol. 186, 57–73 (2009).

49. Salomon, J. et al. Contractile forces at tricellular contacts modulate epithelial organization and monolayer integrity. Nat. Commun. 8, (2017).

50. Vives, V. et al. ASPP2 is a haploinsufficient tumor suppressor that cooperates with p53 to suppress tumor growth. Genes Dev. 20, 1262–7 (2006).

51. Wang, Y. et al. ASPP2 controls epithelial plasticity and inhibits metastasis through β-catenin-dependent regulation of ZEB1. Nat. Cell Biol. 16, (2014).

52. Tordella, L. et al. ASPP2 suppresses squamous cell carcinoma via RelA/p65-mediated repression of p63. Proc. Natl. Acad. Sci. U. S. A. 110, 17969–74 (2013).

53. Bertran, M. T. et al. ASPP proteins discriminate between PP1 catalytic subunits through their SH3 domain and the PP1 C-tail. Nat. Commun. 10, (2019).

54. Kas, S. M. et al. Insertional mutagenesis identifies drivers of a novel oncogenic pathway in invasive lobular breast carcinoma. Nat. Genet. 49, 1219–1230 (2017).

55. Hayashi, S., Lewis, P., Pevny, L. & McMahon, A. P. Efficient gene modulation in mouse epiblast using a Sox2Cre transgenic mouse strain. Mech. Dev. 119, S97–S101 (2002).

56. Muzumdar, M. D., Tasic, B., Miyamichi, K., Li, N. & Luo, L. A global double-fluorescent cre reporter mouse. Genesis 45, 593–605 (2007).

57. Huff, J. The Airyscan detector from ZEISS: confocal imaging with improved signal-to-noise ratio and super-resolution. Nat. Methods 12, I–II (2015).

58. Tse, J. R. & Engler, A. J. Preparation of hydrogel substrates with tunable mechanical properties. Current Protocols in Cell Biology vol. 47 10.16.1-10.16.16 (2010).

59. Bazzi, H., Soroka, E., Alcorn, H. L., Anderson, K. V & Hogan, B. L. M. STRIP1, a core component of STRIPAK complexes, is essential for normal mesoderm migration in the mouse embryo. Proc. Natl. Acad. Sci. U. S. A. 114, E10928–E10936 (2017).

60. Petrie, R. J., Doyle, A. D. & Yamada, K. M. Random versus directionally persistent cell migration. Nat. Rev. Mol. Cell Biol. 10, 538–549 (2009).

61. Nichols, J. & Jones, K. Derivation of mouse embryonic stem (ES) cell lines using small-molecule inhibitors of Erk and Gsk3 signaling (2i). Cold Spring Harb. Protoc. 2017, 379–386 (2017).

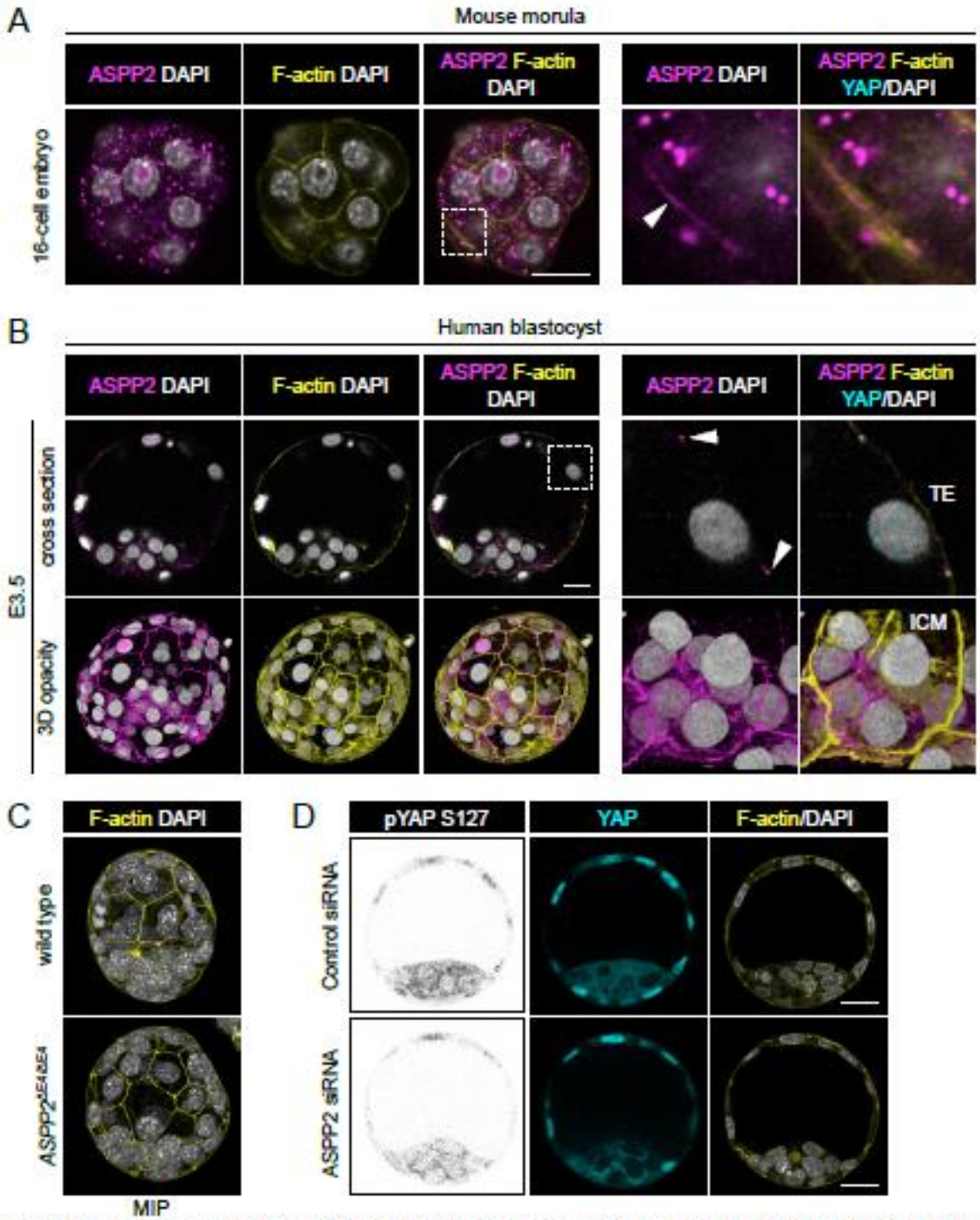

Figure S1: ASPP2 is not required during preimplantation development. A. Localisation pattern of ASPP2 in 16-cell embryos. A cross section through the equatorial plane of a representative embryo is shown. The F-actin cytoskeleton and nuclei were visualised using Phalloidin and DAPI respectively. The dashed area is magnified on the right. The white arrowhead shows ASPP2 and F-actin colocalising at an apical junction between two outside cells. Scale bars: 20 µm (left panel) and 5 µm (right panel). B. localisation pattern of ASPP2 in human blastocysts. The top panel shows a cross section through the equatorial plane of a representative embryo. The dashed area is magnified on the right to highlight the colocalisation between ASPP2 and F-actin at the level of apical junctions in the trophectoderm (TE) (white arrowheads). The bottom row shows a 3D opacity rendering of the same embryo in its totality (left panel) and a focus on its inner cell mass (right panel). TE: trophectoderm; ICM: inner cell mass. Scale bar: 20 µm. C. F-actin is normally distributed at the level of apical junctions in the TE of *ASPP2*$^{\Delta E4/\Delta E4}$ embryos. Maximum intensity projections of representative wild type and *ASPP2*$^{\Delta E4/\Delta E4}$ embryos stained with Phalloidin and DAPI. D. ASPP2 knockdown in E3.5 embryos using siRNA targeting ASPP2 mRNA. Note that the localisation pattern of pYAP S127 was similar in control and ASPP2-depleted embryos. Scale bar: 20 µm.

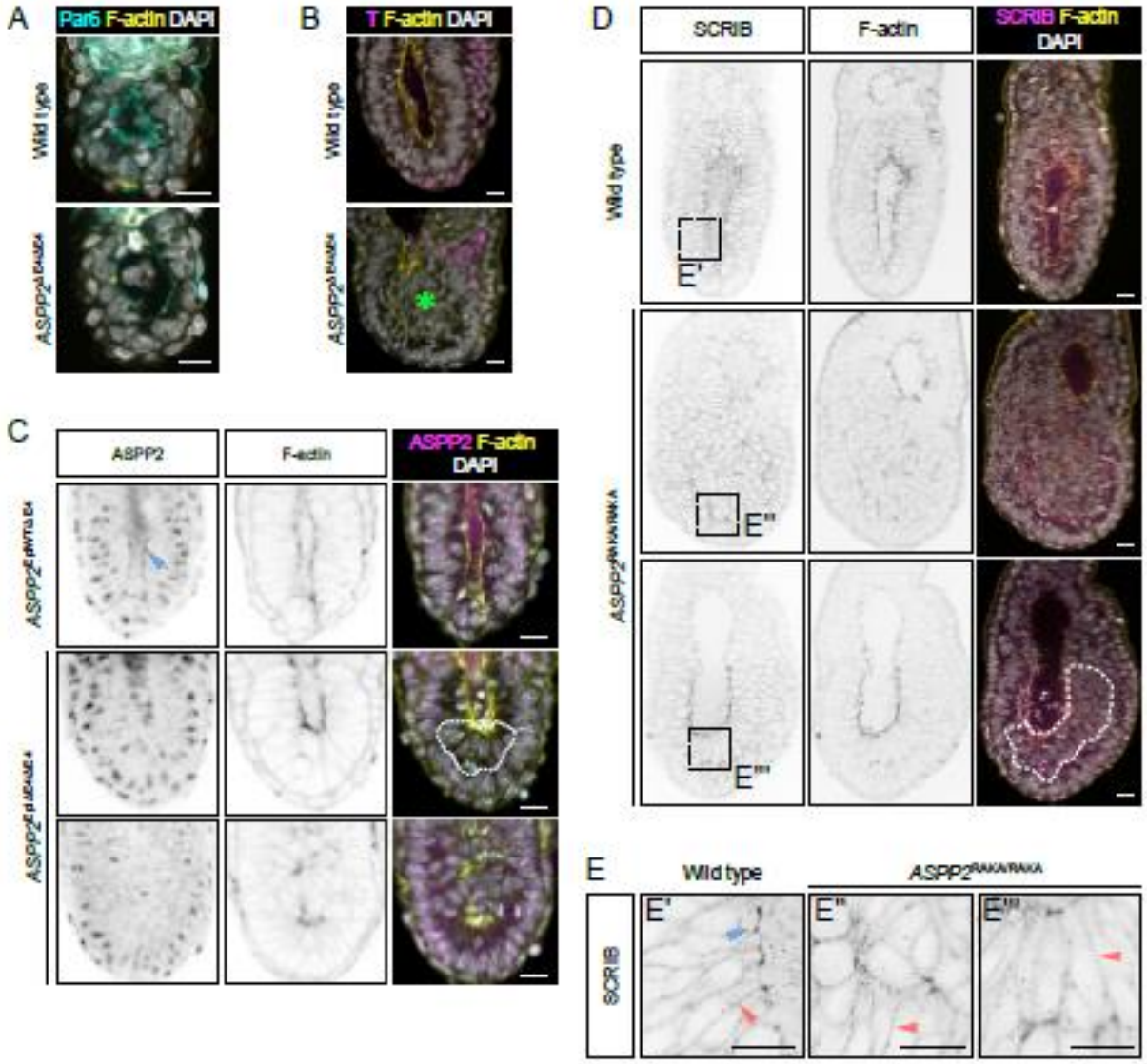

Figure S2: ASPP2 is required specifically in the epiblast during proamniotic cavity formation. A. Immunofluorescence of wild type and *ASPP2*$^{\Delta E4/\Delta E4}$ E5.5 embryos using an anti-Par6 antibody. B. Phenotype of *ASPP2*$^{\Delta E4/\Delta E4}$ embryos at E7.5. Brachyury (T) localisation was analysed by indirect immunofluorescence. The ectopic accumulation of cells in the proamniotic cavity of *ASPP2*$^{\Delta E4/\Delta E4}$ embryos is indicated by a green star. C. ASPP2 expression was conditionally prevented in the epiblast to test whether ASPP2 was specifically required in the epiblast (*ASPP2*$^{flox\Delta E4/\Delta E4}$ embryos). ASPP2 expression pattern was analysed by indirect immunofluorescence. ASPP2 proteins were completely absent at the apical junction of epiblast cells in *ASPP2*$^{flox\Delta E4/\Delta E4}$ embryos. Note that the ASPP2 antibody results in non-specific nuclear signal (also seen in Figure 1C when depleting ASPP2 by siRNA). The dashed area highlights the ectopic accumulation of cells in the epiblast. D. SCRIB expression pattern was analysed by indirect immunofluorescence in wild type and *ASPP2*$^{RAKA/RAKA}$ embryos. The ectopic accumulations of cells in the epiblast of *ASPP2*$^{RAKA/RAKA}$ embryos was highlighted by a dashed line. E. Magnification of the corresponding regions in D. The blue arrowhead points to the enrichment of SCRIB at the apical junctions. Red arrowheads point to basolateral SCRIB. The F-actin cytoskeleton and nuclei were visualised using Phalloidin and DAPI respectively. Scale bars: 20 µm.

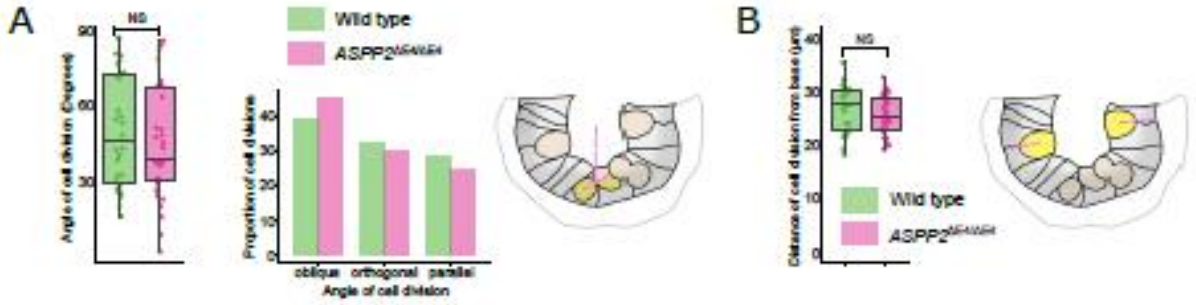

Figure S3: The angle of cell division and their relative position from the base of the epiblast is unaffected in the absence of ASPP2. A. Quantification of cell division angles in the epiblasts of wild type (n=3 embryos, 28 cells) and *ASPP2*$^{\Delta E4/\Delta E4}$ embryos (n=3 embryos, 33 cells). Left panel: Comparison of all cell division angles in wild type and *ASPP2*$^{\Delta E4/\Delta E4}$ embryos. NS: non-significant (nested ANOVA). right panel: Cell division angles were defined as either parallel (0° to 30°), oblique (30° to 60°) or orthogonal (60° to 90°). NS: non-significant (Fisher's exact test of independence). B. Position of cell division events in wild type and *ASPP2*$^{\Delta E4/\Delta E4}$ embryos. The relative position of cell division events was expressed as the distance between mother cell position immediately prior to a division event and the base of the epithelium. NS: non-significant (nested ANOVA).

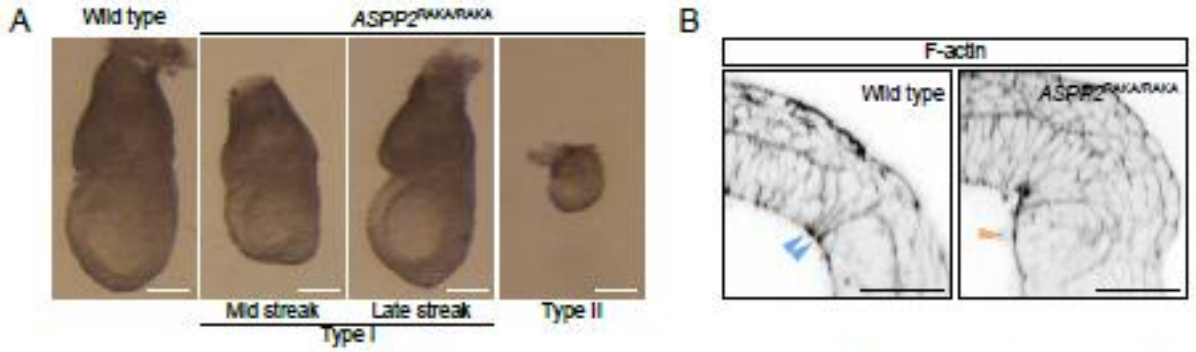

Figure S4: Gross defects in ASPP2*$^{RAKA/RAKA}$ *embryos in a BALB/c background at E7.5. A. Bright field images of wild type and type I (34/41, 82.9%) and type II (7/41, 17.1%) phenotypes observed in *ASPP2*$^{RAKA/RAKA}$ embryos. Type I embryos exhibited a strong accumulation of cells in their posterior. B. Cells ectopically accumulating in the primitive streak region are unable to apically constrict and do not have enriched F-actin at the apical junctions (orange arrowhead) in comparison to wild type (blue arrow heads). The F-actin cytoskeleton was visualised using Phalloidin. Scale bars: 20 µm.

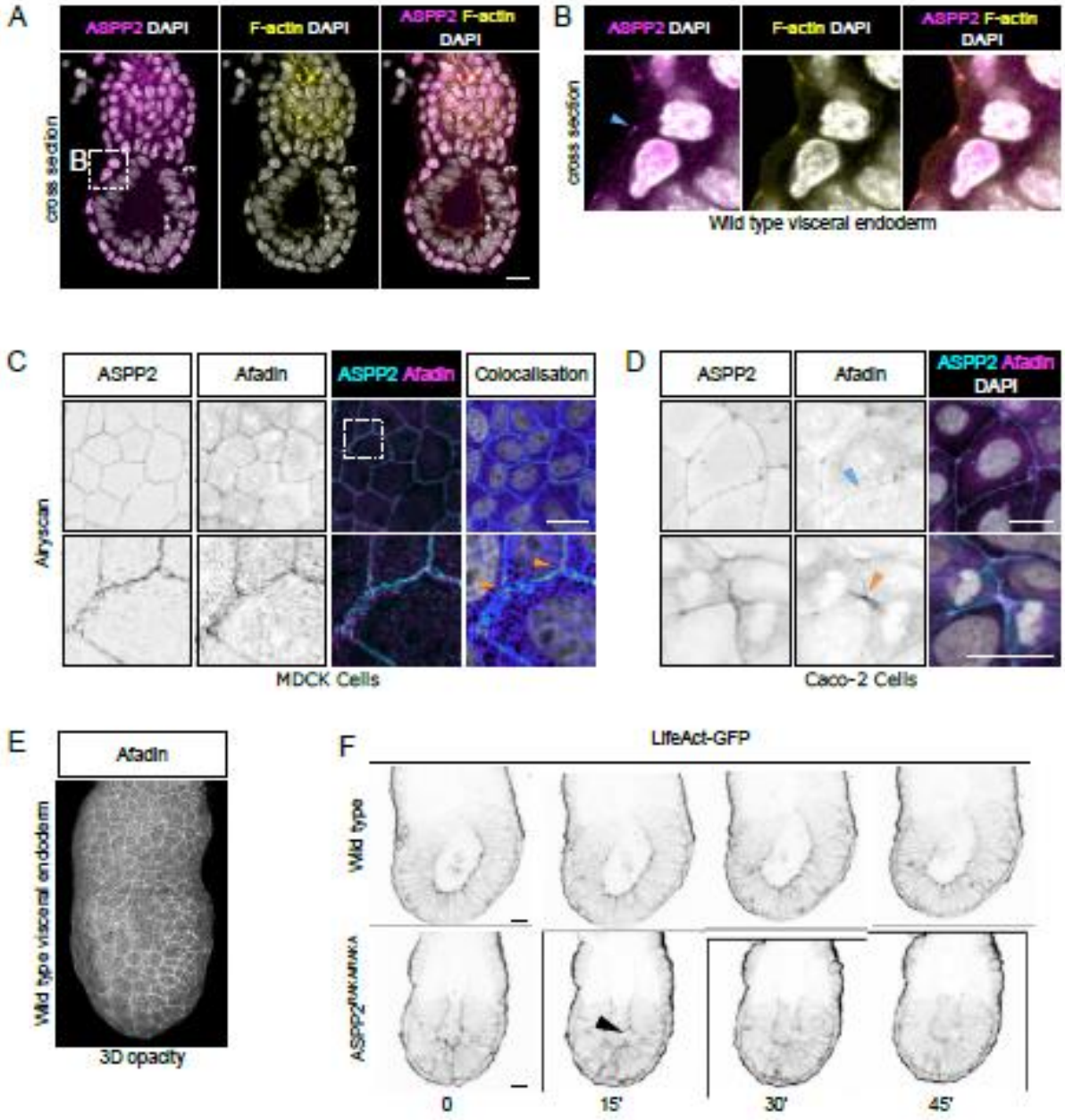

Figure S5: ASPP2 is required for the integrity of the F-actin cytoskeleton in the epiblast as cells divide. A. The localisation pattern of ASPP2 was analysed in wild type E5.5 embryos by immunofluorescence. B. Magnification of the boxed region in A, showing the localisation pattern of ASPP2 in the VE at the apical junctions (blue arrowhead). Note that ASPP2's nuclear signal is non-specific. C. Super-resolution Airyscan imaging of MDCK cells immunostained for ASPP2 and Afadin. Orange arrowheads highlight the colocalisation of Afadin and ASPP2 at tricellular junctions. D. The localisation pattern of ASPP2 and Afadin was analysed in Caco-2 cells. Afadin and ASPP2, in addition to being enriched at tricellular junctions, could also be found colocalising at bicellular junctions (blue arrowhead) and were in close proximity at the cleavage furrow (orange arrowhead). E. 3D opacity rendering showing the localisation at the apical junctions of the VE in an E6.5 wild type embryo. F. Time-lapse imaging of wild type and *ASPP2*$^{RAKA/RAKA}$ LifeAct-GFP positive embryos. Note how apical F-actin is disrupted in *ASPP2*$^{RAKA/RAKA}$ LifeAct-GFP positive embryos following a cell division event (black arrowhead). Nuclei and the F-actin cytoskeleton were visualised with DAPI and Phalloidin respectively. Scale bars: 20 μm.

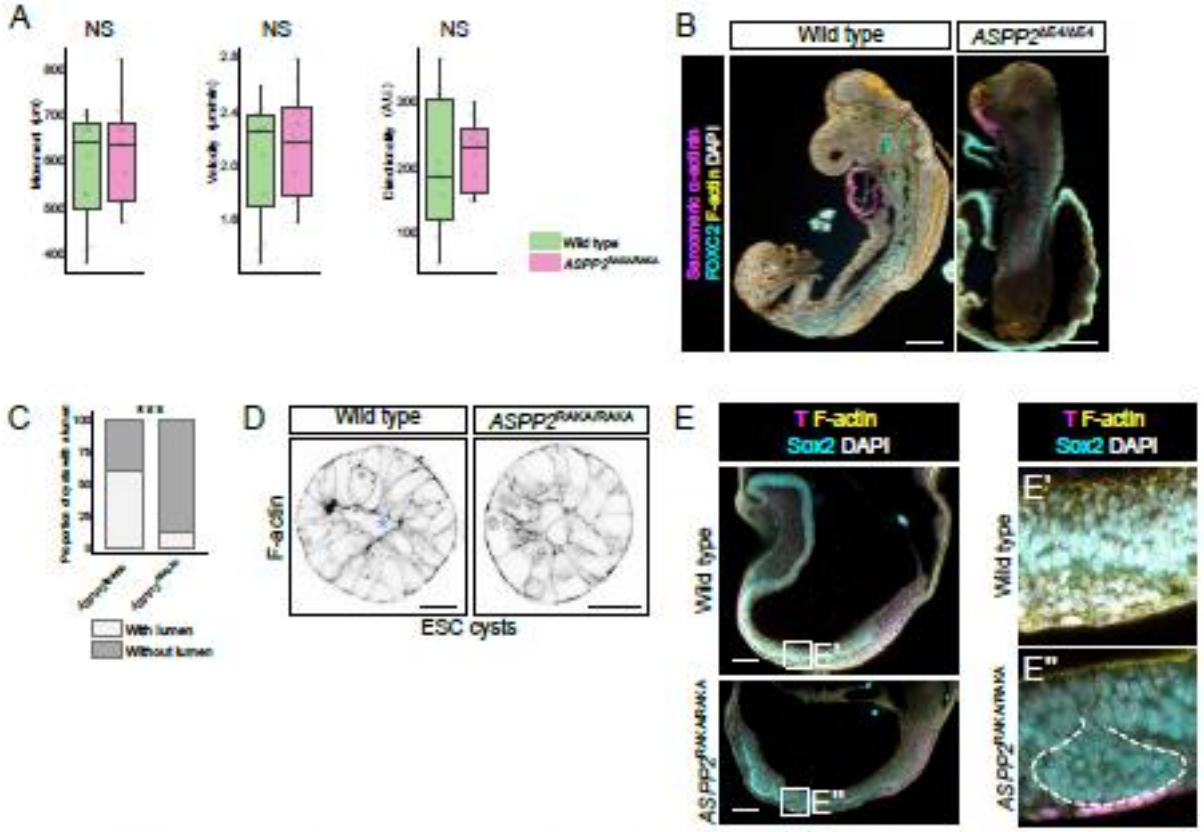

Figure S8: ASPP2 is required for cavity architecture in ESC cysts. A. Mesoderm cell migration is unaffected in the absence of ASPP2. Cell movement, velocity, and directionality from wild type (n=4 explants, 3 cells per explant) and *ASPP2*$^{RAKA/RAKA}$ (n=4 explants, 3 cells per explant) mesoderm explants were quantified. NS: non-significant (nested ANOVA). B. E9.5 wild type and *ASPP2*$^{\Delta E4/\Delta E4}$ embryos labelled by immunofluorescence with antibodies against FOXC2 (somitic mesoderm) and sarcomeric α-actinin (sarcomeres in cardiomyocytes). Nuclei and the F-actin cytoskeleton were visualised with DAPI and Phalloidin respectively. Scale bars: 200 µm. C. Quantification of the proportion of *ASPP2*$^{\Delta E4/\Delta E4}$ and *ASPP2*$^{\Delta E4/\Delta E4}$ ESC-derived cysts with lumens after three days in culture in Matrigel. D. Representative images of wild type and *ASPP2*$^{RAKA/RAKA}$ ESC-derived cysts after three days in culture in Matrigel. The blue star indicates the presence of a cavity in the wild type cyst. E. Cells from the ectoderm occasionally delaminate basally into the underlying mesoderm in E8.5 *ASPP2*$^{RAKA/RAKA}$ embryos. The F-actin cytoskeleton was visualised with Phalloidin respectively. Scale bars: 20 µm.

MOVIE LEGENDS

Movie 1: Time lapse imaging of wild type and ASPP2$^{\Delta N/\Delta N}$ embryos with mT/mG-labelled cell membranes

Movie 2: Airyscan imaging and 3D rendering of F-actin in the primitive streak region of representative wild type and ASPP2$^{RARA/RARA}$ embryos

Movie 3: D rendering showing that the primitive streak expands comparatively in E7.5 wild type and ASPP2$^{\Delta N/\Delta N}$ embryos. Mesoderm cells were labelled by immunofluorescence using an antibody against Brachyury (T). Nuclei and the F-actin cytoskeleton were visualised with DAPI and Phalloidin respectively.

Movie 4: Time lapse imaging of wild type and ASPP2$^{RARA/RARA}$ mesoderm explants positive for the LifeAct-GFP transgene